TABLE OF CONTENTS

8007300645

TABLE OF CONTENTS (Contd)

LIST OF TABLES

LIST OF FIGURES

(At Rear of Section)

LIST OF FIGURES (Contd)

00164

LIST OF FIGURES (Contd)

LIST OF APPENDICES

Number	Title
3A	Modal Analysis of Xenon-Induced Oscillations

LIST OF FIGURES

(At Rear of Section)

3 REACTOR

3.1 DESIGN BASES

The reactor is designed to meet the performance objectives specified in 3.1.1 without exceeding the limits of design and operation specified in 3.1.2.

3.1.1 PERFORMANCE OBJECTIVES

The reactor is designed to operate initially at 2,452 MWt(*) with sufficient design margins to accommodate transient operation and instrument error without damage to the core and without exceeding the pressure at the relief valve settings in the reactor coolant system. The ultimate operating power level of the reactor core is expected to be 2,552 MWt. This section of the report describes only reactor operation at the initial power level.

The fuel rod cladding is designed to maintain its integrity for the anticipated core life. The effects of gas release, fuel dimensional changes, and corrosion- or irradiation-induced changes in the mechanical properties of cladding are considered in the design of fuel assemblies.

Reactivity is controlled by control rod assemblies (CRA), burnable poison rod assemblies (BPRA), and soluble boron in the coolant. Sufficient CRA worth is available to shut the reactor down ($k_{eff} \leq 0.99$) in the hot condition at any time during the life cycle with the most reactive CRA stuck in the fully withdrawn position. Equipment is provided to add soluble boron to the reactor coolant to insure a similar shutdown capability when the reactor coolant is cooled to ambient temperatures.

The reactivity worth of CRA, and the rate at which reactivity can be added, is limited to insure that credible reactivity accidents cannot cause a transient capable of damaging the reactor coolant system or causing significant fuel failure.

3.1.2 LIMITS

3.1.2.1 Nuclear Limits

The core has been designed to the following nuclear limits:

a. Fuel has been designed for a maximum burnup of 55,000 MWd/MTU.

b. The power Doppler coefficient is negative, and the control system is capable of compensating for reactivity changes resulting from nuclear coefficients, either positive or negative.

c. Control systems will be available to handle core xenon instabilities should they occur during operation, without jeopardizing the safety conditions of the reactor coolant system.

- - - - -

(*) Full (rated) core thermal power.

d. The core will have sufficient excess reactivity to produce the design power level and lifetime without exceeding the control capacity or shutdown margin.

e. Controlled reactivity insertion rates have been limited to 9.2×10^{-5} $(\Delta k/k)$/sec for a single regulating CRA group withdrawal, and 7×10^{-6} $(\Delta k/k)$/sec for soluble boron removal.

f. Reactor control and maneuvering procedures will not produce peak-to-average power distributions greater than those listed in Table 3-1. The low worth of CRA groups inserted during power operation limits power peaks to acceptable values.

3.1.2.2 Reactivity Control Limits

The control system and the operational procedures will provide adequate control of the core reactivity and power distribution. The following control limits will be met:

a. Sufficient control will be available to produce an adequate shutdown margin.

b. The shutdown margin will be maintained with the CRA of highest worth stuck out of the core.

c. CRA withdrawal limits the reactivity insertion to 9.2×10^{-5} $(\Delta k/k)$/sec on a single regulating group. Boron dilution is also limited to a reactivity insertion of 7×10^{-6} $(\Delta k/k)$/sec.

3.1.2.3 Thermal and Hydraulic Limits

The reactor core is designed to meet the following limiting thermal and hydraulic conditions:

a. No central melting in the fuel at the design overpower (114 percent).

b. A 99 percent confidence that at least 99.5 percent of the fuel rods in the core are in no jeopardy of experiencing a departure from nucleate boiling (DNB) during continuous operation at the design overpower.

c. Essentially 100 percent confidence that at least 99.96 percent of the fuel rods in the core are in no jeopardy of experiencing a DNB during continuous operation at rated power.

d. The generation of net steam in the hottest core channels is permissible, but steam voids will be low enough to prevent flow instabilities.

The design overpower is the highest credible reactor operating power permitted by the safety system. Normal overpower to trip is significantly less than the design overpower. Core rated power is 2,452 MWt.

3.1.2.4 Mechanical Limits

3.1.2.4.1 Reactor Internals

The reactor internal components are designed to withstand the stresses resulting from start-up; steady state operation with two, three, or four reactor coolant pumps running; and shutdown conditions. No damage to the reactor internals will occur as a result of loss of pumping power.

Reactor internals will be fabricated from SA-240 (Type 304) material and will be designed within the allowable stress levels permitted by the ASME Code, Section III, for normal reactor operation and transients. Structural integrity of all core support assembly circumferential welds will be assured by compliance with ASME Code, Sections III and IX, radiographic inspection acceptance standards, and welding qualifications.

The core support structure will be designed as a Class I structure, as defined in Appendix 5A of this report, to resist the effects of seismic disturbances. The basic design guide for the seismic analysis will be AEC publication TID-7024, "Nuclear Reactors and Earthquakes."

Lateral deflection and torsional rotation of the lower end of the core support assembly will be limited to prevent excessive movements resulting from seismic disturbance and thus prevent interference with control rod assemblies (CRA). Core drop in the event of failure of the normal supports will be limited so that the CRA do not disengage from the fuel assembly guide tubes.

The structural internals will be designed to maintain their functional integrity in the event of a major loss-of-coolant accident as described in 3.2.4.1. The dynamic loading resulting from the pressure oscillations because of a loss-of-coolant accident will not prevent CRA insertion.

Internals vent valves are provided to relieve pressure generated by steaming in the core, following a postulated reactor coolant inlet pipe rupture, so that the core will remain sufficiently cooled.

3.1.2.4.2 Fuel Assemblies

The fuel assemblies are designed to operate satisfactorily to design burnup and to retain adequate integrity at the end of life to permit safe removal from the core.

The assemblies are designed to operate safely during steady state and transient conditions under the combined effects of flow-induced vibration, cladding strain caused by reactor pressure, fission gas pressure, fuel growth, and differential thermal expansion. The cold-worked Zircaloy-4 cladding is designed to be freestanding. Fuel rods are held in place by mechanical spacer grids that are designed to maintain dimensional control of the fuel rod spacing throughout the design life without impairing cladding integrity. Contact loads are limited to minimize fret[illegible]

The spacer grids are also designed to permit differential thermal expansion of the fuel rods without restraint that would cause distortion of the rods. The fuel assembly upper end fitting and the control rod guide tube in the internals structure are both indexed to the grid plate above the fuel assemblies, thus insuring continuous alignment of the guide channels for the CRA. The control rod travel is designed so that the rods are always engaged in the fuel assembly guide tubes, thus insuring that CRA can always be inserted. The assembly structure is also designed to withstand handling loads, shipping loads, and earthquake loads.

Stress and strain for all anticipated normal and abnormal operating conditions will be limited as follows:

a. Stresses that are not relieved by small deformations of the material will be prevented from leading to failure by not permitting these stresses to exceed the yield strength of the material nor to exceed levels that would use in excess of 75 percent of the stress rupture life of the material. An example of this type of stress is the circumferential membrane stress in the clad due to internal or external pressure.

b. Stresses that are relieved by small deformations of the material, and the single occurrence of which will not make a significant contribution to the possibility of a failure, will be permitted to exceed the yield strength of the material. Where such stresses exceed the material yield strength, strain limits will be set, based on low-cycle fatigue techniques, using no more than 90 percent of the material fatigue life. Evaluations of cyclic loadings will be based on conservative estimates of the number of cycles to be experienced. An example of this type of stress is the thermal stress resulting from the thermal gradient across the clad thickness.

c. Combinations of these two types of stresses, in addition to the individual treatment outlined above, will be evaluated on the low-cycle fatigue basis of Item b. Also, clad plastic strain due to diameter increases resulting from thermal ratcheting and/or creep, including the effects of internal gas pressure and fuel swelling, will be limited to about 1 percent.

d. Minimum clad collapse pressure margins will be required as follows:

(1) 10 percent margin over system design pressure, on short-time collapse, at end void.

(2) End void must not collapse (must be either freestanding or have adequate support) on a long-time basis.

(3) 10 percent margin over system operating pressure, on short-time collapse, at hot spot average temperature through the clad wall.

(4) Clad must be freestanding at design pressure on a short-time basis at 725 F hot spot average temperature through the clad wall.

3.1.2.4.3 Control Rod Assembly (CRA)

The control rod clad is designed to the same criteria as the fuel clad, as applicable. Adequate clearance will be provided between the control rods and the guide tubes, which position them within the fuel assembly, so that control rod overheating will be avoided and unacceptable mechanical interference between the control rod and the guide tube will not occur under any operating condition, including earthquake.

Overstressing of the CRA components during a trip will be prevented by minimizing the shock loads by snubbing and by providing adequate strength.

3.1.2.4.4 Control Rod Drive

The control rod drives provide control rod assembly (CRA) insertion and withdrawal rates consistent with the required reactivity changes for reactor operational load changes. This rate is based on the worths of the various rod groups, which have been established to limit power-peaking flux patterns to design values. The maximum reactivity addition rate is specified to limit the magnitude of a possible nuclear excursion resulting from a control system or operator malfunction. The normal insertion and withdrawal velocity has been established as 30 in./min.

The control rod drives provide a "trip" of the CRA which results in a rapid shutdown of the reactor for conditions that cannot be handled by the reactor control system. The trip is based on the results of various reactor emergency analyses, including instrument and control delay times and the amount of reactivity that must be inserted before deceleration of the CRA occurs. The maximum travel time for a 2/3 insertion on a trip command of a CRA has been established as 1.4 sec.

The control rod drives can be coupled and uncoupled to their respective CRA without any withdrawal movement of the CRA.

All pressure-containing components are designed to meet the requirements of the ASME Code, Section III, Nuclear Vessels, for Class A vessels.

Materials selected for the control rod drive are capable of operating within the specified reactor environment for the life of the mechanism without any deleterious effects. Adequate clearance will be provided between the stationary and moving parts of the control rod drives so that the CRA trip time to full insertion will not be adversely affected by mechanical interference under all operating conditions and seismic disturbances.

Structural integrity and adherence to allowable stress limits of the control rod drive and related parts during a trip will be achieved by establishing a limit on impact loads through snubbing.

3.1.2.4.5 Methods of Load Analysis To Be Employed for Reactor Internals and Core

Static or dynamic analyses will be used as appropriate. In general, dynamic analysis will be used for earthquakes and the subcooled portion of the

loss-of-coolant accident (LOCA). For the relatively steady state portion of the LOCA, a static analysis will be used.

Where it is indicated that substantial coupling, ie, interrelationship, exists between major components of the Nuclear Steam System (NSS) such as between the steam generator, the piping, and the vessel, the dynamic analysis will include the response of the entire coupled system. However, where coupling is found to be small, the component or groups of components will be treated independently of the overall system.

The dynamic analysis for LOCA will use predicted pressure-time histories as input to a lumped-mass model. For earthquakes, actual earthquake records, normalized to appropriate ground motion, will be used as input to the model. The output from the analysis will be in the form of internal motions (displacements, velocities, and accelerations), motions of individual fuel assemblies, impact loads between adjacent fuel assemblies, and impact loads between peripheral fuel assemblies and the core shroud.

In addition, seismic analysis will also be performed using a modal superposition and response spectra approach.

For the simultaneous occurrence of LOCA and the maximum earthquake (E'), both time-history excitations will be input to the system simultaneously. Relative starting times will be changed until maximum structural motions, indicating maximum stresses, are obtained. Output will be those mentioned above.

Using the output from the lumped-mass model and additional information such as pressure-time histories on separate internals and core components (including control rods), stresses and deflections will be calculated. These stresses and deflections will be compared to the allowable limits for the various loading combinations as established in Appendix 5A to insure that they are less than these allowables.

3.2 REACTOR DESIGN

3.2.1 GENERAL SUMMARY

The important core design, thermal, and hydraulic characteristics are tabulated in Table 3-1.

Table 3-1

Core Design, Thermal, and Hydraulic Data

Reactor	
Type	Pressurized Water
Rated Heat Output, MWt	2,452
Vessel Coolant Inlet Temperature, F	555
Vessel Coolant Outlet Temperature, F	602.8
Core Outlet Temperature, F	604.3
Operating Pressure, psig	2,185
Core and Fuel Assemblies	
Total Number of Fuel Assemblies in Core	177
Number of Fuel Rods per Fuel Assembly	208
Number of Control Rods per Control Rod Assembly	16
Number of In-Core Instrumentation Positions per Fuel Assembly	1
Fuel Rod Outside Diameter, in.	0.430
Clad Thickness, in.	0.0265
Fuel Rod Pitch, in.	0.568
Fuel Assembly Pitch Spacing, in.	8.587
Unit Cell Metal/Water Ratio (Volume Basis)	0.82
Clad Material	Zircaloy-4 (Cold-Worked)
Fuel	
Material	UO_2
Form	Dished-End, Cylindrical Pellets
Diameter, in.	0.370
Active Length, in.	144
Density, % of Theoretical	93.5
Heat Transfer and Fluid Flow at Rated Power	
Total Heat Transfer Surface in Core, ft^2	49,734
Average Heat Flux, Btu/hr-ft^2	163,725
Maximum Heat Flux, Btu/hr-ft^2	510,300
Average Power Density in Core, kW/l	79.60
Average Thermal Output, kW/ft of Fuel Rod	5.4
Maximum Thermal Output, kW/ft of Fuel Rod	16.83
Maximum Clad Surface Temperature, F	654
Average Core Fuel Temperature, F	1,345
Maximum Fuel Central Temperature at Hot Spot, F	4,150
Total Reactor Coolant Flow, lb/hr	131.32 x 10^6
Core Flow Area (Effective for Heat Transfer), ft^2	49.19
Core Coolant Average Velocity, fps	15.2
Coolant Outlet Temperature at Hot Channel, F	642.8

00174

Table 3-1 (Contd)

Power Distribution

Maximum/Average Power Ratio, Radial x Local ($F_{\Delta h}$ Nuclear)	1.78
Maximum/Average Power Ratio, Axial (F_z Nuclear)	1.70
Overall Power Ratio (F_q Nuclear)	3.03
Power Generated in Fuel and Cladding, %	97.3

Hot Channel Factors

Power Peaking Factor (F_Q)	1.011
Flow Area Reduction Factor (F_A)	
Interior Bundle Cells	0.98
Peripheral Bundle Cells	0.97
Local Heat Flux Factor (F_Q")	1.014
Hot Spot Maximum/Average Heat Flux Ratio (F_q nuc and mech)	3.12

DNB Data

Design Overpower Ratio	1.14
DNB Ratio at Design Overpower (W-3)	1.71
DNB Ratio at Rated Power (W-3)	2.21

3.2.2 NUCLEAR DESIGN AND EVALUATION

The basic design of the core satisfies the following requirements:

a. Sufficient excess reactivity is provided to achieve the design power level over the specified fuel cycle.

b. Sufficient reactivity control is provided to permit safe reactor operation and shutdown at all times during core lifetime.

3.2.2.1 Nuclear Characteristics of the Design

3.2.2.1.1 Excess Reactivity

The nuclear design characteristics are given in Table 3-2. The excess reactivities associated with various core conditions are tabulated in Table 3-3. The core will operate for 460 full-power days for the first cycle and will have a 310 full-power day equilibrium cycle. Design limits will be held with respect to reactivity control and power distribution. In-core instrumentation will be used to indicate power peaking levels. Single fuel assembly reactivity information is also included in Table 3-3.

Table 3-2

Nuclear Design Data

Fuel Assembly Volume Fractions	
Fuel	0.303
Moderator	0.580
Zircaloy	0.102
Stainless Steel	0.003
Void	0.012
	1.000
Total UO_2 (BOL, First Core), Metric Tons	94.5
Core Dimensions, in.	
Equivalent Diameter	128.9
Active Height	144.0
Unit Cell H_2O to U Atomic Ratio (Fuel Assembly)	
Cold	2.85
Hot	2.04
Full-Power Lifetime, Days	
First Cycle	460
Each Succeeding Cycle	310
Fuel Irradiation, MWd/MTU	
First Cycle Average	13,540
Succeeding Cycle Average	9,125
Feed Enrichments, w/o U-235	
First Cycle	2.30/2.30/2.64 (by Zone)
Control Data	
Control Rod Material	Ag-In-Cd
Number of Full-Length Control Rod Assemblies	49
Number of Xenon (Part-Length) Control Rod Assemblies	8
Total Full-Length Control Rod Worth ($\Delta k/k$), %	8.0
Control Rod Cladding Material	Type 304 SS

Table 3-3

Excess Reactivity Conditions

Effective Multiplication, k_{eff}[a]	
Cold, Zero Power, No Burnable Poison	1.271
Hot, Zero Power, No Burnable Poison	1.218
Hot, Rated Power, No Burnable Poison	1.200
Hot, Rated Power, With Burnable Poison	1.115
Hot, Equilibrium Xenon, Rated Power, With Burnable Poison	1.084
Single Fuel Assembly[b]	
Hot	0.77
Cold[c]	0.87

(a) First Cycle at Beginning of Life (BOL)

(b) Based on Highest Probable Enrichment of 3.5 Weight Percent

(c) A Center-to-Center Assembly Pitch of 21 Inches Is Required for This k_{eff} in Cold, Nonborated Water With No Xenon or Samarium

The minimum critical mass, with and without xenon and samarium poisoning, may be specified as a single assembly or as multiple assemblies in various geometric arrays. The unit fuel assembly has been investigated for comparative purposes. A single cold, clean assembly containing a maximum probable enrichment of 3.5 weight percent is subcritical. Two assemblies side-by-side are supercritical except when both equilibrium xenon and samarium are present. Three assemblies side-by-side are supercritical with both equilibrium xenon and samarium present.

3.2.2.1.2 Reactivity Control Distribution

Control of excess reactivity is shown in Table 3-4.

Table 3-4

First Cycle Reactivity Control Distribution

	% Δk/k
1. Controlled by Soluble Boron	
a. Moderator Temperature Deficit (70 to 520 F)	3.4
b. Equilibrium Xenon and Samarium	3.5
c. Fuel Burnup and Fission Product Buildup	7.2

Table 3-4 (Contd)

		% Δk/k
2.	Controlled by Burnable Poison Rod Assemblies (BPRA)	
	Fuel Burnup and Fission Product Buildup	6.0
3.	Controlled by Inserted Control Rod Assemblies	
	Transient Xenon (Normally Inserted)	0.8
4.	Controlled by Movable Control Rod Assemblies (CRA)	
	a. Doppler Deficit (0 to 100% Rated Power)	1.2
	b. Moderator Temperature Deficit (0 to 15% Power at End of Life, 520 to 579 F)	0.8
	c. Dilution Control	0.2
	d. Shutdown Margin	1.0
	Total Movable Control Worth Required	3.2
5.	Available Control Rod Assembly Worths	
	a. Total CRA Worth	8.0
	b. Stuck Rod Worth (Rod of Highest Reactivity Value)	(-) 2.5
	c. Minimum Available CRA Worth	5.5
	d. Minimum Movable CRA Worth Available	4.5

Explanation of Items Above

1. Soluble Boron

Boron in solution is used to control the following relatively slow-moving reactivity changes:

a. The moderator deficit in going from ambient to operating temperatures. The value shown is for the maximum change which would occur toward the end of the cycle.

b. Equilibrium xenon and samarium.

c. The excess reactivity required for fuel burnup and fission product buildup throughout cycle life.

Figure 3-1 shows the typical variation in boron concentration with life for Cycle 1 and the equilibrium cycle.

00178

2. Burnable Poison

The 16 control rod holes in 72 of the fuel assemblies not equipped with control rod assemblies will be utilized as locations for burnable poison rods. The 72 element locations are shown in Figure 3-4.

3. Inserted Control .

Sufficient rod worth remains inserted in the core during normal operation to overcome the peak xenon transient following a power reduction of 50 percent of rated power for 90 percent of the fuel cycle. This override capability facilitates the return to normal operating conditions without extended delays. The presence of these rods in the core during operation does not produce power peaks above the design value, and the shutdown margin of the core is not adversely affected. Axial power peak variation, resulting from partial or full insertion of xenon override rods, is described fully in Figures 3-2 and 3-3. The loss of movable reactivity control due to the insertion of this group produces no shutdown difficulties and is reflected in Table 3-5.

4. Movable Control

a. Power level changes (Doppler) and regulation.

b. Between 0 and 15 percent of rated power, reactivity compensation by CRA may be required as a result of the linear increase of reactor coolant temperature from 520 F to the normal operating value.

c. Additional reactivity is held by a group of partially inserted CRA (25 percent insertion maximum) to allow periodic rather than continuous soluble boron dilution. The CRA are inserted to the 25 percent limit as the boron is diluted. Automatic withdrawal of these CRA during operation is allowed to a 5 percent insertion limit where the dilution procedure is again initiated and this group of CRA is reinserted.

d. A shutdown margin of 1 percent $\Delta k/k$ below the hot critical condition is also considered as part of the reactivity controlled by CRA.

5. Rod Worth

A total of 3.2 percent $\Delta k/k$[(a)] is required in movable control. Analysis of the 49 full-length CRA under the reference fuel arrangement predicts a total CRA worth of at least 8.0 percent $\Delta k/k$. The stuck-out CRA worth was also evaluated at a value no larger than 2.5 percent $\Delta k/k$[(b)]. This evaluation included selection of the highest worth CRA under the first CRA-out condition. The minimum available CRA worth of 4.5 percent $\Delta k/k$[(a)] is sufficient to meet movable control requirements. The eight

- - - - -

(a) Does not include transient control. See Table 3-4.
(b) First cycle. See Table 3-4.

xenon control rods (XCRA) are worth from 0.2 to 0.4 percent Δk/k. This value is not included in the 8.0 percent Δk/k rod worth reported above.

3.2.2.1.3 Reactivity Shutdown Analysis

The ability to shut down the core under both hot and cold conditions is illustrated in Table 3-5. In this tabulation both the first and equilibrium cycles are evaluated at the beginning of life (BOL) and the end of life (BOL) for shutdown capability.

Table 3-5

Shutdown Reactivity Analysis

Reactivity Effects, % Δk/k	First Cycle BOL	First Cycle EOL	Equilibrium BOL	Equilibrium EOL
1. Maximum Shutdown CRA Requirement				
Doppler (100 to 0% Power)	1.2	1.5	1.2	1.5
Moderator Deficit (15 to 0% Power)	0.0	0.8	0.0	0.8
Total	1.2	2.3	1.2	2.3
2. Maximum Available CRA Worth[(a)]	-8.0	-8.0	-8.0	-8.0
Transient Xe Insertion Worth	0.8	0.0	0.8	0.0
Possible Dilution Insertion	0.2	0.2	0.2	0.2
3. Minimum Available CRA Worth				
All CRA In	-7.0	-7.8	-7.0	-7.8
One CRA Stuck-Out[(b)]	-4.5	-5.3	-4.5	-5.3
4. Minimum Hot Shutdown Margin				
All CRA In	-5.8	-5.5	-5.8	-5.5
One CRA Stuck-Out	-3.3	-3.0	-3.3	-3.0

(a) Total Worth of 49 CRA

(b) CRA of Highest Reactivity Value

Examination of Table 3-5 for Minimum Hot Shutdown Margin (Item 4) shows that, with the highest worth CRA stuck out, the core can be maintained in a subcritical condition. Normal conditions indicate a minimum hot shutdown margin of 5.5 percent Δk/k at the end of life.

Under conditions where a cooldown to reactor building ambient temperature is required, concentrated soluble boron will be added to the reactor coolant to produce a shutdown margin of at least 1 percent Δk/k. Beginning-of-life boron levels for several core conditions are listed in Table 3-6 along with boron worth values. The conditions shown with no CRA illustrate the highest requirements.

Table 3-6

Soluble Boron Levels and Worth
(First Cycle)

Core Conditions	BOL Boron Levels, ppm
1. Cold, k_{eff} = 0.99	
No CRA In	1,290
All CRA In	810
One Stuck CRA	960
2. Hot, Zero Power, k_{eff} = 0.99	
No CRA In	1,250
All CRA In	450
One Stuck CRA	700
3. Hot, Rated Power, k_{eff} = 1.00	
No CRA In	1,030
4. Hot, Equilibrium Xe and Sm, Rated Power, k_{eff} = 1.00	
No CRA In	680

Core Condition	Boron Worth, (% Δk/k)/ppm
Hot	1/100
Cold	1/75

3.2.2.1.4 Reactivity Coefficients

Reactivity coefficients form the basis for digital studies involving normal and abnormal reactor operating conditions. These coefficients have been investigated as part of the analysis of this core and are described below as to function and overall range of values.

a. Doppler Coefficient

The Doppler coefficient reflects the change in reactivity as a function of fuel temperature. A rise in fuel temperature results in an increase in the effective absorption cross section of the fuel (the Doppler broadening of the resonance peaks) and a corresponding reduction in neutron production. The range for the Doppler coefficient under operating conditions is expected to be -1.1×10^{-5} to -1.7×10^{-5} $(\Delta k/k)/F$.

b. Moderator Void Coefficient

The moderator void coefficient relates the change in neutron multiplication to the presence of voids in the moderator. The expected range for the void coefficient is -4.0×10^{-4} to -3.0×10^{-3} $(\Delta k/k)$/percent void.

c. Moderator Pressure Coefficient

The moderator pressure coefficient relates the change in moderator density, resulting from a reactor coolant pressure change, to the corresponding effect on neutron production. This coefficient is opposite in sign and considerably smaller when compared to the moderator temperature coefficient. A typical range of pressure coefficients over a life cycle would be $+4 \times 10^{-7}$ to $+3 \times 10^{-6}$ $(\Delta k/k)$/psi.

d. Moderator Temperature Coefficient

The moderator temperature coefficient relates a change in neutron multiplication to the change in reactor coolant temperature. Reactors using soluble boron as a reactivity control have fewer negative moderator temperature coefficients than do cores controlled solely by movable or fixed CRA. The major temperature effect on the coolant is a change in density. An increasing coolant temperature produces a decrease in water density and an equal percentage reduction in boron concentration. The concentration change results in a positive reactivity component by reducing the absorption in the coolant. The magnitude of this component is proportional to the total reactivity held by soluble boron.

The moderator temperature coefficient has been calculated for three conditions of the hot, clean (no xenon) core with 1030 ppm boron in the moderator.

Zero Power	$\alpha_m \approx 0$
15 Percent Power	$\alpha_m = -0.32 \times 10^{-4}$ $(\Delta k/k)/F$
100 Percent Power	$\alpha_m = -0.42 \times 10^{-4}$ $(\Delta k/k)/F$

Since equilibrium xenon is covered by soluble poison, it follows that at the full-power condition with xenon, the moderator temperature coefficient will be even more negative than shown above.

The moderator temperature coefficient will be -3.0×10^{-4} $(\Delta k/k)/F$ at the end of the equilibrium fuel cycle.

e. pH Coefficient

Currently, there is no definite correlation to predict pH reactivity effects between various operating reactors. pH effects versus

reactor operating time at power, and changes in effects with various clad, temperature, and water chemistry. Yankee (Rowe, Mass.), Saxton, and Con Edison Indian Point Station No. 1 have experienced reactivity changes at the time of pH changes, but there is no clear-cut evidence that pH is the direct influencing variable without considering other items such as clad materials, fuel assembly crud deposition, system average temperature, and prior system water chemistry.

Saxton experiments have indicated a pH reactivity effect of 0.16 percent reactivity per pH unit change with and without local boiling in the core. Operating reactor data and the results of applying Saxton observations to the reference reactor are as follows:

(1) The proposed system pH will vary from a cold measured value of approximately 5.5 to a hot calculated value of 7.8 with 1,400 ppm boron and 3 ppm KOH in solution at the beginning of life. Lifetime bleed dilution to 20 ppm boron will reduce pH by approximately 0.8 pH units to a hot calculated pH value of 7.0.

(2) Considering the system make-up rate of 70 gpm, the corresponding changes in pH are 0.071 pH units per hour for boron dilution and 0.231 pH units per hour for KOH dilution. Applying pH worth values of 0.16 percent $\Delta k/k$ per pH unit, as observed at Saxton, insertion rates are 3.16×10^{-6} (percent $\Delta k/k$)/sec and 1.03×10^{-5} (percent $\Delta k/k$)/sec, respectively. These insertion rates correspond to 1.03 percent power/hour and 3.4 percent power/hour, respectively, which are easily compensated by the operator or the automatic control system.

3.2.2.1.5 Reactivity Insertion Rates

Figure 7-7 displays the integrated rod worth of three overlapping rod banks as a function of distance withdrawn. The indicated groups are those used in the core during power operation. Using approximately 1.2 percent $\Delta k/k$ CRA groups and a 25 in./min drive speed in conjunction with the reactivity response given in Figure 7-7 yields a maximum reactivity insertion rate of 9.2×10^{-5} $(\Delta k/k)$/sec. The maximum reactivity insertion rate for soluble boron removal is 7×10^{-6} $(\Delta k/k)$/sec.

3.2.2.1.6 Power Decay Curves

Figure 3-5 displays the beginning-of-life power decay curves for the CRA worths corresponding to the 1 percent hot shutdown margin with and without a stuck rod. The power decay is initiated by the trip release of the CRA with a 300 msec delay from initiation to start of CRA motion. The time required for 2/3 rod insertion is 1.4 sec.

3.2.2.1.7 Neutron Flux Distribution and Spectrum

The neutron flux levels at the core edge and the pressure vessel wall are given in Table 3-7. At both locations, the values shown include an axial peaking factor of 1.3, a scaling factor of 2, and a safety margin of 1.9.

Table 3-7

Exterior Neutron Levels and Spectra

Flux Group		Neutron Flux Levels, neut/cm^2-s	
		Core Edge (x 10^{13})	Interior Wall of Pressure Vessel (x 10^{10})
1	0.821 MeV to 10 MeV	6.0	3.4
2	1.230 keV to 0.821 MeV	9.0	7.5
3	0.414 eV to 1.230 keV	6.2	5.7
4	Less Than 0.414 eV	7.1	2.1

The calculations were performed using The Babcock & Wilcox Company's LIFE code (BAW-293, 3.6.3) to generate input data for the transport code, TOPIC.[1] A 4-group edit is obtained from the LIFE output which includes diffusion coefficients, absorption, removal, and fission cross sections, and the zeroth and first moments of the scattering cross section. TOPIC is an S_n code designed to solve the 1-dimensional transport equation in cylindrical coordinates for up to six groups of neutrons. For the radial and azimuthal variables, a linear approximation to the transport equation is used; for the polar angle, Gauss quadrature is used. Scattering functions are represented by a Legendre series. The azimuthal angle can be partitioned into 4 to 10 intervals on the half-space between 0 and π. The number of mesh points in the radial direction is restricted by the number of these intervals. For the core exterior flux calculations, four intervals on the azimuthal were used. This allows the maximum number of mesh points (240) in the "r" direction to describe the shield complex. An option is available to use either equal intervals on the azimuthal angle or equal intervals on the cosine of the angle. Equal intervals on the cosine were chosen since this provides more detail in the forward direction of the flux (toward the vessel). Five Gauss quadrature points were used on the cosine of the polar angle in the half-space between 0 and π.

Results from the above method of calculation have been compared with thermal flux measurements through an array of iron and water slabs in the LIDO pool reactor.[2] Although this is not a direct comparison with fast neutron measurements, it does provide a degree of confidence in the method since the magnitude of the thermal flux in shield regions is governed by fast neutron penetration.

Results of the comparison showed that fluxes predicted by the LIFE-TOPIC calculation were lower, in general, by about a factor of 2. Results of the fast flux calculations are, consequently, increased by a factor of 2 to predict the nvt in the reactor vessel.

The following conservatisms were also incorporated in the calculations:

a. Neutron fluxes outside the core are based on a maximum power density of 41 watts/cc at the outer edge of the core rather than

an estimated average of 28 watts/cc over life, resulting in a safety margin of about 45 percent.

b. A maximum axial power peaking factor of 1.7 was used. This is about 30 percent greater than the 1.3 expected over life.

Uncertainties in the calculations include the following:

1. The use of only four neutron groups to describe the neutron energy spectrum.

2. Use of the LIFE code to generate the 4-group cross sections. In the LIFE program, the 4-group data in all regions are computed from a fission spectrum rather than a leakage spectrum.

3. Having only four intervals, ie, n = 4 in the S_n calculation, to describe the angular segmentation of the flux.

It is expected that the combination of 1 and 2 above will conservatively predict a high fast neutron flux at the vessel wall because it underestimates the effectiveness of the thermal shield in reducing the fast flux. In penetration through water, the average energy of the neutrons in the group above 1 MeV increases above that of a fission spectrum, ie, the spectrum in this group hardens. For neutrons above 1 MeV, the nonelastic cross section of iron increases rapidly with energy. Therefore, the assumption of a fission spectrum to compute cross sections in the thermal shield, and the use of a few-group model to cover the neutron energy spectrum, would underestimate the neutron energy loss in the thermal shield and the subsequent attenuation by the water between the vessel and thermal shield. The results from 34-group P3MG1(3) calculations show that reduction of the flux above 1 MeV by the thermal shield is about a factor of 4 greater than that computed from the 4-group calculations.

The effect of 3 above is expected to underestimate the flux at the vessel wall. In calculations at ORNL using the S_n technique, a comparison between an S_4 and an S_{12} calculation was made in a penetration through hydrogen. The results for a variety of energies over a penetration range of 140 cm showed the S_4 calculation to be lower than the S_{12} by about a factor of 2 at maximum. Good agreement was obtained between the S_{12} and moments method calculations.

The above uncertainties indicate that the calculation technique should overestimate the fast flux at the reactor vessel wall. However, the comparison with thermal flux data indicates a possible underestimate. Until a better comparison with data can be made, we have assumed that the underestimate is correct and accordingly have increased the flux calculations by a factor of 2 to predict the nvt in the reactor vessel.

The reactor utilizes a larger water gap and thinner thermal shield between the core and the reactor vessel wall when compared to currently licensed plants. The effect of this steel-water configuration on (a) the neutron irradiation, and (b) the thermal stresses in the reactor vessel wall, were evaluated as follows:

a. Neutron Irradiation

Calculations were performed in connection with the reactor vessel design to determine the relative effects of varying the baffle and thermal shield thicknesses on the neutron flux (>1 MeV) at the vessel wall. These calculations were performed with the P1 option of the P3MG1 code[3] using 34 fast neutron groups. The results showed that the neutron flux level at the vessel wall is dependent, for the most part, on the total metal and water thickness between the core and the vessel. However, there was some variation in fluxes depending upon the particular configuration of steel-water laminations. Also, the gain in neutron attenuation by replacing water with steel diminishes somewhat with increasing steel thickness.

In general, however, the results showed that for total steel thicknesses in the range of 3 to 6 in., 1 in. of steel in place of 1 in. of water would reduce the neutron flux above 1 MeV by about 30 percent. In pure water, the calculations showed that the neutron flux would be reduced, on the average, by a factor of 6 in 6 in. of water.

Based on the above analysis, a comparison has been made of the neutron attenuation in this reactor vessel with those in San Onofre, Turkey Point 3 and 4, Indian Point 2, and Ginna. The total distance between this core and the reactor vessel is 21 in. This provides from 1.5 to as much as 5.75 in. more distance between the core and the vessel than in the other reactors. For neutrons above 1 MeV, it was found that this additional distance would provide additional attenuation ranging from a factor of 1.1 to 5 times greater than that in the other PWR considered.

b. Thermal Stresses

The gamma heating in the reactor vessel is produced by primary gammas from the core and by secondary gammas originating in the core baffle plate, barrel, thermal shield, and the vessel itself. In this reactor design, the major portion of the heat is generated by gamma rays from the core and by secondary gamma rays from the core baffle plate and barrel.

Since the gammas from each of these sources must penetrate the thermal shield to reach the vessel, the vessel heating rate is dependent on the thermal shield thickness.

For designs which employ thicker thermal shields, or in which internals are to be exposed to higher neutron fluxes, gamma rays originating in the thermal shield or in the vessel itself may govern the vessel heating rates. Since gamma rays from these sources would have to penetrate only portions or none of the thermal shield to reach the vessel, the vessel heating in such cases would be less dependent on thermal shield thickness than in this reactor design.

00 86

A comparison was made between the gamma attenuation provided by the water and metal in this reactor vessel and that in other PWR by assuming that, in each design, the vessel heating was dependent on the gamma ray attenuation provided by the thermal shield. This approach would be conservative since, as noted above for some designs, gamma sources other than those attenuated by the thermal shield may contribute appreciably to the vessel heating. The results of the comparison showed that the difference in gamma attenuation between this reactor and other PWR ranged from a negligible difference to a factor of 5.3 less for this reactor design.

The maximum steady-state stress resulting from gamma heating in the vessel has been calculated to be 3,190 psi (tension). This is a relatively low value, and no problems are anticipated from thermal stresses in the reactor vessel wall.

3.2.2.2 Nuclear Evaluation

Analytical models and the application of these models are discussed in this section. Core instabilities associated with xenon oscillation are also described, with threshold data evaluated under reference conditions.

3.2.2.2.1 Analytical Models

Reactor design calculations are made with a large number of computer codes. The choice of which code set or sets to use depends on which phase of the design is being analyzed. A list of codes used in core analysis with a brief discussion follows in 3.2.2.2.2.

a. Reactivity Calculations

Calculation of the reactivity of a pressurized water reactor core is performed in one, two, or three dimensions. The geometric choice depends on the type of calculations to be made. In a clean type of calculation where there are no strong, localized absorbers of a type differing from the rest of the lattice, 1-dimensional analysis is satisfactory. This type of problem is handled quite well by the B&W 1-dimensional depletion package code LIFE. LIFE is a composite of MUFT (Ref 4), KATE (Ref 5), RIP, WANDA (Ref 6), and a depletion routine. Normally, the MUFT portion is used with 34-energy groups, an exact treatment of hydrogen, the Greuling-Goertzel approximation for elements of mass less than 10, and Fermi age for all heavier elements. The KATE portion normally uses a Wigner-Wilkins spectrum. In WANDA, 4-energy groups are utilized. Disadvantage factors for input to the thermal group are calculated with the THERMOS (Ref 7) code. This code set has been shown to give reliable results for a reactivity calculation of this type. Recent check calculations on critical experiments have a standard deviation of less than 0.5 percent $\Delta k/k$.

A 1-dimensional analysis of a geometric arrangement, where there are localized strong absorbers such as CRA, requires a preliminary 2-dimensional analysis. The required properties of the 1-dimensional

system are then matched to the 2-dimensional analysis. In this manner, it is possible to analyze the simpler 1-dimensional system in a depletion survey problem with only a small loss in accuracy.

The 1-dimensional calculations are used as preliminary guides for the more detailed 2-dimensional analysis that follows. Values of reactivity coefficients, fuel cycle enrichments, lifetimes, and soluble poison concentrations can be found to improve the intial conditions specified for 2-dimensional analysis.

Two-dimensional reactivity calculations are done with either the PDQ (Ref 8) or TURBO (Ref 9) diffusion and/or depletion codes. These codes have mesh limitations on the size of a configuration which can be shown explicitly and are often studied with quarter core symmetry. Symmetry is desirable in the design, and no loss in generality occurs. The geometric description includes each fuel assembly and as much detail as is possible, ie, usually each unit in the fuel assembly. Analysis of this type permits detailed power distribution studies as well as reactivity analysis. The power distribution in a large PWR core which has zone loading cannot be predicted reliably with 1-dimensional calculations. This is particularly true when local power peaking as a function of power history is of interest. It is necessary to study this type of problem with at least a 2-dimensional code, and in some cases, 3-dimensional calculations are necessary.

Use of the 2-dimensional programs requires the generation of group constants as a function of material composition, power history, and geometry. For regions where diffusion theory is valid, MUFT and KATE with THERMOS disadvantage factors are used to generate epithermal and thermal coefficients. This would apply at a distance of a few mean paths from boundaries or discontinuities in the fuel rod lattice. Discontinuities refer to water channels, instrumentation ports, and CRA guide tubes. The interfaces between regions of different enrichment are considered to be boundaries as well as the outer limit of the core.

To generate coefficients for regions where diffusion theory is inappropriate several methods are utilized. The arrangement of structural material, water channels and adjacent fuel rod rows can be represented well in slab geometry. The coefficients so generated are utilized in the epithermal energy range. Coefficients for the thermal energy range are generated by a slab THERMOS calculation. The regions adjacent to an interface of material of different enrichment are also well represented with the P3MG code.

The arrangement of instrumentation ports and control rod guide tubes lends itself to cylindrical geometry. DTF-IV (Ref 10) is quite effective in the analysis of this arrangement. Input to DTF-IV is from GAM (Ref 11) and THERMOS or KATE. Iteration is required between the codes. The flux shape is calculated by DTF-IV and cross sections by the others. The outer boundary of the core where there is a transition from fuel to reflector and baffle is also represented by the DTF-IV code. The 3-dimensional analysis

is accomplished by extending the techniques of 2-dimensional representation.

b. Control Rod Analysis

B&W has developed a procedure for analyzing the reactivity worth of small Ag-In-Cd rods in fuel lattices. Verification of this procedure was made by the comparative analysis of 14 critical experiments with varying rod and rod assembly configurations.[13,14] Critical lattice geometries were similar to those of the reference core design. Boron concentration ranged from 1,000 to 1,500 ppm. The Ag-In-Cd rods were arranged in various geometrical configurations which bracket the reference design. Water holes, simulating withdrawn rods, were included as part of the lattice study. The resulting comparison of the analytical and experimental worths are shown in Table 3-8. Details of the critical configurations are given in References 13 and 14.

Table 3-8

Calculated and Experimental Rod and Rod Assembly Comparison

Core No.	Assemblies Per Core	Ag-In-Cd Rods Per Assembly	H_2O Holes Per Core	Rod Assembly - Calculated Worth, % Δk/k	Rod Assembly - Experimental Worth, % Δk/k
5-B	4	4	252	2.00	1.98
4-F	4	9	0	3.38	3.34
5-C	2	12	276	2.38	2.35
4-D	1	16	0	1.43	1.42
5-D	2	16	284	2.80	2.82
4-E	1	20	0	1.54	1.52
5-E	2	20	292	3.05	3.01

The mean error in calculating these configurations is shown to be less than 1 percent. Comparison of the power shape associated with the 16-rod reference assemblies showed good similarity. Point-to-average power had a maximum variation of less than 2 percent with experimental data.

The analytical method used for this analysis is based on straight diffusion theory. Thermal coefficients for a control rod are obtained from THERMOS by flux-weighting. Epithermal coefficients for the upper energy groups are generated by the B&W LIFE program. The resulting coefficients are used in the 2-dimensional code PDQ to obtain the required eigenvalues.

GAKER and LIBPM are used to prepare data for THERMOS. GAKER generates scattering cross sections for hydrogen by the Nelkin technique. LIBPM uses the Brown and St John free gas model for generating the remaining scattering cross sections.

THERMOS is used in two steps. First, the critical fuel cell is analyzed to obtain a velocity-weighted disadvantage factor. This is used

in the homogenization of fuel cells and gives a first order correction for spatial and spectral variation. The ratio of flux in the moderator to flux in the fuel was analyzed to within 2 percent of experimental values using the velocity-weighting technique. The second step is to use THERMOS in a calculation where the Ag-In-Cd rod is surrounded by fuel. This is used to generate the flux-weighted control rod cell coefficients as a function of boron concentration. As a check on the validity of the THERMOS approach, extrapolation distances were compared to those given by the Spinks method.(15) The agreement was within 2.2 percent for a set of cases wherein the number densities of Ag-In-Cd were varied in a range up to 250 percent. All other coefficients are generated by LIFE in much the same manner as with THERMOS. The data are used in a 2-dimensional PDQ layout where each fuel rod cell is shown separately.

c. Determination of Reactivity Coefficients

This type of calculation is different from the reactivity analysis only in application, ie, a series of reactivity calculations being required. Coefficients are determined for moderator temperature, voiding, and pressure, and for fuel temperature. These are calculated from small perturbations in the required parameter over the range of possible values of the parameter.

The moderator temperature coefficient is determined as a function of soluble poison concentration and moderator temperature, and fuel temperature or Doppler coefficient as a function of fuel temperature. The coefficient for voiding is calculated by varying the moderator concentration or percent void.

3.2.2.2.2 Codes for Reactor Calculations

This section contains a brief description of codes mentioned in the preceding sections.

THERMOS (Ref 7) - This code solves the integral form of the Boltzmann Transport Equation for the neutron spectrum as a function of position. A diagonalized connection to the isotropic transfer matrix has been incorporated allowing a degree of anisotropic scattering.

MUFT (Ref 4) - This program solves the P_1 or B_1 multigroup equation for the first two Legendre coefficients of the directional neutron flux, and for the isotropic and anisotropic components of the slowing down densities due to a cosine-shaped neutron source. Coefficients are generated with MUFT for the epithermal energy range.

KATE (Ref 5) - The code solves the Wigner-Wilkins differential equation for a homogeneous medium moderated by chemically unbound hydrogen atoms in thermal equilibrium. Coefficients for the thermal energy range are generated by KATE.

RIP - This program averages cross sections over an arbitrary group structure, calculates resonance integrals for a set of resolved peaks, and computes L-factors for input to MUFT, P1MG, and P3MG.

WANDA (Ref 6) - This code provides numerical solutions of the 1-dimensional few-group neutron diffusion equations.

LIFE - This is a 1-dimensional depletion package code which is a combination of MUFT, KATE, RIP, and WANDA. The combination mechanizes the procedures for using the codes separately.

GAM (Ref 11) - This code is a multigroup coefficient generation program that solves the P_1 equations and includes anisotropic scattering. Inelastic scattering and resonance parameters are also treated by GAM.

P3MG (Ref 3) - The code solves the multienergy transport equation in various geometries. The code is primarily used for epithermal coefficient generations.

DTF (Ref 10) - This code solves the multigroup, 1-dimensional Boltzmann transport equation by the method of discrete ordinates. DTF allows multigroup anisotropic scattering as well as up and down scattering.

PDQ (Ref 8) - This program solves the 2-dimensional neutron diffusion-depletion problem with up to five groups. It has a flexible representation of time-dependent cross sections by means of fit options.

TURBO (Ref 9) - This code is similar in application to the PDQ depletion program. It, however, lacks the great flexibility of the PDQ fit options.

CANDLE (Ref 9) - This code is similar to TURBO, but solves the diffusion equations in one dimension.

TNT (Ref 9) - This code is similar in application to TURBO, but is a 3-dimensional code extended from DRAC

3.2.2.2.3 Xenon Stability Analysis

Initial studies of the reference core indicate that underdamped xenon oscillation should be considered. Features have been provided in the design to allow control of axial oscillations and to make the core stable against azimuthal oscillations. (Radial oscillations are unlikely.) These features are discussed below.

As to axial oscillations, certain of the control rod assemblies will contain poison only in a portion of their lengths. They will be positioned during the operation of the unit to maintain an acceptable distribution of power for any

particular operating condition in the core, thereby reducing the tendency for axial oscillations. Instructions will be made available to the operator concerning positioning of the partially poisoned control rods to achieve desirable axial power shapes.

In regard to azimuthal oscillations, fixed poison in the form of burnable poison will be used in fuel assemblies (see Figure 3-4) as necessary to insure azimuthal stability in the core for the design power density.

A brief description of the studies performed to date follows:

a. Method

(1) Modal Analysis

The details of the methods and initial results of the modal analysis are described in Appendix 3-A.

(2) One- and Two-Group Methods and Modal Coupling

One- and two-group treatments[16] have been compared. A one-group model is satisfactory for large, water-moderated, low leakage cores such as the reference design. The effects of modal coupling have been examined and shown to be of no consequence for cores similar to the reference design. Values of critical parameters varied no more than 1 to 2.8 percent for the same core with and without modal coupling. The lower value was computed with a zero-power coefficient and was not conservative without modal coupling. The higher value was computed with the reference power coefficient and was conservative without modal coupling.

(3) Digital Analysis

Xenon stability studies are continuing with codes in various geometries which have thermal-nuclear iteration capability for both fuel and moderator temperature feedback. The one-dimensional feedback code LIFE handles the iteration in the following manner:

$$\Delta T_i = (T_{out} - T_{in})_i = c \int_{Z_{in}}^{Z_{out}} PD(Z)dZ \qquad (A)$$

where ΔT_i = temperature change in region "i"

$PD(Z)$ = power density in the Z direction

Z_{in}, Z_{out} = region "i" boundaries

and

$$c = \frac{\Delta T_{core}}{\int_0^H PD(Z)df} \qquad (B)$$

where H is the active fuel height.

Equation (A) is solved to T_{out} of region "i." Since T_{in} is known from core inlet conditions, the average fluid temperature is defined as follows:

$$\overline{T}_{fluid_i} = \frac{T_{out} + T_{in}}{2} i \qquad (C)$$

The newly computed, region-averaged fluid temperatures are used to compute new fluid densities. These fluid densities are then used to adjust the number densities for water and soluble poison. Local or bulk boiling is not permitted in the model, but incorporation would increase stability. The average fuel temperature for each axial core region is then computed from the average fluid temperature and power densities as follows:

$$\overline{T}_{fuel_i} = f(\overline{PD}_i) + \overline{T}_{fluid_i}$$

where $\overline{PD}_i$ is the average power density of region "i," and

$f(\overline{PD}_i)$ is a tabular function relating fuel temperature increase and power density obtained from auxiliary calculations.

After the new fluid temperatures, moderator densities, and fuel temperatures are obtained, these quantities are used as new LIFE input to obtain a new power distribution until a convergence criterion is met.

This analysis used an exact solution in that the spectrum was recalculated for each zone (11 axial zones described the reactor) for each iteration at every time step. This included the effects of the moderator temperature coefficient.

This LIFE package was used to determine the effects of the uncertainty in the power Doppler on the stability of the core.

The uncertainty in the Doppler was more than compensated with a reduction in fuel temperature of 500 degrees. The reference core was analyzed with core average fuel temperatures of 1,400 F and 900 F. Figure 3-6 compares the cyclic response of these two cases following the 3-ft insertion and removal (after two hours) of a 1.2 percent $\Delta k/k$ rod bank near the beginning of life. These studies were made at beginning-of-life boron levels of approximately 1,900 ppm. This level is approximately 800 ppm above the predicted beginning-of-life level and, consequently, reflects a positive moderator temperature coefficient which is not expected.

Case 1 on Figure 3-6 depicts the behavior of the core if the heat transfer equations were not included in the calculation. Figure 3-7 shows the effect of fuel temperature toward the end of life. It is easily verified that the 900 F fuel temperature case approached the threshold condition for axial oscillation in this core. On the basis of the information presented, it can be said that for a realistic fuel temperature this core does not exhibit axial instability at any time during the initial cycle.

The one-dimensional model was used to determine a method of controlling the core without taking into account the stabilizing effect of the power Doppler. Normally, this would produce a divergent oscillation as shown in Figure 3-8. A study was completed wherein a 1 percent $\Delta k/k$ rod bank with a 3-ft-long section of regular control rod material was successfully maneuvered to control the core after a perturbation of the power shape at a point about 3/4 of the way through Cycle 1. The controlled results are also shown in Figure 3-8. The minimum rod motion was 1 foot, and the time step employed was 4.8 hours. More precise rod movement over shorter time periods would produce a much smoother power ratio curve. This control mechanism appears to be quite adequate.

Stability in "R-Z" or "X-Y" geometry is studied with the HARMONY[8] code, which in either case can be used with fuel and moderator temperature feedback. This code is used with fitted coefficients to obtain a more complete solution to the perturbed behavior of the reference design.

The digital results are processed by first fitting power distribution results to an equation of the following form by a least square technique:

where $$P' = Ae^{zt} \sin \frac{2\pi t}{T}$$

P' = excess power

z = stability index

T = oscillation period

The calculated stability index is then extrapolated to zero-length time steps by the procedures of References 20 and 21 as follows:

$$Z = Z_o \frac{(1 - e^{T_r})}{T_r} - \frac{\lambda_i}{2}\left[1 + e^{-T_r} - 2\frac{(1 - e^{T_r})}{T_r}\right]$$

$$T_r = \langle A \rangle T$$

$$\langle A \rangle = \lambda_x + \sigma_x \phi_o$$

where Z_o = extrapolated stability index

T_r = time step length

ϕ_o = average thermal flux

Reasonable agreement has been found between the initial modal analysis and one-dimensional results.

(4) Control of an Axial Oscillation

The one-dimensional model was used to determine a method of controlling the axial power distribution without considering the stabilizing effects of thermal-nuclear feedback. Normally, this calculation would show a divergent oscillation. A study was completed in which a 3-ft section of control rod poison material was successfully maneuvered to control the core after introduction of a perturbation. The minimum rod motion was 12 in. with a 4.8-hour minimum period for rod movement. More precise movement over a shorter minimum period would improve control. The procedure will be extended to two dimensions.

b. Conclusions

The following conclusions have been made as a result of the studies to date:

(1) Instability in the radial direction will not occur.

(2) The core design under examination will not be susceptible to diverging azimuthal oscillations.

(3) Potential axial oscillations will be thwarted or controlled by the part length control rods.

The nominal and minimum (accounting for the uncertainties correction listed above) stability indices are described in the Appendix 3-A.

3.2.3 THERMAL AND HYDRAULIC DESIGN AND EVALUATION

3.2.3.1 Thermal and Hydraulic Characteristics

3.2.3.1.1 Fuel Assembly Heat Transfer Design

a. Design Criteria

The criterion for the heat transfer design is to be safely below Departure From Nucleate Boiling (DNB) at the design overpower (114 percent of rated power). The analysis is described in detail in 3.2.3.2.2, Statistical Core Design Technique.

The input information for the statistical core design technique and for the evaluation of individual hot channels is as follows:

(1) Heat transfer critical heat flux equations and data correlations.

(2) Nuclear power factors.

(3) Engineering hot channel factors.

(4) Core flow distribution hot channel factors.

(5) Maximum reactor overpower.

These inputs have been derived from test data, physical measurements, and calculations as outlined below.

b. Heat Transfer Equation and Data Correlation

The heat transfer relationship used to predict limiting heat transfer conditions is presented in References 22 and 23. The equations are as follows:

(1) W-3 uniform flux DNB correlation for single channel with all walls heated:

$$\frac{Q''_{DNB,eu}}{10^6} = \{ (2.022 - 0.0004302\ P) + (0.1722 - 0.0000984\ P) \exp [(18.177 - 0.004129\ P)x]\} \times [0.1484 - 1.596\ x + 0.1729\ x\ |x|\ \frac{G}{10^6} + 1.037] \times [1.157 - 0.869\ x] \times [0.2664 + 0.8357 \exp (-3.151\ D_e)] \times [0.8258 + 0.000784(H_{sat} - H_{in})]$$

where Q'' = flux, Btu/h-ft^2

P = pressure, psia

G = mass velocity, lb/h-ft^2

x = quality, expressed as fraction

D_e = equivalent diameter, in.

H = enthalpy, Btu/lb

(2) W-3 nonuniform flux DNB correlation for single channel with all walls heated:(22)

$$Q''_{DNB,N} = Q''_{DNB,eu}/F$$

where $Q''_{DNB,N}$ = DNB heat flux for the nonuniformly heated channel

$Q''_{DNB,eu}$ = equivalent uniform DNB flux

$$F = \left\{ \frac{C}{Q''_{local}\left[1 - \exp\left(-C\,\ell_{DNB,eu}\right)\right]} \right\} \times \left\{ \int_0^{\ell_{DNB}} Q''(Z) \exp\left[-C(\ell_{DNB,N} - Z)\right] dZ \right\}$$

$$C = 0.44 \frac{(1 - x_{DNB})^{7.9}}{\left(\frac{G}{10^6}\right)^{1.72}} \text{ in.}^{-1}$$

(3) W-3 uniform flux DNB correlation for single channel with unheated walls:(23)

$$\frac{Q''_{DNB,\text{ with unheated wall}}}{Q''_{DNB,\text{ using } D_h \text{ to replace } D_e}} = (1.36 + 0.12\, e^{9x}) \times (1.2 - 1.6\, e^{-1.92 D_h}) \times (1.33 - 0.237\, e^{5.66 x})$$

where D_e = equivalent diameter based on all the wetted perimeter, in.

D_h = equivalent diameter based on only the heated perimeter, in.

Individual channels are analyzed to determine a DNB ratio, ie, the ratio of the heat flux at which a DNB is predicted to occur to the heat flux in the channel being investigated. This DNB ratio is related to the data correlation as shown in Figure 3-9. A confidence and population value is associated with every DNB ratio as described

in the Statistical Core Design Technique (3.2.3.2.2). The plot of DNB versus P is for a confidence of 99 percent. The criterion for evaluating the thermal design margin for individual channels or the total core is the confidence-population relationship. The DNB ratios required to meet the basic criteria or limits are a function of the experimental data and heat transfer correlation used, and vary with the quantity and quality of data. The recommended minimum design DNB ratio for the W-3 correlation is 1.30.

The DNB and population relationship for a design limit of 1.30 in the hot channel corresponds to a 99 percent confidence that at least 94.3 percent of the population of all such hot channels is in no jeopardy of experiencing a DNB. The DNB ratios and the fraction of the core in no jeopardy of experiencing a DNB at design conditions are considerably higher than those given in the design limits outlined in 3.1.2.3.

c. Nuclear Power Factors

The heated surfaces in every flow channel in the core are examined for heat flux limits. The heat input to the fuel rods in a coolant channel is determined from a nuclear analysis of the core and fuel assemblies. The results of this analysis are as follows:

(1) The nominal nuclear peaking factors for the worst time in core life are

$$F\Delta n = 1.77$$

$$Fz = 1.70$$

$$Fq = 3.01$$

(2) The design nuclear peaking factors for the worst time in core life are

$$F\Delta h = 1.78$$

$$Fz = 1.70$$

$$Fq = 3.03$$

where $F\Delta h$ = max/avg total power ratio (radial x local nuclear)

Fz = max/avg axial power ratio (nuclear)

Fq = $F\Delta h$ x Fz (nuclear total)

The nominal values are the maximum values calculated with nominal spacing of fuel assemblies. The design values are obtained by examining maximum, nominal, and minimum fuel assembly spacing and determining the worst values for the combined effect of flow and rod peaking.

The axial nuclear factor, Fz, is illustrated in Figure 3-10. The distribution of power expressed as $P/\overline{P}$ is shown for two conditions of reactor operation. The first condition is an inlet peak with a max/avg value of 1.70 resulting from partial insertion of a CRA group for transient control following a power level change. This condition results in the maximum local heat flux and maximum linear heat rate. The second power shape is a symmetrical cosine which is indicative of the power distribution with xenon override rods withdrawn. The flux peak max/avg value is 1.50 in the center of the active core. Both of these flux shapes have been evaluated for thermal DNB limitations. The limiting condition is the 1.50 cosine power distribution. The inlet peak shape has a larger maximum value. However, the position of the 1.50 cosine peak farther up the channel results in a less favorable flux to enthalpy relationship. This effect has been demonstrated in DNB tests of nonuniform flux shapes.(24) The 1.50 cosine axial shape has been used to determine individual channel DNB limits and to make the associated statistical analysis.

The nuclear factor for total radial x local rod power, $F_{\Delta h}$, is calculated for each rod in the core. A distribution curve of the fraction of the core fuel rods operating above various peaking factors is shown in Figure 3-11 for a typical fuel cycle condition with the maximum fuel rod peaking factor of 1.78.

d. Engineering Hot Channel Factors

Power peaking factors obtained from the nuclear analysis are based on mechanically perfect fuel assemblies. Engineering hot channel factors are used to describe variations in fuel loading, fuel and clad dimensions, and flow channel geometry from perfect physical quantities and dimensions.

The application of hot channel factors is described in detail in 3.2.3.2.2, Statistical Core Design Technique. The factors are determined statistically from fuel assembly as-built or specified data where F_Q is a heat input factor, F_Q'' is a local heat flux factor at a hot spot, and F_A is a flow area reduction factor describing the variation in coolant channel flow area. Several subfactors are combined statistically to obtain the final values for F_Q, F_Q'', and F_A. These subfactors are shown in Table 3-9. The factor, the coefficient of variation, the standard deviation, and the mean value are tabulated.

00200

Table 3-9

Coefficients of Variation

CV No.	Description	σ	$\bar{x}$	CV
1	Flow Area			
	Interior Bundle Cells	0.00190	0.17740	0.01072
	Peripheral Bundle Cells	0.00346	0.21546	0.01608
2	Local Rod Diameter	0.000647	0.430	0.00151
3	Average Rod Diameter (Die-Drawn, Local and Average Same)	0.000647	0.430	0.00151
4	Local Fuel Loading			0.00698
	Subdensity	0.00647	0.935	0.00692
	Subfuel Area (Diameter Effect)	0.000094	0.1075	0.00088
5	Average Fuel Loading			0.00557
	Subdensity	0.00485	0.935	0.00519
	Sublength	0.26294	144	0.00183
	Subfuel Area (Diameter Effect)	0.000094	0.1075	0.00088
6	Local Enrichment	0.00421	2.30	0.00183
7	Average Enrichment	0.00421	2.30	0.00183

CV Coefficient of Variation $\sigma/\bar{x}$
σ Standard Deviation of Variable
$\bar{x}$ Mean Value of Variable

(Enrichment values are for worst case normal assay batch; maximum variation occurs for minimum enrichment.)

e. Core Flow Distribution Hot Channel Factors

The physical arrangement of the reactor vessel internals and nozzles results in a nonuniform distribution of coolant flow to the various fuel assemblies. Reactor internal structures above and below the active core are designed to minimize unfavorable flow distribution. A 1/6 scale model test of the reactor and internals is being performed to demonstrate the adequacy of the internal arrangements. The final variations in flow will be determined when the tests are completed. Interim factors for flow distribution effects have been calculated from test data on reactor vessel models for previous pressurized water reactor designs.

A flow distribution factor is determined for each fuel assembly location in the core. The factor is expressed as the ratio of fuel assembly flow to average fuel assembly flow. The finite values of the

00201

ratio may be greater or less than 1.0 depending on the position of the assembly being evaluated. The flow in the central fuel assemblies is in general larger than the flow in the outermost assemblies due to the inherent flow characteristics of the reactor vessel.

The flow distribution factor is related to a particular fuel assembly location and the quantity of heat being produced in the assembly. A flow-to-power comparison is made for all of the fuel assemblies. The worst condition in the hottest fuel assembly is determined by applying model test isothermal flow distribution data and heat input effects at power as outlined in 3.2.3.2.3. Two assumptions for flow distribution have been made in the thermal analysis of the core as follows:

(1) For the maximum design condition and for the analysis of the hottest channel, all fuel assemblies receive minimum flow for the worst condition, regardless of assembly power or location.

(2) For the most probable design conditions predicted, average flows have been assigned for each fuel assembly consistent with location and power. The flow factor assumed for the maximum design condition is conservative. Application of vessel flow test data and individual assembly flow factors in the detailed core design will result in improved statistical statements for the maximum design condition.

f. Maximum Reactor Design Overpower

Core performance is assessed at the maximum design overpower. The selection of the design overpower is based on an analysis of the reactor protection system as described in Section 7. The reactor trip point is 107.5 percent rated power, and the maximum overpower, which is 114 percent, will not be exceeded under any conditions.

g. Maximum Design Condtions Analysis Summary

The Statistical Core Design Technique described in 3.2.3.2.2 was used to analyze the reactor at the maximum design conditions described previously. The total number of fuel rods in the core that have a possibility of reaching DNB is shown in Figure 3-12 for 100 to 130 percent overpower for the maximum design conditions. Point B on Line 1 is the maximum design point for 114 percent power with the design $F\Delta h$ nuclear of 1.78 and minimum flow to every channel in the core. This Point B forms the basis for this statistical statement:

> There is a 99 percent confidence that at least 99.98 percent of the fuel rods in the core are in no jeopardy of experiencing a departure from nucleate boiling (DNB) during continuous operation at the design overpower of 114 percent.

At 100 percent power (2,452 MWt) as shown by Point A, the statistical number of fuel rods in jeopardy is less than one, resulting in a

population protected in excess of 99.997 percent. The limit imposed by a W-3 DNB ratio of 1.3 is 70 fuel rods in jeopardy or a population protected of 99.810 percent.

An additional analysis of fuel rods in jeopardy for all the maximum design conditions except fuel assembly flow distribution is shown as Line 2 in Figure 3-12. Each assembly was assumed to receive average flow for the assembly power conditions. The final consideration of flow distribution will result in values within the bounds of the two lines. Statistical results for the maximum design condition calculation, as shown by Figure 3-12, may be summarized as follows in Table 3-10.

Table 3-10

DNB Results - Maximum Design Condition
(99% Confidence Level)

Point	Power, % of 2,452 MWt	FΔh	Possible DNB	Population Protected, %	Hot Channel DNB Ratio (W-3)
A	100	1.78	<1	>99.997	2.21
B	114	1.78	5.0	99.986	1.71
C	128	1.78	70.0	99.810	1.30

h. Most Probable Design Condition Analysis Summary

The previous maximum design calculation, as shown by Line 1, Figure 3-12, indicates the total number of rods that may be in jeopardy when it is conservatively assumed that every rod in the core has the mechanical and heat transfer characteristics of a hot channel as described in 3.2.3.2.2. For example, all channels are analyzed with F_A (flow area factor) less than 1.0, F_Q (heat input factor) greater than 1.0, and with minimum fuel assembly flow. It is physically impossible for all channels to have hot channel characteristics. A more realistic indication of the number of fuel rods in jeopardy may be obtained by the application of the statistical heat transfer data to average rod power and mechanical conditions.

An analysis for the most probable conditions has been made based on the average conditions described in 3.2.3.2.2. The results of this analysis are shown in Figure 3-13. The analysis may be summarized as follows in Table 3-11.

00203

Table 3-11

DNB Results - Most Probable Condition

Point	Power, % of 2,452 MWt	FΔh	Possible DNB	Population Protected, %	Hot Channel DNB Ratio (W-3)
D	100	1.78	<1	>99.997	2.48
E	114	1.78	1.7	99.995	1.97
F	130	1.78	9.9	99.973	1.51

The analysis was made from Point D at 100 percent power to Point F at 130 percent power to show the sensitivity of the analysis with power. The worst condition expected is indicated by Point E at 114 percent power where it is shown statistically that there is a small possibility that 1.7 fuel rods may be subject to a departure from nucleate boiling (DNB). This result forms the basis for the following statistical statement for the most probable design conditions:

> There is at least a 99 percent confidence that at least 99.995 percent of the rods in the core are in no jeopardy of experiencing a DNB, even with continuous operation at the design overpower of 114 percent.

i. Distribution of the Fraction of Fuel Rods Protected

The distribution of the fraction (P) of fuel rods that have been shown statistically to be in no jeopardy of a DNB has been calculated for the maximum design and most probable design conditions. The computer programs used provide an output of (N) number of rods and (P) fraction of rods that will not experience a DNB grouped for ranges of (P). The results for the most probable design condition are shown in Figure 3-14.

The population protected, (P), and the population in jeopardy, (1-P), are both plotted. The integral of (1-P) and the number of fuel rods gives the number of rods that are in jeopardy for given conditions as shown in Figures 3-12 and 3-13. The number of rods is obtained from the product of the percentage times the total number of rods being considered (36,816). Two typical distributions shown in Figure 3-14 are for the most probable condition analysis of Points E and F on Figure 3-13. The lower line of Figure 3-14 shows P and (1-P) at the 114 percent power condition represented by Point E of Figure 3-13. The upper curve shows P and (1-P) at the 130 percent power condition represented by Point F of Figure 3-13. The integral of N and (1-P) of the lower curve forms the basis for the statistical statement at the most probable design condition described in (h) above.

j. Hot Channel Performance Summary

The hottest unit cell with all surfaces heated has been examined for hot channel factors, DNB ratios, and quality for a range of reactor

00204

powers. The cell has been examined for the maximum value of $F_{\Delta h}$ nuclear of 1.78. The hot channel was assumed to be located in a fuel assembly with 95 percent of the average fuel assembly flow. The heat generated in the fuel is 97.3 percent of the total nuclear heat. The remaining 2.7 percent is assumed to be generated in the coolant as it proceeds up the channel within the core and is reflected as an increase in ΔT of the coolant.

Error bands of 65 psi operating pressure and ±2 F are reflected in the total core and hot channel thermal margin calculations in the direction producing the lowest DNB ratios or highest qualities. The DNB ratio versus power is shown in Figure 3-15. The DNB ratio in the hot channel at the maximum overpower of 114 percent is 1.71 which corresponds to a 99 percent confidence that at least 99.82 percent of the fuel channels of this type are in no jeopardy of experiencing a DNB. The engineering hot channel factors used in the design analysis are described in 3.2.3.2.2 and listed below:

$$F_Q = 1.011$$

$$F_{Q''} = 1.014$$

$$F_A = 0.98 \text{ (Interior Cells)}$$

$$F_A = 0.97 \text{ (Wall Cells)}$$

The hot channel exit quality for various powers is shown in Figure 3-16. The combined results may be summarized for 2,120 psig as follows:

Reactor Power, %	DNB Ratio (W-3)	Exit Quality, %
100	2.21	-1.0[(a)]
107.5 (Trip Setting)	1.91	1.5
114 (Maximum Power)	1.71	3.9
128	1.30	9.1
138	1.00	13.5

(a) Subcooled

3.2.3.1.2 Fuel and Cladding Thermal Conditions

a. Fuel

A digital computer code is used to calculate the fuel temperature. The program uses nonuniform volumetric heat generation across the fuel diameter, and external coolant conditions and heat transfer coefficients determined for thermal-hydraulic channel solutions. The fuel thermal conductivity is varied in a radial direction as a function of the temperature variation. Values for fuel conductivity were used as shown in Figure 3-17, a plot of fuel conductivity

00285

versus temperature. The heat transfer from the fuel to the clad is calculated with a fuel and clad expansion model proportional to temperatures. The temperature drop is calculated using gas conductivity at the beginning-of-life conditions when the gas conductivity is 0.09 Btu-ft/h-F-ft^2. The gas conduction model is used in the calculation until the fuel thermal expansion relative to the clad closes the gap to a dimension equivalent to a contact coefficient. The contact coefficient is dependent upon pressure and gas conductivity.

A plot of fuel center temperature versus linear heat rate in kW/ft is shown in Figure 3-18 for beginning-of-life conditions. The linear heat rate at the maximum overpower of 114 percent is 19.2 kW/ft. The corresponding center fuel temperature shown in Table 1-2 is 4,450 F. The center and average temperatures at 100 percent power are 4,150 and 1,345 F as shown in Table 3-1.

The peaking factors used in the calculation are

$$F\Delta h = 1.78$$

$$Fz = 1.70$$

$$F_{Q''} = 1.03$$

$$F_q \text{ (nuc and mech)} = 3.12$$

A conservative value of 1.03 was assumed for the heat flux peaking factor, $F_{Q''}$. The assigned value corresponds to a 99 percent population-protected relationship as described in the statistical technique.

b. Clad

The assumptions in the preceding paragraph were applied in the calculation of the clad surface temperature at the maximum overpower. Boiling conditions prevail at the hot spot, and the Jens and Lottes relationship(25) for the coolant-to-clad ΔT for boiling was used to determine the clad temperature. The resulting maximum calculated clad surface temperature is 654 F at a system operating pressure of 2,185 psig.

3.2.3.2 Thermal and Hydraulic Evaluation

3.2.3.2.1 Introduction

Summary results for the characteristics of the reactor design are presented in 3.2.3.1. The Statistical Core Design Technique employed in the design represents a refinement in the methods for evaluating pressurized water reactors. Corresponding single hot channel DNB data were presented to relate the new method with previous criteria. A comprehensive description of the new technique is included in this section to permit a rapid evaluation of the methods used.

00206

A detailed evaluation and sensitivity analysis of the design has been made by examining the hottest channel in the reactor for DNB ratio, quality, and fuel temperatures. The W-3 correlation has been used in this analysis.

3.2.3.2.2 Statistical Core Design Technique

The core thermal design is based on a Statistical Core Design Technique developed by B&W. The technique offers many substantial improvements over older methods, particularly in design approach, reliability of the result, and mathematical treatment of the calculation. The method reflects the performance of the entire core in the resultant power rating and provides insight into the reliability of the calculation. This section discusses the technique in order to provide an understanding of its engineering merit.

The statistical core design technique considers all parameters that affect the safe and reliable operation of the reactor core. By considering each fuel rod, the method rates the reactor on the basis of the performance of the entire core. The result then will provide a good measure of the core safety and reliability since the method provides a statistical statement for the total core. This statement also reflects the conservatism or design margin in the calculation.

A reactor safe operating power has always been determined by the ability of the coolant to remove heat from the fuel material. The criterion that best measures this ability is the DNB, which involves the individual parameters of heat flux, coolant temperature rise, and flow area, and their intereffects. The DNB criterion is commonly applied through the use of the departure from nucleate boiling ratio (DNBR). This is the minimum ratio of the DNB heat flux (as computed by the DNB correlation) to the surface heat flux. The ratio is a measure of the margin between the operating power and the power at which a DNB might be expected to occur in that channel. The DNBR varies over the channel length, and it is the minimum value of the ratio in the channel of interest that is used.

The calculation of DNB heat flux involves the coolant enthalpy rise and coolant flow rate. The coolant enthalpy rise is a function of both the heat input and the flow rate. It is possible to separate these two effects; the statistical hot channel factors required are a heat input factor, F_Q, and a flow area factor, F_A. In addition, a statistical heat flux factor, F_Q'' is required; the heat flux factor statistically describes the variation in surface heat flux. The DNBR is most limiting when the burnout heat flux is based on minimum flow area (small F_A) and maximum heat input (large F_Q), and when the surface heat flux is large (large F_Q''). The DNB correlation is provided in a best-fit form, ie, a form that best fits all of the data on which the correlation is based. To afford protection against DNB, the DNB heat flux computed by the best-fit correlation is divided by a DNB factor (BF) greater than 1.0 to yield the design DNB surface heat flux. The basic relationship

$$DNBR = \frac{Q''_{DNB}}{BF} \times f(F_A, F_Q) \times \frac{1}{Q''_{surface} \times F_Q''}$$

00207

involves as parameters statistical hot channel and DNB factors. The DNB factor (BF) above is usually assigned a value of unity when reporting DNB ratios so that the margin at a given condition is shown directly by a DNBR greater than 1.0, ie, 1.30 in the hot channel.

Selected heat transfer data are analyzed to obtain a correlation. Since thermal and hydraulic data generally are well represented with a Gaussian (normal) distribution (Figure 3-19), mathematical parameters that quantitatively rate the correlation can be easily obtained for the histogram. These same mathematical parameters are the basis for the statistical burnout factor (BF).

In analyzing a reactor core, the statistical information required to describe the hot channel subfactors may be obtained from data on the as-built core, from data on similar cores that have been constructed, or from the specified tolerances for the proposed core. Regardless of the source of data, the subfactors can be shown graphically (Figures 3-20 and 3-21).

All the plots have the same characteristic shape whether they are for subfactors, hot channel factors, or burnout factor. The factor increases with either increasing population or confidence. The value used for the statistical hot channel and burnout factor is a function of the percentage of confidence desired in the result, and the portion of all possibilities desired, as well as the amount of data used in determining the statistical factor. A frequently used assumption in statistical analyses is that the data available represent an infinite sample of that data. The implications of this assumption should be noted. For instance, if limited data are available, such an assumption leads to a somewhat optimistic result. The assumption also implies that more information exists for a given sample than is indicated by the data; it implies 100 percent confidence in the end result. The B&W calculational procedure does not make this assumption, but rather uses the specified sample size to yield a result that is much more meaningful and statistically rigorous. The influence of the amount of data for instance can be illustrated easily as follows: Consider the heat flux factor which has the form

$$F_{Q"} = 1 + K\sigma_{F_{Q"}}$$

where $F_{Q"}$ is the statistical hot channel factor for heat flux

K is a statistical multiplying factor

$\sigma_{F_{Q"}}$ is the standard deviation of the heat flux factor, including the effects of all the subfactors

If $\sigma_{F_{Q"}} = 0.05$ for 300 data points, then a K factor of 2.608 is required to protect 99 percent of the population. The value of the hot channel factor then is

$$F_{Q"} = 1 + (2.608 \times 0.050) = 1.1304$$

00708

and will provide 99 percent confidence for the calculation. If, instead of using the 300 data points, it is assumed that the data represent an infinite sample, then the K factor for 99 percent of the population is 2.326. The value of the hot channel factor in this case is

$$F_Q'' = 1 + (2.326 \times 0.050) = 1.1163$$

which implies 100 percent confidence in the calculation. The values of the K factor used above are taken from SCR-607[26]. The same basic techniques can be used to handle any situation involving variable confidence, population, and number of points.

Having established statistical hot channel factors and statistical DNB factors, we can proceed with the calculation in the classical manner. The statistical factors are used to determine the minimum fraction of rods protected, or that are in no jeopardy of experiencing a DNB at each nuclear power peaking factor. Since this fraction is known, the maximum fraction in jeopardy is also known. It should be recognized that every rod in the core has an associative DNB ratio that is substantially greater than 1.0, even at the design overpower, and that theoretically no rod can have a statistical population factor of 100 percent, no matter how large its DNB ratio.

Since both the fraction of rods in jeopardy at any particular nuclear power peaking factor and the number of rods operating at that peaking factor are known, the total number of rods in jeopardy in the whole core can be obtained by simple summation. The calculation is made as a function of power, and the plot of rods in jeopardy versus reactor overpower is obtained (Figure 3-12). The summation of the fraction of rods in jeopardy at each peaking factor summed over all peaking factors can be made in a statistically rigorous manner only if the confidence for all populations is identical. If an infinite sample is not assumed, the confidence varies with population. To form this summation then, a conservative assumption is required. B&W total core model assumes that the confidence for all rods is equal to that for the least-protected rod, ie, the minimum possible confidence factor is associated with the entire calculation.

The result of the foregoing technique, based on the maximum design conditions (114 percent power), is this statistical statement:

> There is at least a 99 percent confidence that at least 99.98 percent of the rods in the core are in no jeopardy of experiencing a DNB, even with continuous operation at the design overpower.

The maximum design conditions are represented by these assumptions:

a. The maximum design values of $F_{\Delta h}$ (nuclear max/avg total fuel rod heat input) are obtained by examining the maximum, nominal, and minimum fuel assembly spacing and determining the worst value for rod peaking.

b. The maximum value of F_z (nuclear max/avg axial fuel rod heat input) is determined for the limiting transient or steady-state condition.

c. Every coolant channel in the core is assumed to have less than the nominal flow area represented by engineering hot channel factors, F_A, less than 1.0.

d. Every channel is assumed to receive the minimum flow associated with core flow maldistribution.

e. Every fuel rod in the core is assumed to have a heat input greater than the maximum calculated value. This value is represented by engineering hot channel heat input factors, F_Q and F_Q", which are greater than 1.0.

f. Every channel and associated fuel rod has a heat transfer margin above the experimental best-fit limits reflected in DNB ratios greater than 1.0 at maximum overpower conditions.

The statistical core design technique may also be used in a similar manner to evaluate the entire core at the most probable mechanical and nuclear conditions to give an indication of the most probable degree of fuel element jeopardy. The result of the technique based on the most probable design conditions leads to a statistical statement which is a corollary to the maximum design statement:

> There is at least a 99 percent confidence that at least 99.995 percent of the rods in the core are in no jeopardy of experiencing a DNB, even with continuous operation at the design overpower.

The most probable design conditions are assumed to be the same as the maximum design conditions with these exceptions:

a. Every coolant channel is assumed to have the nominal flow area ($F_A = 1.0$).

b. Every fuel rod is assumed to have (1) the maximum calculated value of heat input, and (2) F_Q and F_Q" are assigned values of 1.0.

c. The flow in each coolant channel is based on a power analysis without flow maldistribution factors.

d. Every fuel rod is assumed to have a nominal value for $F\Delta h$ nuclear.

The full meaning of the maximum and most probable design statements requires additional comment. As to the 0.02 percent or 0.005 percent of the rods not included in the statements, statistically, it can be said that no more than 0.02 percent or 0.005 percent of the rods will be in jeopardy, and that in general the number in jeopardy will be fewer than 0.002 percent or 0.005 percent. The statements do not mean to specify a given number of DNB, but only acknowledge the possibility that a given number could occur for the conditions assumed.

00210

In summary, the calculational procedure outlined here represents a substantially improved design technique in two ways:

a. It reflects the performance and safety of the entire core in the resultant power rating by considering the effect of each rod on the power rating.

b. It provides information on the reliability of the calculation and, therefore, the core through the statistical statement.

3.2.3.2.3 Evaluation of the Thermal and Hydraulic Design

a. Hot Channel Coolant Quality and Void Fraction

An evaluation of the hot channel coolant conditions provides additional confidence in the thermal design. Sufficient coolant flow has been provided to insure low quality and void fractions. The quality in the hot channel versus reactor power is shown in Figure 3-16. The sensitivity of channel outlet quality with pressure and power level is shown by the 2,185 and 2,120 psig system pressure conditions examined. These calculations were made for an FΔh of 1.78. Additional calculations for a 10 percent increase in FΔh to 1.96 were made at 114 percent power. The significant results of both calculations are summarized in Table 3-12.

Table 3-12

Hot Channel Coolant Conditions

Power, %	FΔh	Exit Quality, %	Exit Void Fraction, %	Operating Pressure, psig
100	1.78	(-)3.0[b]	0.4[a]	2,185
114	1.78	1.5	7.9	2,185
128	1.78	6.6	28.7	2,185
114	1.96	7.1[b]	30.5[a]	2,185
100	1.78	-1.0	1.7	2,120
114	1.78	3.9	20.0	2,120
128	1.78	9.1	37.2	2,120
114	1.96	9.5	38.9	2,120

[a] Subcooled voids.

[b] Negative indication of quality denotes subcooling.

The conditions of Table 3-12 were determined with all of the hot channel factors applied. Additional calculations were made for unit cell channels without engineering hot channel factors to show the coolant conditions more likely to occur in the reactor core. A value for FΔh of 1.78 was examined with and without fuel assembly flow distribution hot channel factors at 2,185 psig as shown on Figure 3-22. These results show that the exit qualities

from the hottest cells should in general be considerably lower than the maximum design conditions.

b. Core Void Fraction

The core void fractions were calculated at 100 percent rated power for the normal operating pressure of 2,185 psig and for the minimum operating pressure of 2,120 psig. The influence of core fuel assembly flow distribution was checked by determining the total voids for both 100 and 95 percent total core flow for the two pressure conditions.

The results are as follows:

Flow, %	Pressure, psig	Core Void Fraction, %
100	2,185	0.023
100	2,120	0.050
95	2,185	0.053
95	2,120	0.186

The most conservative condition of 95 percent flow at 2,120 psig results in no more than 0.19 percent void volume in the core. Conservative maximum design values were used to make the calculation.

The void program uses a combination of Bowring's[27] model with Zuber's[28] correlation between void fraction and quality. The Bowring model considers three different regions of forced convection boiling. They are:

(1) Highly Subcooled Boiling

In this region, the bubbles adhere to the wall while moving upward through the channel. This region is terminated when the subcooling decreases to a point where the bubbles break through the laminar sublayer and depart from the surface. The highly subcooled region starts when the surface temperature of the clad reaches the surface temperature predicted by the Jens and Lottes equation. The highly subcooled region ends when

$$T_{sat} - T_{bulk} = \frac{n\phi}{V} \qquad (A)$$

where ϕ = local heat flux, Btu/h-ft^2

$n = 1.863 \times 10^{-5} (14 + 0.0068p)$

V = velocity of coolant, ft/s

p = pressure, psia

The void fraction in this region is computed in the same manner as Maurer,[29] except that the end of the region is determined by Equation (A) rather than by a vapor layer thickness. The nonequilibrium quality at the end of the region is computed from the void fraction as follows:

$$x_d^* = \frac{1}{1 + \frac{\rho f}{\rho g}\left(\frac{1}{a_d} - 1\right)} \qquad (B)$$

where x_d^* = nonequilibrium quality at end of Region 1

a_d = void fraction at $T_{sat} - T_{bulk} = \frac{n\phi}{V}$

ρf = liquid component density, lb/ft^3

ρg = vapor component density, lb/ft^3

(2) Slightly Subcooled Boiling

In this region, the bubbles depart from the wall and are transported along the channel (condensation of the bubbles is neglected). This region transcends to a point where the thermodynamic quality is zero. In general, this is the region of major concern in the design of pressurized water reactors.

The nonequilibrium quality in this region is computed from the following formula:

$$x^* = x_d^* + \frac{P_h}{\dot{m}\, h_{fg}(1 + \epsilon)} \int_{z_d}^{z} (\phi - \phi_{SP})dz \qquad (C)$$

where x^* = nonequilibrium quality in Region 2

h_{fg} = latent heat of vaporization, Btu/lb

$\frac{1}{1 + \epsilon}$ = fraction of the heat flux above the single phase heat flux that actually goes to producing voids

ϕ_{SP} = single phase heat flux, $Btu/h\text{-}ft^2$

$\dot{m}$ = mass flow rate, lb/h

P_h = heated perimeter, ft

z = channel distance, ft

The void fraction in this region is computed from

$$\alpha = \frac{x^*}{C_o\left[x^* + \rho_g/\rho_f(1 - x^*)\right] + \frac{38.3\, A_f \rho_g}{\dot{m}}\left[\frac{\sigma g g_c(\rho_f - \rho_g)}{\rho_f^2}\right]^{1/4}} \quad (D)$$

where g = acceleration due to gravity, ft/s^2

g_c = constant in Newton's Second Law = $32.17 \frac{lb\ m\ ft}{lb\ f\ s^2}$

C_o = Zuber's distribution parameter

A_f = flow area, $in.^2$

σ = surface tension

Equation (D) results from rearranging equations found in Reference (33) and assuming bubbly turbulent flow in determining the relative velocity between the vapor and the fluid. Zuber has shown that Equation (D) results in a better prediction of the void fraction than earlier models based on empirical slip ratios.

(3) Bulk Boiling

In this region, the bulk temperature is equal to the saturation temperature, and all the energy transferred to the fluid results in net vapor generation. Bulk boiling begins when the thermodynamic (heat balance) quality, x, is greater than the nonequilibrium quality, x^*. The void fraction in this region is computed using Equation (D) with the thermodynamic quality, x, replacing x^*.

c. Coolant Channel Hydraulic Stability

Flow regime maps of mass flow rate and quality were constructed in order to evaluate channel hydraulic stability. The confidence in the design is based on a review of both analytical evaluations[30, 31, 32, 33] and experimental results obtained in multiple rod bundle burnout tests. Bubble-to-annular and bubble-to-slug flow limits proposed by Baker[30] are consistent with the B&W experimental

data in the range of interest. The analytical limits and experimental data points have been plotted to obtain the maps for the four different types of cells in the reactor core. These are shown in Figures 3-23, 3-24, 3-25, and 3-26. The experimental data points represent the exit conditions in the various types of channels just previous to the burnout condition for a representative sample of the data points obtained at design operating conditions in the nine rod burnout test assemblies. In all of the bundle tests, the pressure drop, flow rate, and rod temperature traces were repeatable and steady, and did not exhibit any of the characteristics associated with flow instability.

Values of hot channel mass velocity and quality at 114 percent and 130 percent power for both nominal and design conditions are shown on the maps. The potential operating points are within the bounds suggested by Baker. Experimental data points for the reactor geometry with much higher qualities than the operating conditions have not exhibited unstable characteristics.

d. Hot Channel DNB Comparisons

DNB ratios for the hottest channel have been determined for the W-3 correlation, and the results are shown in Figure 3-15. DNB ratios are shown for the design 1.50 axial max/avg symmetrical cosine flux shape from 100 to 150 percent power. The W-3 DNB ratio at the maximum design power of 114 percent is 1.71. This compares with the suggested W-3 design value of 1.3. A ratio of 1.3 is reached at 128 percent power at an exit quality of 9.1 percent, which is within the prescribed quality limits of the correlation.

The sensitivity of the DNB ratio with Fz nuclear was examined from 100 to 150 percent power. The detailed results are labeled in Figure 3-27. A cosine flux shape with an Fz of 1.80 and an $F\Delta h$ of 1.78 results in a W-3 DNB ratio of 1.44 at 114 percent power. Similar results are shown for a value of Fz of 1.65 and for the design value of 1.5. The W-3 values are well above suggested design values.

The influence of a change in $F\Delta h$ was determined by analyzing the hot channel for an $F\Delta h$ of 1.96. This value is 10 percent above the maximum design value of 1.78. The resulting W-3 DNB ratio is 1.28 at 114 percent power. This value is well above the correlation best-fit values of 1.0 for the severe conditions assumed.

e. Reactor Flow Effects

Another significant variable to be considered in evaluating the design is the total system flow. Conservative values for system and reactor pressure drop have been determined to insure that the required system flow is obtained in the as-built plant. The experimental programs previously outlined in 1.5.2 will confirm the pressure drop and related pump head requirements. It is anticipated that the as-built reactor flow will exceed the design value and will lead to increased power capability.

The reactor core flow and power capability were evaluated by determining the steady-state power DNB rates versus flow. Analyses were made for (a) variations of power capability with total reactor flow for a constant DNB ratio of 1.30, (b) DNB ratios for design flow with variations in hot channel mixing coefficients and (c) DNB ratios for gross flow variations of ± 10 percent. The results are shown in Figures 3-28 and 3-29. For the analysis shown in Figure 3-28 for design hot channel condition, the flow was determined that would give a DNB ratio of 1.30 for a range of reactor powers. This analysis shows, for example, that a DNB ratio of 1.30 can be maintained in the hot channel at 114 percent power with a total reactor flow of 109 x 10^6 lb/hr as compared with the available design flow of 131.3 x 10^6 lb/hr. The results shown by Line 2 in Figure 3-29 are the DNB ratios for rated flow of 131.3 x 10^6 lb/hr versus power. The limiting condition is 128 percent power for a DNB ratio of 1.30. Lines 1 and 3 show the DNB ratios versus power where the total system flow has been varied by ±10 percent. Adequate DNB ratios can be maintained with a substantial reduction in reactor coolant system flow.

The foregoing sensitivity analyses were made using a fuel assembly design mixing coefficient of 0.02. The final design value may be as high as 0.06. A smooth tube value for mixing without spacer planes is 0.03. A sensitivity analysis for this range of coefficients was made for the rated flow condition. The results are shown by Lines 4 and 5 of Figure 3-29 and discussed in more detail in 3.2.3.2.3.j.

f. Reactor Inlet Temperature Effects

The influence of reactor inlet temperature on power capability at design flow was evaluated. A variation of 1 F in reactor inlet temperature will result in a power capability change of 0.6 percent at a given DNB ratio.

g. Fuel Temperature

(1) Method of Calculation

A fuel temperature and gas pressure computer code was developed to calculate fuel temperatures, expansion, densification, equiaxed and columnar grain growth, center piping of fuel pellets, fission gas release, and fission gas pressure. Program and data comparisons were made on the basis of the fraction of the fuel diameter within these structural regions:

(a) Outer limit of equiaxed grain growth - 2,700 F.

(b) Outer limit of columnar grain growth - 3,200 F.

(c) Outer limit of molten fuel (UO_2) - 5,000 F.

00216

Data from References 34 through 37 were used to compare calculated and experimental fractions of the rod in grain growth and central melting.

The radial expansion of the fuel pellet is computed from the mean fuel temperature and the average coefficient of linear expansion for the fuel over the temperature range considered. This model combined with the model for calculating the heat transfer coefficient was compared with the model developed by Notley et al(38) of AECL. The difference in fuel growth for the two calculation models was less than the experimental scatter of data.

The fuel may be divided into as many as 30 radial and 70 axial increments for the analysis. An iterative solution for the temperature distribution is obtained, and the thermal conductivity of the fuel is input as a function of temperature. The relative thermal expansion of the fuel and cladding is taken into account when determining the temperature drop across the gap between the fuel and cladding surfaces. The temperature drop across the gap is a function of width, mean temperature, and gas conductivity. The conductivity of the gas in the gap is determined as a function of burnup and subsequent release of fission product gases. In the event of fuel clad contact, contact coefficients are determined on the basis of methods suggested by Ross and Stoute(41). The contact coefficient is determined as a function of the mean conductivity of the interface materials, the contact pressure, the mean surface roughness, the material hardness, and the conductivity of the gas in the gap.

The analytical model computes the amount of central void expected whenever the temperature approaches the threshold temperature for fuel migration, and readjusts the density according to the new geometry.

The program uses a polynominal fit relationship for fuel thermal conductivity. Three relationships were used to evaluate the effects of conductivity on fuel temperatures. The B&W reference design curve which yields an integrated thermal conductivity of 93 w/cm, is a modification of the relationship presented in GEAP-4624.(39)

The conductivity relationships in GEAP-4624 and CVNA-246(40) are compared with the reference design in Figure 3-30. McGrath (40) concludes that the CVNA-246 values are lower limits for the high temperature conditions. Fuel center temperatures for all three of the conductivity relationships at the peaking factors given in 3.2.3.1.2 have been calculated to evaluate the margin to central melting at the maximum overpower and to show the sensitivity of the calculation regarding thermal conductivity. Since the power peaks will be burned off with irradiation, the peaking factors used are conservative at the end of life.

00217

(2) Fuel Center Temperature Results

The results of the analysis for center temperatures with the methods described above are shown in Figures 3-31 and 3-32 for beginning- and end-of-life conditions. The beginning- and end-of-life gas conductivity values are 0.09 and 0.01 Btu/h-ft^2-F. The calculated end-of-life center fuel temperatures are higher than the beginning-of-life values because of the reduction in the conductivity of the gas in the gap. The effect is apparent even though a contact condition prevails. The calculation includes the effect of fuel swelling due to irradiation, but does not consider the effect of fuel cracking and expansion due to thermal gradients. Credit is also taken for the flux depression in the center of the rod because of the self-shielding effect of UO_2 (nonuniform power generation). The calculated contact pressures are conservatively lower than those expected at end-of-life conditions in the hottest fuel rods, and the fuel temperatures shown in the figures above are conservatively high.

The B&W model gives very good results when compared to the results of others in the field as is shown in Figure 3-32. In the linear heat range of most interest, ie, approximately 20 kW/ft, there is only about 200 F difference between the maximum and minimum values calculated. Also the small differences between the B&W curve and the other curves indicate the relative insensitivity of the results to the shape of the conductivity at the elevated temperatures.

The most conservative assumptions, using GEAP-4624 data with relatively little increase in thermal conductivity above 3,000 F, result in central fuel melting at about 22 kW/ft, which is about 3 kW/ft higher than the maximum design value of 19.2 kW/ft at 114 percent power.(3-32) Further evaluation of the two figures shows that central fuel melting is predicted to occur between 22 and 26 kW/ft depending on the time-in-life and conductivity assumptions.

The transient analyses at accident and normal conditions have been made using the design fuel thermal conductivity curve (Figure 3-17) to reflect a conservative value for the maximum average temperature and stored energy in the fuel. Use of this curve results in a higher temperature and, therefore, a lower Doppler coefficient, since it decreases with temperature. Thus, the resultant Doppler effect is also conservative.

(3) Equilibrium Cycle Average Fuel Temperatures

An analysis has been made to show equilibrium average fuel conditions in the core. A typical fuel cycle, end-of-life, condition was used to determine the fraction of fuel at a given average condition. The results are shown in Figure 3-33

where the average temperature varies from 1,300 to 3,300 F, and the entire core average temperature is about 1,800 F. The bundle average powers as shown in Figure 3-34 were used to obtain the fuel rod heat rates. A symmetrical cosine axial power distribution with a 1.50 max/avg value as shown in Figure 3-10 was used to predict the axial heat rate distribution. It was assumed that 97.3 percent of the power is generated in the fuel. The fuel rods were divided into 14 axial and 10 radial segments to obtain the temperature distribution for this analysis. The heat rate for every fuel rod in the core was increased by a local peaking factor of 1.05 to account for uncertainties in the calculation of local peaks. This has the bulk effect of raising reactor power to 105 percent.

The fuel conductivity values from GEAP-4624[39] were used to provide conservative values for fuel conductivity. The maximum powers occurred in fuel assemblies with one and two cycles of operation as shown in Figure 3-34, and the assemblies with the highest burnup did not exceed 1.043 times the average power for the typical case analyzed. The results shown in Figure 3-33 were made by grouping all segments of fuel by temperature. Typical 6 and 10 kW/ft rod radial temperature profiles are shown in Figure 3-35. Typical fuel-to-clad heat transfer coefficients used were 240 and 480 Btu/h-ft^2-F for 6 and 10-kW/ft heat rates, respectively. The corresponding beginning-of-life coefficients are about 500 and 700 Btu/h-ft^2-F for 6 and 10-kW/ft heat rates.

The temperature calculations are conservatively based on nominal fuel dimensions without fuel irradiation swelling or cracking. Fuel swelling and cracking will result in higher fuel-to-clad heat transfer coefficients than those used in the analysis. The volumetric heat generation rate is higher at the outer periphery of the fuel than in the center region, and the operating temperatures will be lower than those predicted by the uniform radial power condition assumed in the analysis.

h. Fission Gas Release

The fission gas release is based on results reported in GEAP-4596,[42] Additional data from GEAP-4314[43], AECL-603[44], and CF-60-12-14[45] have been compared with the suggested release rate curve. The release rate curve[42] is representative of the upper limit of release data in the temperature region of most importance. A design release rate of 43 percent and an internal gas pressure of 3,300 psi are used to determine the fuel clad internal design conditions reported in 3.2.4.2, Fuel Assemblies.

The design values for fission gas release from the fuel and for the maximum clad internal pressure were determined by analyzing various operating conditions and assigning suitable margins for possible increases in local or average burnup in the fuel. Adequate margins are

provided without utilizing the initial porosity voids present in the UO_2 fuel. A detailed analysis of the design assumptions for fission gas release, and the relationship of burnup, fuel growth, and initial diametral clearance between the fuel and clad, are summarized in the following paragraphs. An evaluation of the effect of having the fuel pellet internal voids available as gas holders is also included.

(1) Design Assumptions

(a) Fission Gas Release Rates

The fission gas release rate is calculated as a function of fuel temperature at 114 percent of rated power. The procedures for calculating fuel temperatures are discussed in 3.2.3.2.3.g. The fission gas release curve and the supporting data are shown in Figure 3-36. Most of the data are on or below the design release rate curve. A release rate of 51 percent is used for the portion of the fuel above 3,500 F. The fuel temperatures were calculated using the B&W design fuel thermal conductivity curve which yields conservatively high values for fuel temperatures.

(b) Axial Power and Burnup Assumptions

The temperature conditions in the fuel are determined for the most severe axial power peaking expected to occur. Two axial power shapes have been evaluated to determine the maximum release rates. These are 1.50 and 1.70 max/avg shapes as shown in Figure 3-10 and repeated as part of Figure 3-37 of this analysis. The quantity of gas released is found by applying the temperature-related release rates to the quantities of fission gas produced along the length of the hot fuel rod.

The quantity of fission gas produced in a given axial location is obtained from reactor core axial region equilibrium burnup studies. Three curves showing the axial distribution of burnup as a local-to-average ratio along the fuel rod are shown in Figure 3-37. Values of 100, 300, and 930 days of operation are shown.

The 930-day, or end-of-life condition, is the condition with the maximum fission gas inventory. The average burnup at the end of life in the hot fuel rod is 38,150 MWd/MTU which has been determined as follows:

Calculated Hot Bundle Average Burnup, MWd/MTU	33,000
Hot Fuel Rod Burnup Factor	1.05
Margin for Calculation Accuracy	1.10
Hot Rod Maximum Average Burnup, MWd/MTU	38,150

00230

The local burnup along the length of the fuel rod is the product of the hot rod maximum average value above and the local-to-average ratio shown in Figure 3-37. The resulting hot rod local maximum burnup for the 930-day, end-of-life condition is about 42,000 MWd/MTU. This is the maximum calculated value. However, local values to 55,000 MWd/MTU have been evaluated to insure adequate local fuel cladding strength for possible increases in average or local burnup over the life of the fuel for various fuel management procedures.

(c) Hot Rod Power Assumptions

The maximum hot rod total power occurring at any time in the life of the fuel has been used to calculate the overpower temperature conditions. A hot rod power of 1.78 times the average rod power has been applied. This results in a maximum linear heat rate of 19.2 kW/ft which corresponds to 114 percent of the maximum thermal output (16.83 kW/ft) shown in Table 3-1. This is a conservative assumption when coupled with the end-of-life fission gas inventory since bundle and individual fuel rod power is expected to decrease with fuel burnup. A study of the power histories of all of the fuel assemblies to equilibrium conditions shows that the powers in the bundles during the last 300 days of operation are not more than 1.3 times the average bundle power. The peak bundle ratio of 1.69 (1.78 ÷ hot rod ratio) will only occur during the first two fuel cycles when the fission gas inventory is less than the maximum value.

(d) Fuel Growth Assumptions

The fuel growth was calculated as a function of burnup as indicated in 3.2.4.2.1. Fuel pellet dimensions in the thermal temperature and gas release models were increased to the end-of-life conditions as determined above.

(e) Gas conductivity and Contact Heat Transfer Assumptions

The quantity of fission gas released is a function of fuel temperature. The temperatures are influenced by three factors: (a) the conductivity of the fission gas in the gap between the fuel and clad, (b) the diametral clearance between fuel and clad, and (c) the heat transfer conditions when the fuel expands enough to contact the clad.

A gas conductivity of 0.01 Btu/h-ft^2-F based on 43 percent release of fission gas at the end-of-life condition was used in the analysis. Diametral clearances of 0.0025 to 0.0075 inch reflecting minimum and maximum clearances after fuel growth were analyzed. The contact heat transfer coefficients were calculated as suggested in Reference 42.

00239

(2) Summary of Results

The fission gas release rates were determined in the first evaluation. Rates were found for various cold diametral clearances and axial power peaking and burnup shapes. The results are shown in Figure 3-38. The lowest curve is the expected condition for a 1.70 axial power shape with a 930-day axial burnup distribution as shown in Figure 3-37. The increase in release rate with diametral clearance results from the fact that the fuel temperature must be raised to higher values before contact with the fuel clad is made. The release rate at the minimum clearance of 0.0045 inch is 15 percent. This condition is equivalent to a 0.0025 inch gap after irradiation growth and produces the maximum clad stress (maximum sized pellets with minimum internal diameter cladding). The release rate of 34 percent for the maximum diametral clearance of 0.0095 inch will not occur with the maximum stress condition due to fuel growth, since the fuel has more room to grow into the clearance.

Two additional cases were examined to check the sensitivity of the calculations to axial power and burnup shapes. The results are shown by the upper two curves in Figure 3-38. The top curve is a plot of the release rates when it is assumed that both the axial power and burnup inventory of fission gas are distributed with a 1.50 max/avg ratio as shown on Figure 3-55. Similar results are shown for the 1.70 max/avg power ratio with a 1.50 max/avg burnup ratio. These curves show the release rates expected are not strongly influenced by the various power and burnup shapes.

The second evaluation shows the resulting internal pressures due to the release of fission product gases. Plots of internal clad pressures for the expected 930-day axial burnup distribution and a 1.70 max/avg axial power shape are shown in Figure 3-39. The lower curve is a plot of internal gas pressure assuming that 6.5 percent of the fuel volume is available to hold the released gas (open porosity). The present design condition being used in clad-stress calculations assumes a closed pore condition with all released gas contained outside the fuel pellets in spaces between the expanded dished ends of the pellets, the radial gaps (if any), and the void spaces at the ends of the fuel rods. The effects of fuel densification and grain growth described in 3.2.3.2.3.g are included in the analysis. The calculation of maximum pressure is also relatively insensitive to the axial burnup distribution as shown by the line in Figure 3-39 for a 1.50 max/avg axial power and burnup shape. (This corresponds to a local burnup peak of 57,000 MWd/MTU.)

There is evidence that the UO_2 pellets in a nuclear reactor[46, 47,48] are usually cracked. A sensitivity analysis on fuel-to-clad gap conductance was performed to illustrate the effects

of fuel cracking. Two independent fuel models were developed to simulate this phenomenon. In one model, the cold minimum fuel diameter was increased by 0.0025 inch in order to decrease the diametral gap and increase the gap conductance (2.5-mil cracking effect). In the other model, the methods of Ross and Stoute[41] were used to evaluate gap conductance with the fuel-to-clad contact pressure equal to zero ("0-contact" cracking effect). This model assumes that the fuel cracks enough to come into contact with the clad, but not enough to exert pressure against the clad. As the higher heat rates are reached, the thermal growth of the fuel causes a contact pressure which is used in the calculations. Fuel-to-clad gap conductance as a function of linear heat rate is plotted on Figure 3-40 to show the marked increase in gap heat transfer due to fuel cracking. To further illustrate the effects of fuel cracking, a sensitivity analysis on rod internal pressure was performed using the foregoing fuel models. Figure 3-41 shows the results of this study for the two cracked fuel models and the ideal thermal expansion model at the most conservative fuel-to-clad heat transfer conditions (largest gap, end-of-life gas conductivity, etc). The fuel cracking models show a marked reduction in internal gas pressure from the design conditions.

A parametric study on gas pressure versus reactor power was performed to further illustrate the conservatisms involved in the gas pressure analysis. Figure 3-42 shows the results for the two cracked models and the ideal thermal expansion model at the worst fuel-to-clad heat transfer conditions. A conservative steady-state reactor power level of 2,795 MWt (114 percent of rated power) was used to obtain fission gas release. This analysis shows that power increases from rated power, 2,452 to 3,000 MWt result in very small increases in fuel rod internal gas pressure. Final design consideration of power conditions and fuel cracking will result in lower fuel temperature and associated internal gas pressures.

The allowable design internal pressure of 3,300 psi is well above the maximum values of internal pressures calculated for open or closed pellet pores, and the maximum internal pressure should only occur with the maximum diametral clearance condition. An increase in average fuel burnup can be tolerated within the prescribed internal pressure design limits.

It has been indicated in Reference 38 and in AECL-1598 that the UO_2 fuel is plastic enough to flow under low stresses when the temperature is above 1,800 F. That fraction of the fuel below this temperature may retain a large portion of the original porosity and act as a fission gas holder. The hottest axial locations producing the highest clad stresses will have little if any fuel below 1,800 F. However, the ends of the fuel rods will have some fuel below this temperature.

The approximate fraction of the fuel below 1,800 F at overpower for a 1.70 axial power shape is as follows for various cold diametral clearances.

Clearance, in.	Percent of Fuel Below 1,800 F, %
0.0045	40
0.0070	20
0.0095	5

The retention of fuel porosity in the low temperature and low burnup regions will result in modest reductions in internal gas pressure.

i. Hot Channel Factors Evaluation

(1) Rod Pitch and Bowing

A flow area reduction factor is determined for the as-built fuel assembly by taking channel flow area measurements and statistically determining an equivalent hot channel flow area reduction factor. A fuel assembly has been measured, and the results are shown in Table 3-9. Interior channel measurements and measurements of the channels formed by the outermost fuel rods with adjacent assemblies have been analyzed. Coefficients of variation for each type of channel have been determined. In the analytical solution for a channel flow, each channel flow area is reduced over its entire length by the F_A factors shown in Figure 3-20 for the desired population protected at a 99 percent confidence. The hot channels have been analyzed using values for 95 percent population protected, or F_A in the interior cells of 0.98 and F_A in the wall cells of 0.97 as listed in 3.2.3.1.1.j.

Special attention is given to the influence of water gap variation between fuel assemblies when determining rod powers. Nuclear analyses have been made for the nominal, maximum, and minimum spacing between adjacent fuel assemblies. The nominal and maximum hot assembly fuel rod powers are shown in Figures 3-43 and 3-44. The hot channel nuclear power factor ($F^N_{\Delta h}$ nuclear) of 1.78 shown in 3.2.3.1.1 is based on Figure 3-44 for the worst water gap between fuel assemblies. The factor of 1.783 is a product of the hot assembly factor of 1.68 times the 1.061 hot rod factor. This power factor is assigned to the hottest unit cell rod which is analyzed for burnout. Peaking factors for other channels are obtained in a similar manner. In all cases, the combined flow spacing and power peaking producing the lowest DNB ratio is used.

(2) Fuel Pellet Diameter, Density, and Enrichment Factors

Variations in the pellet size, density, and enrichment are reflected in coefficients of variation Numbers 2 through 7 of Table 3-9. These variations have been obtained from the measured or specified tolerances and combined statistically as described in 3.2.3.2.2 to give a power factor on the hot rod. For 99 percent confidence and 95 percent population conditions, this factor, F_Q, is 1.011 and is applied as a power increase over the full length of the hot channel fuel rod. The local heat flux factor, $F_Q"$, for similar conditions is 1.014. These hot channel values are shown in Table 3-1. The corresponding values of F_Q and $F_Q"$ with 99.99 percent population protected are 1.025 and 1.03, respectively. A conservative value of $F_Q"$ of 1.03 for 99 percent confidence and 99.99 percent population is used for finding the maximum fuel linear heat rates as shown in 3.2.3.1.2.

These factors are used in the direct solution for channel enthalpies and are not expressed as factors on enthalpy rise as is often done. The coefficients of variation will be under continuous review during the final design and development of the fuel assembly.

(3) Flow Distribution Effects

Inlet Plenum Effects

The final inlet plenum effects will be determined from the 1/6 scale model flow test now in progress. The initial runs indicate satisfactory flow distribution. Although the final nuclear analysis and flow test data may show that the hot bundle positions receive average or better flow, it has been assumed that the flow in the hot bundle position is 5 percent less than average bundle flow under isothermal conditions corresponding to the model flow test conditions. An additional reduction of flow due to hot assembly power is described below.

Redistribution in Adjacent Channels of Dissimilar Coolant Conditions

The hot fuel assembly flow is less than the flow through an average assembly at the same core pressure drop because of the increased pressure drop associated with a higher enthalpy and quality condition. This effect is allowed for by making a direct calculation for the hot assembly flow. The combined effects of upper and lower plenum flow conditions and heat input to the hot assemblies have been used to determine hot assembly flows. The worst flow maldistribution effect has been assumed in the initial design, and the minimum hot assembly flow has been calculated to be 89 percent of the average assembly flow at 114 percent overpower. Actual hot assembly flows are calculated rather than applying an equivalent hot channel enthalpy rise factor.

00225

Physical Mixing of Coolant Between Channels

The flow distribution within the hot assembly is calculated with a mixing code that allows an interchange of heat between channels. Mixing coefficients have been determined from multirod mixing tests. The fuel assembly, consisting of a 15 x 15 array of fuel rods, is divided into unit, wall, control rod, and corner cells as shown by the heavy lines in Figure 3-43. The mixed enthalpy for every cell is determined simultaneously so that the ratio of cell to average assembly enthalpy rise (Enthalpy Rise Factor) and the corresponding local enthalpy are obtained for each cell. Typical enthalpy rise factors are shown in Figures 3-43 and 3-44 for the hot and surrounding cells. The assumptions used to describe the channels for the peaking and enthalpy rise factors shown are given in 3.2.3.2.3.j, which follows.

j. Evaluation of the DNB Ratios in the Unit, Wall, Control Rod, and Corner Cells

DNB Results at Rated Flow

The DNB ratios in the hot unit cell at the maximum design condition described in 3.2.3.1 are shown in Figure 3-15. The relationship shown is based on the application of the W-3 correlation. An additional sensitivity analysis of the assembly corner, wall, and control rod cells has been made for the worst combination of fuel assembly spacing and power peaking.

The sensitivity of the assembly design with respect to variations of mass velocity (G), channel spacing, mixing intensity, and local peaking on the DNB ratios in the fuel assembly channels has been evaluated by analyzing the nominal conditions and a postulated worst case condition. The summary results are shown below in Table 3-13 for the nominal case and 3-14 for the maximum design or postulated worst case. The unit cell DNB ratios are repeated for comparison. All of the DNB ratios are for 114 percent overpower.

Table 3-13

DNB Ratios in the Fuel Assembly Channels (W-3)

Nominal Case

Cell Type	G, lb/h-ft^2 x 10^{-6}	DNBR (W-3) (114% Power)
Unit	2.55	1.97
Corner	2.59	1.97
Wall	2.59	2.03
Control Rod	2.45	2.15

Table 3-14

DNB Ratios in the Fuel Assembly Channels (W-3)

Postulated Worst Case (Design)

Cell Type	G, lb/h-ft^2 x 10^{-6}	DNBR (W-3) (114% Power)
Unit	2.31	1.71
Corner	2.18	1.81
Wall	2.24	1.78
Control Rod	2.20	1.83

The DNB ratios in all channels are high enough to insure a confidence-population relationship equal to or better than that outlined in 3.2.3.1.1 for the hot unit cell channel. All of the wall, corner, and control rod cells have DNB ratios equal to or lower than that of the unit cell hot channel. This results from a more favorable flow to power ratio in these cells associated with relatively larger flow areas.

The DNB ratios were obtained by comparing the fuel rod local heat fluxes and channel coolant conditions with the limitations predicted by the correlation. Typical results are shown in Figures 3-45 and 3-46 for the nominal and worst case conditions in the unit cell.

Fuel Rod Power Peaks and Cell Coolant Conditions

The nominal case local-to-average rod powers and the local-to-average exit enthalpy rise ratios are shown in Figure 3-43 for the hot corner, wall, control rod, and unit cells in the hot fuel assembly. Values shown are for nominal water gaps between the hot fuel

assembly and adjacent fuel assemblies with nominal flow to hot fuel assembly, and with a minimum intensity of turbulence, α,(*) equal to 0.02.

Additional tests are being run to determine the maximum values of intensity of turbulence associated with the fuel assembly. The expected value is greater than 0.02 since a value of 0.03 is obtained in smooth tubes. The fuel assembly spacer grids will induce turbulence and improve coolant mixing.

The postulated worst case local-to-average rod powers (nuclear peaking factor) and exit enthalpy rise factors in the hot fuel assembly are shown in Figure 3-44. The factors were determined for this case with the minimum water gap between the hot fuel assembly and adjacent fuel assemblies, with minimum flow to the hot fuel assembly, and with a minimum assumed intensity of turbulence, α, equal to 0.02. An evaluation of minimum, nominal, and maximum spacing between assemblies showed the minimum to have the lowest DNB ratios.

A mixing coefficient of 0.02 was used for both nominal and design worst case analyses. Final design values of about 0.06 are likely. The influence of mixing coefficients is shown in Figure 3-29, which shows values ranging from 0.01 to 0.06. The value of 0.02 is sufficiently conservative for design evaluation. The conditions analyzed to obtain the DNB ratios for various values of the mixing coefficients shown in Figure 3-29 were outlined previously in 3.2.3.2.3.i.

Fuel Assembly Power and Rated Flow Conditions

The nominal and postulated worst cases were run at 114 percent reactor power with the nominal and worst $F\Delta h$ factors shown in 3.2.3.1.1.c. The 1.50 modified cosine axial power shape of Figure 3-10 was used to describe the worst axial condition.

The hot assembly flow under nominal conditions without a flow maldistribution effect is 96 percent of the average assembly flow, and the reduction in flow is due entirely to heat input effects. The hot assembly flow under the worst postulated

- - - - -

(*) The intensity of turbulence, α, is defined as

$$\sqrt{v_t'^2}/V$$

where V_t' is the transverse component of the fluctuating turbulent velocity, and V is the coolant velocity in the axial direction. This method of computing mixing is described by Sandberg, R. O., and Bishop, A. A., CVTR Thermal-Hydraulic Design for 65 MW Gross Fission Power, CVNA-227.

00238

conditions is 89 percent of the average assembly flow and considers the worst combined effects of heat input and flow maldistribution.

k. DNB Results for Postulated Loss of an Internals Vent Valve

The reactor arrangement includes vent valves above the core to equalize the pressure between inlet and outlet regions during a loss-of-coolant accident. The effective core flow will be reduced in the unlikely event that a valve disc breaks off. A DNB analysis was made to show the design margin for a postulated accidental failure of one valve disc.

An arrangement consisting of valves with a 14-inch diameter throat was investigated. In the event the disc from one of these valves is completely removed, a small reduction in effective core flow for heat removal will be experienced. Approximately 5.7 percent of the incoming flow will bypass the core through the valve opening. However, the reduction of resistance results in an increase in total system flow of about 1.1 percent. The net reduction of flow for core heat removal is 4.6 percent.

The minimum DNB ratios for the reduced effective core flow compare with the full flow ratios as follows:

Percent Rated Power	DNBR (Full Flow)	DNBR (Reduced Flow)
100	2.21	2.05
107.5 (Trip Set Point)	1.91	1.76
114	1.71	1.55

DNB ratios were determined for the worst corner, control rod, wall, or unit cell. The DNB ratios in the hot unit cell were the lowest. The minimum DNB ratio at the trip set point of 107.5 percent power is well above the minimum recommended value of 1.30. The DNB ratio of 1.30 is maintained up to 123 percent power for the postulated worst case design conditions.

A complete sensitivity analysis has been made to determine the effects of design flow and unexpected core bypass flow from the inlet to the outlet chambers in the reactor vessel. The results are shown in Figure 3-47. Bypass flow was varied from 0 to 10 percent while holding a constant core average temperature of 580 F. A design allowance of 2 percent (2.63×10^6 lb/hr) bypass flow for vent valve seat and fitup leakage is included in all calculations for nominal or maximum design DNB ratios. This design condition is indicated by Line 2 and is identical with rated conditions in Figure 3-15 as previously discussed. Line 5 shows the DNB ratios versus power for a condition of the loss of one vent valve disc

plus a 2 percent bypass. Additional lines are shown for 0, 5, and 10 percent variations in bypass flow.

3.2.3.2.4 Evaluation of Internals Vent Valve

A vapor lock problem could arise if water is trapped in the steam generator blocking the flow of steam from the top of the reactor vessel to a cold leg leak. Under this condition, the steam pressure at the top of the reactor would rise and force the steam bubbles through the water leg in the bottom of the steam generator. This same differential pressure that develops a water leg in the steam generator will develop a water leg in the reactor vessel which could lead to uncovering of the core.

The most direct solution to this problem is to equalize the pressure across the core support shield, thus eliminating the depression of the water level in the core. This can be accomplished by vent valves in the core support shield which provide direct communication between the reactor plenum and the top of the annulus. These vent valves open on a very low-pressure differential to allow steam generated in the core to flow directly to the leak from the reactor vessel. Although the flow path in the steam generator is blocked, this is of no consequence since there is an adequate flow path to remove the steam being generated in the core.

The preliminary design of this valve is shown in Figure 3-51. The valve disc hangs closed in its natural position. A flat, stainless steel seat inclined 5 degrees from vertical insures against flow from the annulus to the upper plenum chamber assembly. In the event of an accident, the reverse pressure differential will open the valve. At all times during normal reactor operation, the pressure in the annulus on the outside of the core support shield is greater than the pressure in the plenum chamber on the inside of the core support shield. Accordingly, the vent valve will be held closed during normal operation. With four reactor coolant pumps operating, the pressure differential is 42 psi resulting in a several thousand pound closing force on the vent valve.

Under accident conditions, the valve will begin to open with a pressure differential in a direction opposite to the normal pressure differential of about 0.3 psi develops. At this point, the opening force on the valve counteracts the natural closing force of the valve. With a pressure differential of no greater than 1.5 psi, the valve would be fully open. With this pressure differential, the water level in the core would be at about the top of the core. In order for the core to be half uncovered, assuming solid water in the bottom half of the core, a pressure differential of 3.7 psi would have to be developed. This would provide an opening force of about 3 times that required to open the valve completely. This is a conservative limit since it assumes equal density in the core and the annulus surrounding the core. The hot, steam-water mixture in the core will have a density much less than that of the cold water in the annulus, and somewhat greater pressure differentials could be tolerated before the core is more than half uncovered.

00230

Assumptions

At the present time, an analog computer simulation is being developed to evaluate the performance of the vent valves in the plenum chamber. This analysis will be used to demonstrate that adequate steam relief exists so that cooling of the core will be accomplished.

The basic model is a simulation of the reactor coolant system which includes the effect of the emergency cooling by the ECCS, the effect of steam generation in the once-through steam generators, the effect of steam generation in the core, and the effect of operation of the vent valves. The model is composed of four basic regions that simulate the water volume in the annulus between the reactor vessel and the core, the water volume in the core, the steam volume above the core water level, and the steam volume in the region between the vent valves and the break location. Fluid flow between each of these regions, flow from the emergency injection system, steam flow through the break, and possible water spillage from the break are all considered. The core volumetric heat generation and heat transfer to a changing water level in a five-section core is considered.

Using the computer program, the required number and capacity of valves will be obtained. Conservative assumptions on core decay heat, flow losses, heat transfer coefficients, and the available capacity from the emergency injection systems will be used.

The exact number of valves and their size will be specified upon completion of this analytical study. The performance of the valves must meet the criterion for core cooling that has been defined in 14.2.2.3.2 of the PSAR and is quoted below:

> "The performance criterion for the emergency core cooling equipment is to limit the clad temperature transient below the clad melting point so that fuel geometry is maintained to provide core cooling capability. This equipment has been conservatively sized to limit the clad temperature transient to 2,300 F or less as temperatures in excess of this value promote a faster zirconium-water reaction rate, and the termination of the transient near the melting point would be difficult to demonstrate."

00231

3.2.4 MECHANICAL DESIGN LAYOUT

3.2.4.1 Internal Layout

Reactor internal components include the plenum assembly and the core support assembly (consisting of the core support shield, vent valves, core barrel, lower grid, flow distributor, in-core instrument guide tubes, thermal shield, and surveillance holder tubes). Figure 3-48 shows the reactor vessel, reactor vessel internals arrangement, and the reactor coolant flow path. Figure 3-49 shows a cross section through the reactor vessel, and Figure 3-50 shows the core flooding arrangement.

Reactor internal components do not include fuel assemblies, orifice rod assemblies, control rod assemblies (CRA), surveillance specimen assemblies, or in-core instrumentation. Fuel assemblies are described in 3.2.4.2, control rod assemblies and drives in 3.2.4.3, surveillance specimen assemblies in 4.4.3, and in-core instrumentation in 7.3.3.

The reactor internals are designed to support the core, maintain fuel assembly alignment, limit fuel assembly movement, and maintain CRA guide tube alignment between fuel assemblies and control rod drives. They also direct the flow of reactor coolant, provide gamma and neutron shielding, provide guides for in-core instrumentation between the reactor vessel lower head and the fuel assemblies, support the surveillance specimen assemblies in the annulus between the thermal shield and the reactor vessel wall, and support the internals vent valves. These vent valves are provided to relieve pressure generated by steaming in the core following a reactor coolant inlet pipe rupture so that the core will remain sufficiently covered with coolant. All reactor internal components can be removed from the reactor vessel to allow inspection of the reactor internals and the reactor vessel internal surface.

In anticipation of lateral deflection of the lower end of the core support assembly as a result of horizontal seismic loadings, integral weld-attached, deflection-limiting spacer blocks have been placed on the reactor vessel inside wall. In addition, these blocks limit the rotation of the lower end of the core support assembly which could conceivably result from flow-induced torsional loadings. The blocks allow free vertical movement of the lower end of the internals for thermal expansion throughout all ranges of reactor operating conditions, but in the unlikely event of a flange, circumferential weld, or bolted joint failure the blocks will limit the possible core drop to 1/4 in. or less. The final elevation plane of these blocks will be established near the same elevation as the vessel support skirt attachment to minimize dynamic loading effects on the vessel shell or bottom head. Preliminary calculations indicate the impact loading on the stop blocks for a 1/4 in. core drop would be approximately 5 g total. Block location and geometry will be evaluated and determined to transfer this loading through the vessel support skirt to the reactor building concrete. A significant reduction in impact loading can be achieved through proper stop block design and detailed analysis. A 1/4 in. core drop will not allow the lower end of the CRA neutron absorber rods to disengage from their respective fuel assembly guide tubes if the CRA are in the full-out position, since approximately 6-1/2 in. of rod length would remain in the fuel assembly guide tubes. A core drop of 1/4 in. will not result in a significant reactivity change. The core cannot rotate and bind the drive lines because rotation of the core support assembly is prevented by the stop blocks.

The failure of the core support shield and core barrel upper flanges, or related flanges and other circumferential joints, is not considered credible on the basis of the conservative design criteria and large safety factors employed in the internals design. The final internals design will be capable of withstanding various combinations of forces and loadings resulting from the static weight of internals (225,000 lb total, not including the plenum assembly which weighs 100,000 lb), core with control rod drive line (303,000 lb total), dynamic load from trip (10 g gives 207,000 lb), seismic (0.10 g vertical gives 53,000 lb), coolant flow hydraulic loading (230,000 lb), and other related loadings. The algebraic sum of this simplified loading case is 559,000 lb. This results in a tensile stress of about 585 psi in the core support shield shell, which is approximately 3 percent of the material yield strength. Final internals component weights, seismic analysis, dynamic loadings from flow-induced vibration, detailed stress analysis with consideration for thermal stress during all transients, and resolution of fabrication details such as shell rolling tolerances and weld joint preparation details will increase the stress levels listed above. As a final design criterion, the core support components will meet the stress requirements of the ASME Code, Section III, during normal operation and transients. The structural integrity of all core support circumferential weld joints in the internals shells will be insured by compliance with the radiographic inspection requirements in the code above. The seismic analysis will include detailed calculations to determine the maximum structural response of the reactor vessel and internals. This analysis will be performed as described in 3.1.2.4.

In the event of a major loss-of-coolant accident, such as a 36-in. diameter reactor coolant pipe break near the reactor vessel outlet, the fuel assembly and vessel internals would be subjected to dynamic loadings resulting from an oscillating differential pressure across the core. Some deflection of the internals structures would occur, but internals component failure will not occur. The occurrence of a loss-of-coolant accident and resulting loadings will be evaluated during the detailed design period for the fuel assemblies and related internals structural components.

The deflections and movements described above would not prevent CRA insertion because the control rods are guided throughout their travel, and the guide-to-fuel-assembly alignment cannot change regardless of related component deflections. CRA trip could conceivably be delayed momentarily as a result of the oscillating pressure differential. However, the CRA travel time to full insertion would remain relatively unaffected as transient pressure oscillations are dampened out in approximately 0.5 sec. On this basis, the CRA travel time to 2/3 insertion on a trip command will be approximately 1.6 sec instead of the specified 1.40 sec. Also, this possible initial minor delay in trip initiation would not contribute to the severity of the loss-of-coolant accident because at the initiation of CRA trip, the core would be subcritical from voids.

Material for the reactor internals bolting will be subjected to rigid quality control requirements to insure structural integrity. The bolts will be inspected for surface flaw indications after all fabrication operations have been completed. Torque values will be specified for the final assembly to develop full-bolting capability. All fasteners will be lock-welded to insure assembly integrity.

3.2.4.1.1 Plenum Assembly

The plenum assembly is located directly above the reactor core and is removed as a single component before refueling. It consists of a plenum cover, upper grid, CRA guide tube assemblies, and a flanged plenum cylinder with openings for reactor coolant outlet flow. The plenum cover is a series of parallel flat plates intersecting to form square lattices with a perforated top plate and flange, and is attached to the plenum cylinder top flange. Three lifting lugs are provided for the plenum assembly handling. The CRA guide tubes are welded to the plenum cover top plate and bolted to the upper grid. CRA guide assemblies provide CRA guidance and protect the CRA from the effects of coolant cross-flow, and provide structural attachment of the grid assembly to the plenum cover.

Each CRA guide assembly consists of an outer tube housing, a mounting flange, 12 perforated slotted tubes and four sets of tube segments which are properly oriented and attached to a series of castings to provide continuous guidance for the CRA full stroke travel. Design clearances in the guide tube will accommodate some degree of misalignment between the CRA guide tubes and the fuel assemblies. Final design clearances will be established by tolerance studies and by the results of the Control Rod Drive Line Facility (CRDL) prototype tests. Preliminary test results are described in 3.2.4.3.5.

The upper grid assembly consists of parallel flat bars intersecting to form square lattices. The bars are attached to a flange which is bolted to the plenum cylinder lower flange. The upper grid assembly locates the lower end of the individual CRA guide tube assembly relative to the upper end of the corresponding fuel assembly.

Locating keyways in the plenum assembly cover flange engage the reactor vessel top flange locating keys to align the plenum assembly with the reactor vessel, reactor closure head control rod drive penetrations, and the core support assembly. The bottom of the plenum assembly is guided by the inside surface of the lower flange of the core support shield.

3.2.4.1.2 Core Support Assembly

The core support assembly consists of the core support shield, core barrel, lower grid assembly, flow distributor, thermal shield, in-core instrument guide tubes, surveillance specimen holder tubes, and internals vent valves.

Static loads from the assembled components and fuel assemblies, and dynamic loads from CRA trip, hydraulic flow, thermal expansion, seismic disturbances, and loss-of-coolant accident considerations, are all carried by the core support assembly.

The core support assembly components are described as follows:

a. Core Support Shield

The core support shield is a large flanged cylinder which mates with the reactor vessel opening. The top flange rests on a circumferential ledge in the reactor vessel top closure flange. The core support shield lower flange is bolted to the core barrel. The cylinder wall

has two nozzle openings for reactor coolant outlet flow. The inside surface of the lower flange guides and aligns the plenum assembly relative to the core support shield. Three lifting lugs are provided to handle the core support shield. These lugs are also used to handle the core support assembly.

The core support shield outlet nozzles are sealed to the reactor vessel outlet nozzles by the differential thermal expansion between the stainless steel core support shield and the carbon steel reactor vessel. The nozzle seal surfaces are finished and fitted to a predetermined cold gap providing clearance during core support assembly installation and removal. At reactor operating temperature the mating metal surfaces are in contact to make a seal without exceeding allowable stresses in either the reactor vessel or internals. Internals vent valves are installed in the core support shield cylinder wall to relieve the pressure generated by steaming in the core following a postulated cold leg (reactor coolant inlet) pipe rupture (see 3.2.4.1).

b. Core Barrel

The core barrel supports the fuel assemblies, lower grid, flow distributor, and in-core instrument guide tubes. The core barrel consists of a flanged cylinder, a series of internal former plates bolted to the cylinder, and a series of baffle plates bolted to the inner surfaces of the former plates to form an inner wall enclosing the fuel assemblies. Construction of the core barrel will be similar to that of the reactor internals component developed by B&W for the Indian Point Station Unit No. 1.

Coolant flow is downward along the outside of the core barrel cylinder and upward through the fuel assemblies contained in the core barrel. A small portion of the coolant flows upward through the space between the core barrel cylinder and the baffle plate wall.

The upper flange of the core barrel cylinder is bolted to the mating lower flange of the core support shield assembly, and the lower flange is bolted to the mating flange of the lower grid assembly. All bolts will be inspected and installed as described in 3.2.4.1, and will be lock-welded after final assembly. Lifting lugs attached to the core barrel are provided for core support assembly handling.

c. Lower Grid Assembly

The lower grid assembly provides alignment and support for the fuel assemblies, supports the thermal shield and flow distributor, and aligns the in-core instrument guide tubes with the fuel assembly instrument tubes. The lower grid consists of two lattice structures separated by short tubular columns surrounded by a flanged cylinder. The top flange is bolted to the lower flange of the core barrel. A perforated flat plate located midway between the two lattice structures aids in distributing coolant flow.

d. Flow Distributor

The flow distributor is a perforated, dished head with an external flange which is bolted to the bottom flange of the lower grid. The flow distributor supports the in-core instrument guide tubes and distributes the reactor coolant entering the bottom of the core.

e. Thermal Shield

A cylindrical, stainless steel, thermal shield is installed in the annulus between the core barrel cylinder and the reactor vessel inner wall. The thermal shield reduces the neutron and gamma internal heat generation in the reactor vessel wall and thereby reduces the resulting thermal stresses.

The thermal shield is supported on, positioned by, and attached to the lower grid top flange. The thermal shield upper end is positioned by spacers between the thermal shield and the core barrel outer cylinder to minimize the possibility of thermal shield vibration. The thermal shield attachment is designed to avoid shear loads on fasteners. All fasteners are lock-welded after final assembly.

f. Surveillance Specimen Holder Tubes

Surveillance specimen holder tubes are installed on the core support assembly outer wall to contain the surveillance specimen assemblies. The tubes extend from the top flange of the core support shield to the lower end of the thermal shield. The tubes will be rigidly attached to prevent flow-induced vibration. Slip joints at the intermediate supports and top end of the assemblies accommodate axial motion caused by differential thermal expansion.

g. In-Core Instrument Guide Tube Assembly

The in-core instrument guide tube assemblies guide the in-core instrument assemblies between the instrume penetrations in the reactor vessel bottom head and the instrument tubes in the fuel assemblies. Minor horizontal misalignment is accommodated between the reactor vessel instrument penetrations and the instrument guide tubes assembled with the flow distributor. A perforated shroud tube, concentric with the instrument guide tube, adds rigidity to the assembly and reduces the effect of coolant flow forces. Forty-six in-core instrument guide tubes are provided. The in-core instrument guide tubes are designed so they will not be affected by the core drop described in 3.2.4.1.

h. Internals Vent Valves

Internals vent valves are installed in the core support shield to prevent a pressure unbalance which might interfere with core cooling following a loss-of-coolant accident. Under all normal operating conditions, the vent valves will be closed. In the event of a loss-of-coolant accident in the cold leg of the reactor loop, the valves

will open to permit steam generated in the core to flow directly to the leak and will prevent the core from becoming more than 1/2 uncovered after emergency core coolant has been supplied to the reactor vessel. The design of the internals vent valve is shown in Figure 3-51.

Each valve assembly consists of a hinged disc, valve body with sealing surfaces, split-retaining ring, and fasteners. Each valve assembly is installed into a machined mounting ring, integrally welded in the core support shield wall. The mounting ring contains the necessary features to retain and seal the perimeter of the valve assembly. Also, the mounting ring includes an alignment device to maintain the correct orientation of the valve assembly for hinged-disc operation. Each valve assembly will be remotely handled as a unit for removal or installation. Valve component parts, including the disc, are of captured-design to minimize the possibility of loss of parts to the coolant system, and all fasteners include a positive locking device. The hinged-disc includes a device for remote inspection of disc function.

The arrangement consists of 14-in. diam vent valve assemblies installed in the cylindrical wall of the internals core support shield (refer to Figure 3-48). The valve centers are coplanar and are 42 in. above the plane of the reactor vessel coolant nozzle centers. In cross section, the valves are spaced around the circumference of the core support shield wall.

The hinge assembly consists of a shaft, two valve body journal receptacles, two valve disc journal receptacles, and four flanged shaft journals (bushings). Loose clearances are used between the shaft and journal inside diameters, and between the journal outside diameters and their receptacles.

This feature provides eight loose rotational clearances to minimize any possibility of impairment of disc-free motion in service. In the event that one rotational clearance should bind in service, seven loose rotational clearances would remain to allow unhampered disc-free motion. In the worst case, at least four clearances must bind or seize solidly to affect adversely valve disc-free motion.

In addition, the valve disc contains a self-alignment feature so that the external differential pressure adjusts the disc seal face to the valve body seal face. This feature minimizes the possibility of increased leakage and pressure-induced deflection loadings on the hinge parts in service.

The external side of the disc is contoured to absorb the impact load of the disc on the reactor vessel inside wall without transmitting excessive impact loads to the hinge parts as a result of a loss-of-coolant accident.

3.2.4.2 Fuel Assemblies

3.2.4.2.1 Description

a. General Description

The fuel for the reactor is sintered pellets of low-enriched uranium dioxide clad in Zircaloy-4 tubing. The clad, fuel pellets, end caps, and the fuel support components form a "Fuel Rod." Two hundred and eight fuel rods, 16 control rod guide tubes, one instrumentation tube, eight spacer grids, and two end fittings make up the basic "Fuel Assembly" (Figure 3-52). The guide tubes, spacer grids, and end fittings form a structural cage which contains the 208 fuel rods in a 15 x 15 array. The center position in the assembly is reserved for instrumentation. The remaining 16 locations in the array are provided for the guide tubes which guide the control rods and provide the vertical support of the assembly.

The complete core has 177 fuel assemblies which are arranged on a square lattice to approximate the shape of a cylinder. All assemblies are identical in mechanical construction and interchangeable in the core and are designed to accept the control rod assemblies (CRA). The reactivity of the core under operating conditions is controlled by 57 CRA, of which 8 are xenon control rod assemblies. These xenon control rod assemblies are identical in physical configuration to the CRA but have poison in the lower portion of the rod only. In the fuel assemblies containing no CRA, an orifice rod assembly (Figure 3-53) or a burnable poison rod assembly (Figure 3-54) is inserted into the upper ends of the guide tubes. These assemblies minimize guide tube bypass coolant flow. The lumped burnable poison rod assemblies allow a lower boric acid concentration in the reactor coolant, thereby lowering the moderator temperature coefficient. Because of mechanical and geometric identity, the CRA, xenon control rods, burnable poison rod assemblies, and orifice rod assemblies are designed to be interchangeable among fuel assemblies.

00238

Table 3-15

Fuel Assembly Components, Materials, and Dimensions

Item	Material	Dimensions, in.
Fuel	UO_2 Sintered Pellets	0.370 diam
Fuel Clad	Zircaloy-4	0.430 OD x 0.377 ID x 152.875 long
Fuel Rod Pitch		0.568
Fuel Assembly Pitch		8.587
Active Fuel Length		144
Overall Length		≈165
Control Rod Guide Tube	Zircaloy-4	0.530 OD x 0.015 wall
Instrumentation Tube	Zircaloy-4	0.530 OD x 0.402 ID
Spacer Grid	Inconel-718 Strips	0.016 thick
End Fittings	Stainless Steel, Tp-304	

b. Fuel

The fuel is sintered and ground pellets of uranium dioxide which are fabricated from previously unirradiated material. These slightly enriched pellets are right circular cylinders with dished ends and a ground diameter. The pellet ends are dished to minimize the difference in axial expansion between the fuel and the cladding. The nominal density of the fuel is 93.5 percent of theoretical.

Average design burnup of the fuel is 27,490 MWd/MTU. Peak design burnup is 55,000 MWd/MTU. At the peak burnup, the fuel growth is calculated to be 9-1/2 volume percent by the method given in Reference 49. Radial growth of the fuel during burnup is accommodated by pellet porosity, by radial clearance between the pellets and the cladding, and by a small amount of permanent strain in the cladding.

Below each fuel column is a support that axially locates the bottom of the fuel column and separates the fuel from the lower end cap. Means are provided at the top to maintain the fuel column in place during shipping and handling.

Fission gas release from the fuel is accommodated by voids within the fuel, by the radial gap between the pellets and the cladding, and by a void space at the top and bottom ends of the fuel rods.

c. Fuel Assembly Structure

(1) General

The fuel assembly shown in Figure 3-52 is the canless type in which the spacer grids, end fittings, and the guide tubes form the basic structure. Fuel rods are supported at each spacer grid by contact points integral with the walls of the fuel cell boundary. The guide tubes are permanently attached to the upper and lower end fittings tying the assembly together. The use of similar material in the guide tubes and the fuel rods results in minimum differential thermal expansion. The fuel rods bottom on the grid of the lower end fitting.

(2) Spacer Grids

Spacer grids are constructed from strips which are slotted and fitted together in "eggcrate" fashion. Each grid has 32 strips, 16 perpendicular to 16, which form the 15 x 15 lattice for the fuel rods. The square walls formed by the interlaced strips provide support for the fuel rods in two perpendicular directions. Contact points on the walls of each square opening are integrally punched dimples in the strips.

(3) Lower End Fitting

The lower end fitting positions the assembly when inserted in the lower core grid plate and supports the fuel assembly weight. The lower ends of the fuel rods rest on the grid of the lower end fitting. Penetrations in the fitting are provided for attaching the control rod guide tubes and for access of the instrumentation tube.

(4) Upper End Fitting

The upper end fitting positions the upper end of the fuel assembly in the upper core grid plate structure and provides means for coupling the handling equipment. An identifying number on each upper end fitting provides positive identification when handling.

An internal hollow post, welded in the center of the end fitting provides means for retention of the orifice rod assembly and burnable poison rod assembly.

Attached to the upper end fittings are four holddown springs. These springs provide a positive holddown margin to oppose hydraulic forces.

00240

(5) Control Rod Guide Tubes

The Zircaloy guide tubes provide continuous guidance to the control rods within the fuel assembly during operation and provide structural continuity for the fuel assembly. Welded to each end of a guide tube are flanged and threaded sleeves, which attach the tubes to the end fittings by lock-welded nuts. Radial restraint of the guide tubes is provided by the spacer grids.

(6) Instrumentation Tube

This Zircaloy tube serves as a channel to guide, position, and contain the in-core instrumentation in the center of the fuel assembly. The instrumentation string is guided up through the lower end fitting and through the tube to the desired core elevation. The instrumentation tube provides no structural support of the assembly and is retained axially by the end fittings and radially by the spacer grids.

00241

3.2.4.2.2 Evaluation

a. Fuel Rod Assembly

(1) General

The basis for the design of the fuel rod is discussed in 3.1.2.4. Materials testing and actual operation in reactor service with Zircaloy cladding have demonstrated that Zircaloy-4 material has sufficient corrosion resistance and mechanical properties to maintain the integrity and serviceability required for design burnup.

(2) Clad Stress and Strain

The cladding of fuel rods is subjected to hydrostatic pressure, gradually increasing internal pressure, thermal stresses, vibration, and to the effects of differential expansion of the fuel and cladding caused by thermal expansions and by fuel growth due to irradiation effects. In addition, the properties of the cladding are influenced by thermal and irradiation effects, which are analyzed below.

Stress analysis for cladding is based on several conservative assumptions that make the actual margins of safety greater than those calculated. For example, it is assumed that the clad with the thinnest wall, the smallest fuel-clad gap, and the greatest ovality permitted by the specification is operating in the region of the core where performance requirements are most severe. Fission gas release rates, fuel growth, and changes in mechanical properties with irradiation are based on a conservative evaluation of currently available data. Thus, it is unlikely that failure of the cladding will result during operation.

Pressure Effects

Clad stresses due to external and internal pressure are considerably below the yield strength. Circumferential stress due to external pressure, calculated using those combinations of clad dimensions, ovality, and eccentricity that produce the highest stress, is shown in Table 3-16. The maximum stress of 33,000-psi compression, at the system design pressure of 2,500 psi, is the sum of 22,000-psi compressive membrane stress plus 11,000-psi compressive bending stress due to ovality at the clad OD in the expansion void and at the beginning of life. The maximum stress in the heat-producing zone is 32,000 psi at design pressure and 27,000 psi at operating pressure. At this stress, the material may creep enough to allow an increase in ovality until further creep is restrained by support from the fuel. Contact loads between fuel and cladding for this case are about 20 lb/in. of length.

At the end of life, fission gas pressure may exceed operating pressure when the fuel rod is at operating temperature. The calculation of fission gas release is discussed in 3.2.3.2.3.h. The value of 3,300 psi is used as a design internal pressure. The maximum design pressure differential of 1,115 psi gives a resultant circumferential stress of 9,000 psi. This is about 1/4 of the yield strength and, therefore, is not a potential source of short-time burst. The possibility of stress-rupture burst has been investigated using finite-difference methods to estimate the long-time effects of the increasing pressure on the clad. The predicted pressure-time relationship produces stresses that are less than 1/3 of the stress levels that would produce stress rupture at the end of life. Outpile stress-rupture data were used, but the greater than 3:1 margin on stress is more than enough to account for decreased stress-rupture strength due to irradiation.

Table 3-16

Clad Circumferential Stresses

Operating Condition	Calc. Stress, psi	Yield Stress, psi	Ultimate Tensile Stress, psi
1. BOL[a] - Operating at Design Pressure			
Conditions			
Total Stress (Membrane + Bending) Due to 2,500 psig System Design Pressure Minus 100 psig Fuel Rod Internal Pressure			
Stress			
Average Clad Temperature - Approximately 625 F (Expansion Void)	-33,000	46,000	
2. EOL - Maximum Overpower			
Conditions			
System Pressure - 2,185 psig			
Fuel Rod Internal Pressure - 3,300 psig			
Average Temperature Through Clad Thickness at Hot Spot - Approximately 725 F			
Stress			
Pressure Stress Only[b]	9,000		
Including 4,000 psi Thermal Stress	13,000	36,000	38,000
3. EOL - Shutdown			
Immediately After Shutdown			
Conditions			
Syste Pressure - 2,200 psig			
Fuel Rod Internal Pressure - 1,750 psig			

(a) Cladding will be specified with 45,000 psi minimum yield strength and 10 percent minimum elongation, both at 650 F. Minimum room temperature strengths will be approximately 75,000 psi yield strength (0.2 percent offset) and 95,000 psi ultimate tensile strength.

(b) Cladding stresses due to fuel swelling are discussed further on another page of 3.2.4.2.2.

Table 3-16 (Contd)

Operating Condition	Calc. Stress, psi	Yield Stress, psi	Ultimate Tensile Stress, psi
Stress			
Average Clad Temperature - Approximately 575 F	-4,000	45,000	48,000
3 Hours Later			
Conditions			
(50 F/h Pressurizer Cooldown Rate)			
Fuel Rod Internal Pressure - 1,050 psig			
System Pressure - 680 psig			
Stress			
Average Clad Temperature - Approximately 425 F	3,300	52,000	55,000

The total production of fission gas in the hottest fuel rod assembly is based on the hot rod average burnup of 38,000 MWd/MTU. The corresponding maximum design burnup at the hot fuel rod midpoint is 55,000 MWd/MTU.

The fission gas release is based on temperature versus release fraction as shown in Figure 3-36. Fuel temperatures are calculated for small radial and axial increments. The total fission gas release is calculated by integrating the incremental releases.

The maximum release and gas pressure buildups are determined by evaluating the following factors for the most conservative conditions:

(a) Gas conductivity at the end of life with fission gas present.

(b) Influence of the pellet-to-clad radial gap and contact heat transfer coefficient on fuel temperature and release rate.

(c) Unrestrained radial and axial thermal growth of the fuel pellets relative to the clad.

(d) Hot rod local peaking factors.

(e) Radial distribution of fission gas production in the fuel pellets.

00245

(f) Fuel temperatures at reactor design overpower.

The fuel temperatures used to determine fission gas release and internal gas pressure have been calculated at the reactor overpower condition (114 percent). Fuel temperatures, total free gas volume, fission gas release, and internal gas pressure have been evaluated for a range of initial diametral clearances. This evaluation shows that the highest internal pressure results when the maximum diametral gap is assumed because of the resulting high average fuel temperature. The release rate increases rapidly with an increase in fuel temperature, and unrestrained axial growth reduces the relatively cold gas end plenum volumes. A conservative ideal thermal expansion model is used to calculate fuel temperatures as a function of initial cold diametral clearance. Considerably lower resistance to heat transfer between the fuel and clad is anticipated at the end of life due to fuel fracture, swelling, and densification. The resulting maximum fission gas release rate is 43 percent.

Collapse Margins

Short-time collapse tests have demonstrated a clad collapsing pressure in excess of 4,000 psi at expansion void maximum temperature. Collapse pressure margin is approximately 1.7. Extrapolation to hot spot average clad temperature (≈725 F) indicates a collapse pressure of 3,500 psi and a margin of 1.4, which also greatly exceeds requirement. Outpile creep collapse tests have demonstrated that the clad meets the long-time (creep-collapse) requirement.

Fuel Irradiation Growth and Fuel-Clad Differential Thermal Expansion

The results of tests and the operation of Zircaloy-clad UO_2 fuel rods indicate that the rods can be safely operated to the point where total permanent strain is 1-1/2 percent, or higher, in the temperature range applicable to PWR cladding.(50) The allowable design strain is about 1 percent (3.1.2.4.2.c).

Fuel rod operating conditions pertinent to fuel swelling considerations are listed below for end-of-life conditions.

Burnup (Design Value), MWd/MTU	55,000
Minimum Fuel-to-Clad Gap (Beginning of Life), in.	0.0045
Pellet Nominal Diameter, in.	0.370
Pellet Density (Percent of Theoretical), %	93.5
Cladding (Zircaloy-4), in.	0.0265 Wall

The capability of Zircaloy-clad UO_2 fuel in solid rod form to perform satisfactorily in service has been demonstrated through operation of the SA-1 assembly in the Dresden and Shippingport cores, and through results of their supplementary development programs, up to approximately 40,000 MWd/MTU.

As outlined below, existing experimental information supports the various individual design parameters and operating conditions up to and perhaps beyond the maximum design burnup of 55,000 MWd/MTU, but not in a single experiment. However, the B&W High Burnup Irradiation Program currently in progress does combine the primary items of concern in a single experiment, and the results will be available to contribute to the final design.

Application of Experimental Data to Design Adequacy of the Clad-Fuel Initial Gap To Accommodate Clad-Fuel Differential Thermal Expansion

Experimental Work

Six rabbit capsules, each containing three Zr-2 clad rods of 5-in. fuel length, were irradiated in the Westinghouse Test Reactor[51] at power levels up to 24 kW/ft. The 94 percent theoretical density (TD) UO_2 pellets (0.430 OD) had initial clad-fuel diametral gaps of 6, 12, and 25 mils. No dimensional changes were observed. Central melting occurred at 24 kW/ft only in the rods that had the 25 mil initial gap.

Two additional capsules were tested.[52] The specimens were similar to those described above except for length and initial gap. Initial gaps of 2, 6, and 12 mils were used in each capsule. In the A-2 capsule, three 38-in.-long rods were irradiated to 3,450 MWd/MTU at 19 kW/ft maximum. In the A-4 capsule, four 6-in.-long rods were irradiated to 6,250 MWd/MTU at 22.2 kW/ft maximum. No central melting occurred in any rod, but diameter increases up to 3 mils in the A-2 capsule and up to 1.5 mils in the A-4 capsule were found in the rods with the 2 mil initial gap.

Application

In addition to demonstrating the adequacy of Zircaloy-clad UO_2 pellet rods to operate successfully at the power levels of interest (and without central melting), these experiments demonstrate that the design initial clad-fuel gap of 4 to 8 mils is adequate to prevent unacceptable clad diameter increase due to differential thermal expansion between the clad and the fuel at beginning of life. A maximum local diametral increase of less than 0.001 in. is indicated for fuel rods having the minimum initial gap, operating at the maximum overpower condition.

Adequacy of the Available Voids To Accommodate Differential Expansion of Clad and Fuel, Including the Effects of Fuel Swelling

Experimental Work

Zircaloy-clad, UO_2 pellet-type rods have performed successfully in the Shippingsport reactor up to approximately 40,000 MWd/MTU. Bettis Atomic Power Laboratory[49] has irradiated plate-type UO_2 fuel (96-98 percent TD) up to 127,000 MWd/MTU and at fuel center temperatures between 1,300 and 3,800 F. This work indicates fuel swelling rates of 0.16 percent $\Delta V/10^{20}$ f/cc until fuel internal voids are filled, then 0.7 percent $\Delta V/10^{20}$ f/cc after internal voids are filled. This point of "breakaway" appears to be independent of temperature over the range studied and dependent on clad restraint and the void volume available for collection of fission products. The additional clad restraint and greater fuel plasticity (from higher fuel temperatures) of rod-type elements tend to reduce these swelling effects by providing greater resistance to radial swelling and lower resistance to longitudinal swelling than was present in the plate-type test specimens.

This is confirmed in part by the work of Frost, Bradbury, and Griffiths of Harwell[53] in which 1/4-in. diameter UO_2 pellets clad in 0.020 in. stainless steel with a 2 mil diametral gap were irradiated to 53,300 MWd/MTU at a fuel center temperature of 3,180 F without significant dimensional change.

In other testing[54] 0.150-in. OD, 82-96 percent TD oxide pellets (20 percent Pu, 80 percent U) clad with 0.016-in. stainless steel with 6-8 mil diametral gaps have been irradiated to 77,000 MWd/MTU at fuel temperatures high enough to approach central melting without apparent detrimental results. Comparable results were obtained on rods swaged to 75 percent TD and irradiated to 100,000 MWd/MTU.

Application

Based on the BAPL experimental data, swelling of the fuel rods is estimated as outlined below.

The fuel is assumed to swell uniformly in all directions, conservatively neglecting axial plastic flow into the end dishes. Thermal expansions are calculated as described in 3.2.3.2.3.g. If the fuel cracks, the crack voids are assumed to be available to absorb fuel growth.

The external effect of fuel swelling is assumed to occur at 0.16 percent $\Delta V/10^{20}$ f/cc until the as-fabricated void

in the 93.5 percent pellets is filled. From that time on, swelling is assumed to take place at 0.7 percent $\Delta V/10^{20}$ f/cc until the maximum burnup of 13.6 x 10^{20} f/cc (55,000 MWd/MTU) is reached.

Studies of clad strain at various gaps indicate that the rod with the minimum gap experiences the greatest clad strain in spite of its improved gap conductivity. Clad permanent strain reaches a maximum at the end of life, and is 0.7 percent for nominal density fuel. Clad strain for fuel rods with maximum density allowed by the specification will also meet the design's maximum allowable permanent strain.

Fuel Swelling Studies at B&W

Experimental fuel swelling studies under inpile conditions simulating large reactor environments are under way. Parameters contributing to swelling are burnup, heating rate, fuel density and grain size, and clad restraint. These are being studied systematically by irradiating a series of capsules containing fuel rods. Test variables are shown in Table 3-17, and the program's schedule is given in Table 3-18. See also 3.3.3.3.3.

Test variables include heat rate, burnup, clad thickness, and fuel-to-clad gap. Postirradiation examination will include investigation of dimensional changes, metallographic examination of fuel and cladding, fission gas release correlations with test conditions, and other related observations.

Table 3-17
B&W High Burnup Irradiation Program - Capsule Fuel Test

Identification			Burnup			Heat Rate			
Capsule	Fuel Rod	Irradiation Facility	MWD/MTU $x 10^{-3}$	Fissions/cc $x 10^{-20}$(1)	Irradiation Time, calendar months(2)	Initial, kw/ft	Final, kw/ft	Diametral Gap, mils	Clad Thickness, mils
B-1	B-1	RS-3	10	2.5	4	18	17.5	4-5	25
	B-2			2.5			17.5	7-8	25
	B-3			2.5			17.5	7-8	15
B-2	B-20	RS-4	17	3.8	10	18	16.9	Powder	25
	B-19		26	6.5			16.9	4-5	25
B-3	B-7	RS-6	30	[illegible].5	11	18	16.1	4-5	25
	B-8			7.5			16.1	7-8	25
	B-9			7.5			16.1	7-8	15
B-4	B-10	RS-1	45	10.05	17	18	14.9	Powder	25
	B-11			11.25			14.9	4-5	25
B-5	B-13	RS-5	55	13.75	21	18	14.1	4-5	25
	B-14			13.75			14.1	7-8	25
	B-15			13.75			14.1	7-8	15
B-6	B-31	RS-2	70	15.63	26	18	13.3	Powder	25
	B-17			17.5			13.3	7-8	25
B-7	B-5	RS-5	80	17.87	30	18	12.5	Powder	25
	B-4			20.0			12.5	7-8	25
B-8	B-22	RL-1	30	7.5	11	21-1/2	20.5	4-5	25
	B-23			7.5			20.5	7-8	25
	B-33			7.5			20.5	7-8	15
B-9	B-25	RL-2	55	13.75	21	21-1/2	19.3	4-5	25
	B-26			13.75			19.3	7-8	25
	B-27			13.75			19.3	7-8	15
B-10	B-28	RL-3	80	20.0	30	21-1/2	17.8	7-8	25
	B-29			20.0			17.8	7-8	25
	B-30			20.0			17.8	7-8	15
B-11	B-24	RL-4	70	17.5	26	21-1/2	16.5	7-8	15
	B-34			17.5			16.5	7-8	25
	B-35			17.5			16.5	7-8	25
B-12	B-16	RS-3	65	14.50	24	18	13.3	Powder	25
	B-32			16.24			13.3	7-8	15

(1) Based on 200 Mev per fission.

(2) Based on 80 per cent reactor efficiency.

Table 3-18

B&W High Burnup Irradiation Program Schedule

(Based on BAW-TM-192)

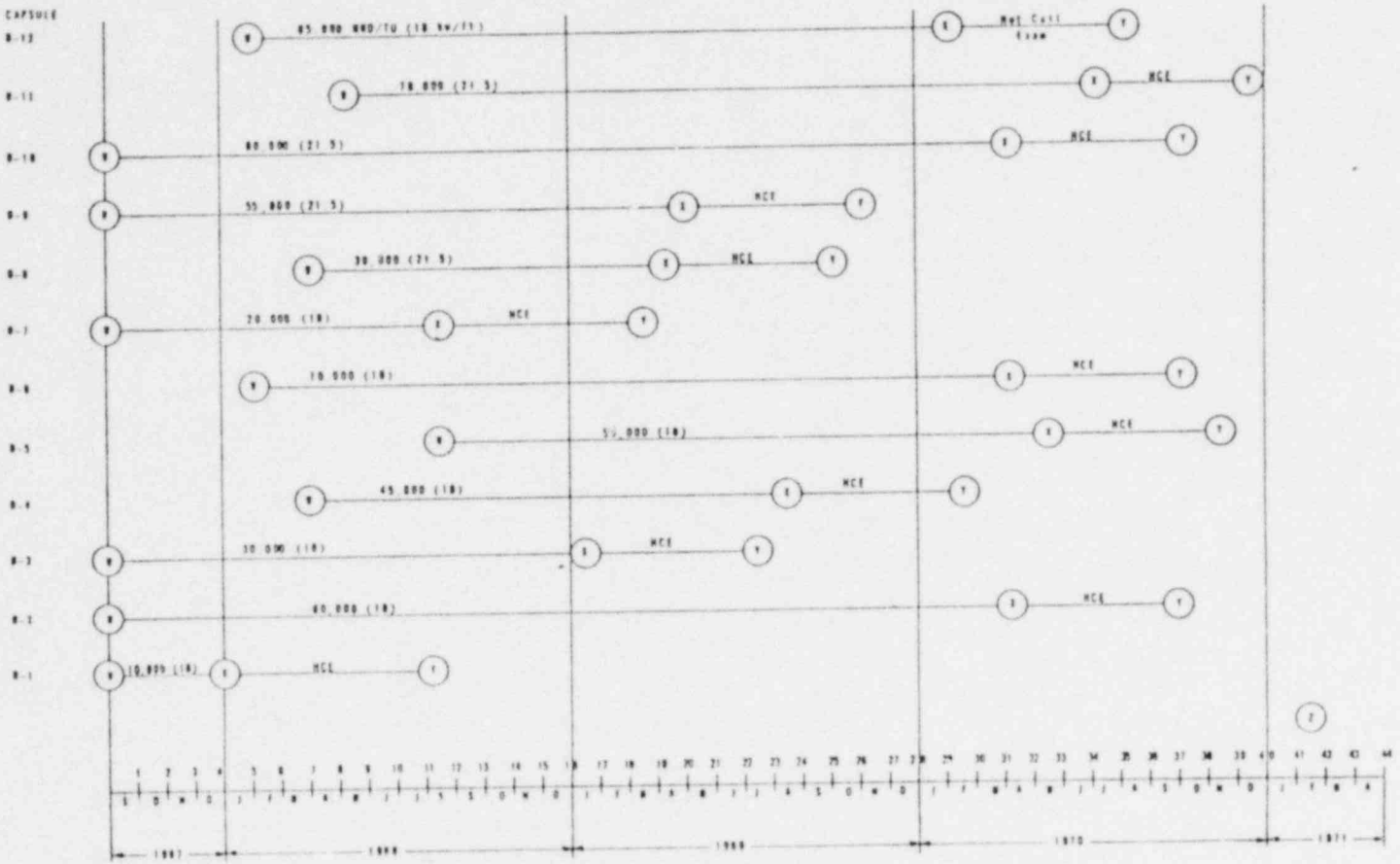

LEGEND

B - Start irradiation

E - Complete irradiation

I - Interim Report Issued

F - Final Report Issued

Capsules B-1 thru B-13

Effect of Zircaloy Creep

The effect of Zircaloy creep on the amount of fuel rod growth due to fuel swelling has been investigated. Clad creep has the effect of producing a nearly constant total pressure on the clad ID by permitting the clad diameter to increase as the fuel diameter increases. Based on out-of-pile data,(55) 1 percent creep will result in 10,000 h (corresponding approximately to the end-of-life diametral swelling rate) from a stress of about 22,000 psi at the 720 F average temperature through the clad at the hot spot. At the start of this high swelling period (roughly the last 1/3 of the core life), the reactor coolant system pressure would more or less be balanced by the rod internal pressure, so the total pressure to produce the clas stress of 22,000 psi would have to come from the fuel. Contact pressure would be 2400 psi. At the end of life, the rod internal pressure exceeds the system pressure by about 1100 psi, so the clad fuel contact pressure would drop to 1300 psi. Assuming that irradiation produces a 3:1 increase in creep rates, the clad stress for 1 percent strain in 10,000 h would drop to about 15,000 psi. Contact pressures would be 1800 psi at the beginning of the high swelling period, 700 psi at the end of life. Since the contact pressure was assumed to be 825 psi in calculating the contact coefficient used to determine the fuel pellet thermal expansion, there is only a short period at the very end of life (assuming the 3:1 increase in creep rates due to irradiation) when the pellet is slightly hotter than calculated. The effect of this would be a slight increase in pellet thermal expansion and therefore in clad strain. Considering the improbability that irradiation will actually increase creep rates by 3:1, no change is anticipated.

b. Overall Assembly

(1) Assurance of Control Rod Assembly Free Motion

The 0.060 in. diametral clearance between the control rod guide tube and the control rod is provided to cool the control rod and to insure adequate freedom to insert the control rod. As indicated below, studies have shown that fuel rods will not bow sufficiently to touch the guide tube. Thus, the guide tube will not undergo deformation caused by fuel rod bowing effects. Initial lack of straightness of fuel rod and guide tube, plus other adverse tolerance conditions, conceivably could reduce the 0.093 in. nominal gap between fuel rod and guide tube to a minimum of about 0.055 in., including amplification of bowing due to axial friction loads from the spacer grid. The maximum expected flux gradient of 1.176 across a fuel rod will produce a temperature difference of 12 F, which will result in a thermal bow of less than 0.002 in. Under these conditions, for the fuel rod to touch the guide tube, the thermal gradient across the fuel rod diameter would have to be on the order of 300 F.

The effect of a DNB occurring on the side of a fuel rod adjacent to a guide tube would result in a large temperature difference. In this case, however, investigation has shown that the clad temperature would be so high that insufficient strength would be available to generate a force of sufficient magnitude to cause a significant deflection of the guide tube. In addition, the guide tube would experience an opposing gradient that would resist fuel rod bowing, and its internal cooling would maintain temperatures much lower than those in the fuel rod cladding, thus retaining the guide tube strength.

(2) Vibration

The semiempirical expression developed by Burgreen[56] was used to calculate the flow-induced vibratory amplitudes for the fuel assembly and fuel rod. The calculated amplitude is 0.010 in. for the fuel assembly and less than 0.005 in. for the fuel rod. The fuel rod vibratory amplitude correlates with the measured amplitude obtained from a test on a 3 x 3 fuel rod assembly. In order to substantiate what is believed to be a conservatively calculated amplitude for the fuel assembly, a direct measurement will be obtained for a full size prototype fuel assembly during testing of the assembly in the Control Rod Drive Line Facility (CRDL) at the B&W Research Center, Alliance, Ohio.

(3) Demonstration

In addition to the specific items discussed above, the overall mechanical performance of the fuel assembly and its individual components is being demonstrated in an extensive experimental program in the CRDL.

3.2.4.3 Control Rod Drive System

3.2.4.3.1 Description

The control rod drive system includes drive mechanisms which actuate control rod assemblies and xenon control rod assemblies, drive controls, power supplies, position indication, operating panels and indicators, safety devices, enclosures, housings, and mountings. Criteria applicable to drive mechanisms for both control rod assemblies and xenon control rod assemblies are given in 3.2.4.3.1.1. Additional requirements for the mechanisms which actuate only control rod assemblies are given in 3.2.4.3.1.2.

3.2.4.3.1.1 General Design Criteria

a. Single Failure

No single failure shall inhibit the protective action of the control rod drive system. The effect of a single failure shall be limited to one control rod drive.

b. Uncontrolled Withdrawal

No single failure or sequence of dependent failures shall cause uncontrolled withdrawal of any control rod assembly (CRA).

c. Equipment Removal

The disconnection of plug-in connectors, modules, and subassemblies from the protective circuits shall be annunciated or shall cause a reactor trip.

d. Position Indication

Continuous position indication, as well as an upper and lower position limit indication, shall be provided for each control rod drive. The accuracy of the position indicators shall be consistent with the tolerance set by reactor safety analysis.

e. System Monitoring

The control rod drive control system shall include provisions for monitoring conditions that are important to safety and reliability. These include rod position deviation and power supply voltage.

f. Drive Speed

The control rod drive control system shall provide for single uniform speed of the mechanism. The drive controls, or mechanism and motor combination, shall have an inherent speed limiting feature. The speed of the mechanism shall be 30 in./min ±6 percent of the predetermined value for both insertion and withdrawal. The withdrawal speed shall be limited so as not to exceed 25 percent overspeed in the event of speed control fault.

g. Mechanical Stops

Each control rod drive shall have positive mechanical stops at both ends of the stroke or travel. The stops shall be capable of receiving the full operating force of the mechanisms without failure.

3.2.4.3.1.2 Additional Design Criteria

The following criteria are applicable only to the mechanisms which actuate control rod assemblies.

a. CRA Positioning

The control rod drives shall provide for controlled withdrawal or insertion of the control rod assemblies (CRA) out of, or into, the reactor core to establish and hold the power level required. The drives are also capable of rapid insertion or trip for emergency reactor conditions.

00254

b. CRA Trip

The trip command shall have priority over all other commands. Trip action shall be positive and nonreversible. Trip circuitry shall provide the final protective action and shall be direct-acting, incur minimum delay, and shall not require external power. Circuit-interrupting devices shall not prevent reactor trip. Fuses, where used, shall be provided with blown indicators. Circuit breaker position information shall also be indicated.

c. Group Withdrawal

The control rod drive system allows only two out of three regulating CRA groups to withdraw at any time subject to the conditions described in 7.2.2.1.2.

3.2.4.3.2 Control Rod Drive Mechanisms

The control rod drives provide for controlled withdrawal or insertion of the control rod assemblies out of or into the core and are capable of rapid insertion or trip. The drives are hermetically sealed, reluctance motor-driven screw units. The control rod drive data are listed in Table 3-19.

Table 3-19

Control Rod Drive Design Data

Item	Data
Number of Drives	57
Type	Hermetically Sealed, Reluctance Motor-Driven Screw
Location	Top-Mounted
Direction of Trip	Down
Velocity of Normal Withdrawal and Insertion, in./min	30
Maximum Travel Time for 2/3 Trip Insertion (93 in.), s	1.40
Length of Stroke, in.	139
Design Pressure, psig	2500
Design Temperature, F	650

The drive mechanism consists of a motor tube which houses a lead screw and its rotor assembly, and a buffer. The end of the motor tube is closed by a

00255

cap and vent assembly. A motor stator is placed down over the motor tube pressure vessel, and position indication switches are arranged outside the motor tube extension.

The control rod drive output element is a translating screw shaft which is coupled to the control rod. The screw is driven by an anti-friction nut element which is rotated magnetically by a motor stator located outside the pressure boundary. Current impressed on the stator causes the separable nut halves to engage; a mechanical spring causes them to disengage the screw in the absence of a current. For rapid insertion, the nut separates to release the screw shaft which then falls into the core by gravity. A buffer within the upper housing decelerates the falling assembly to a low speed a short distance above its full-in position. The final deceleration is accommodated by the down-stop buffer spring.

This mechanism incorporates proven principles and material combinations and is based on extensive analytical, developmental, design, test, and manufacturing experience obtained over the years for Shippingport and the Nuclear Navy.

The control rod drive is shown in Figures 3-55 and 3-56. Subassemblies of the control rod drive are described as follows:

a. Motor Tube

The motor tube is a three-piece welded assembly designed and manufactured in accordance with the requirements of the ASME Code, Section III, for Class A nuclear pressure vessels. The motor tube wall between the rotor assembly and the stator is constructed of magnetic material in order to present a small air gap to the motor. This region of the motor tube is of low alloy steel clad on the inside diameter with stainless steel or with Inconel. The upper end of the motor tube acts only as an enclosure for the withdrawn lead screw; this end is made of a stainless steel and is transition-welded to the upper end of the low alloy motor section. The lower end of the low alloy tube section is welded to a stainless centrifugal casting which is flanged at the face in contact with the vessel's control rod nozzle. Double gaskets with a test port between are used at the connection between the motor tube and the reactor vessel.

b. Motor

The motor is a synchronous, canned reluctance unit with a slip-on stator. The rotor element is described in Paragraph (f) below. The stator is a 48-slot, four-pole arrangement with water cooling coils wound on the outside of its casing. The stator is encapsulated after winding to establish a hermetically sealed unit. It is six phase, star-connected for operation in a pulse-stepping mode, advancing 15 mechanical degrees and 30 electrical degrees per step. The stator assembly is mounted over the motor tube housing as shown in Figure 3-56.

00286

c. Cap and Vent Valve

The upper end of the motor tube is closed by a cap containing a vapor bleed port and vent valve. The valve and bleed port and the cap-to-motor tube closures are arranged to have double seals. The cap is retained by a bolting ring threaded to the outside of the motor tube. The retaining bolts are assembled to the bolting ring so that they cannot be dropped. The bolts are made long so as to be elastic enough to provide positive seal preload at any assembly temperature from 20 to 650 F. The minimum preload is equal to the 3750 psig proof pressure force.

d. Actuator

The actuator consists of the translating screw shaft, its rotating nut assembly, and a torque restraint for the screw. The actuator travel is about 12 feet.

e. Screw Shaft

The screw shaft has a lead of 0.750 in. The thread is a double entry with a spacing of 0.375 in. Thread lead error is held to 0.0005 in. maximum in any 6 in., so that good load sharing is obtained with the roller nuts. The thread form is a modified ASME with a flank angle that allows the roller to disengage without lifting the screw.

f. Rotor Assembly

The rotor assembly is a pair of scissors arms containing ball bearing-mounted threaded rollers skewed at the lead screw helix angle so as to engage the screw thread. The scissors arms are pivoted on a hollow support member (rotor tube), so that the rollers can alternately engage or disengage with the screw thread. The rotor tube member is mounted on ball bearings supported by the motor tube.

g. Roller Nut

The roller nut assembly is a cylinder with circumferential rings matching the form and spacing of the screw shaft thread. It contains integral, angular contact, ball thrust bearing races at each end through which it is supported by a shaft fixed at the screw helix angle to the scissors arms. Two such assemblies are mounted to each scissors arm, so that the four together form a complete nut to match the screw shaft.

h. Scissors Arms

The scissors arms are magnetically acted upon by motor stator. The end of the arms below the pivot support the roller nuts and a separating spring. Current in the motor causes the arms to move radially closer to the motor tube's inner wall, thereby engaging

00257

the rollers with the centrally located screw shaft. A rotating field, three phase current in the motor stator acts on the magnetic arms to rotate the assembly.

i. Rotor Tube

The rotor tube is a hollow member serving to support and limit the travel of the scissors arms. The scissors arms pivot on the lower end of the rotor tube with their upper ends being caged at the top of the tube. The central hole clears the land (outside) diameter of the screw shaft by 0.10 in., so that no impedance to a trip occurs. The tube is supported by a large, angular contact, ball thrust bearing at its lower end and by a radial ball bearing at its upper end. Both of these bearings pilot into the magnetic portion of the motor tube and, therefore, provide direct control of the motor air gap. A second radial bearing mounted to the upper end of the rotor tube has its outer race pinned to both the scissors arms, thereby synchronizing their motion during engagement and disengagement.

j. Torque Restraint

The torque restraint for the screw shaft is a tubular assembly containing a keyway that extends the full length of the screw travel. The assembly is supported vertically and in torque by the upper end of the motor tube extension. The lower end of this tube assembly supports the buffer and is the down stop. A set of indexing serrations mate and orient the torque restraint tube and the motor tube just below the cap. The male serrations are machined on a shoulder upset on the torque restraint hanger tube. This shoulder rests against a step in the motor tube inside diameter so as to provide a vertical support. A key fixed to the top of the lead screw is mated with the restraint keyway to provide both radial and tangential positioning of the lead screw. This assembly also contains the position indicator permanent magnet and the buffer piston. The torque restraint keyway is made in a separate member to prevent contact with the motor tube's smooth wall during mechanism operation.

k. Buffer

The buffer assembly is capable of decelerating the translating mass from the unpressurized terminal velocity to zero velocity without applying greater than ten times the gravitational force on the control rod. The buffer consists of a piston fixed to the top end of the screw shaft and a cylinder which is fixed to the lower end of the torque restraint hanger. Twelve inches above the bottom stop, the piston at the top of the screw enters the cylinder. Guiding is accomplished because the piston and torque guide key is on a single part, while the cylinder and key slot are on a single mating part. As the piston travels into the cylinder, water is driven into the center of the lead screw through holes in the

upper section which produce the damping pressure drop. The number of holes presented to the buffer chamber is reduced as the rod moves into the core, so that the damping coefficient increases as the velocity reduces, thereby providing an approximately uniform deceleration. A large helical spring buffer is employed to take the kinetic energy of the drive line at the end of the water buffer stroke. The spring buffer accepts a five-foot per second impact velocity of the drive line and control rod with an instantaneous overtravel of one inch past the normal down stop. The inclusion of this spring buffer permits practical clearances in the water buffer.

1. Lead Screw Guide

The lead screw guide bushing acts as a primary thermal barrier and as a guide for the screw shaft. The bushing acts as a primary thermal barrier by allowing only a small path for free convection of water between the mechanism and the closure head nozzle. Fluid temperature in the mechanism is largely governed by the flow of water up and down through this bushing. The diametral clearance between screw shaft and bushing is large enough to preclude jamming the screw shaft and small enough to hold the free convection to an acceptable value. In order to obtain trip travel times of acceptably small values, it is necessary to provide an auxiliary flow path around the guide bushing. The larger area path is necessary to reduce the pressure differential required to drive water into the mechanism to equal the screw displacement. The auxiliary flow paths are closed for small pressure differentials (several inches of water) by gravity relief valves which prevent the convective flows, but open fully during trip.

m. Position Indication and Controls

The position transducer consists of a series of magnetically operated reed switches mounted in a tube parallel to the motor tube extension. Each switch is hermetically sealed. Switch contacts close when in proximity to a permanent magnet mounted on the upper end of the lead screw extension.

As the lead screw (and the control rod assembly) moves, switches operate sequentially. The closures are detected, and an analog voltage of position is produced at the output of the position converter. The output is utilized for control and meter indication.

The accuracy of position indication is about ±1-1/2 in. Similar switches are used as travel limit transducers, which are energized by the same internal magnet. Switch closure can be used to operate alarm and stop rod motion devices directly.

A position indication is provided by driving a pulse-stepping motor, which in turn drives a position indication potentiometer. This output drives a conventional panel meter. The accuracy of position indication is about ±2-1/2 in.

n. Motor Tube Design Criteria

The motor tube design complies with Section III of the ASME Boiler and Pressure Vessel Code under classification as Class A vessels. The operating transient cycles, which are considered for the stress analysis of the reactor pressure vessel, are also considered in the motor tube design.

Quality standards relative to material selection, fabrication, and inspection are specified to insure safety function of the housings essential to accident prevention. Materials conform to ASTM or ASME, Section II, Material Specifications. All welding shall be performed by personnel qualified under ASME Code, Section IX, Welding Qualifications. These design and fabrication procedures establish quality assurance of the assemblies to contain the reactor coolant safely at operating temperature and pressure.

In the highly unlikely event that a pressure barrier component or the control rod drive assembly does fail catastrophically, ie, ruptured completely, the following results would ensue:

(1) Control Rod Drive Nozzle

The assembly would be ejected upward as a missile until it was stopped by the missile shield over the reactor. This upward motion would have no adverse effect on adjacent assemblies.

(2) Motor Tube

The failure of this component anywhere above the lower flange would result in a missile-like ejection into the missile shielding over the reactor. This upward motion would have no adverse effect on adjacent mechanisms.

3.2.4.3.3 Control Rod Drive Control System (Control Package)

The control system for the control rod drive is designed to energize and position the control rod drive, provide a reactor trip, indicate the control rod assembly (CRA) position in the core, and indicate malfunctions in the system. The control system consists of:

A. System Control

1. Individual and Group CRA Control (Operator's Panel)
2. Position Indication
3. Automatic Sequencing
4. Position Deviation Monitors

B. Power Supply (Motor Controller)

1. SCR Programmer (CRA Speed Standard)
2. SCR Banks
3. CRA Grouping Panel
4. Transfer Control

C. Trip

Figure 3-57 depicts in block diagram form Items B and C with command inputs from Item A.

The reactor operator is provided with an operator panel and controls which permit manual or automatic group operation, manual single rod operation, group sequencing and position indication. All manual commands, including operator-initiated trip, are made from the operator's panel.

Position indication is provided on both individual rods and rod groups. Individual position meters indicating percent withdrawn are visible from the operator's panel. Four group position meters are provided at the operator's panel. These group meters indicate the position of either the four safety rod groups or the regulating groups, whichever is selected by the meter selector switch.

Automatic sequencing of the regulating groups is provided. The sequencer provides overlapped withdrawal and insertion of Groups 5, 6, and 7 within the limits of 7.2.2.1.2. This sequencing is provided in both automatic and manual modes of control. Sequencer logic is derived from position transducer and limit switch signals.

The system control provides the logic to command the proper group power supply. The group power supply provides d-c power from a three-phase source and applies

it as directed by the programmer controlled SCR to the CRA mechanism. The power supply consists of an SCR programmer, SCR gate drivers, SCR banks, transfer relays, input power transformers, and rod group patch panels.

Input commands of in-hold-out are received by the programmer, which in turn generates the gating sequences for the SCR banks. The programmer consists of a synchronous motor operating on 60-cycle, a-c power, driving a coded disk through a light beam. The coded light beam drives photo detectors, and the photo detectors drive SCR gate driver amplifiers, which in turn gate the SCR. The SCR banks apply a steady voltage to successive motor windings and are line-commutated by the input a-c power. The motor is 6-phase, star-connected and produces 15 degrees of mechanical rotation per switching cycle.

The group power supplies contain redundant SCR banks, each fed from a different power source but driven from a common but dual-channel programmer. Eight groups of drives are in the rod drive system, each having its own power supply. A ninth power supply is provided for single rod control and as an operational spare.

Any rod may be operated in the single rod mode by transferring to the ninth power supply.

Reactor trip is initiated by de-energizing two circuit breakers supplying control rod drive power or two contactors supplying SCR gate power. Both circuits have two devices in series.

The reactor protection system trips the power circuit breakers and control circuit contactors through two out of four logic as shown in the block diagram (Figure 3-57).

3.2.4.3.4 Control Rod Drive System Evaluation

a. Design Criteria

The system will be designed, tested, and analyzed for compliance with the design criteria. A preliminary safety analysis of the control rod drive motor control subsystem was conducted to determine failures of logic functions. It was concluded that no single failure in any CRA control would prevent CRA insertion, nor cause inadvertent CRA withdrawal of another CRA or CRA group.

b. Materials Selection

Materials are selected to be compatible with, and operate in, the reactor coolant. Certified mill test reports containing chemical analysis and test data of all materials exposed to the reactor system fluid will be provided and maintained for the control rod drives. Certificates of compliance for other materials and components shall also be provided.

00262

c. Relation to Design Temperature

All parts of the control rod drive exposed to reactor coolant are designed to operate at 650 F, although it is expected that all parts will operate considerably cooler. Some tests have been completed, and additional tests are planned to determine the operating temperature gradients throughout the drive mechanism during all phases of operation. These tests will also provide an indication of the amount of convection that takes place within the water space of the mechanism. The more significant temperature changes will be caused by displacement of reactor coolant in and out of the mechanism water space as the drive line is raised and lowered.

d. Design Life

The expected life of the control rod drive control system is as follows:

(1) Structural portions, such as flanges and pressure housings, have an expected life of 40 years.

(2) Moving parts, such as lead screw and roller nuts have an expected life of 20 years.

(3) Electronic control circuitry has an expected life of 20 years.

3.2.4.3.5 Control Rod Assembly (CRA)

Each control rod assembly is made up of 16 control rods which are coupled to a single Type 304 stainless steel spider (Figure 3-58). Each control rod consists of an absorber section of silver-indium-cadmium poison clad with cold-worked, Type 304 stainless steel tubing and Type 304 stainless steel upper and lower end pieces. The end pieces are welded to the clad to form a water and pressure-tight container for the poison. The control rods are loosely coupled to the spider to permit maximum conformity with the channels provided by the guide tubes. The CRA is inserted through the upper end fitting of the fuel assembly, each control rod being guided by an in-core guide tube. Guide tubes are also provided in the upper plenum assembly above the core so that full length guidance of the control rods is provided throughout the stroke. With the reactor assembled, the CRA cannot be withdrawn far enough to cause disengagement of the control rods from the in-core guide tubes. Pertinent design data are shown in Table 3-20.

Table 3-20

Control Rod Assembly Design Data

Item	Data
Number of Rod Assemblies	49
Number of Control Rods per Assembly	16
Outside Diameter of Control Rod, in.	0.440
Cladding Thickness, in.	0.019
Cladding Material	Type 304 SS, Cold-Worked
Poison Material	80% Ag, 15% In, 5% Cd
Length of Poison Section, in.	134
Stroke of Control Rod, in.	139

This type of CRA has been developed under the USAEC Large Reactor Development Program and offers the following significant advantages:

a. More uniform distribution of absorber throughout the core volume.

b. Shorter reactor vessel and shorter internals owing to elimination of control rod followers.

c. Lower reactor building requirements owing to reduction of reactor coolant inventory.

d. Better core power distribution for a given CRA worth.

A CRA prototype similar to the B&W design has been extensively tested[57] at reactor temperature, pressure, and flow conditions under the LRD program.

The silver-indium-cadmium poison material is enclosed in stainless steel tubes to provide structural strength to the control rod assemblies. These rods are designed to withstand all operating loads including those resulting from hydraulic forces, thermal gradients, and reactor trip deceleration. The cladding of the poison section also prevents corrosion and eliminates possible silver contamination of the reactor coolant.

The ability of the poison clad to resist collapse due to the system pressure has been demonstrated by an extensive collapse test program on cold-worked stainless steel rods. The actual collapse margins are higher than the requirements.

00264

Internal pressure and poison swelling are not expected to cause stressing or stretching of the clad because the Ag-In-Cd alloy poison does not yield a gaseous product under irradiation.

Because of their great length and unavoidable lack of straightness, some slight mechanical interference between control rods and guide tubes must be expected. However, the parts involved, especially the control rods, are so flexible that only very small friction drags will result. Similarly, thermal distortions of the control rods are expected to be small because of the low heat generation and adequate cooling. Consequently, it is not anticipated that the control rod assemblies will encounter significant frictional resistance to their motion in the guide tubes.

Lifetime tests have been performed on a prototype CRA in the CRDL Facility described in 3.3.3.1 and in accordance with the program outlined in 3.3.3.4.1. Approximately 2200 full-stroke cycles and 250 full-stroke trips have been completed with the reference design CRA at reactor operating conditions of pressure, temperature, flow, and water chemistry. This is approximately equivalent to 20 years of operation on the CRA. Evidence of contact was noticed on the lead-in tip of the control rod assembly, but no measurable amount of metal had been removed. Visual inspection of the spider shows an insignificant amount of wear.

At the end of 410 full-stroke cycles and 50 full-stroke trips (the equivalent of three years' operation in one assembly), the in-core guide tubes in the fuel assembly were examined. Wear marks were noted at the entrance of the guide tubes, and these marks extended into the guide tubes approximately 5 in. Approximately 7 mils of metal had been removed longitudinally from the guide tubes at the upper end. Since no change in the time required for two-thirds insertion was noted over the duration of the testing performed to date, it is concluded that wear of the guide tubes and the CRA will not be of concern.

The methods and frequency of CRA in-service inspection as well as the criteria for replacement will be determined during the detailed design.

3.2.4.3.6 Xenon Control Rod Assembly (XCRA)

Each xenon control rod assembly is made up of 16 xenon control rods which are coupled to a single Type 304 stainless steel spider (Figure 3-59). Each xenon control rod consists of an absorber section of silver-indium-cadmium control material clad with cold-worked, Type 304 stainless steel tubing and Type 304 stainless steel upper and lower end pieces. The end pieces are welded to the clad to form a water and pressure-tight container for the poison. The XCRA is inserted through the upper end fitting of the fuel assembly, each control rod being guided by an in-core guide tube. Guide tubes are also provided in the upper plenum assembly above the core so that full length guidance of the control rods is provided throughout the stroke. With the reactor assembled the XCRA cannot be withdrawn far enough to cause disengagement of the control rods from the in-core guide tubes. Pertinent design data are shown in Table 3-21.

00265

Table 3-21

Xenon Control Rod Assembly Design Data

Item	Data
Number of Rod Assemblies	8
Number of Xenon Control Rods per Assembly	16
Outside Diameter of Xenon Control Rod, in.	0.440
Cladding Thickness, in.	0.019
Cladding Material	Type 304 SS, Cold-Worked
Poison Material	80% Ag, 15% In, 5% Cd
Length of Poison Section, in.	36
Stroke of Control Rod, in.	139

3.2.4.3.7 Burnable Poison Rod Assembly (BPRA)

Each burnable poison rod assembly consists of 16 burnable poison rods which are coupled to a single Type 304 stainless steel spider (Figure 3-54). Each burnable poison rod consists of clad B_4C in Al_2O_3. The end pieces are welded to the clad to form a water and pressure-tight container for the burnable poison. The BPRA are guided by the fuel assembly guide tubes, and coupled with the fuel assembly by means of a positive coupling mechanism provided on the burnable poison rod spider and the fuel assembly hold-down latch. In addition to their nuclear function, these BPRA also minimize guide tube bypass coolant flow. Pertinent design data are shown in Table 3-22.

Table 3-22

Burnable Poison Rod Assembly Design Data

Item	Data
Number of Rod Assemblies	72
Number of Burnable Poison Rods per Assembly	16
Outside Diameter of Burnable Poison Rod, in.	0.430
Cladding Thickness, in.	0.035
Poison Material	B_4C in Al_2O_3
Length of Poison Section, in.	126

00266

3.3 TESTS AND INSPECTIONS

3.3.1 NUCLEAR TESTS AND INSPECTION

3.3.1.1 Critical Experiments

An experimental program (58-60) to verify the relative reactivity worth of the CRA has recently been completed. Detailed testing established the worth of the CRA under various conditions similar to those for the reference core. These parameters include control rod arrangement in a CRA, fuel enrichments, fuel element geometry, CRA materials, and soluble boron concentration in the moderator.

Gross and local power peaking were also studied, and three-dimensional power-peaking data were taken as a function of CRA insertion. Detailed peaking data were also taken between fuel assemblies and around the water holes left by withdrawn CRA. The experimental data are being analyzed and will become part of the experimental bench mark for the analytical models used in the design.

3.3.1.2 Zero Power, Approach to Power, and Power Testing

Boron worth and CRA worth (including stuck-CRA worth) will be determined by physics tests at the beginning of each core cycle. Recalibration of boron worth and CRA worth is expected to be performed at least once during each core cycle. Calculated values of boron worth and CRA worth will be adjusted to the test values as necessary. The boron worth and CRA worth at a given time in core life will be based on CRA position indication and calculated data as adjusted by experimental data.

The reactor coolant will be analyzed in the laboratory periodically to determine the boron concentration, and the reactivity held in boron will then be calculated from the concentration and the reactivity worth of boron.

The method of maintaining the hot shutdown margin (hence stuck-CRA margin) is related to operational characteristics (load patterns) and to the power-peaking restrictions on CRA patterns at power. The CRA pattern restrictions will insure that sufficient reactivity is always fully withdrawn to provide adequate shutdown with the stuck-CRA margin. Power peaking as related to CRA patterns and shutdown margin will be monitored by reactivity calculations.

Operation under power conditions will normally be monitored by in-core instrumentation, and the resulting data will be analyzed and compared with multidimensional calculations to provide support for further power escalations.

3.3.2 THERMAL AND HYDRAULIC TESTS AND INSPECTION

3.3.2.1 Reactor Vessel Flow Distribution and Pressure Drop Test

A 1/6-scale model of the reactor vessel and internals will be tested to evaluate:

a. The flow distribution to each fuel assembly of the reactor core and to develop, if necessary, devices required to produce the desired flow distribution.

00267

b. Fluid mixing between the vessel inlet nozzle and the core inlet, and between the inlet and outlet of the core.

c. The overall pressure drop between the vessel inlet and outlet nozzles, and the pressure drop between various points in the reactor vessel flow circuit.

d. The internals vent valves for closing behavior and for the effect on core flow with valves in the open position.

The reactor vessel, thermal shield, flow baffle, core barrel, and plenum assembly are made of clear plastic to allow use of visual flow study techniques. All parts of the model except the core are geometrically similar to those in the prototype reactor. However, the simulated core was designed to maintain dynamic similarity between the model and prototype.

Each of the 177 simulated fuel assemblies contains a calibrated flow nozzle. The test loop is capable of supplying cold water (80 F) to three inlet nozzles and hot water (180 F) to the fourth. Temperature will be measured in the inlet and outlet nozzles of the reactor model and at the inlet and outlet of each of the fuel assemblies. Static pressure taps will be located at suitable points along the flow path through the vessel. This instrumentation will provide the data necessary to accomplish the objectives set forth for the tests.

3.3.2.2 Fuel Assembly Heat Transfer and Fluid Flow Tests

B&W is conducting a continuous research and development program for fuel assembly heat transfer and fluid flow applicable to the design of the reference reactor. Single-channel tubular and annular test sections and multiple rod assemblies have been tested at the B&W Research Center.

The reactor thermal design is based upon burnout heat transfer experiments with (a) multiple rod, heated assemblies with uniform heat flux, and (b) single rod, annular heaters with nonuniform axial heat flux, at design conditions of pressure and mass velocity. These experiments are being extended to test nonuniform multiple rod heater assemblies as described in 1.5.2. The results of these tests will be applied to the final thermal design of the reactor and the specification of operating limits.

3.3.2.2.1 Single-Channel Heat Transfer Tests

A large quantity of uniform flux, single-channel, critical heat flux data has been obtained. References to uniform flux data are given in BAW-168[64] and 3.2.3.2.3 of this report. The effect on the critical heat flux caused by nonuniform axial power generation in a tubular test section at 2,000 psi pressure was investigated as early as 1961.[61] This program was extended to include pressures of 1,000, 1,500, and 2,000 psi and mass velocities up to 2.5×10^6 lb/h-ft^2.[62] The effect on the critical heat flux caused by differences in the radial and axial power distribution in an annular test section was recently investigated at reactor design conditions.[63] Data were obtained at pressures of 1,000, 1,500, 2,000, and 2,200 psi and at mass velocities up to 2.5×10^6 lb/h-ft^2.

00268

The tubular tests included the following axial heat flux shapes where $P/\overline{P}$ is local to average power:

a. Uniform Heat Flux $(P/\overline{P}) = 1.000$ constant

b. Sine Heat Flux $(P/\overline{P})_{max} = 1.396$ @ 50% L

c. Inlet Peak Heat Flux $(P/\overline{P})_{max} = 1.930$ @ 25% L

d. Outlet Peak Heat Flux $(P/\overline{P})_{max} = 1.930$ @ 75% L

Tests of two additional, nonuniform, 72-in. heated length, tubular tests were undertaken to obtain data for peaking conditions more closely related to the reference design. The additional flux shapes being tested are:

a. Inlet Peak Heat Flux $(P/\overline{P})_{max} = 1.65$ @ 28% L

b. Outlet Peak Heat Flux $(P/\overline{P})_{max} = 1.65$ @ 72% L

These tests will cover approximately the same range of pressure, mass velocity and ΔT as the multiple rod fuel assembly tests.

3.3.2.2.2 Multiple Rod Fuel Assembly Heat Transfer Tests

Critical heat flux data have been obtained from 6-ft long, 9-rod fuel assemblies in a 3 x 3 square array. A total of 513 data points was obtained covering the following conditions:

$$10 \leq \Delta T_s \leq 300$$

$$1{,}000 \leq P \leq 2{,}400$$

$$0.2 \times 10^6 \leq G \leq 3.5 \times 10^6$$

where

ΔT_s = inlet subcooling, F

P = pressure, psia

G = mass velocity, $lb/h\text{-}ft^2$

The geometry of this section consisted of nine rods of 0.420-in. diameter on a 0.558-in. square pitch. Analysis of the last data of this set is in process.

3.3.2.2.3 Fuel Assembly Flow Distribution, Mixing, and Pressure Drop Tests

Flow visualization and pressure drop data have been obtained from a 10-times-full-scale (10X) model of a single rod in a square flow channel. These data have been used to refine the spacer ferrule designs with respect to mixing turbulence and pressure drop. Additional pressure drop testing has been conducted using 4-rod (5X), 4-rod (1X), 1-rod (1X), and 9-rod (1X) models.

00269

Testing to determine the extent of interchannel mixing and flow distribution also has been conducted. Flow distribution in a square 4-rod test assembly has been measured. A salt solution injection technique was used to determine the average flow rates in the simulated reactor assembly corner cells, wall cells, and unit cells. Interchannel mixing data were obtained for the same assembly. These data have been used to confirm the flow distribution and mixing relationships employed in the core thermal and hydraulic design. Flow tests on a mockup of two adjacent fuel assemblies have been conducted. Additional mixing, flow distribution, and pressure drop data will be obtained to improve the core power capability. The following fuel assembly geometries will be tested to provide additional data:

a. A 9-rod (3 x 3 array) mixing test assembly, of the same bundle geometry as the DNB bundle described previously, has been constructed to determine flow pressure drop, flow distribution, and degree of mixing present during the DNB investigations. Testing with the assembly is in progress.

b. Several 64-rod assemblies simulating larger regions and various mechanical arrangements within a 15 x 15 fuel assembly and between adjacent fuel assemblies will be flow tested. The hydraulic facility has been constructed.

3.3.3 FUEL ASSEMBLY, CONTROL ROD ASSEMBLY, AND CONTROL ROD DRIVE MECHANICAL TESTS AND INSPECTION

To demonstrate the mechanical adequacy and safety of the fuel assembly, control rod assembly (CRA), and control rod drive, a number of functional tests have been performed, are in progress, or are in the final stages of preparation.

3.3.3.1 Prototype Testing

A full scale prototype fuel assembly, CRA, and control rod drive are presently being tested in the Control Rod Drive Line (CRDL) Facility located at the B&W Research Center, Alliance, Ohio. This full-size loop is capable of simulating reactor environmental conditions of pressure, temperature, and coolant flow. To verify the mechanical design, operating compatibility, and characteristics of the entire control rod drive fuel assembly system, the drive will be stroked and tripped approximately 200 percent of the expected operating life requirements.

A portion of the testing will be performed with maximum misalignment conditions. Equipment is available to record and verify data such as fuel assembly pressure drop, vibration characteristics and hydraulic forces, and to demonstrate control rod drive operation and verify scram times. All prototype components will be examined periodically for signs of material fretting, wear, and vibration/fatigue to insure that the mechanical design of the equipment meets reactor operating requirements. Preliminary test results are given in 3.2.4.3.5.

00270

3.3.3.2 Model Testing

Many functional improvements have been incorporated in the design of the prototype fuel assembly as a result of model tests run to date. For example, the spacer grid to fuel rod contact area was fabricated to 10 times reactor size and tested in a loop simulating coolant flow Reynolds numbers of interest. Thus, visually, the shape of the fuel rod support areas was optimized with respect to minimizing the severity of flow vortices. Also, a 9-rod (3 x 3) actual size model was fabricated (using production fuel assembly materials) and tested at 640 F, 2,200 psi, and 13 fps coolant flow. Principal objectives of this test were to evaluate fuel rod cladding to spacer grid contact wear, and/or fretting corrosion resulting from flow-induced vibration. A wide range of contact loads (including small clearances) was present in this specimen. No significant wear or other flow-induced damage was observed after 210 days of loop operation.

3.3.3.3 Component and/or Material Testing

3.3.3.3.1 Fuel Rod Cladding

Extensive short time collapse testing was performed on Zircaloy-4 tube specimens as part of the B&W overall creep-collapse testing program. Initial test specimens were 0.436-in. OD with wall thicknesses of 0.020 in., 0.024 in., and 0.028 in. Ten 8-in. long specimens of each thickness were individually tested at 680 F at slowly increasing pressure until collapse occurred. Collapse pressures for the 0.020-in. wall thickness specimens ranged from 1,800 to 2,200 psig, the 0.024-in. specimens ranged from 2,800 to 3,200 psig, and the 0.028-in. specimens ranged from 4,500 to 4,900 psig. The material yield strength of these specimens ranged from 65,000 to 72,000 psi at room temperature, and was 35,800 psi at 680 F.

Additional Zircaloy-4 short time collapse specimens were prepared with a material yield stress of 78,000 psi at room temperature and 48,500 psi at 615 F. Fifteen specimens having an OD of 0.410 in. and an ID of 0.365 in. (0.0225-in. nominal wall thickness) were tested at 615 F at increasing pressure until collapse occurred. Collapse pressures ranged from 4,470 to 4,960 psig.

Creep-collapse testing was performed on the 0.436-in. OD specimens. Twelve specimens of 0.024-in. wall thickness and 30 specimens of 0.028-in. wall thickness were tested in a single autoclave at 680 F and 2,050 psig. During this test, two 0.024-in. wall thickness specimens collapsed during the first 30 days and two collapsed between 30 and 60 days. None of the 0.028-in. wall thickness specimens had collapsed after 60 days. Creep-collapse testing was then performed on thirty 0.410-in. OD by 0.365-in. ID (0.0225-in. nominal wall) specimens for 60 days at 615 F and 2,140 psig. None of these specimens collapsed, and there were no significant increases in ovality after 60 days.

Results of the 60-day, creep-collapse testing on the 0.410-in. OD specimens showed no indication of incipient collapse. The 60-day period for creep-collapse testing is used since it exceeds the point of primary creep of the material, yet is sufficiently long to enter the stage when fuel rod pressure begins to build up during reactor operation, ie. past the point of maximum differential pressure that the clad would be subjected to in the reactor.

In order to help optimize the final clad thickness, additional clad-collapse testing is scheduled for 1969 using specimens fabricated to the reference design fuel clad dimensions, material specifications, and operating conditions.

3.3.3.3.2 Fuel Assembly Structural Components

The structural characteristics of the fuel assembly which are pertinent to loadings resulting from normal operation, handling, earthquake, and accident conditions will be investigated experimentally in test facilities such as, the CRDL Facility. Structural characteristics such as natural frequency and damping will be determined at the relatively high amplitude of interest in our seismic and LOCA analysis. Natural frequencies and amplitudes resulting from flow induced vibration will be measured at various temperatures and flow velocities, up to reactor operating conditions.

In the mechanical design of the spacer grids, particular attention is given to the ferrule-to-fuel-rod contact points. Sufficient load must be applied to position the fuel rods and to minimize fuel rod vibration, yet allow axial thermal differential expansion, and not produce fretting wear in the fuel rod cladding. Static load and functional testing of the prototype grids will demonstrate their adequacy to perform within the design requirements.

3.3.3.3.3 High Burnup Fuel Irradiations

The primary purpose of the B&W High Burnup Irradiation Program is to determine the swelling rate of UO_2 as a function of burnup using fuel rods of the same design as the core. In addition to determining the swelling rate, the effect of several other variables including the density, heat rate, and cladding restraint will be investigated.

The program consists of capsules some of which will operate at a heat rate of 18 kW/ft and others at a heat rate of 21.5 kW/ft. The pellets, other than U-235 content, will conform to the reactor fuel specifications. The burnup will range from 10,000 to 80,000 MWd/MTU with eight capsules exceeding 45,000 MWd/MTU. The capsules will not operate with an external pressure. However, two different cladding thicknesses, 0.015 and 0.025 in., will be used to vary the restraint offered by the cladding. The fuel rods will operate with a cladding surface temperature of 650 F. The diametral gaps between the pellets and cladding will vary from 4-5 to 7-8 mils, to give smeared densities of about 92.3 and 90.8 percent, respectively. These gaps and smeared densities are consistent with the fuel rod specifications. The insertion date for the first capsule was September 5, 1967. See Tables 3-17 and 3-18 herein.

The tests are oriented toward the determination of the behavior of materials in an irradiation environment and to determine the optimum geometric and material properties for the specific application. The information is essential for advancement of the art, but is not considered critical in the sense that all of the programs must be completed to insure safe operation.

3.3.3.4 Control Rod Drive Tests and Inspection

3.3.3.4.1 Control Rod Drive Developmental Tests

The prototype roller nut drive is under test at the B&W Research Center, Alliance, Ohio.

00272

Wear characteristics of critical components have indicated that material compatibility and structural design of these components will be adequate for the life of the mechanism.

The development program has been completed, and the complete prototype control rod drive is being subjected to environmental testing under simulated reactor conditions (except radiation) in the Control Rod Drive Line (CRDL) Facility at Alliance. Environmental tests include:

Operational Tests

Operating speeds.

Temperature profiles.

Trip times for full and partially withdrawn control rod assemblies (CRA) for various flow-induced pressure drops across the CRA.

Life Tests

(With internals assembled to maximum misalignment permitted by drawing dimensions and tolerances.)

No. of Partial Stroke Cycles	Stroke Length, in.	Span of Control Rod Stroke From "Full-In" Position, in.
1,550	83	From 56 To 139
5,400	50	71 121
8,500	25	114 139
8,500	13	126 139
No. of Trip Cycles		
500	139	From 0 To 139

Misalignment Tests

100 full strokes and 100 full stroke trips with internals tolerances altered to 1.5 times maximum allowable misalignment.

Coupling Tests

Check of coupling operations after testing.

The cycles above meet the total test requirements of 5,000 full strokes and 500 trips. The assembly will be completely disassembled and inspected at various B&W facilities after completion of environmental tests.

3.3.3.4.2 Control Rod Drive Control System Developmental Tests

A control rod drive power supply unit has been built in group prototype form. Following the combined test of the power supply and mechanism, thermal, life, and simulated failure tests will be conducted. The simulated failure test will be designed to verify the safety analysis.

The control rod drive control system will be tested in conjunction with the control rod drive power supply to insure proper operation. Simulated failure testing will also be performed on the combined system to insure that protective requirements are being met.

The position indicator and limit switch subsystem has been built in prototype form and life-tested mechanically under expected environmental conditions. Further testing, both mechanical and electrical, will be done under expected environmental conditions at the B&W Research Center. Characteristics to be determined will include accuracy, repeatability, linearity, short term stability, and long term stability.

3.3.3.4.3 Production Tests

Production tests discussed in this section will be performed either on the drives installed, or on drives manufactured to the same specifications. The finished control rod drive will be proof-tested as a complete system, ie, mechanisms, motor control, and system control working as a system. This proof-testing will be above and beyond any developmental testing performed in the product development stages.

Mechanism production tests will include:

a. Ambient Tests

Coupling tests.

Operating speeds.

Position indication.

Trip tests.

b. Operational Tests

Operating speeds.

Position indication.

Partial and full stroke cycles.

Partial and full stroke trip cycles.

Control system production tests will be performed as described in the following paragraphs.

The finished hardware will be systematically operated through all of its operating modes, checked over the full range of all set points, and checked for proper operation of all patch plugs. This will check completeness and proper functioning of wiring and components.

The operating modes to be checked will include such things as automatic operation, manual group operation, trim or single CRA operation, position indication of all CRA travel limit on all CRA, trip circuit operations, IN command, OUT command, etc.

The trip circuit or circuits will be tested by repeated operation. The overall trip time will be measured.

The accuracy and repeatability of the position indication and limit switch systems will be tested.

Power supply tests will be performed to determine the upper and lower operating voltage and to prove immunity to switching transients.

Fault conditions will be simulated to prove that no unsafe action results from defective components, circuits, or wiring. Ability to detect unsafe fault conditions at the operating console will be determined. Typical of faults to be simulated are:

a. Defective limit switch or circuit.
b. Improper CRA group patch.
c. Defective patch plugs.
d. Defective group sequencer.
e. Defective clock.
f. Defective automatic control signal.
g. Defective command line.
h. Defective fuses.
i. Defective single CRA control circuit or switch.
j. Defective power supply.
k. Defective motor translator.
l. Defective motor cable.
m. Defective position transmitter.

The finished hardware will be visually inspected for quality of workmanship. This inspection will include an examination of the enclosure, cable entrances, dust-tightness, maintenance features, drawers and cable retractors, fasteners, stiffeners, module mounts, wire harnesses, and other similar details.

3.3.4 INTERNALS TESTS AND INSPECTION

The internals upper and lower plenum hydraulic design will be evaluated and guided by the results from the 1/6-scale model flow test which is described in detail in 3.3.2.1. These test results will indicate areas of gross flow maldistribution and allow verification of vessel flow-pressure drop computations. In addition, the test results will provide measured pressure pulses at specific locations to aid in assessing the vibration response characteristics of the internals components.

The effects of internals misalignment will be evaluated on the basis of the test results from the CRDL tests described in 3.3.3.4. These test results, when correlated with the internals guide tube final design, will insure that the CRA will have the capability for a reactor trip or fast insertion under all modes of reactor operation in the reactor coolant environment. These tests will not include the effects of neutron flux exposure.

With regard to the internals surveillance specimen holder tubes, the material irradiation surveillance program is described in 4.4.3.

All internals components can be removed from the reactor vessel to allow inspection of all vessel interior surfaces (see 4.4.1). Internals components surfaces can be inspected when the internals are removed to the canal storage location.

The internals vent valves are designed to relieve the pressure generated by steaming in the core following the LOCA so that the core will remain sufficiently cooled. The valves are designed to withstand the forces resulting from rupture of either a reactor coolant inlet or outlet pipe.

a. A full-size prototype valve assembly (valve disc retaining mechanism and valve body) has been hydrostatically tested to the maximum pressure expected to result during the blowdown.

b. Sufficient tests have been conducted at zero pressure to determine the frictional loads in the hinge assembly, the inertia of the valve cover, and the cover rebound resulting from impact of the cover on the seat so that the valve response to cyclic blowdown forces may be determined analytically.

c. A prototype valve assembly has been pressurized to determine the pressure differential required to cause the valve to begin to open. A determination of the pressure differential required to open the valve to its maximum open position will be simulated by mechanical means.

d. A prototype valve assembly has been installed and removed remotely in a test stand to confirm the adequacy of the vent valve handling tool.

An analysis indicates that the vent valves will not open during operation as a result of vibration caused by transmission of core support shield vibrations.

To verify this analysis B&W has performed vibration tests on a full scale prototype vent valve. The prototype valve was mounted in a test fixture which duplicated the method of valve mounting in the core support shield. The test fixture with valve installed was attached to a vibration test machine and excited sinusoidally through a range of frequencies which encompassed those which may reasonably be anticipated for the core support shield during reactor operation. The relative motion between the valve disc and seat was monitored and recorded during test. The test results indicate that there was no relative motion of the valve to its seat for conditions simulating operating conditions.

During refueling outages after the reactor vessel head and the internals plenum assembly have been removed, the vent valves will be accessible for visual and mechanical inspection. A hook tool will be provided to engage with the previously mentioned valve disc hook or eye. With the aid of this tool, the valve disc can be manually exercised to evaluate the disc freedom. The hinge design will incorporate special features, as described in 3.2.4.1.2.h, to minimize the possibility of valve disc motion impairment during its service life.

00276

With the aid of the above described hook tool, the valve disc can be raised and a visual inspection of the valve body and disc sealing faces can be performed for evaluation of observed surface irregularities.

Remote installation and removal of the vent valve assemblies will be performed with the aid of vent valve handling tool which will include unlocking and operating features for the retaining ring.

The valve disc, hinge shaft, shaft journals (bushings), disc journal receptacles, and valve body journal receptacles will be designed to withstand without failure the internal and external differential pressure loadings resulting from a loss-of-coolant accident. These valve materials will be nondestructively tested and accepted in accordance with the ASME Code III requirements for Class A pressure vessels.

The hinge materials will be selected on the basis of their corrosion resistance, surface hardness, antigalling characteristics, and compatibility with mating materials in the reactor coolant environment.

A remote inspection of hinge parts is not planned until such time as a valve assembly is removed because its free-disc motion has been impaired. In the unlikely event that a hinge part should fail during normal operation, the most significant indication of such a failure would be a change in the free-disc motion as a result of altered rotational clearances.

3.4 REFERENCES

(1) Putnam, G. E., TOPIC - A Fortran Program for Calculating Transport of Particles in Cylinders, IDO-16968, April 1964.

(2) Avery, A. F., The Prediction of Neutron Attenuation in Iron-Water Shields, AEEW-R125, April 1962.

(3) Bohl, H., Jr., et al., P3MG1, A One-Dimensional Multigroup P-3 Program for the Philco-2000 Computer, WAPD-TM-272.

(4) Bohl, H., Jr. and Hemphill, A. P., MUFT-5, A Fast Neutron Spectrum Program for the Philco-2000, WAPD-TM-218.

(5) Armster, H. J. and Callaghan, J. C., KATE-1, A Program for Calculating Wigner-Wilkins and Maxwellian-Averaged Thermal Constants on the Philco-2000, WAPD-TM-232.

(6) Marlowe, O. J. and Suggs, M. C., WANDA-5, A One-Dimensional Neutron Diffusion Equation Program for the Philco-2000 Computer, WAPD-TM-241.

(7) Honeck, H. C., THERMOS, A Thermalization Transport Theory Code for Reactor Lattices, BNL-5826.

(8) Cadwell, W. R., Buerger, P. F., and Pfeifer, C. J., The PDQ-5 and PDQ-6 Programs for the Solution of the Two-Dimensional Neutron Diffusion-Depletion Problem, WAPD-TM-477.

00277

(25) Owen, D. B., Factors for One-Sided Tolerance Limits and for Variable Sampling Plans, SCR-607, March 1963.

(27) Bowring, R. W., Physical Model, Based on Bubble Detachment, and Calculation of Steam Voidage in the Subcooled Region of a Heated Channel, HPR-10, OECD Halden Reactor Project, December 1962.

(28) Zuber, N. and Findlay, J. A., Average Volumetric Concentrations in Two Phase Flow Systems, Presented at the ASME Winter Meeting, 1964. To be published in the ASME Transactions.

(29) Maurer, G. W., A Method of Predicting Steady-State Boiling Vapor Fractions in Reactor Coolant Channels, Bettis Technical Review, WAPD-BT-19.

(30) Baker, O., Simultaneous Flow of Oil and Gas, Oil and Gas Journal, Vol 53, pp 185-195, 1954.

(31) Rose, S. C., Jr., and Griffith, P., Flow Properties of Bubbly Mixtures, ASME Paper No. 65-HT-38, 1965.

(32) Haberstroh, R. D. and Griffith, P., The Transition From the Annular to the Slug Flow Regime in Two-Phase Flow, MIT TR 5003-28, Department of Mechanical Engineering, MIT, June 1964.

(33) Bergles, A. E. and Suo, M., Investigation of Boiling Water Flow Regimes at High Pressure, NYO-3304-8, February 1, 1966.

(34) Notley, N. J. F., The Thermal Conductivity of Columnar Grains in Irradiated UO_2 Fuel Elements, AECL-1822, July 1963.

(35) Lyons, M. F., et al., UO_2 Fuel Rod Operation With Gross Central Melting, GEAP-4264, October 1963.

(36) Notley, M. J. F., et al., Zircaloy-Sheathed UO_2 Fuel Elements Irradiated at Values of Integral kdθ Between 30 and 83 w/cm, AECL-1676, December 1962.

(37) Bain, A. S., Melting of UO_2 During Irradiations of Short Duration, AECL-2289, August 1965.

(38) Notley, M. J. F., et al., The Longitudinal and Diametral Expansions of UO_2 Fuel Elements, AECL-2143, November 1964.

(39) Lyons, M. F., et al., UO_2 Pellet Thermal Conductivity From Irradiations With Central Melting, GEAP-4624, July 1964

(40) McGrath, R. G., Carolinas-Virginia Nuclear Power Associates, Inc., Research and Development Program, Quarterly Progress Report for the Period April - May - June 1965, CVNA-246.

(41) Ross, A. M. and Stoute, R. L., Heat Transfer Coefficients Between UO_2 and Zircaloy-2, AECL-1552, June 1962.

00278

(9) Marlowe, O. J., Nuclear Reactor Depletion Programs for the Philco-2000 Computer, WAPD-TM-221.

(10) Lathrop, K. P., DTF-IV, A FORTRAN-IV Program for Solving the Multigroup Transport Equation With Anisotropic Scattering, LA-3373.

(11) Joanou, G. D. and Dudek, J. S., GAM-1: A Consistent P_1 Multigroup Code for the Calculation of Fast Neutron Spectra and Multigroup Constants, GA-1850.

(12) Baldwin, M. N., Physics Verification Experiments, CORE I, ρ_{28} and Initial Conversion Ratio Measurements, BAW-TM-454.

(13) Clark, R. H. and Pitts, T. G., Physics Verification Experiments, Core I, BAW-TM-455.

(14) Clark, R. H. and Pitts, T. G., Physics Verification Experiments, Cores II and III, BAW-TM-458.

(15) Spinks, N., "The Extrapolation Distance at the Surface of a Grey Cylindrical Control Rod," Nuclear Science and Engineering, 22, pp 87-93, 1965.

(16) Neuhold, R. J., Xenon Oscillation, BAW-305, 1966.

(17) Randall, D. and St. John, D. S., Xenon Spatial Oscillations, Nucleonics, March 1958.

(18) Randall, D. and St. John, D. S., Xenon Spatial Oscillations, Nuclear Science and Engineering, 14, No. 2, October 1962.

(19) Control of Xenon Instabilities in Large PWR's, WCAP-3680-4, July 1967.

(20) Poncelet, C. G. and Christie, A. M., The Effect of a Finite Time Step Length on Calculated Xenon Stability Characteristics in Large PWR's, ANS Winter Meeting, November 1967.

(21) Clark, R. H., Batch, M. L., and Pitts, T. G., Lumped Burnable Poison Program - Final Report, BAW-3493-1.

(22) Tong, L. S., DNB Prediction for an Axially Nonuniform Heat Flux Distribution, WCAP-5584, September 1965.

(23) Tong, L. S., An Evaluation of the Departure From Nucleate Boiling in Bundles of Reactor Fuel Rods, Nuclear Science and Engineering, 33, pp 7-15, 1968.

(24) U.S.-Euratom Joint R&D Program, Burnout Flow Inside Round Tubes With Nonuniform Heat Fluxes, The Babcock & Wilcox Company, BAW-3238-9, May 1966.

(25) Jens, W. H. and Lottes, P. A., Analysis of Heat Transfer Burnout, Pressure Drop, and Density Data for High-Pressure Water, ANL-4627, May 1951.

00279

(42) Hoffman, J. P. and Coplin, D. H., The Release of Fission Gases From Uranium Dioxide Pellet Fuel Operated at High Temperatures, GEAP-4596, September 1964.

(43) Spolaris, C. N. and Megerth, F. H., Residual and Fission Gas Release From Uranium Dioxide, GEAP-4314, July 1963.

(44) Robertson, J. A. L., et al., Behavior of Uranium Dioxide as a Reactor Fuel, AECL-603, 1958.

(45) Parker, G. W., et al., Fission Product Release From UO_2 by High Temperature Diffusion and Melting in Helium and Air, CF-60-12-14, ORNL, February 1961.

(46) Duncombe, E., Effects of Fuel Cracking, Void Migration, and Clad Collapse in Oxide Fuel Rods, Trans. ANS 11(1), p 132, June 1968.

(47) Bain, A. S., Microscopic, Autoradiographic and Fuel/Sheath Heat Transfer Studies on UO_2 Fuel Elements, AECL-2588, June 1966.

(48) Balfour, M. G., Post-Irradiation Examination of CVTR Fuel Assemblies, WCAP-3850-2, March 1968.

(49) Daniel, R. C., et al., Effects of High Burnup on Zircaloy-Clad, Bulk UO_2, Plate Fuel Element Samples, WAPD-263, September 1962.

(50) Fracture of Cylindrical Fuel Rod Cladding due to Plastic Instability, WAPD-TM-651, April 1967.

(51) Duncan, R. N., Rabbit Capsule Irradiation of UO_2, CVNA-142, June 1962.

(52) Duncan, R. N., CVTR Fuel Capsule Irradiations, CVNA-153, August 1962.

(53) Frost, Bradbury, and Griffiths (AERE Harwell), Irradiation Effects in Fissile Oxides and Carbides at Low and High Burnup Levels, Proceedings of IAEA Symposium on Radiation Damage in Solids and Reactor Materials, Venice, Italy, May 1962.

(54) Gerhart, J. M., The Post-Irradiation Examination of a PuO_2-UO_2 Fast Reactor Fuel, GEAP-3833.

(55) Physical and Mechanical Properties of Zircaloy-2 and -4, WCAP-3269-41, Figure 18.

(56) Burgreen, D., Byrnes, J. J., and Benforado, D. M., "Vibration of Rods Induced by Water in Parallel Flow," Trans. ASME 80, p 991, 1958.

(57) Large Closed-Cycle Water Reactor R&D Program, Progress Report for the Period January 1 to March 31, 1965, WCAP-3269-12.

(58) Clark, R. H., Physics Verification Experiments, Cores IV and V, BAW-TM-178, September 1966.

00280

(59) Clark, R. H., Physics Verification Experiment, Core VI, BAW-TM-179, December 1966.

(60) Clark, R. H., Physics Verification Experiment, Axial Power Mapping on Core IV, BAW-TM-255, December 1966.

(61) Swenson, H. W., Carver, J. R., and Kakarala, C. R., The Influence of Axial Heat Flux Distribution on the Departure From Nucleate Boiling in a Water Cooled Tube, ASME Paper 62-WA-2[illegible].

(62) Burnout for Flow Inside Round Tubes With Nonuniform Heat Fluxes, BAW-3238-9, May 1966.

(63) Nonuniform Heat Generation Experimental Program, BAW-3238-13, July 1966.

(64) Wilson, R. H. and Ferrell, J. K., Correlation of Critical Heat Flux for Boiling Water in Forced Circulation at Elevated Pressures, The Babcock & Wilcox Company, BAW-168, November 1961.

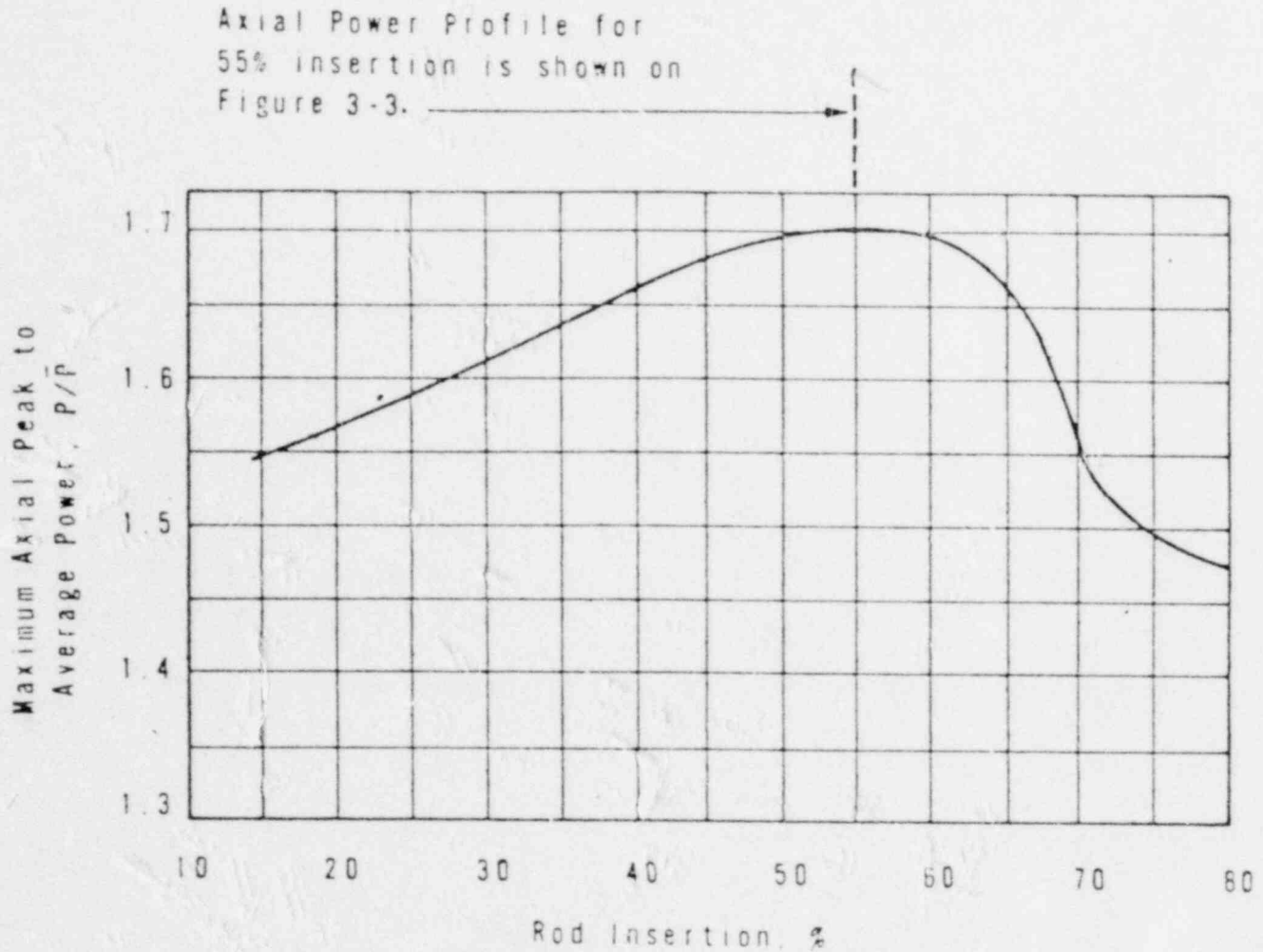

AXIAL PEAK TO AVERAGE POWER
VERSUS XENON OVERRIDE ROD INSERTION

Figure 3-2

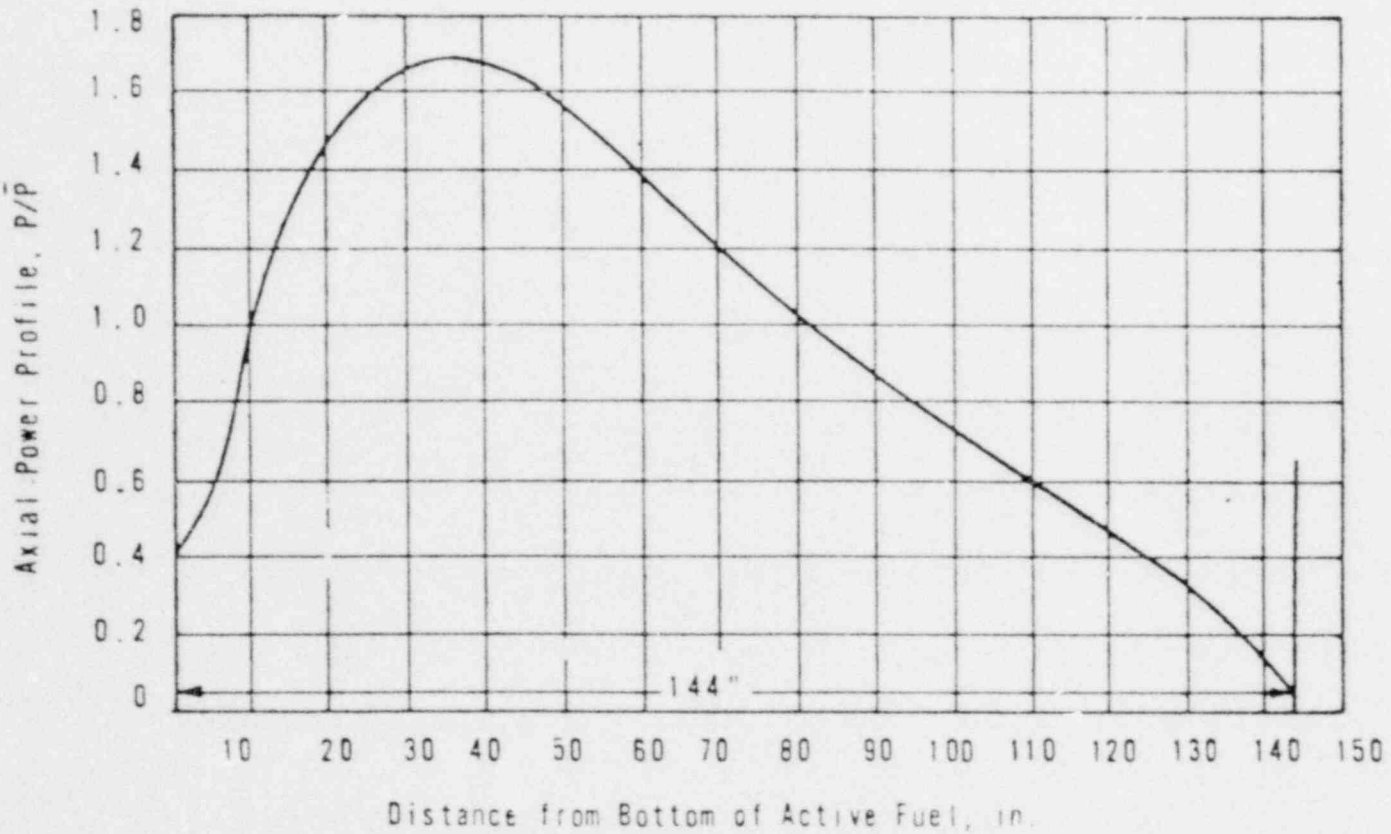

AXIAL POWER PROFILE, XENON OVERRIDE
RODS 55 PER CENT INSERTED

Figure 3-3

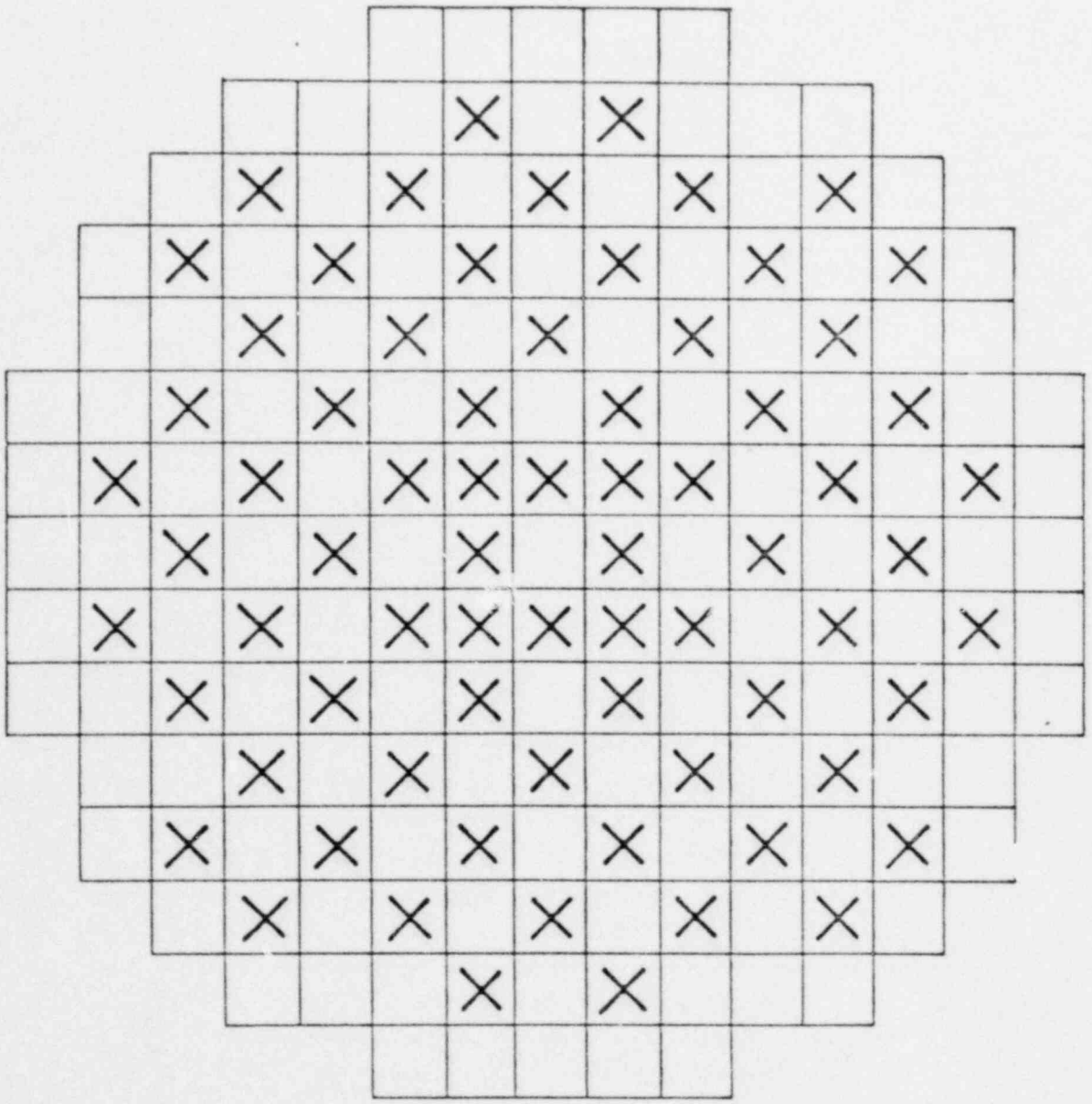

LOCATION OF FUEL ASSEMBLIES CONTAINING
BURNABLE POISON RODS

Figure 3-4

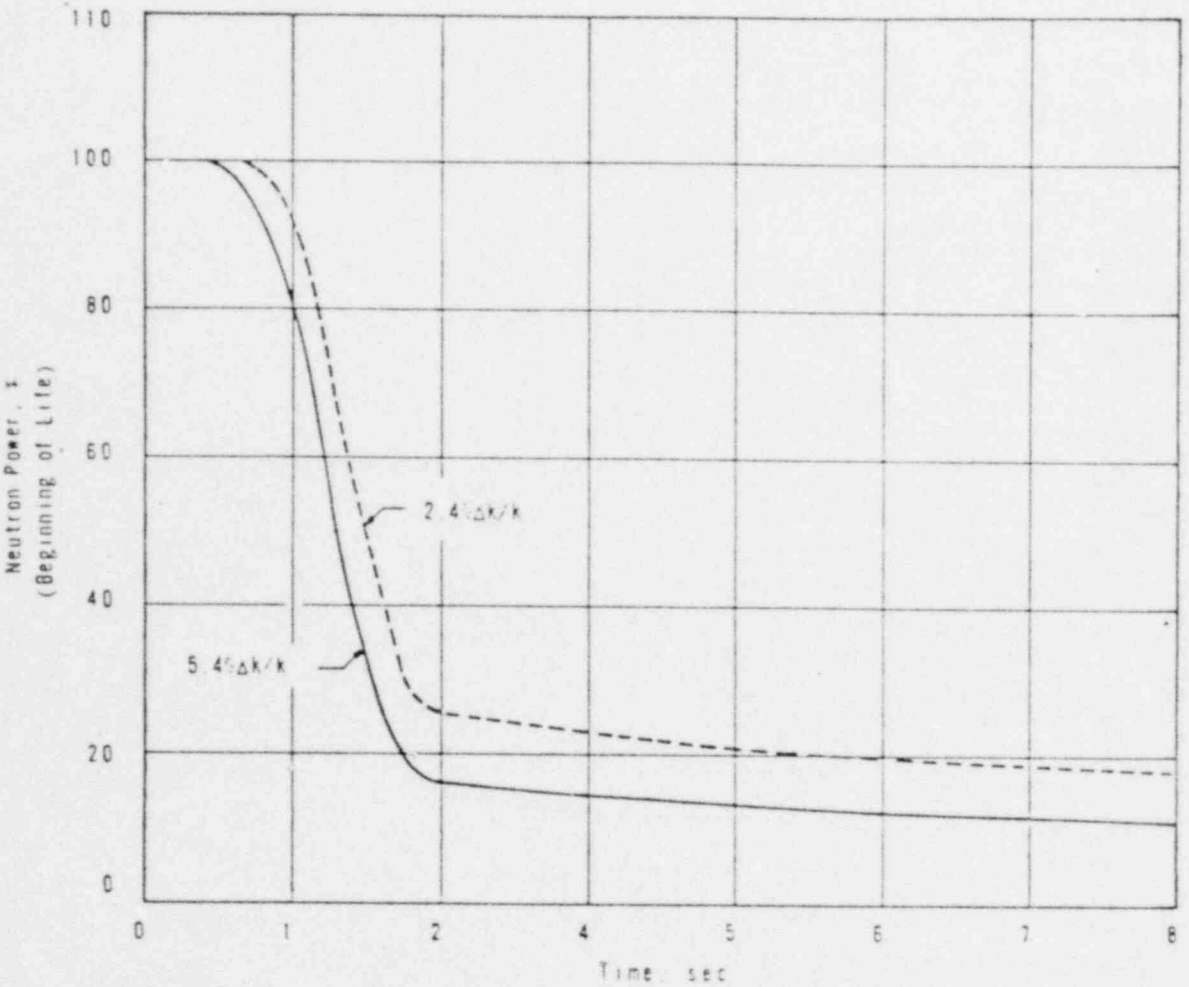

PER CENT NEUTRON POWER
VERSUS TIME FOLLOWING TRIP

Figure 3-5

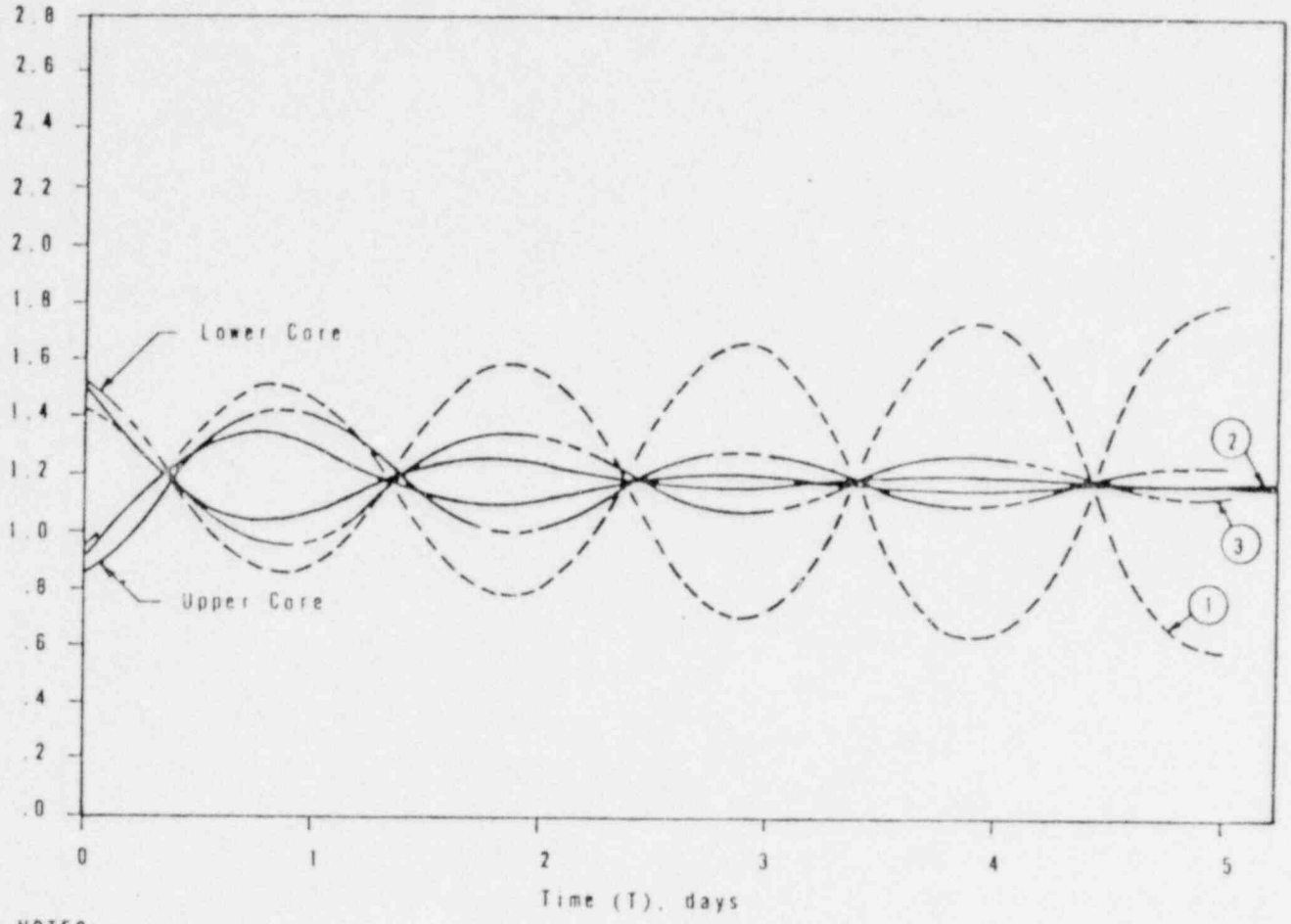

NOTES

1. Power Ratio taken 36 in. from top and bottom of active fuel.
   Case 1 - No temperature iteration, $\bar{T}_{fuel}$ = 1,400 F.
   Case 2 - Temperature iteration with $\bar{T}_{fuel}$ = 1,400 F.
   Case 3 - Temperature iteration with $\bar{T}_{fuel}$ = 900 F.
2. Oscillation initiated at T = 2 days.

EFFECT OF FUEL TEMPERATURE (DOPPLER) ON XENON OSCILLATIONS - BEGINNING OF LIFE

Figure 3-6

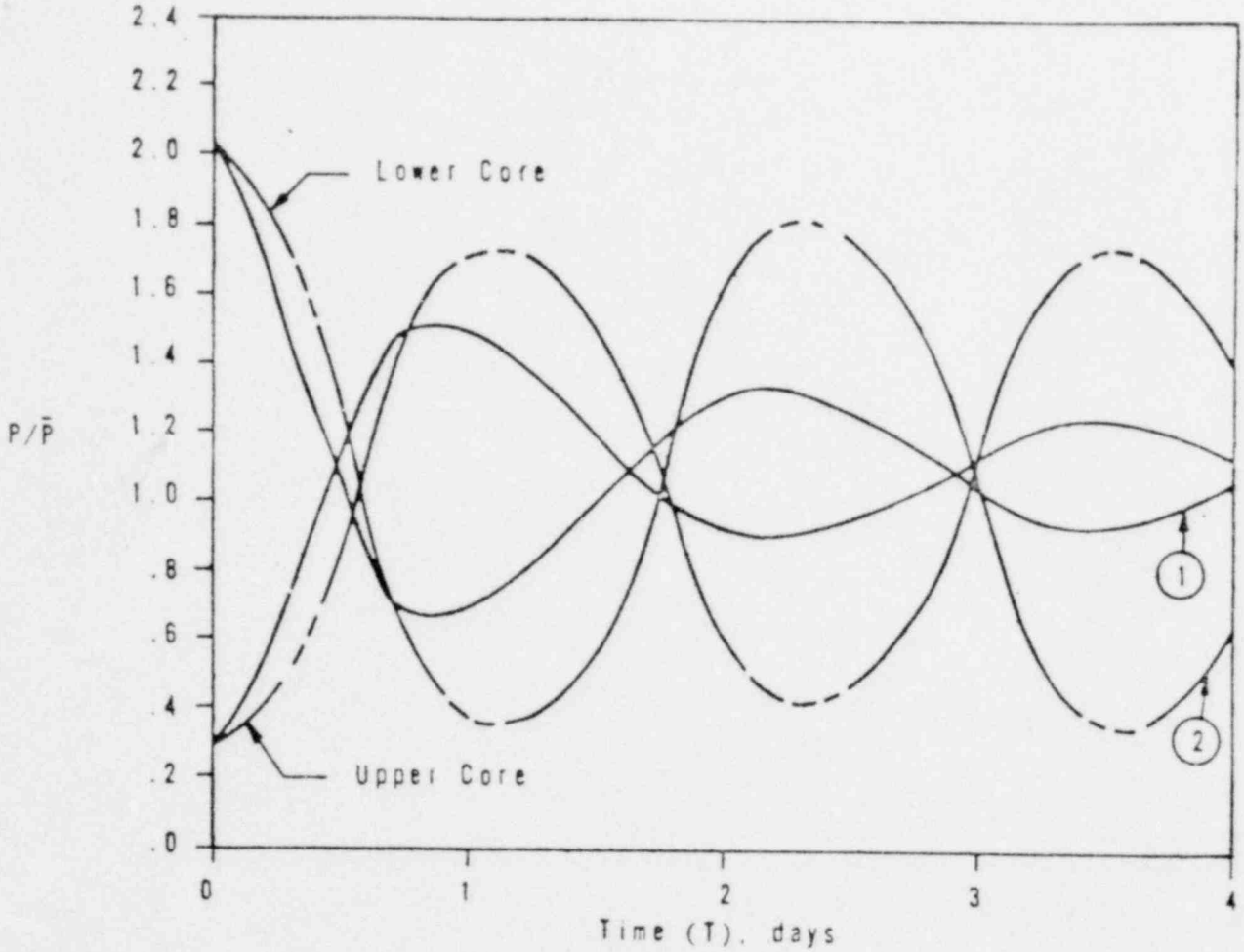

Notes:

1. Power Ratio taken 36 in. from top and bottom of active fuel.
   Case 1 - Temperature Iteration with $\bar{T}_{fuel}$ = 1,400 F.
   Case 2 - Temperature Iteration with $\bar{T}_{fuel}$ = 900 F.
2. Oscillation initiated at T = 300 days.

EFFECT OF FUEL TEMPERATURE (DOPPLER) ON XENON OSCILLATIONS - NEAR END OF LIFE

Figure 3-7

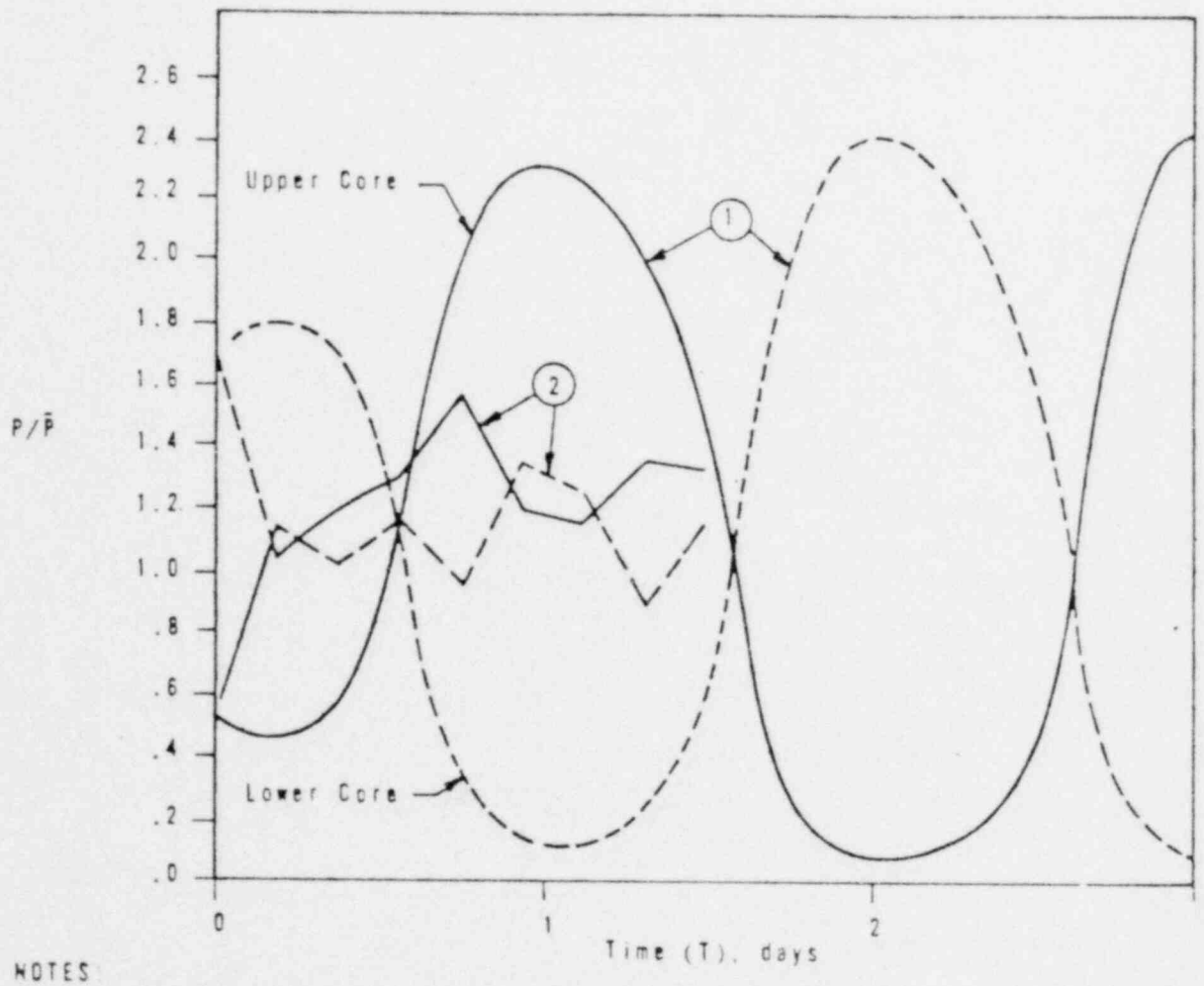

NOTES

1. Case 1 - Divergent oscillation (without temperature iteration).
   Case 2 - Power ratio variation with control (without temperature iteration).
2. Oscillation initiated at T = 200 days.

CONTROL OF AXIAL OSCILLATION
WITH PARTIAL RODS

Figure 3-8

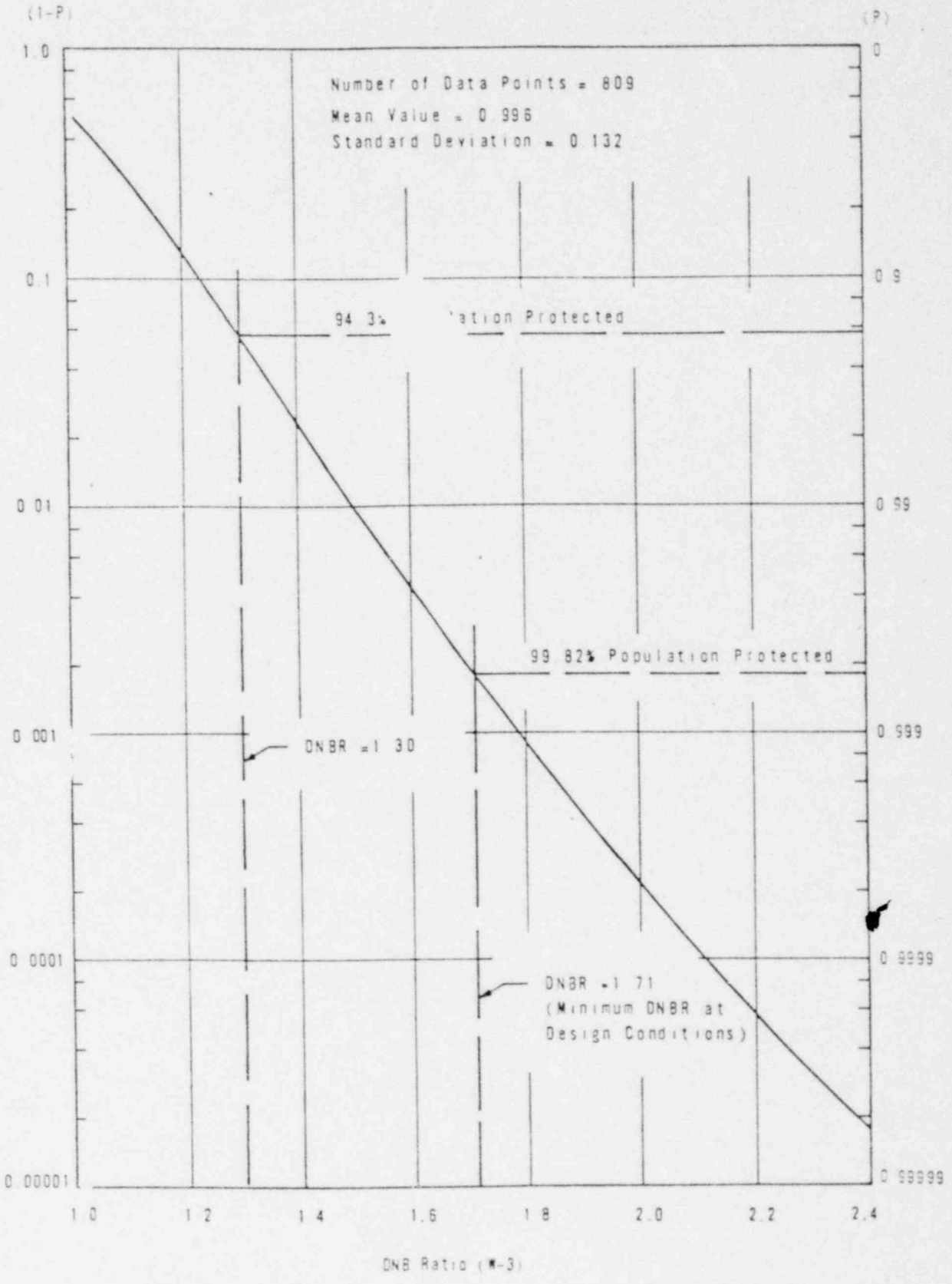

POPULATION PROTECTED, P, AND 1-P
VERSUS DNB RATIO (W-3)

Figure 3-9

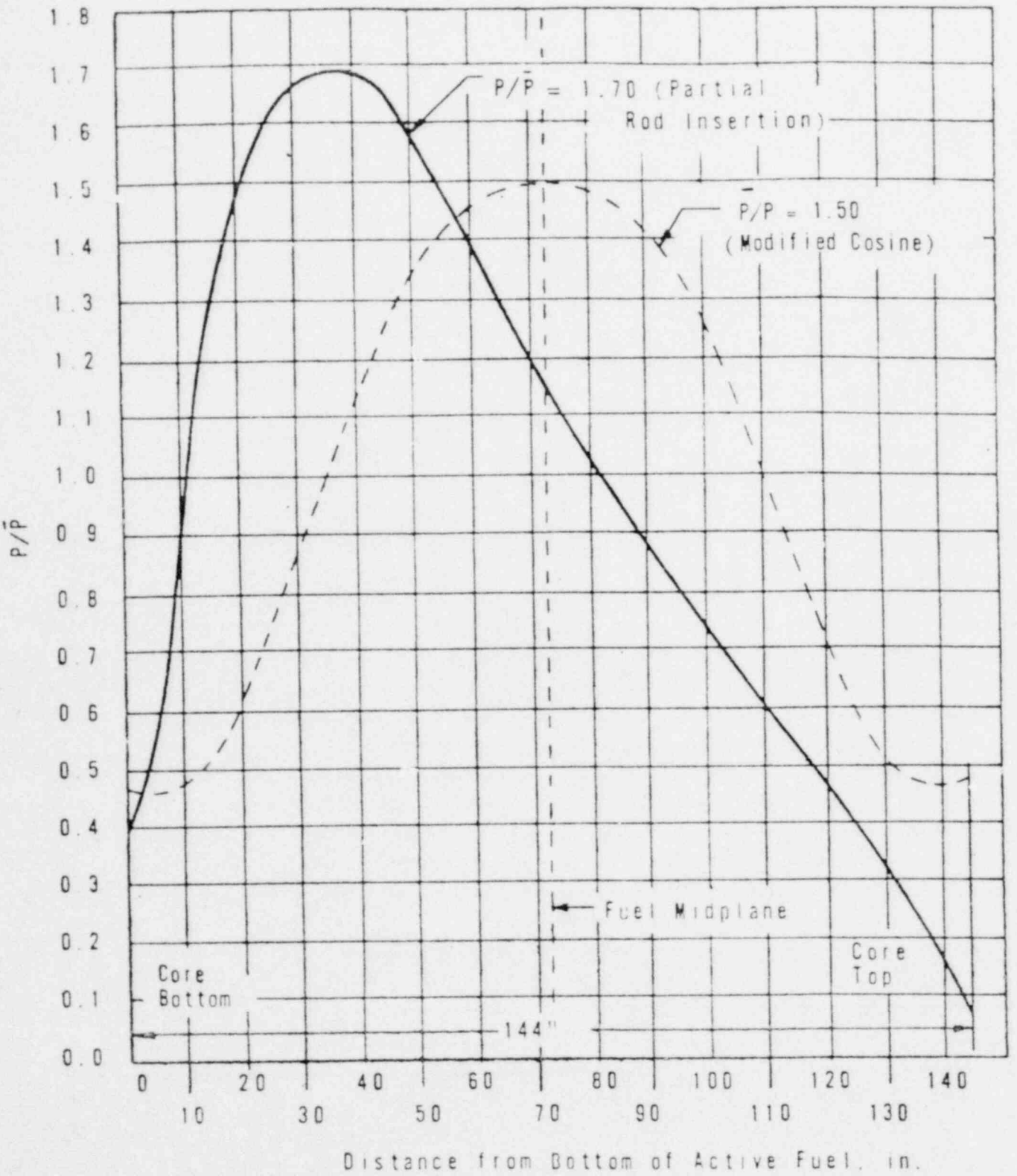

POWER SHAPE REFLECTING INCREASED AXIAL POWER PEAK FOR 144-INCH CORE

Figure 3-10

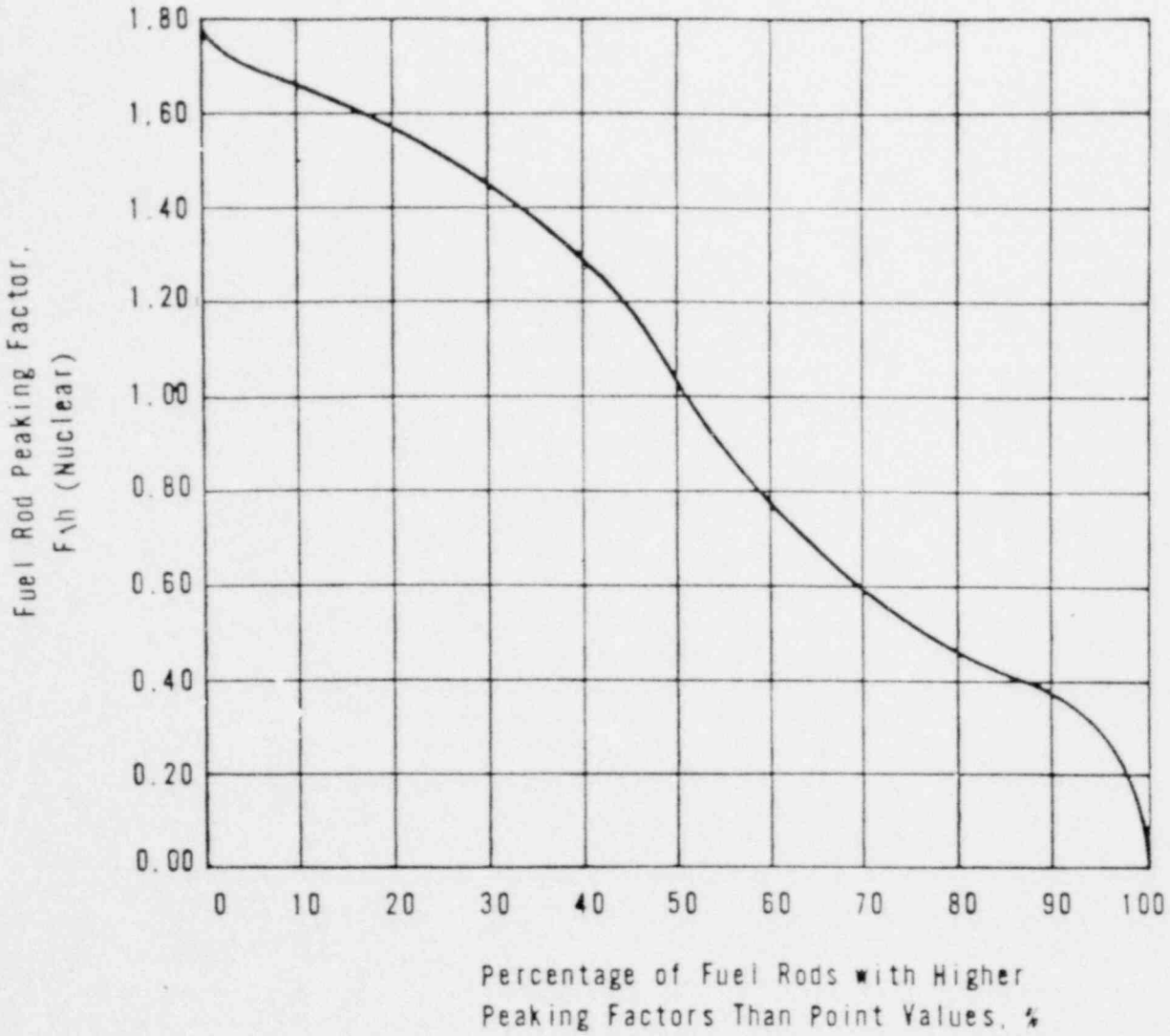

DISTRIBUTION OF FUEL ROD PEAKING

Figure 3-11

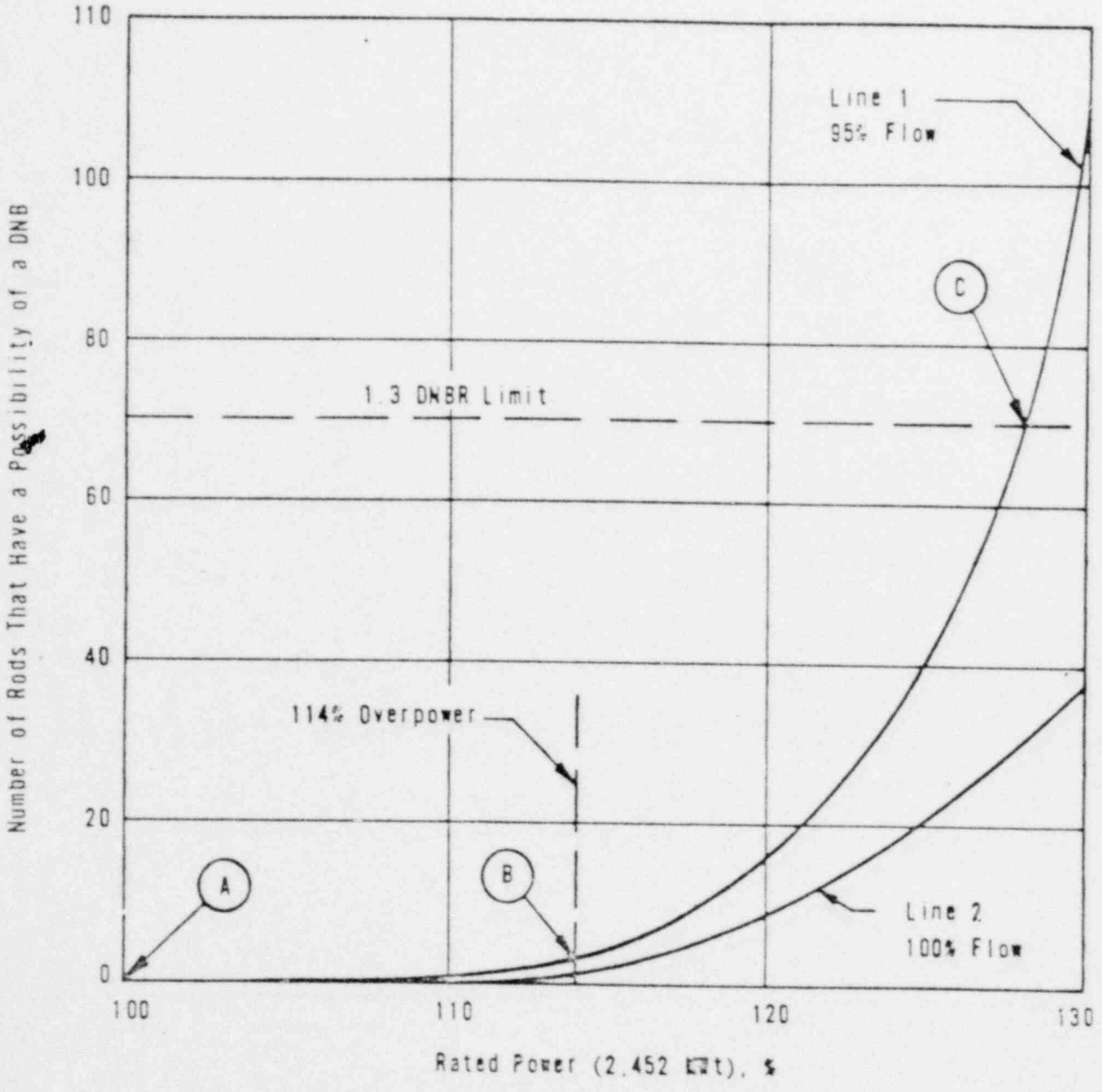

POSSIBLE FUEL ROD DNB'S FOR MAXIMUM DESIGN CONDITIONS - 36,816 - ROD CORE

Figure 3-12

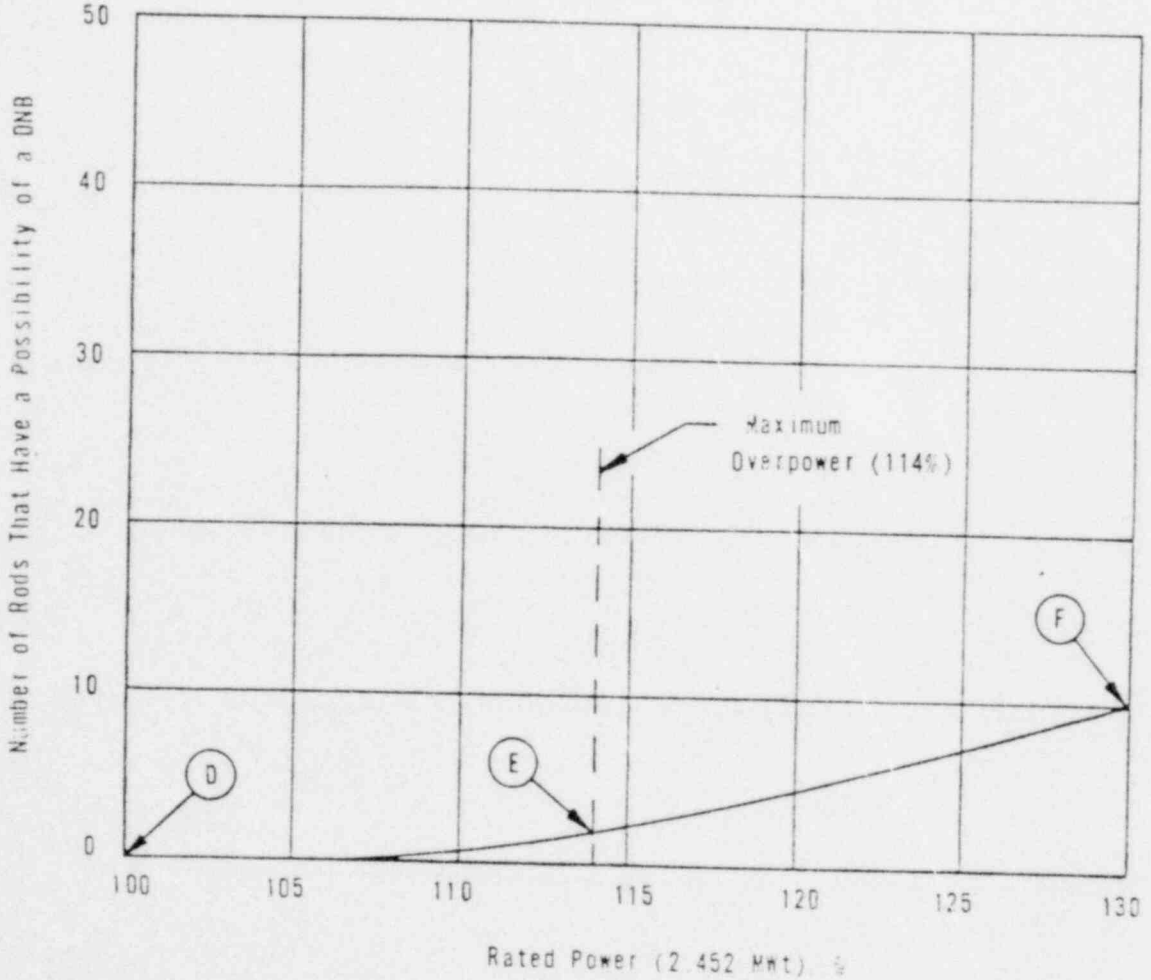

POSSIBLE FUEL ROD DNB S FOR MOST
PROBABLE CONDITIONS - 36 816-ROD CORE

Figure 3-13

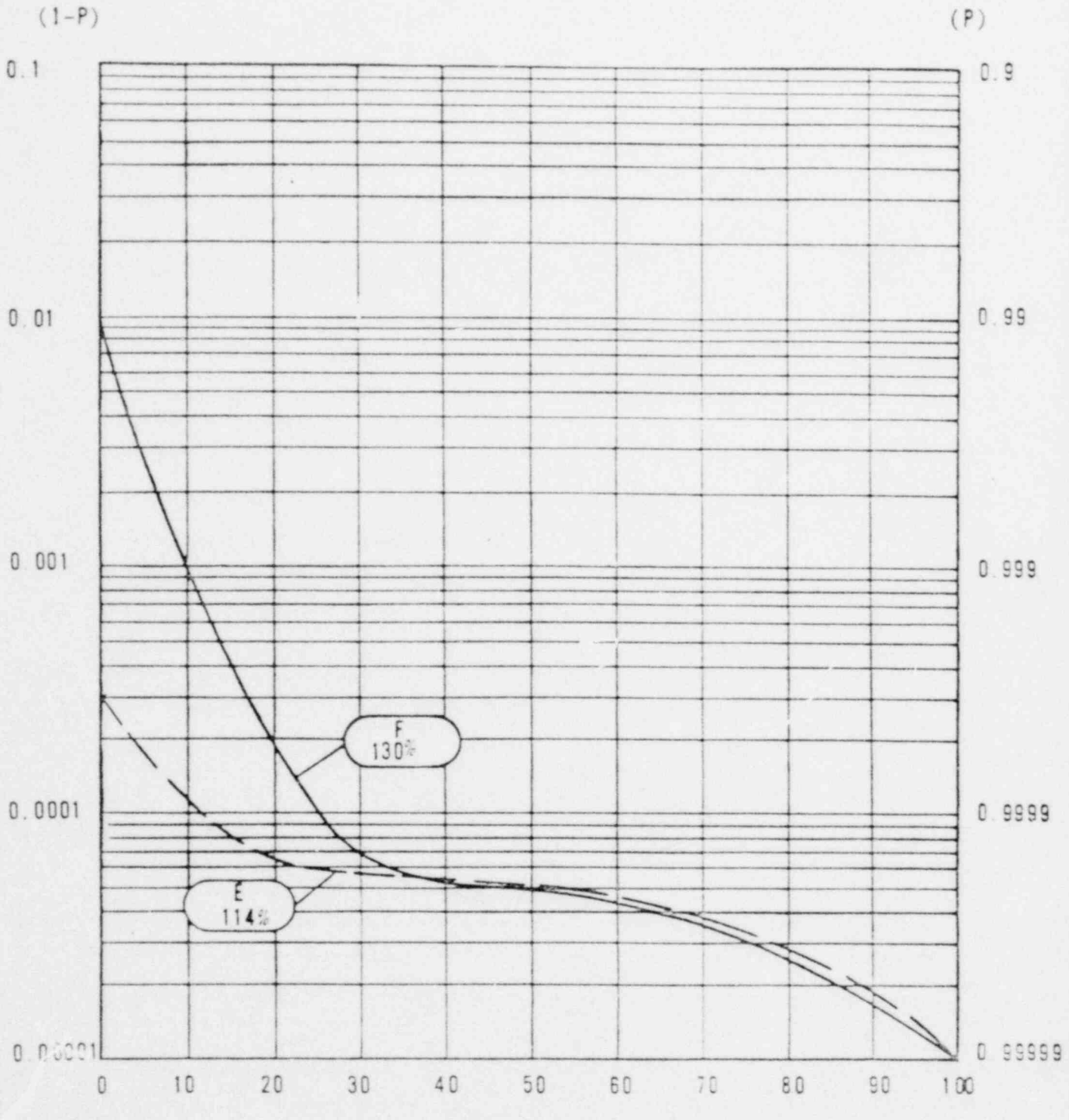

DISTRIBUTION OF POPULATION PROTECTED P, AND 1-P VERSUS NUMBER OF RODS FOR MOST PROBABLE CONDITIONS

Figure 3-14

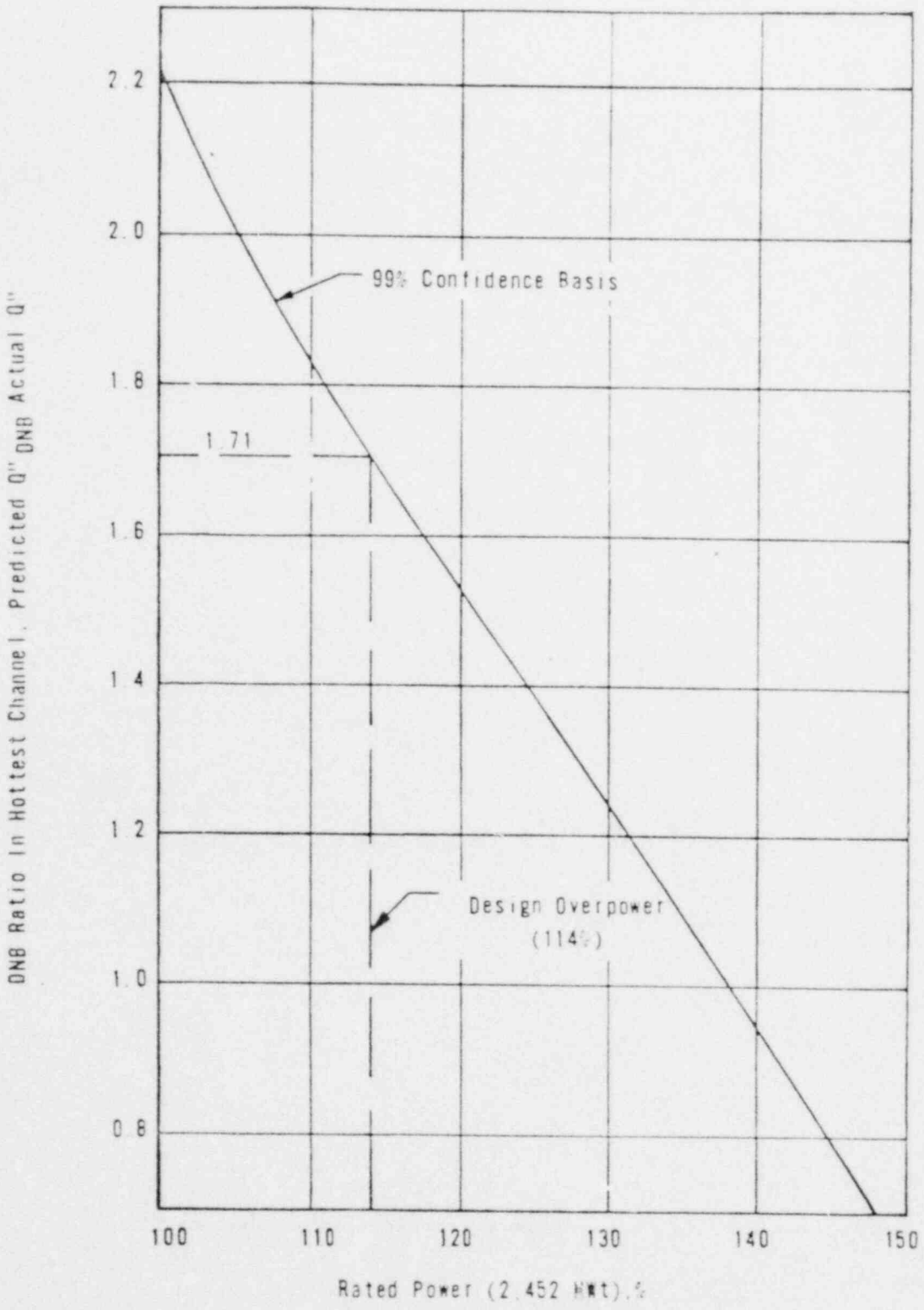

00295

DNB RATIOS (W-3) IN HOT UNIT CELL VERSUS REACTOR POWER

Figure 3-15

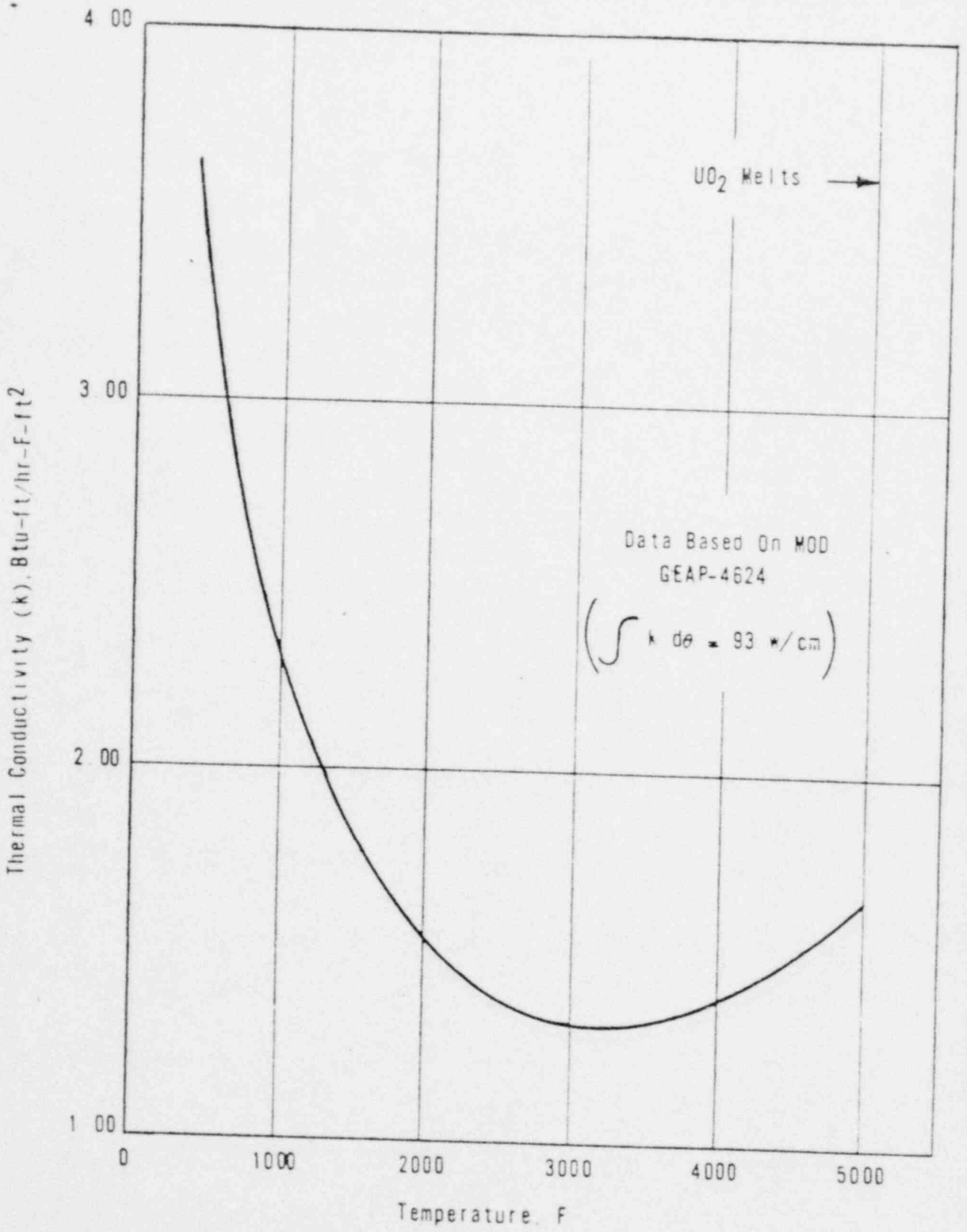

00296

THERMAL CONDUCTIVITY OF UO_2

Figure 3-17

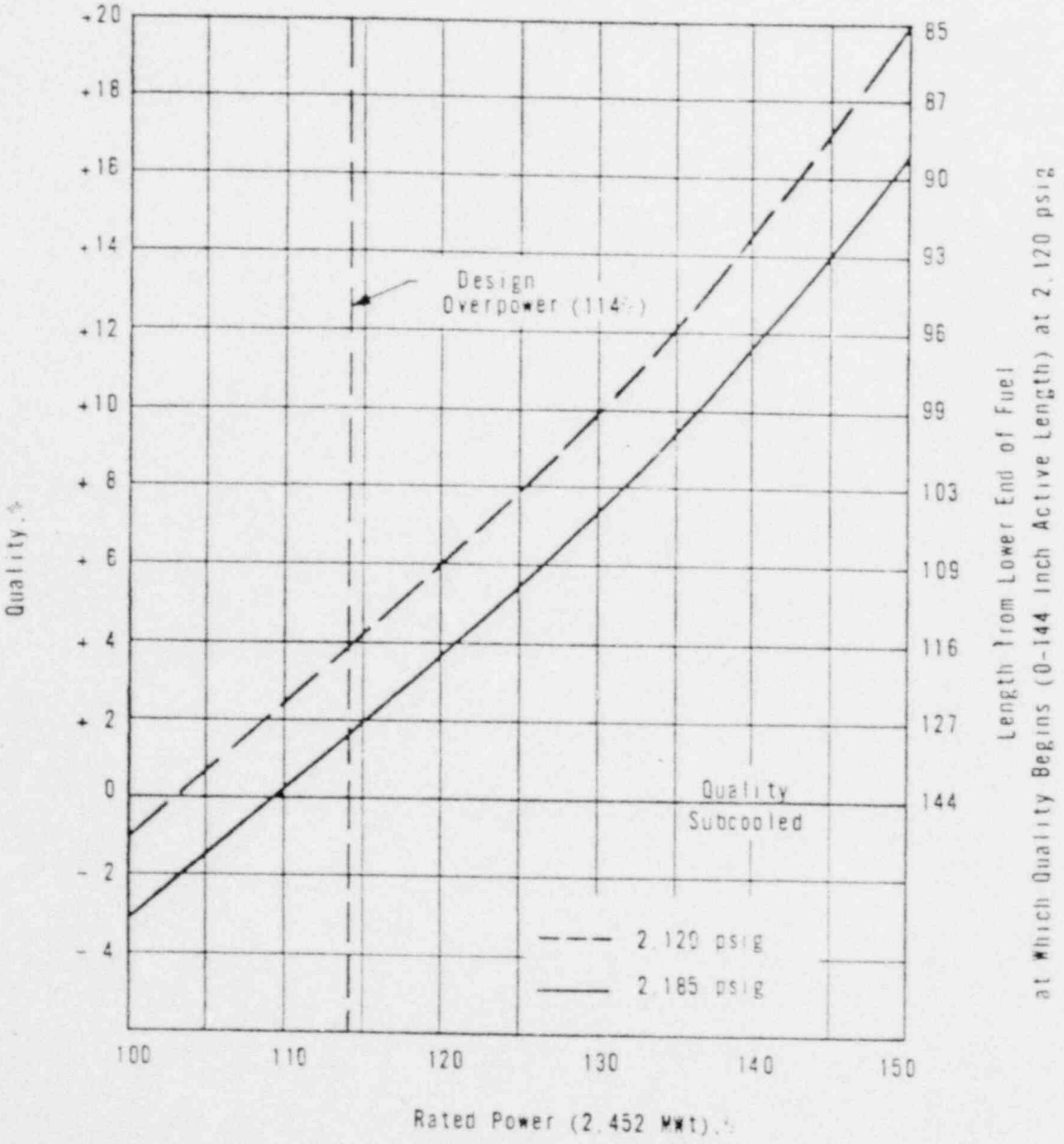

MAXIMUM HOT CHANNEL EXIT QUALITY
VERSUS REACTOR POWER

Figure 3-16

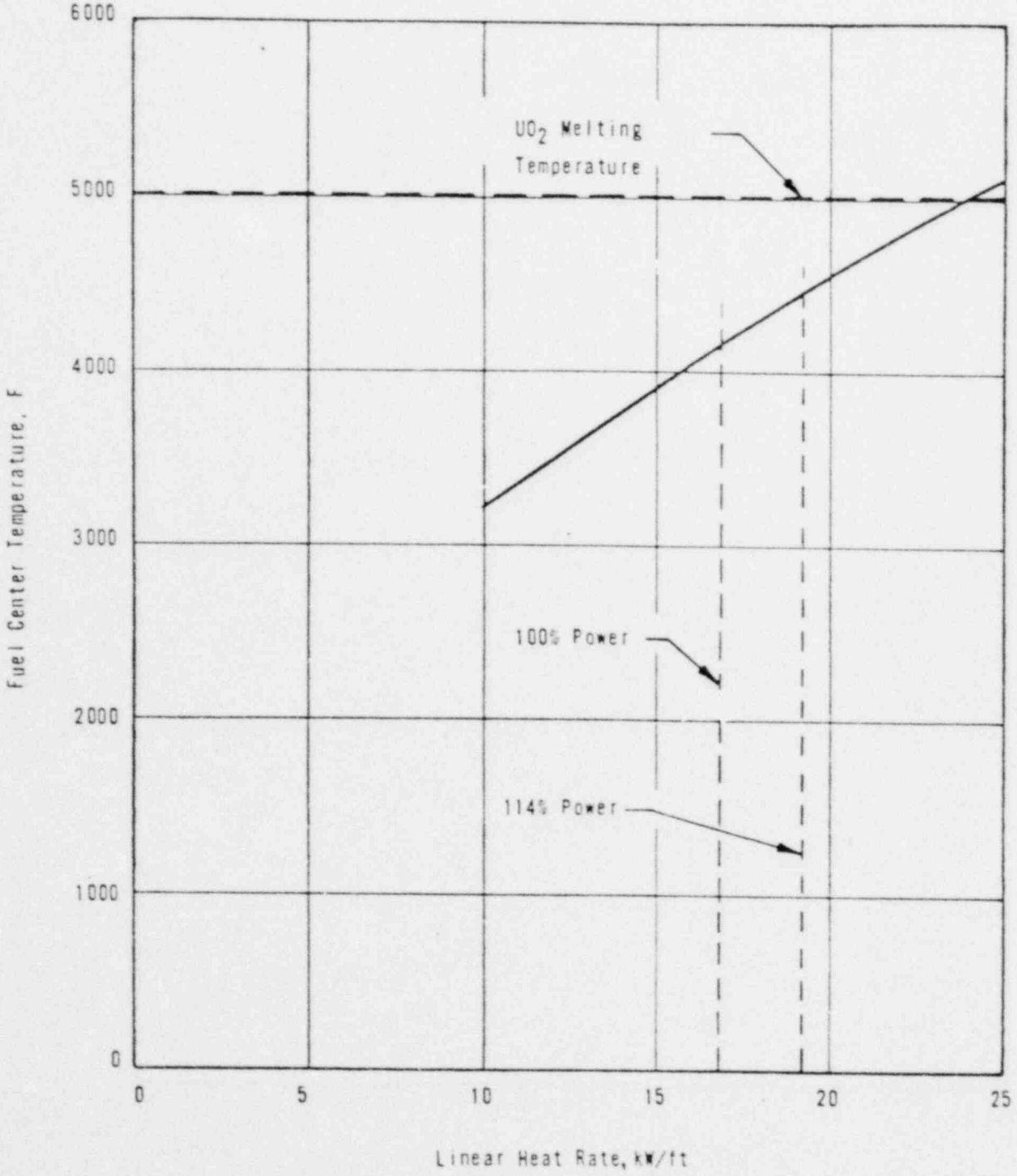

FUEL CENTER TEMPERATURE AT THE HOT SPOT
VERSUS LINEAR POWER

Figure 3-18

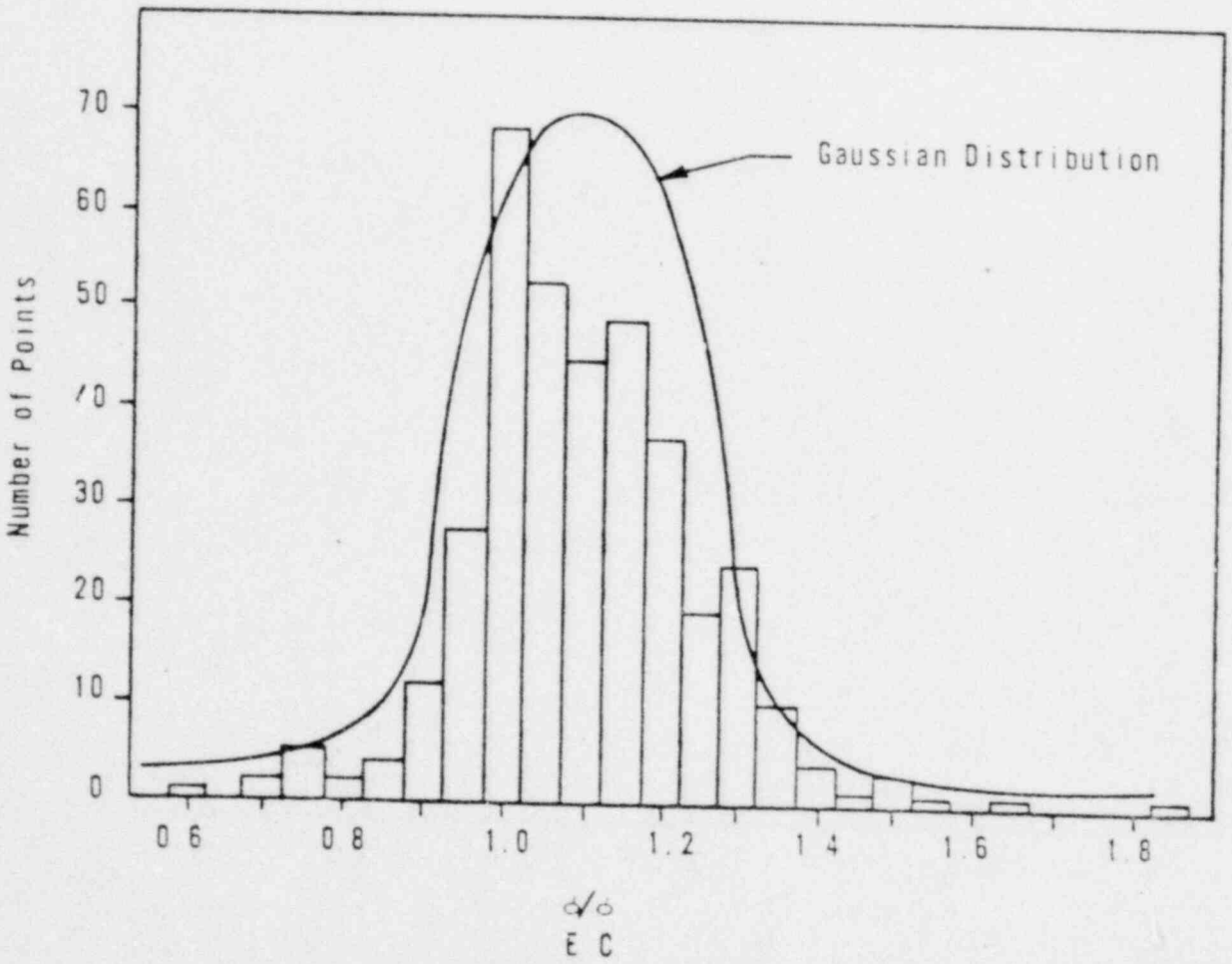

NUMBER OF DATA POINTS VERSUS σE/σC

00249

Figure 3-19

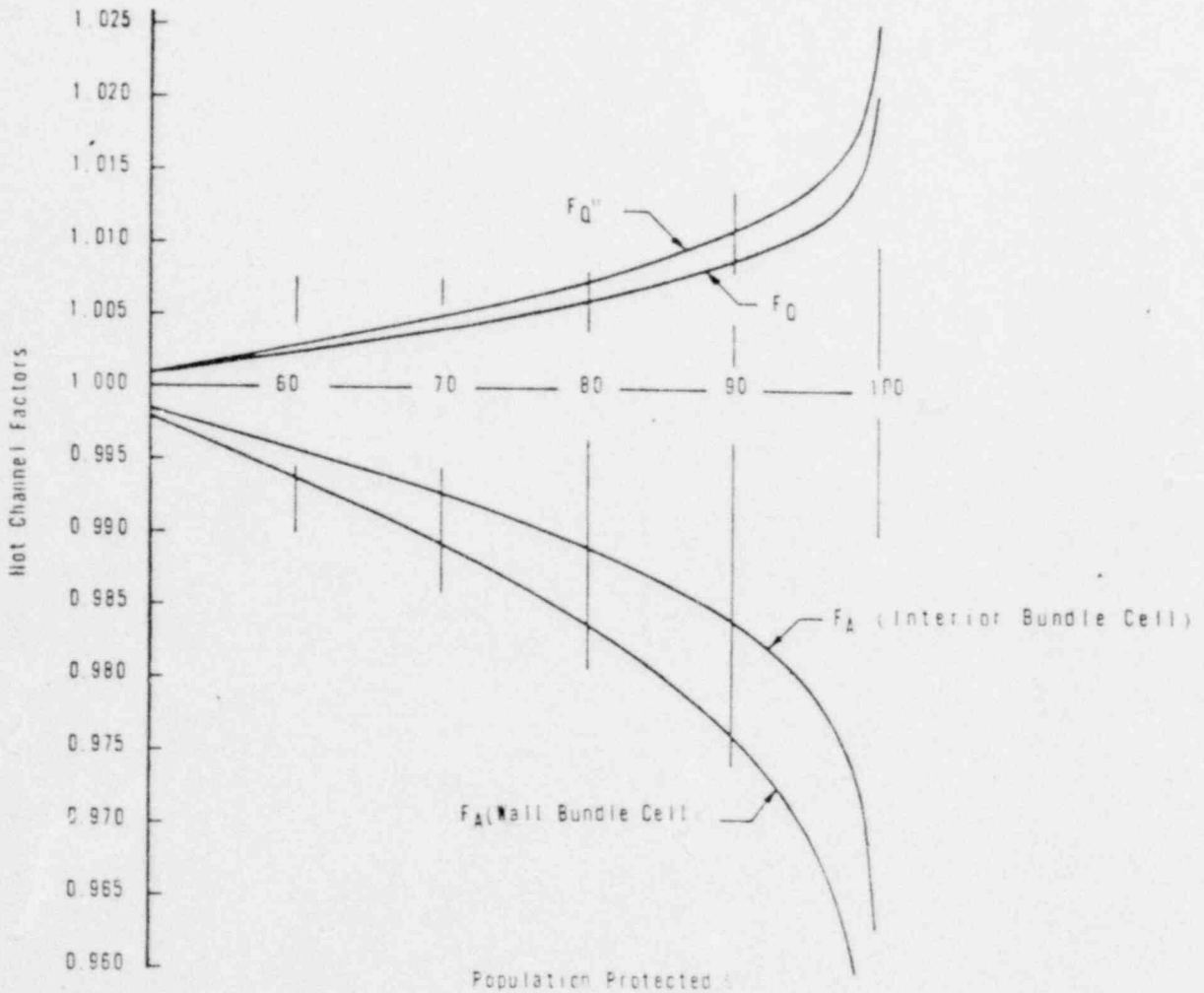

HOT CHANNEL FACTORS VERSUS
PER CENT POPULATION PROTECTED

Figure 3-20

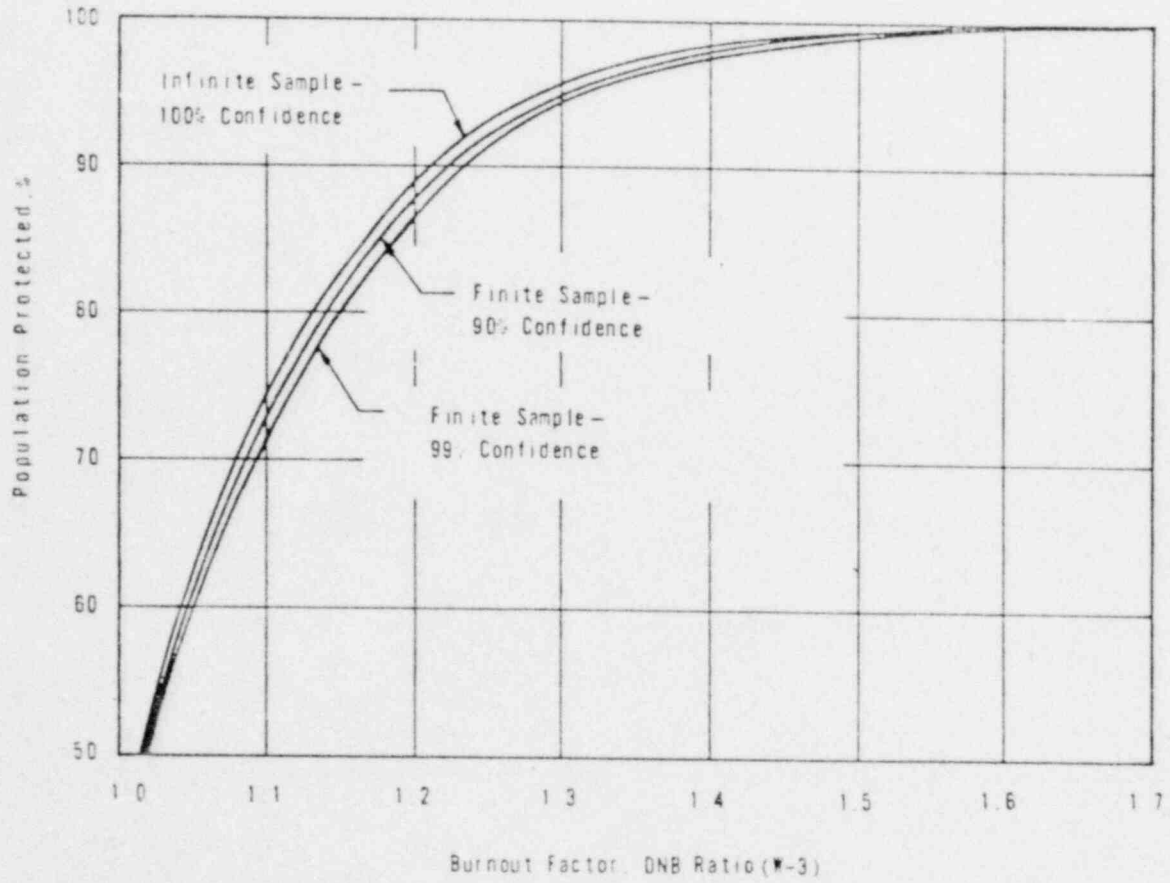

BURNOUT FACTOR (W-3) VERSUS POPULATION
FOR VARIOUS CONFIDENCE LEVELS

Figure 3-21

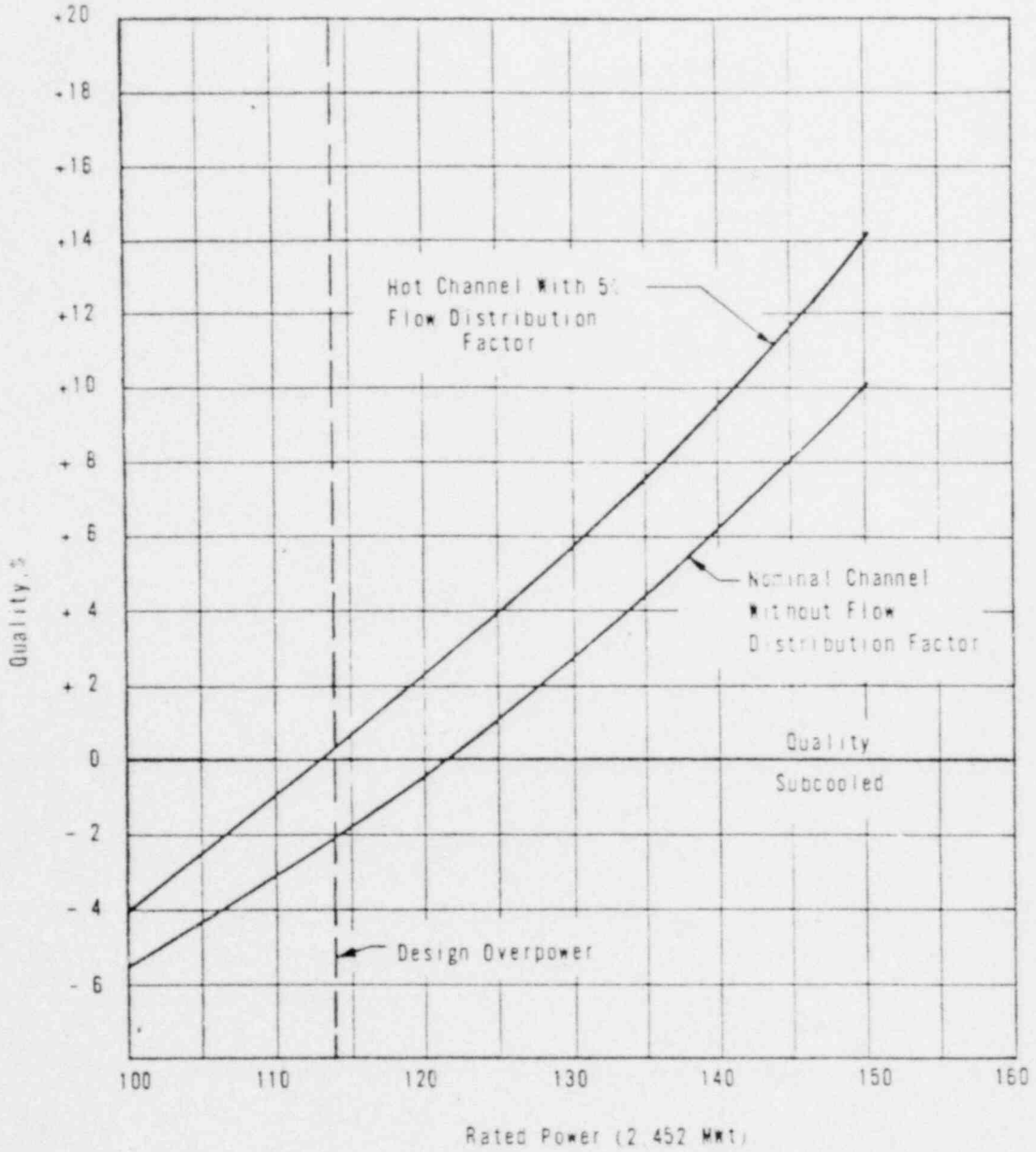

DESIGN HOT CHANNEL AND NOMINAL CHANNEL EXIT QUALITIES VERSUS REACTOR POWER (WITHOUT ENGINEERING HOT CHANNEL FACTORS)

Figure 3-22

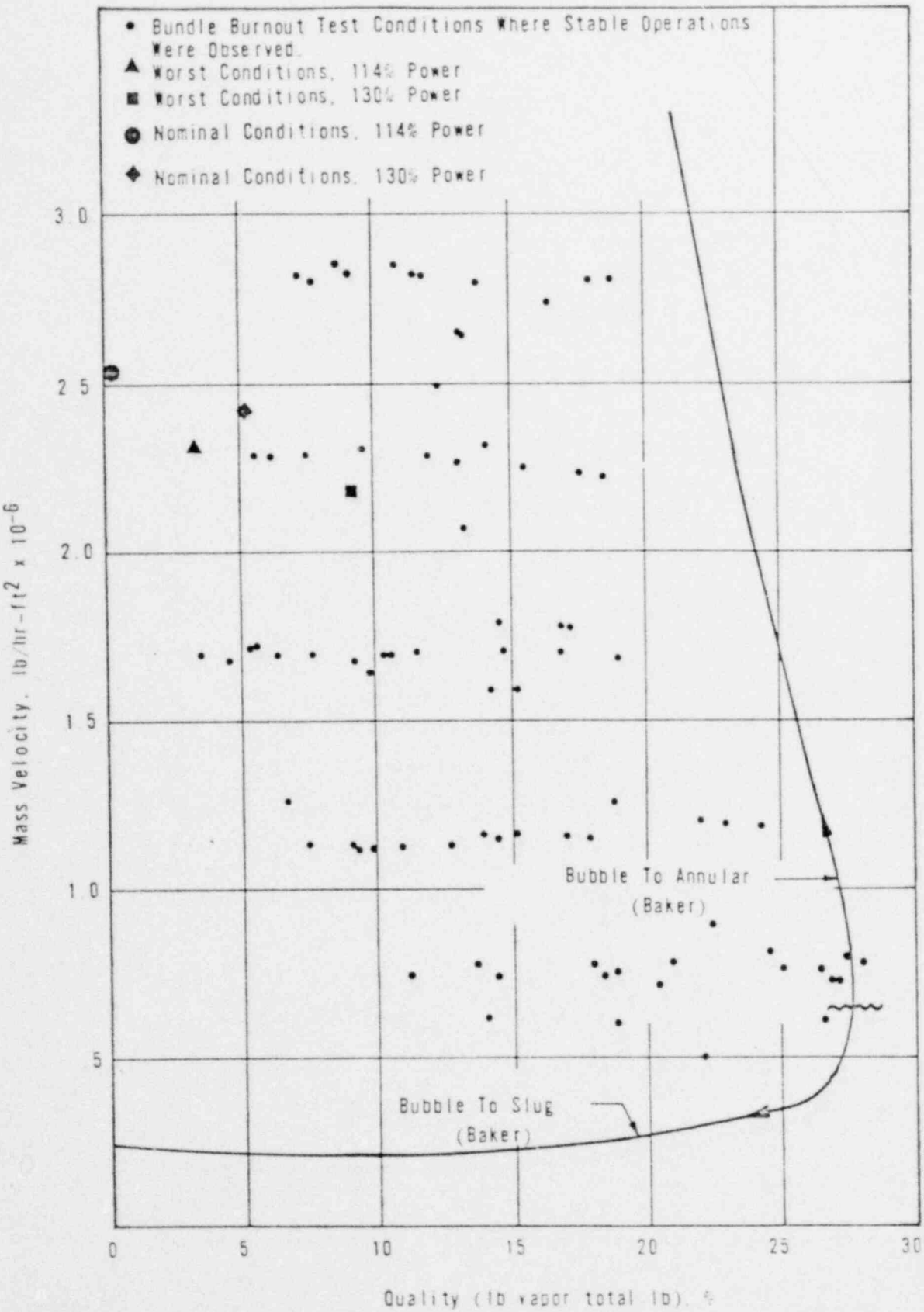

FLOW REGIME MAP FOR THE HOT UNIT CELL

Figure 3-23

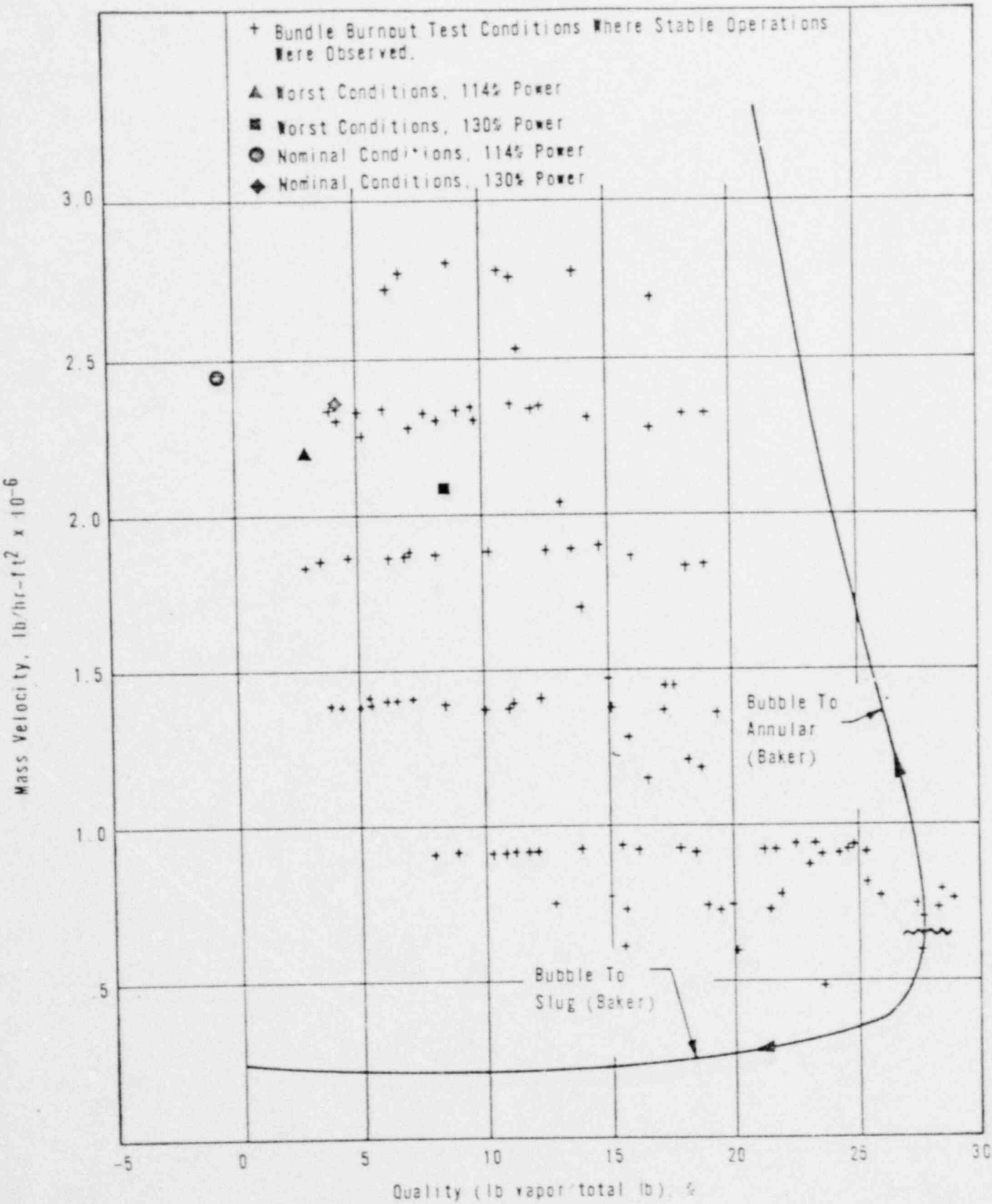

FLOW REGIME MAP FOR THE HOT CONTROL ROD CE

Figure 3-

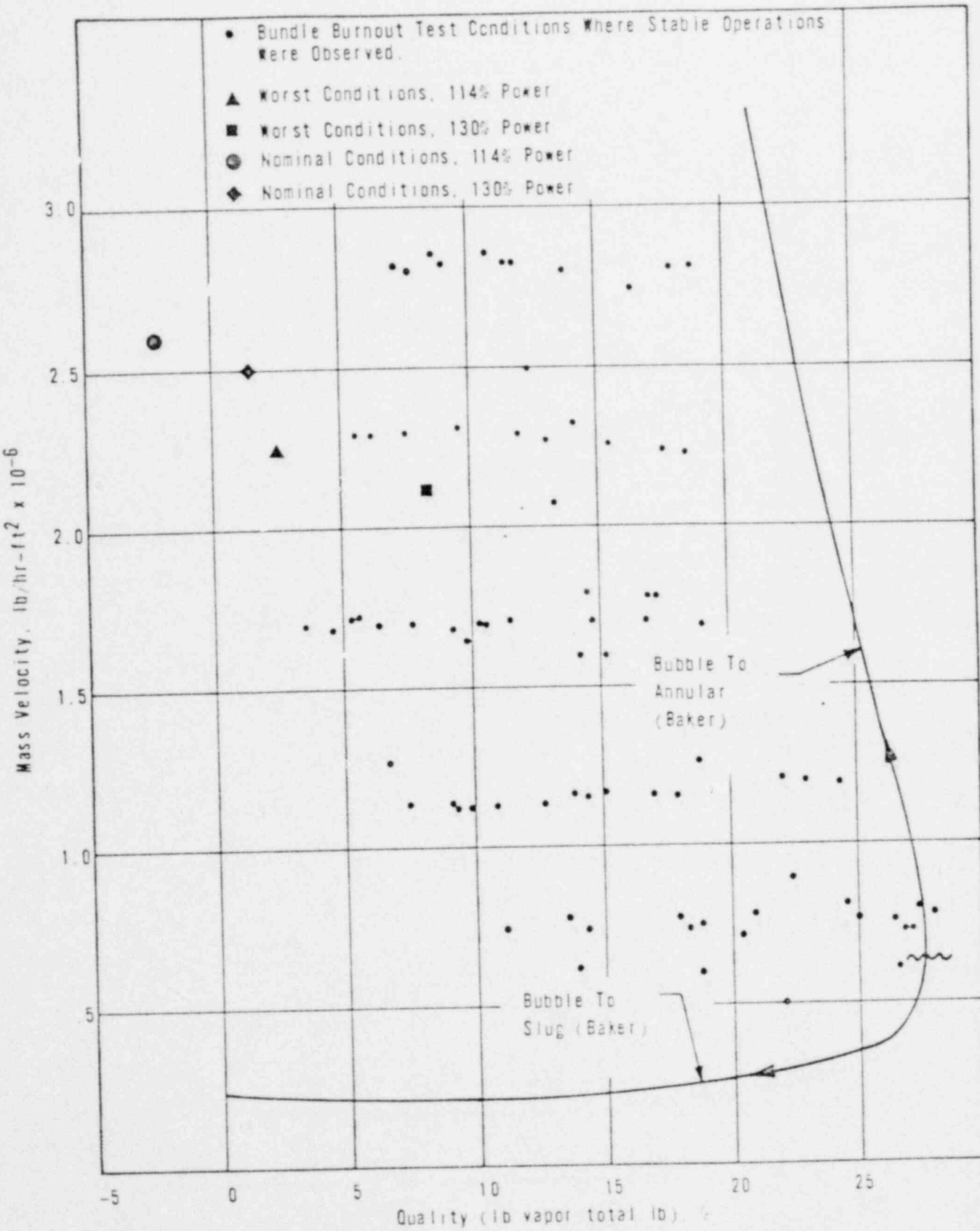

FLOW REGIME MAP FOR THE HOT WALL CELL

Figure 3-25

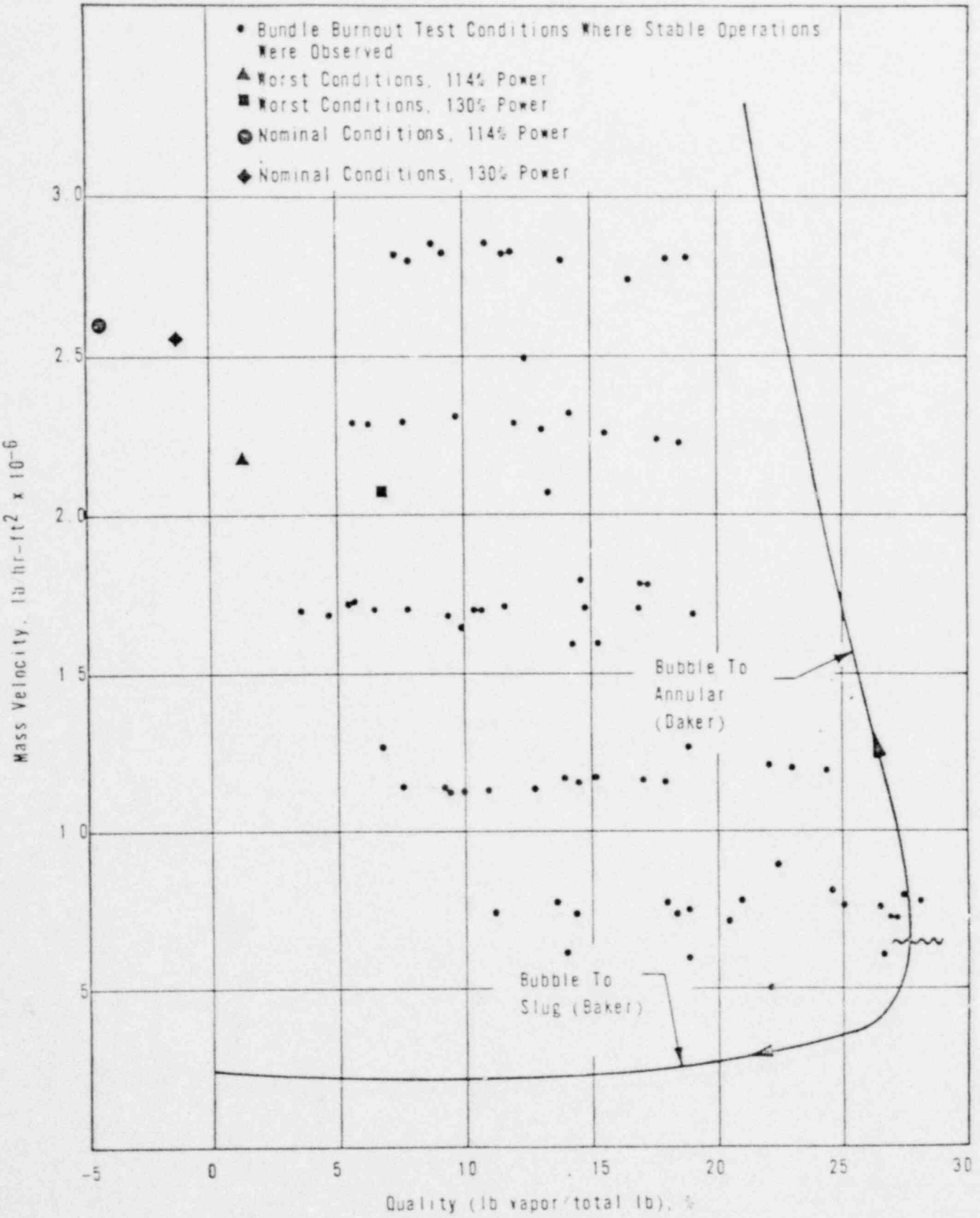

FLOW REGIME MAP FOR THE HOT CORNER CELL

Figure 3-26

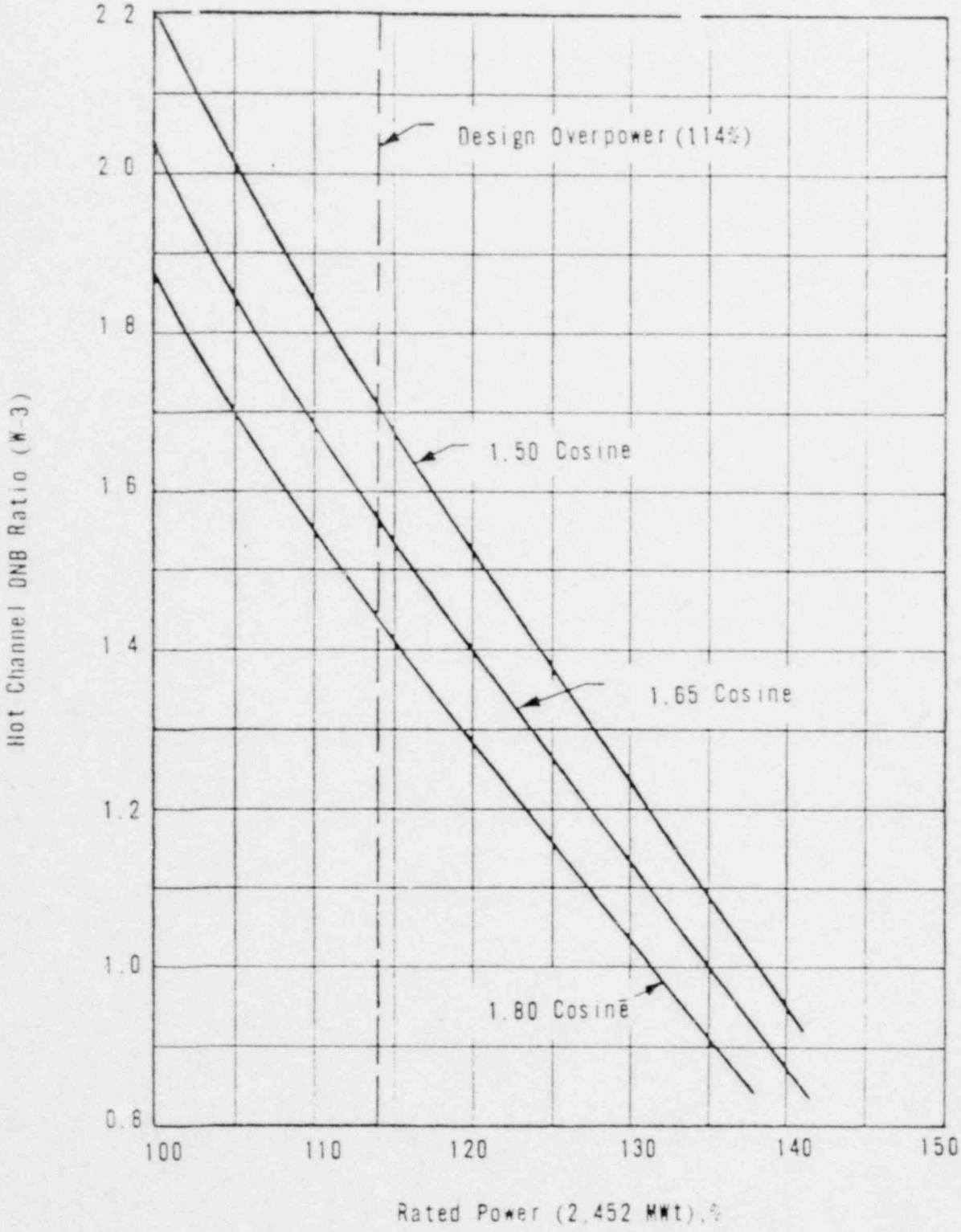

HOT CHANNEL DNB RATIO (W-3) VERSUS POWER FOR VARIOUS AXIAL FLUX SHAPES

Figure 3-27

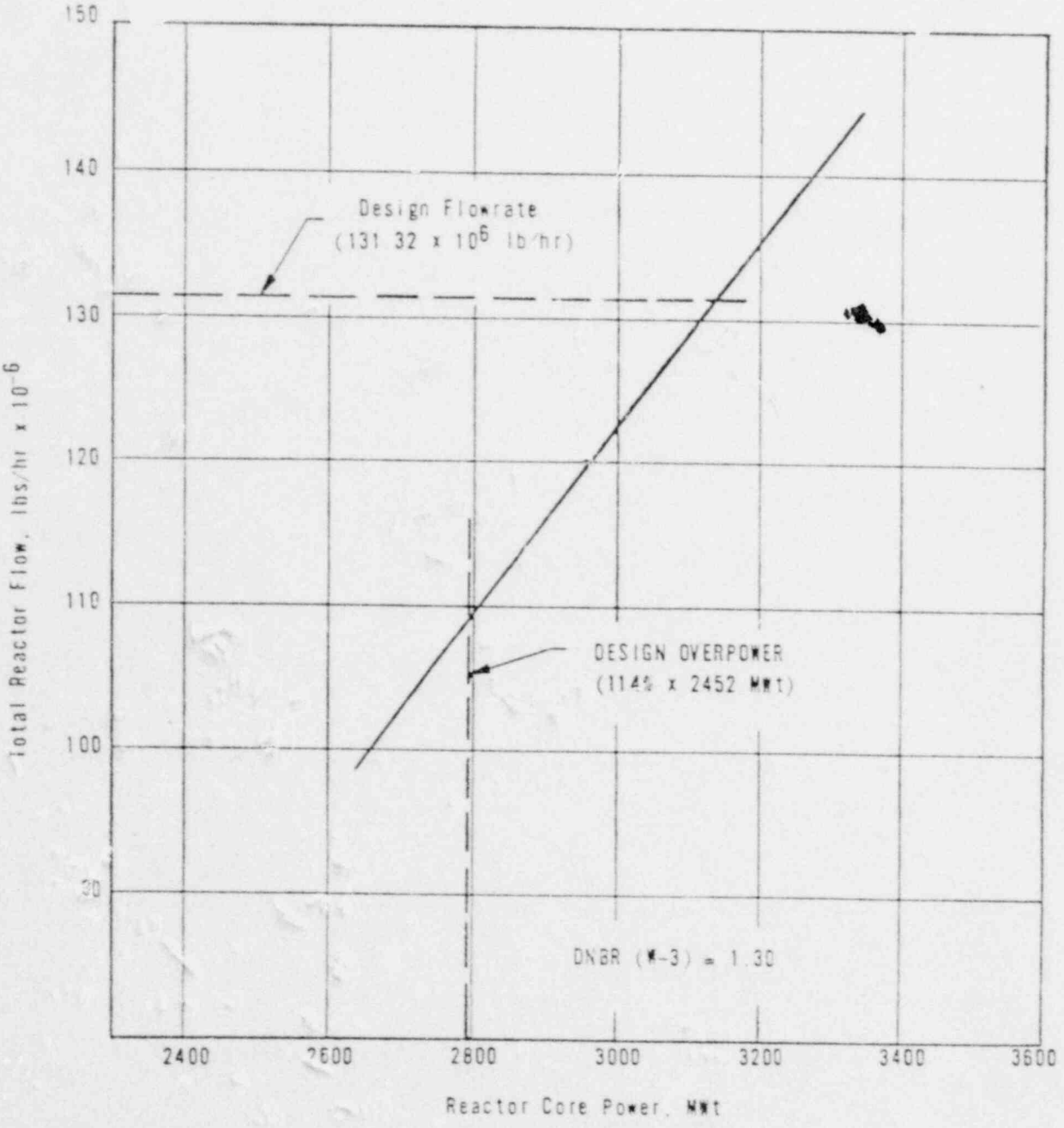

REACTOR COOLANT SYSTEM FLOW VERSUS POWER

Figure 3-28

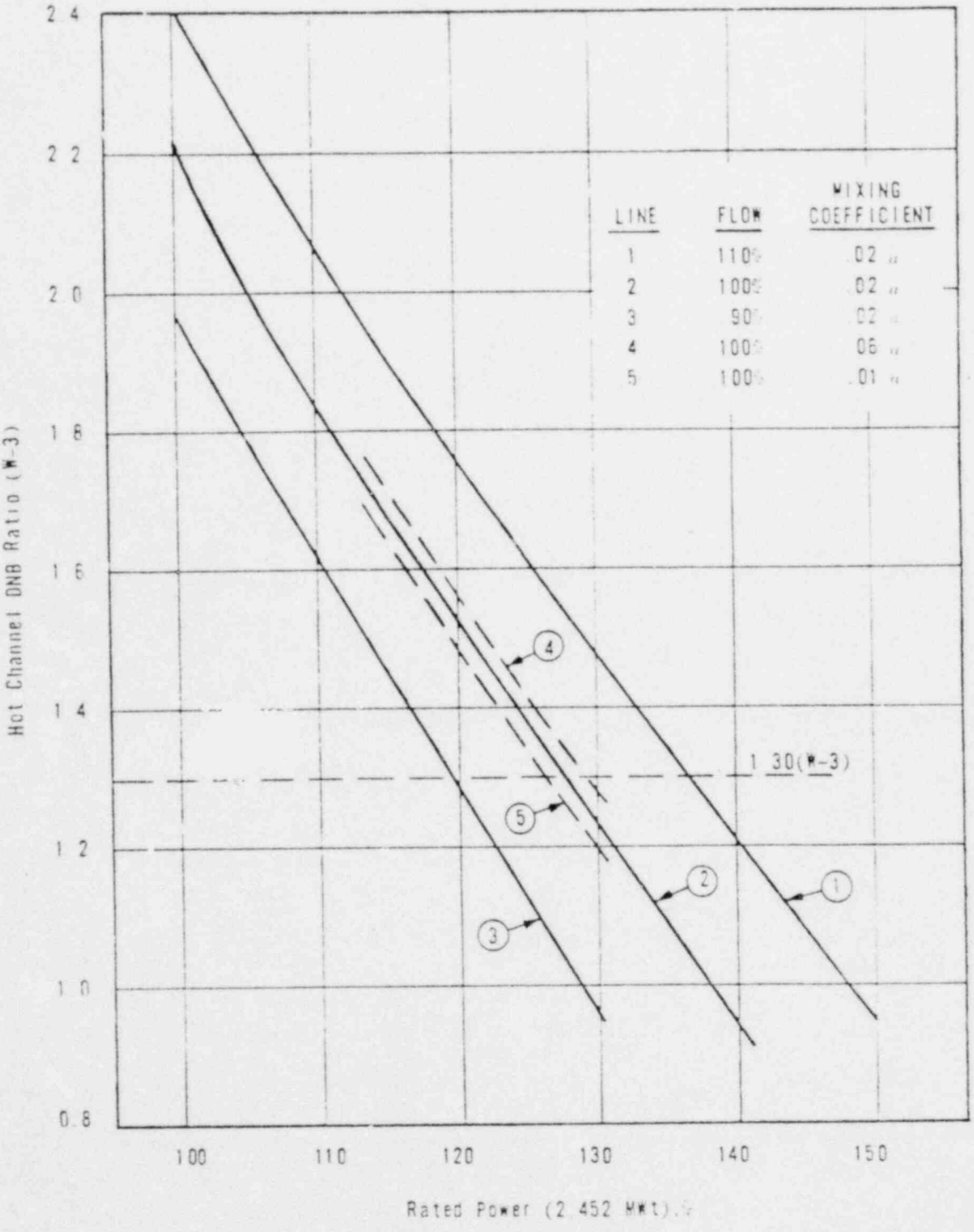

HOT CHANNEL DNB RATIO (W-3) VERSUS POWER WITH REACTOR SYSTEM FLOW AND ENERGY MIXING AS PARAMETERS.

Figure 3-29

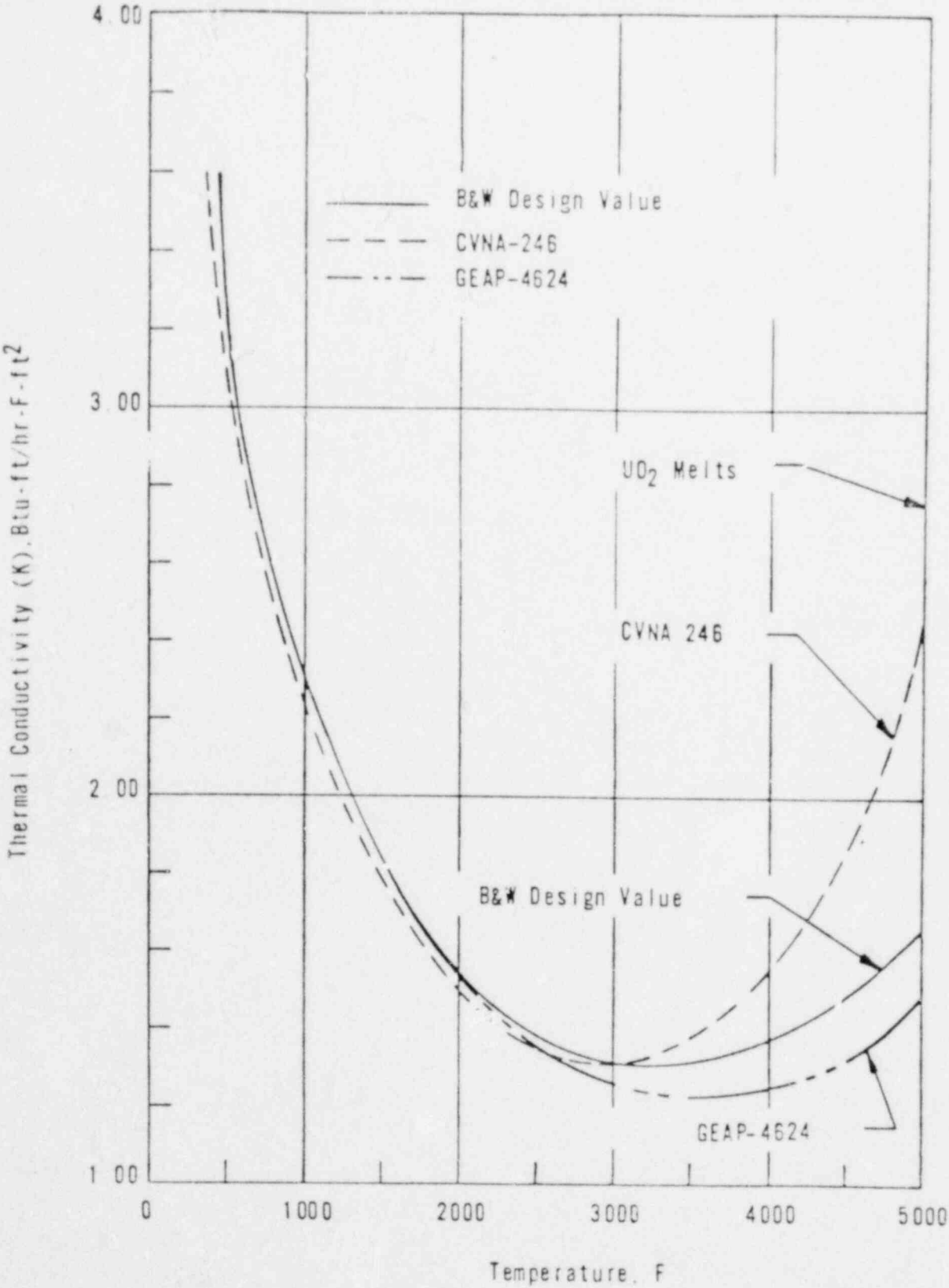

THERMAL CONDUCTIVITY OF 93.5 PER CENT DENSE SINTERED UO_2 PELLETS

00310

Figure 3-30

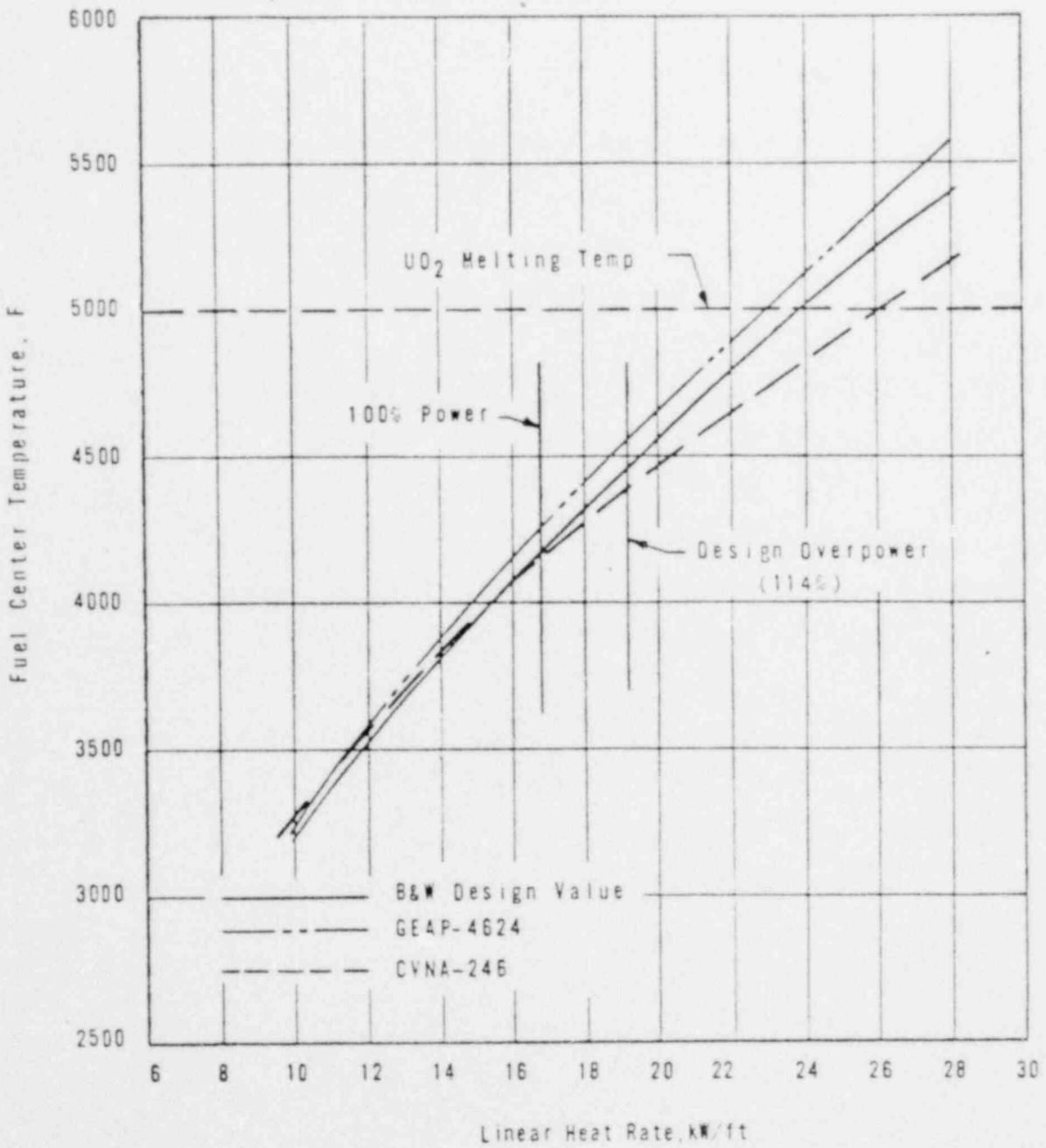

FUEL CENTER TEMPERATURE FOR BEGINNING-OF-LIFE CONDITIONS

Figure 3-31

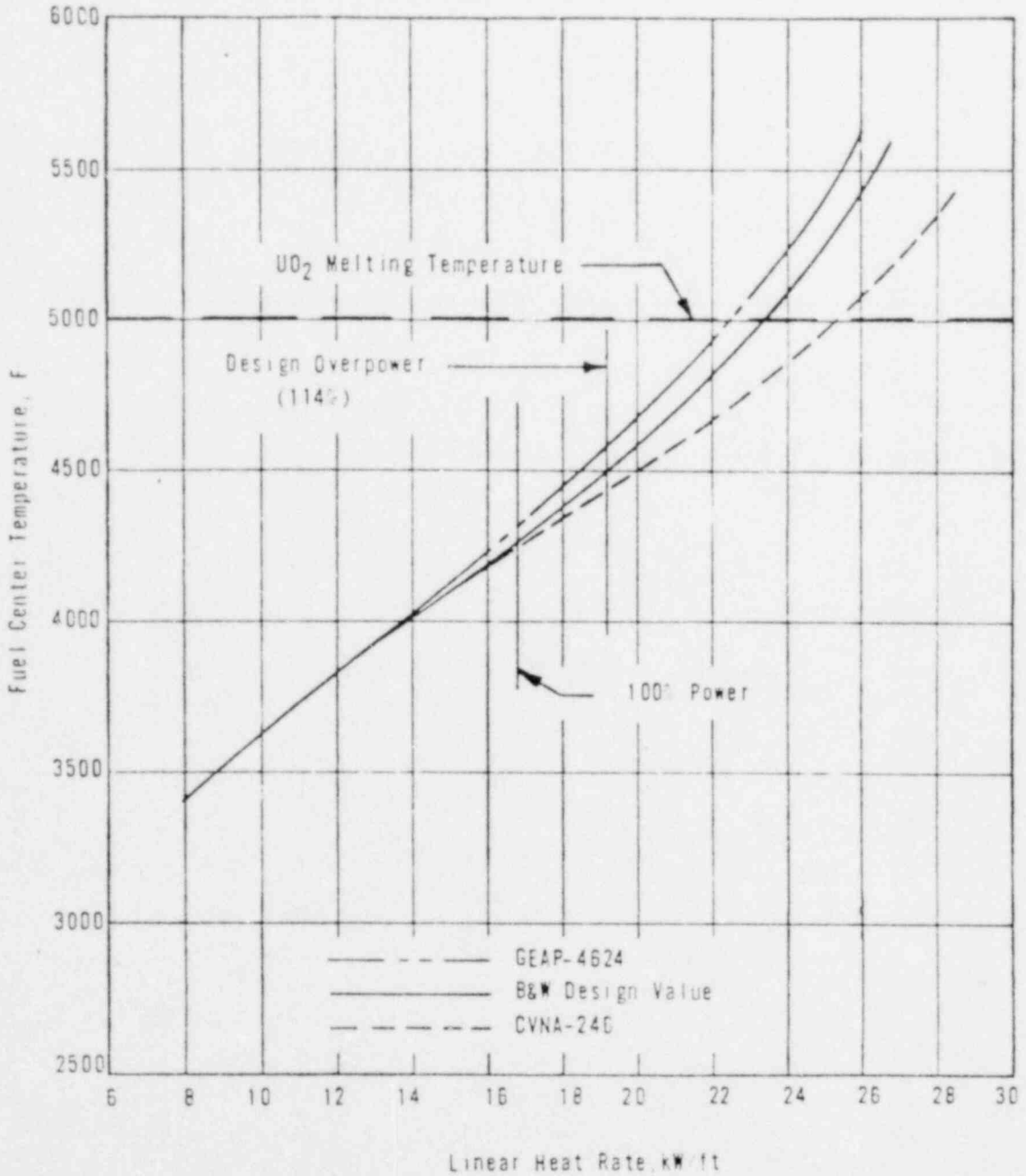

FUEL CENTER TEMPERATURE FOR END-OF-LIFE CONDITIONS

Figure 3-32

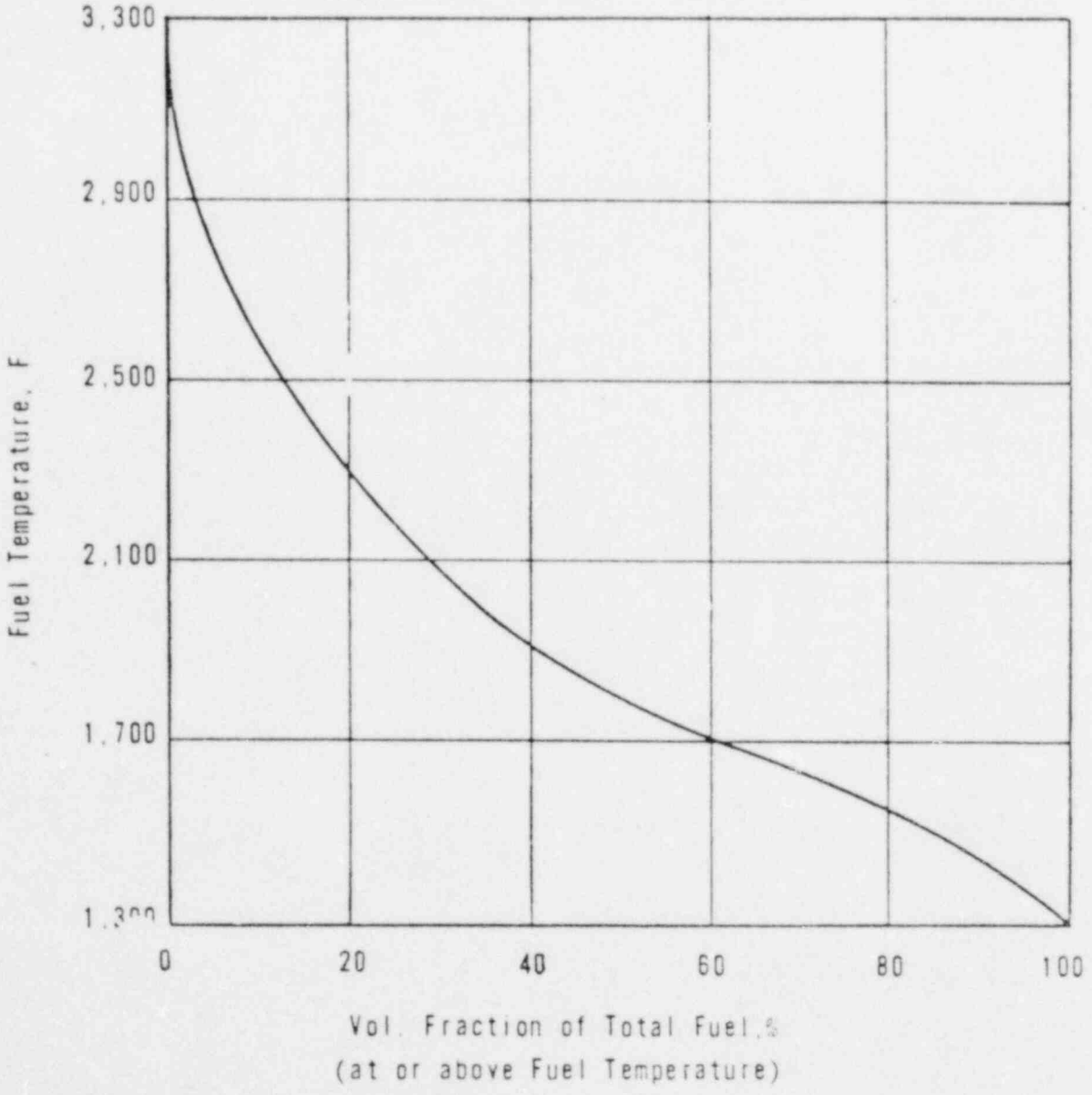

FUEL TEMPERATURE VERSUS TOTAL
FUEL VOLUME FRACTION FOR
EQUILIBRIUM CYCLE AT END OF LIFE

00313

Figure 3-33

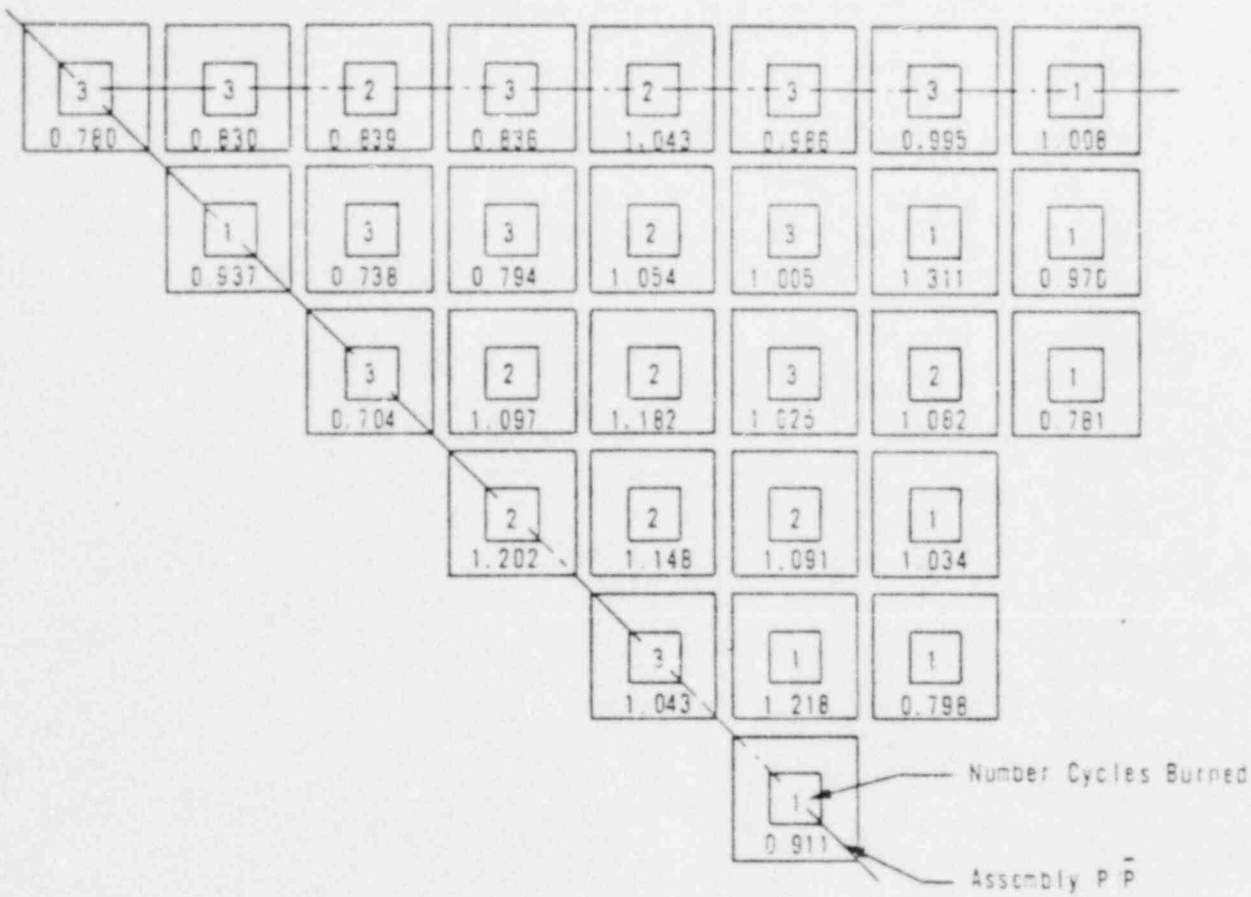

TYPICAL REACTOR FUEL ASSEMBLY POWER
DISTRIBUTION AT END-OF-LIFE EQUILIBRIUM
CYCLE CONDITIONS FOR 1 B CORE

Figure 3-34

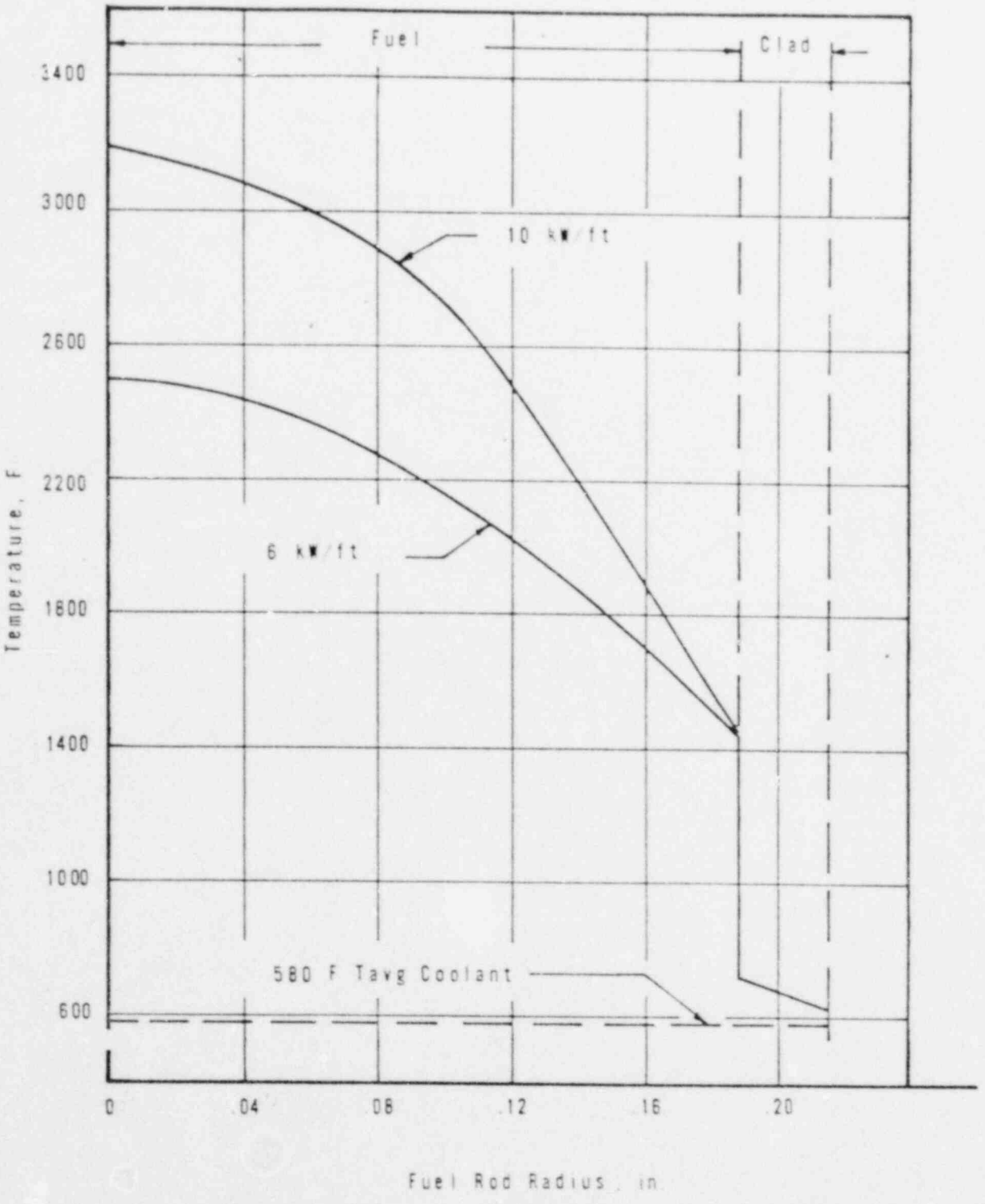

FUEL ROD TEMPERATURE PROFILES AT
6 AND 10 KW FT

Figure 3-35

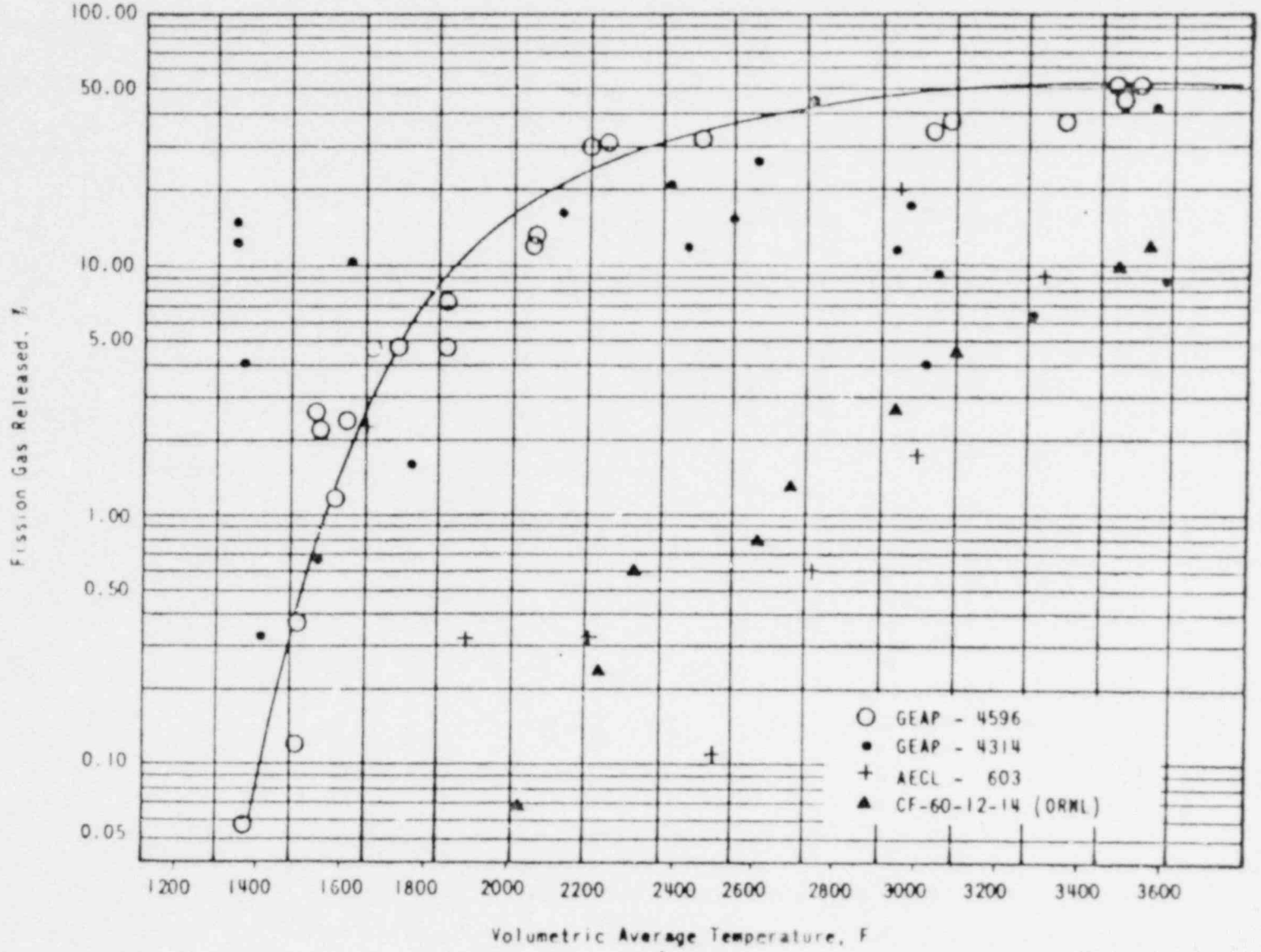

Figure 3-36

PER CENT FISSION GAS RELEASED AS A FUNCTION OF THE AVERAGE TEMPERATURE OF THE UO_2 FUEL

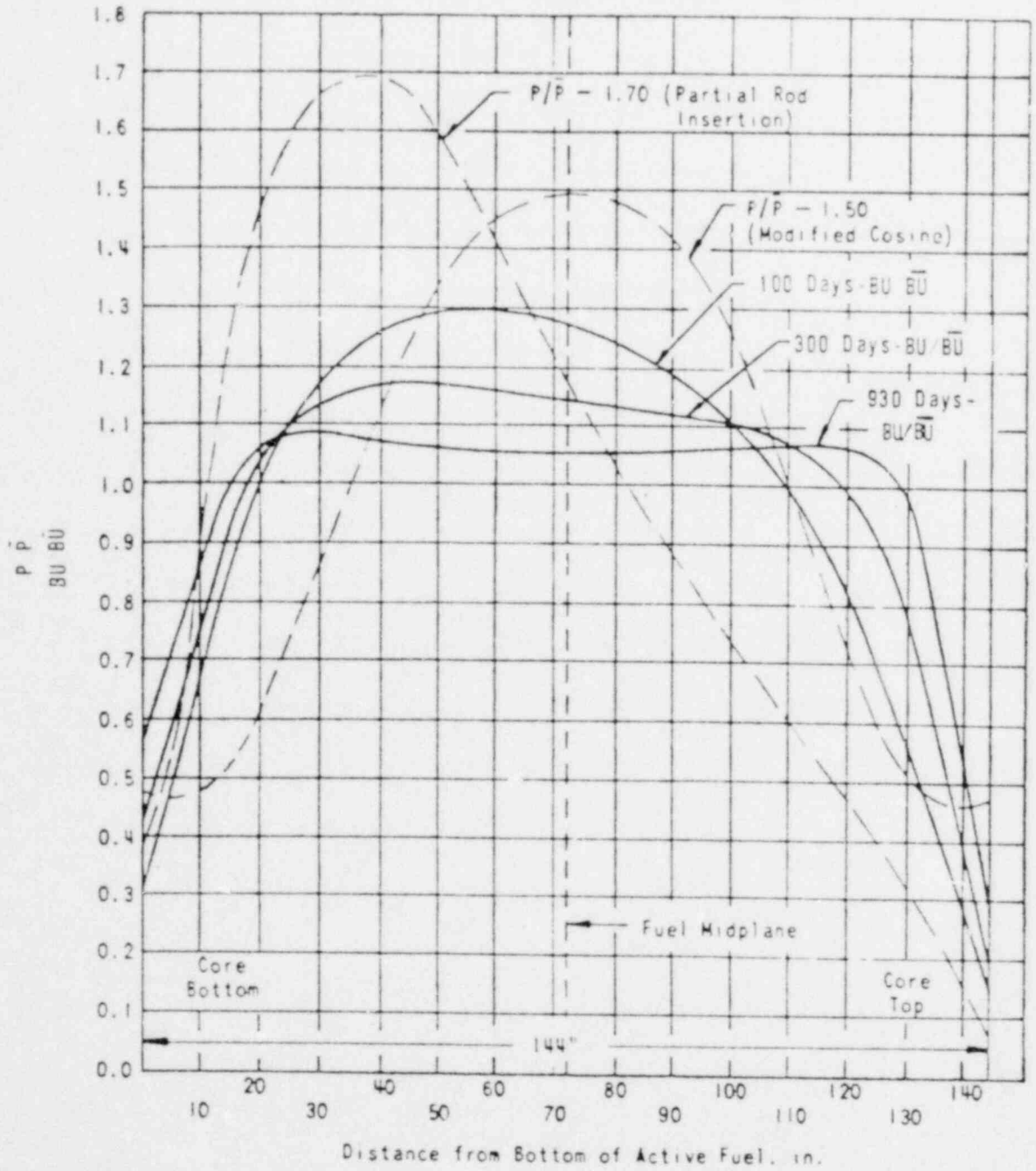

AXIAL LOCAL-TO-AVERAGE BURNUP AND INSTANTANEOUS POWER COMPARISONS

00217

Figure 3-37

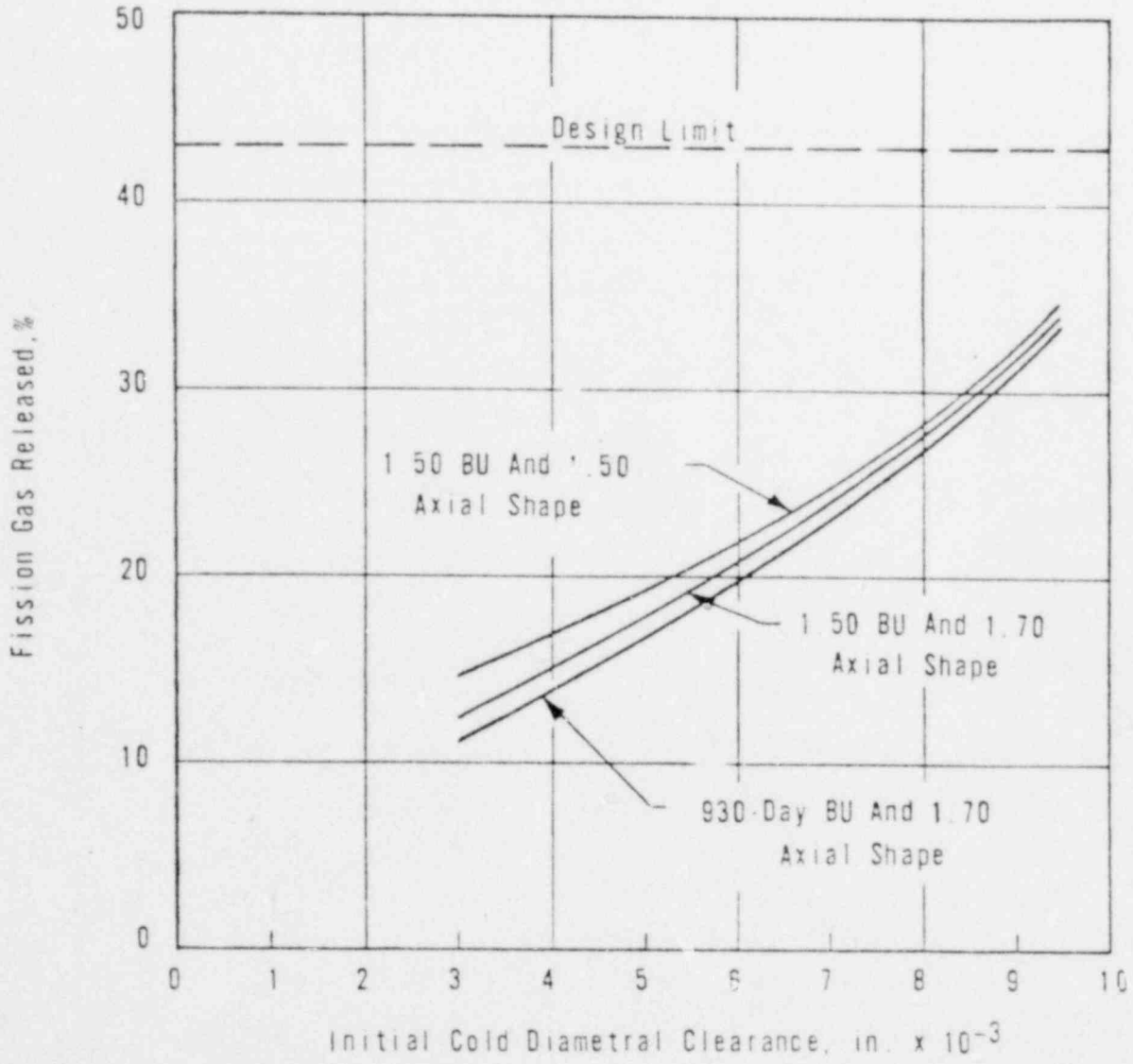

FISSION GAS RELEASE FOR 1 50 AND 1 70
MAX AVG AXIAL POWER SHAPES

Figure 3-38

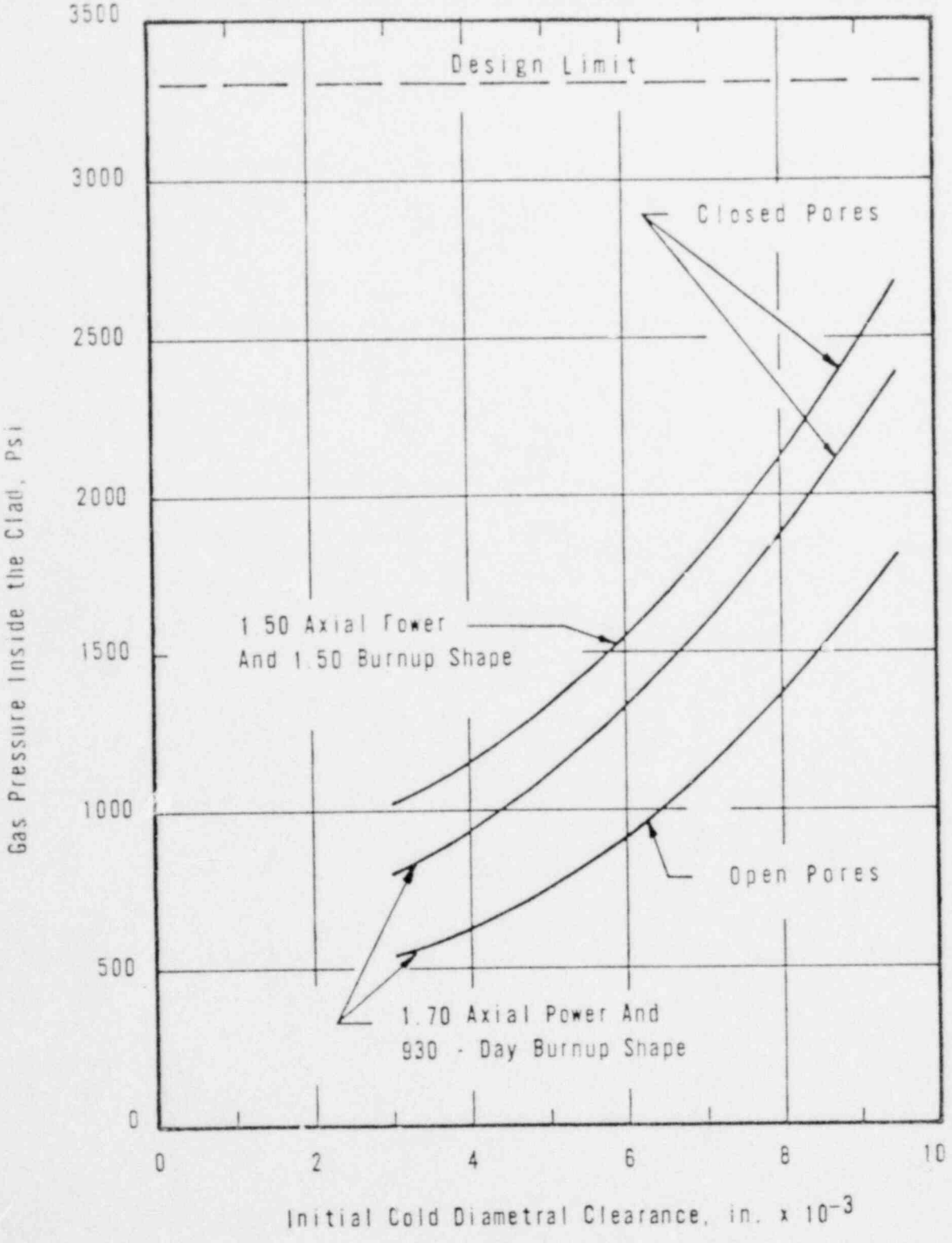

GAS PRESSURE INSIDE THE FUEL CLAD FOR VARIOUS AXIAL BURNUP AND POWER SHAPES FOR IDEAL THERMAL EXPANSION MODEL

Figure 3-35

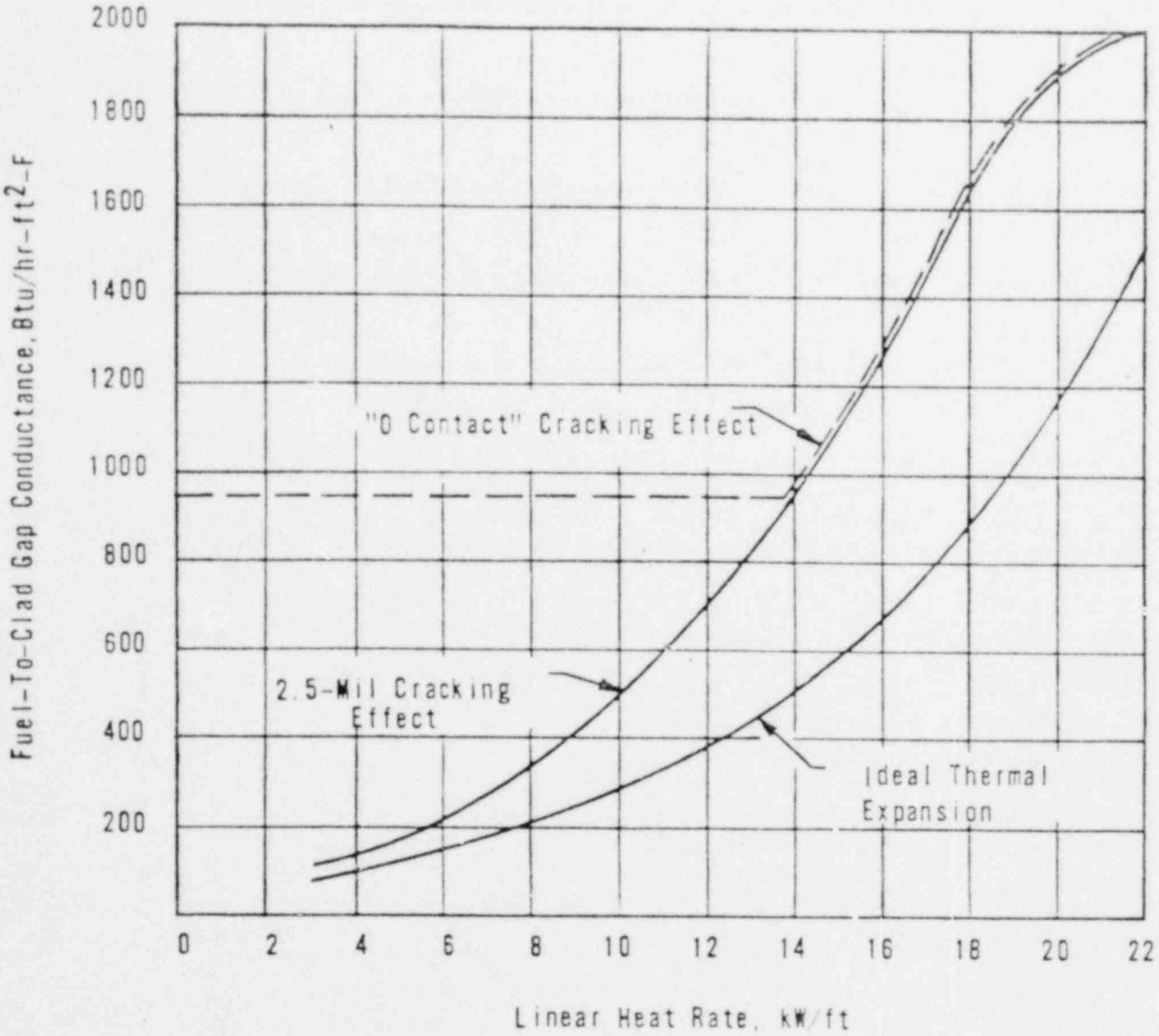

SENSITIVITY ANALYSIS OF THE EFFECTS OF FUEL CRACKING ON FUEL-TO-CLAD GAP CONDUCTANCE

Figure 3-40

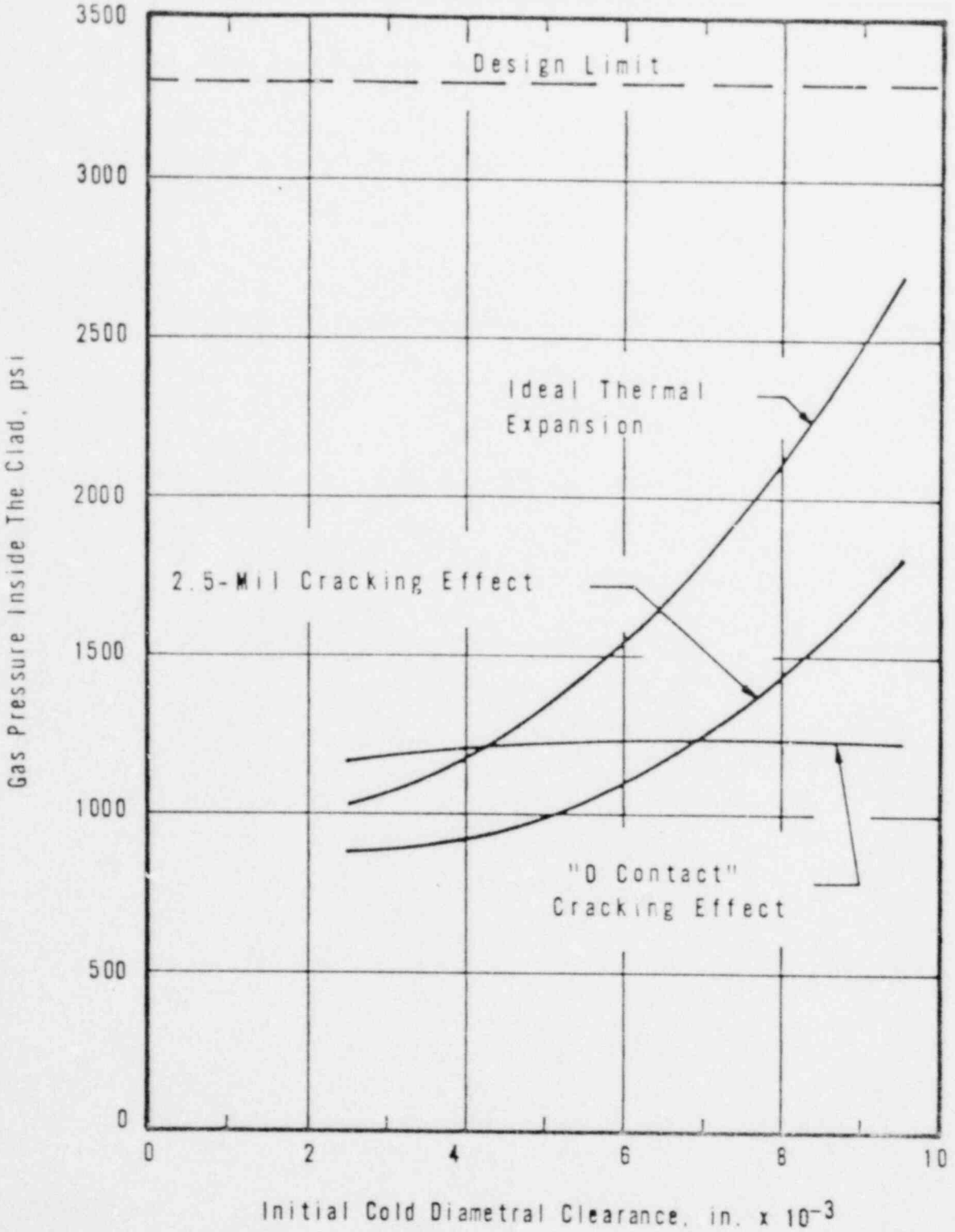

SENSITIVITY ANALYSIS OF THE EFFECTS OF FUEL CRACKING ON INTERNAL PRESSURE

00321

Figure 3-41

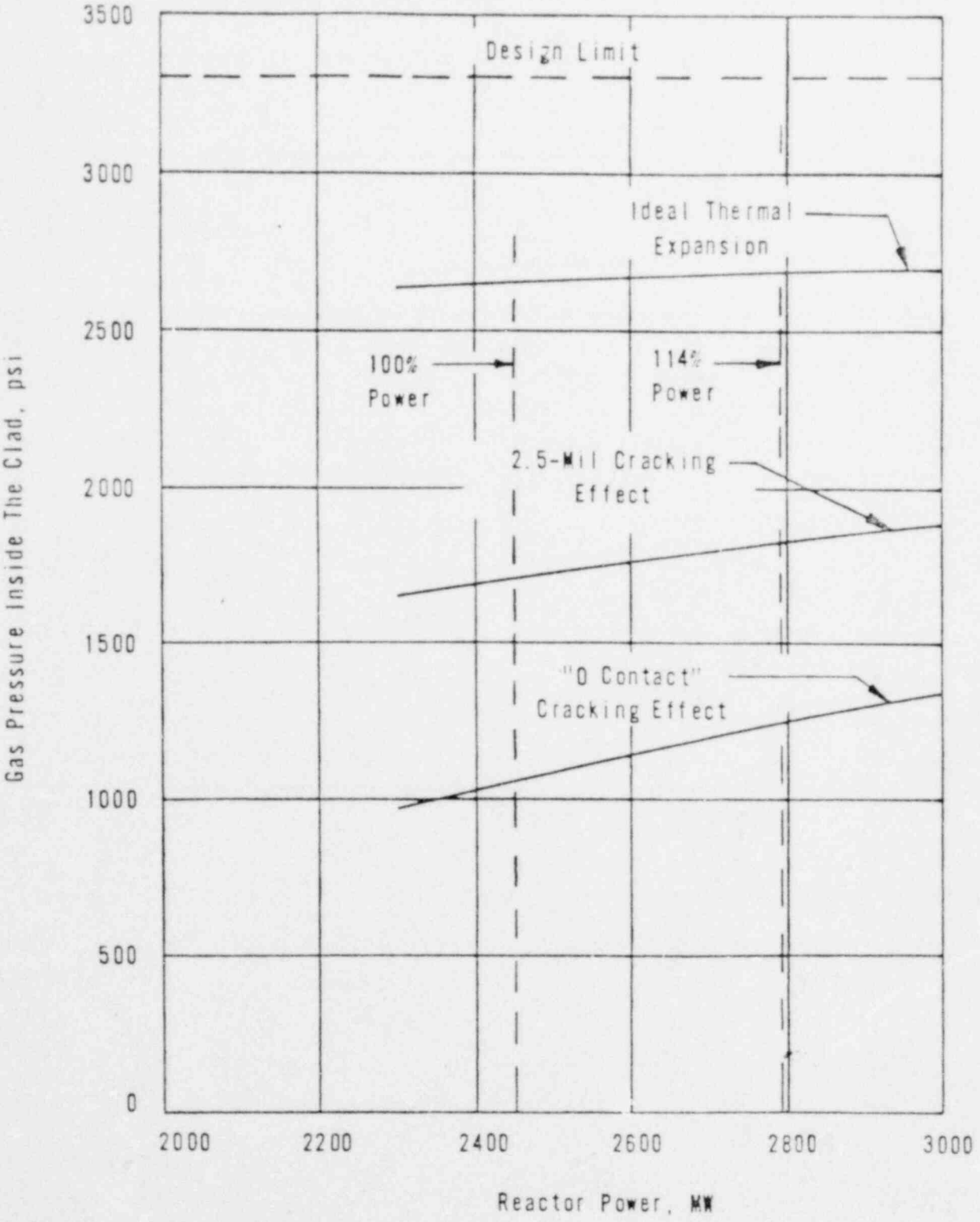

SENSITIVITY ANALYSIS OF THE EFFECTS OF REACTOR POWER ON INTERNAL PRESSURE

Figure 3-42

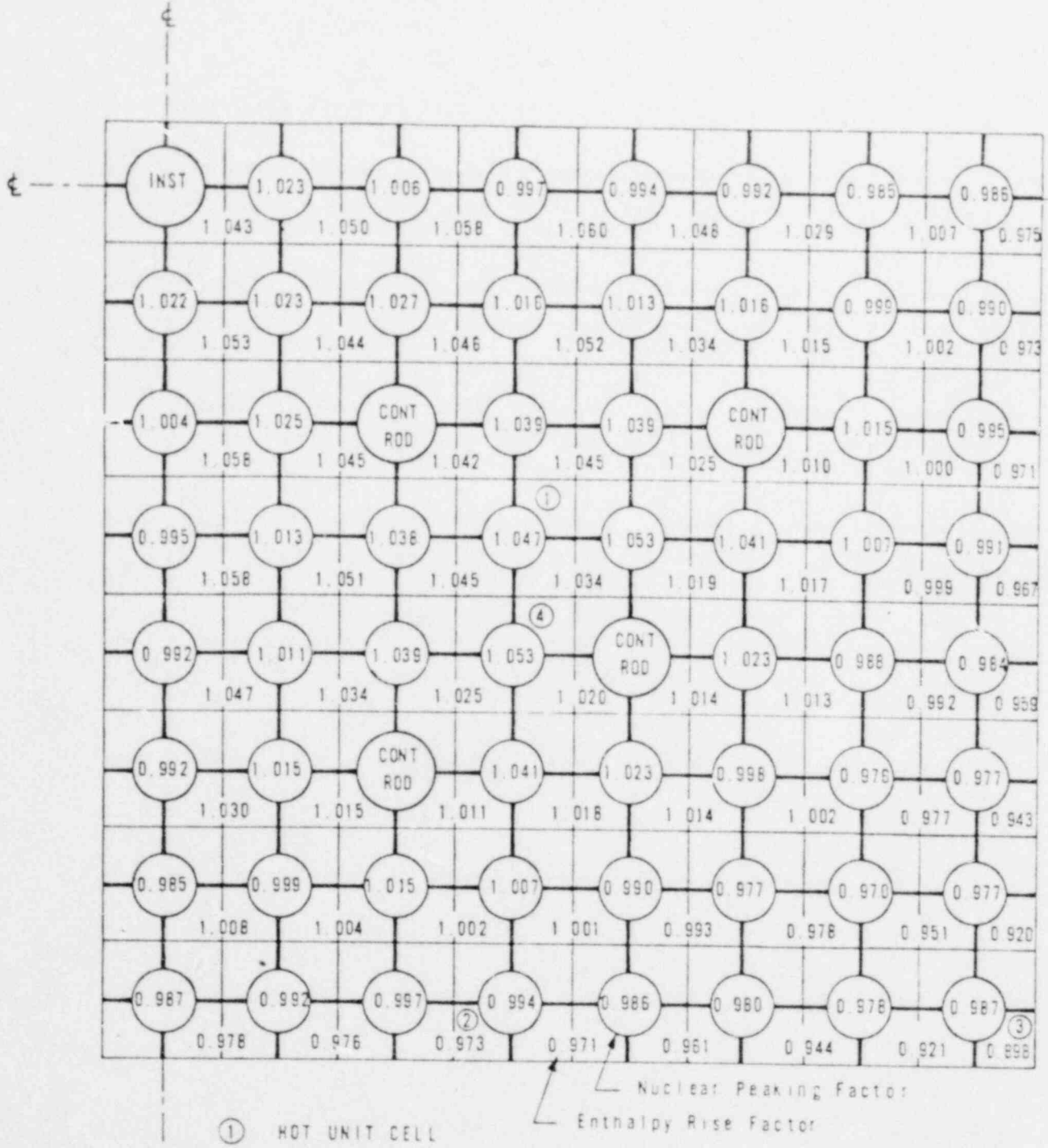

① HOT UNIT CELL

② HOT WALL CELL

③ HOT CORNER CELL

④ HOT CONTROL ROD CELL

NOMINAL FUEL ROD POWER PEAKS AND CELL EXIT ENTHALPY RISE RATIOS

Figure 3-43

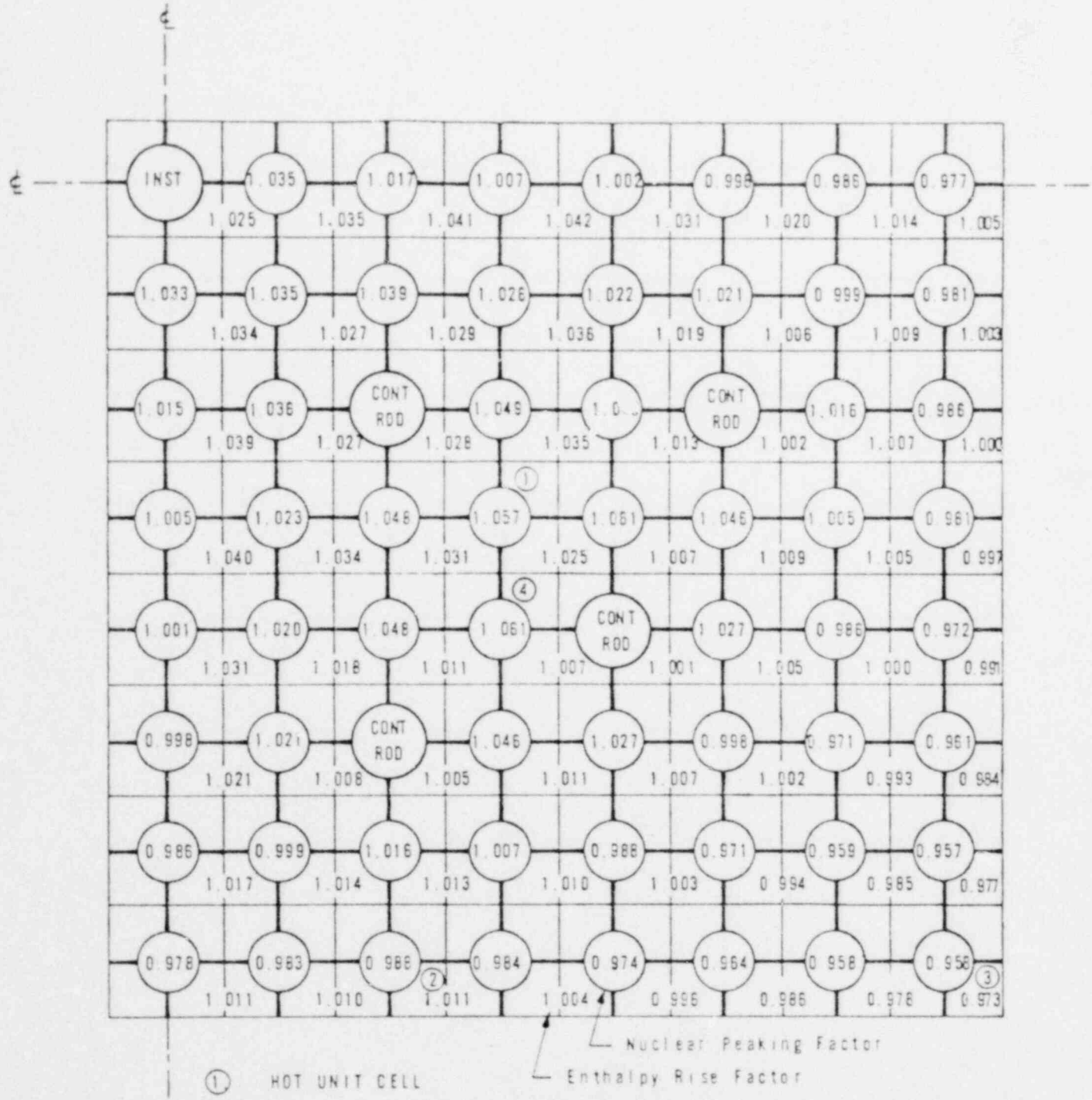

MAXIMUM FUEL ROD POWER PEAKS
AND CELL EXIT ENTHALPY RISE RATIOS

Figure 3-44

00324

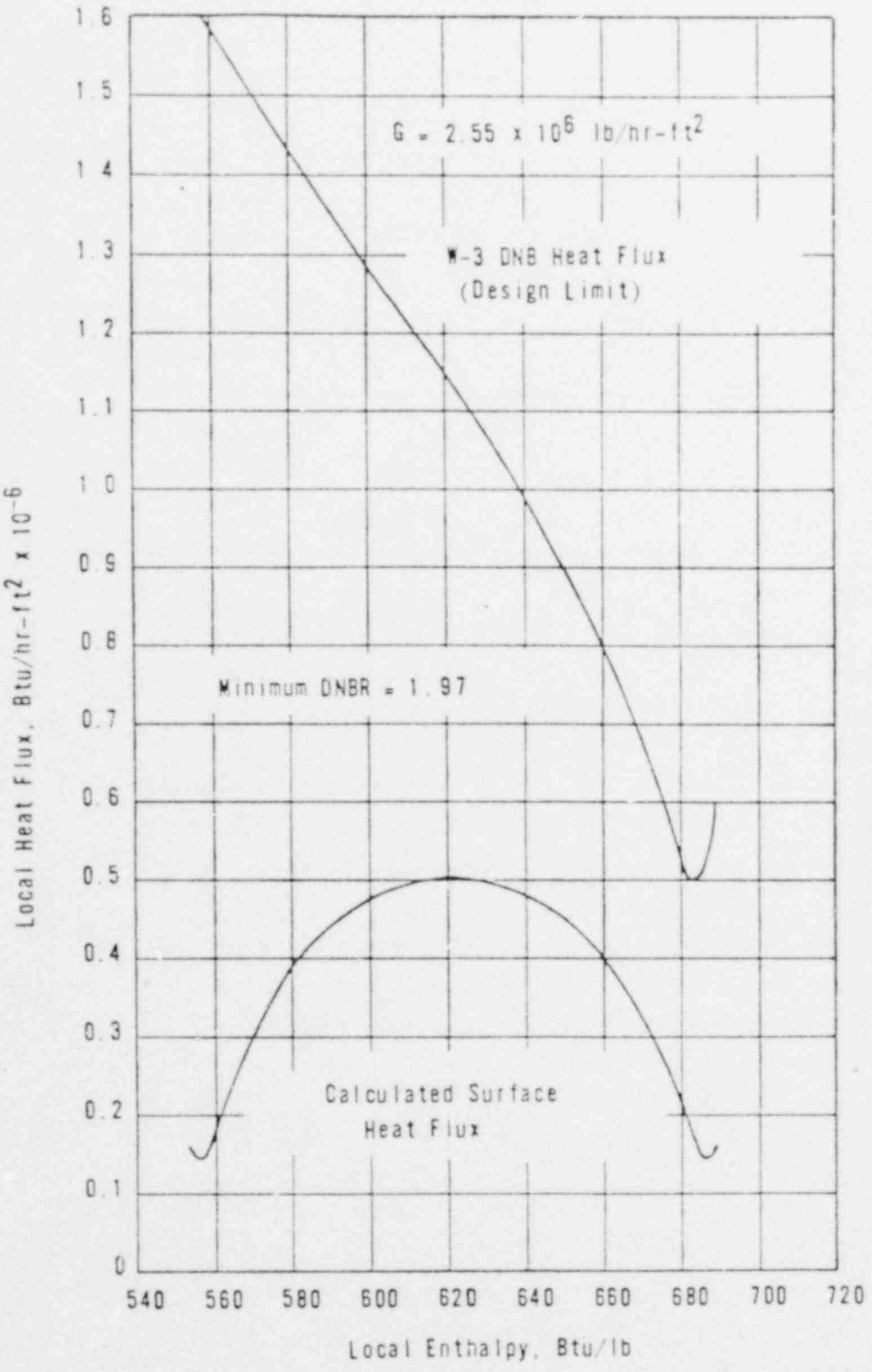

CALCULATED AND DESIGN LIMIT LOCAL HEAT FLUX VERSUS ENTHALPY IN THE HOT UNIT CELL AT THE NOMINAL CONDITION

Figure 3-45

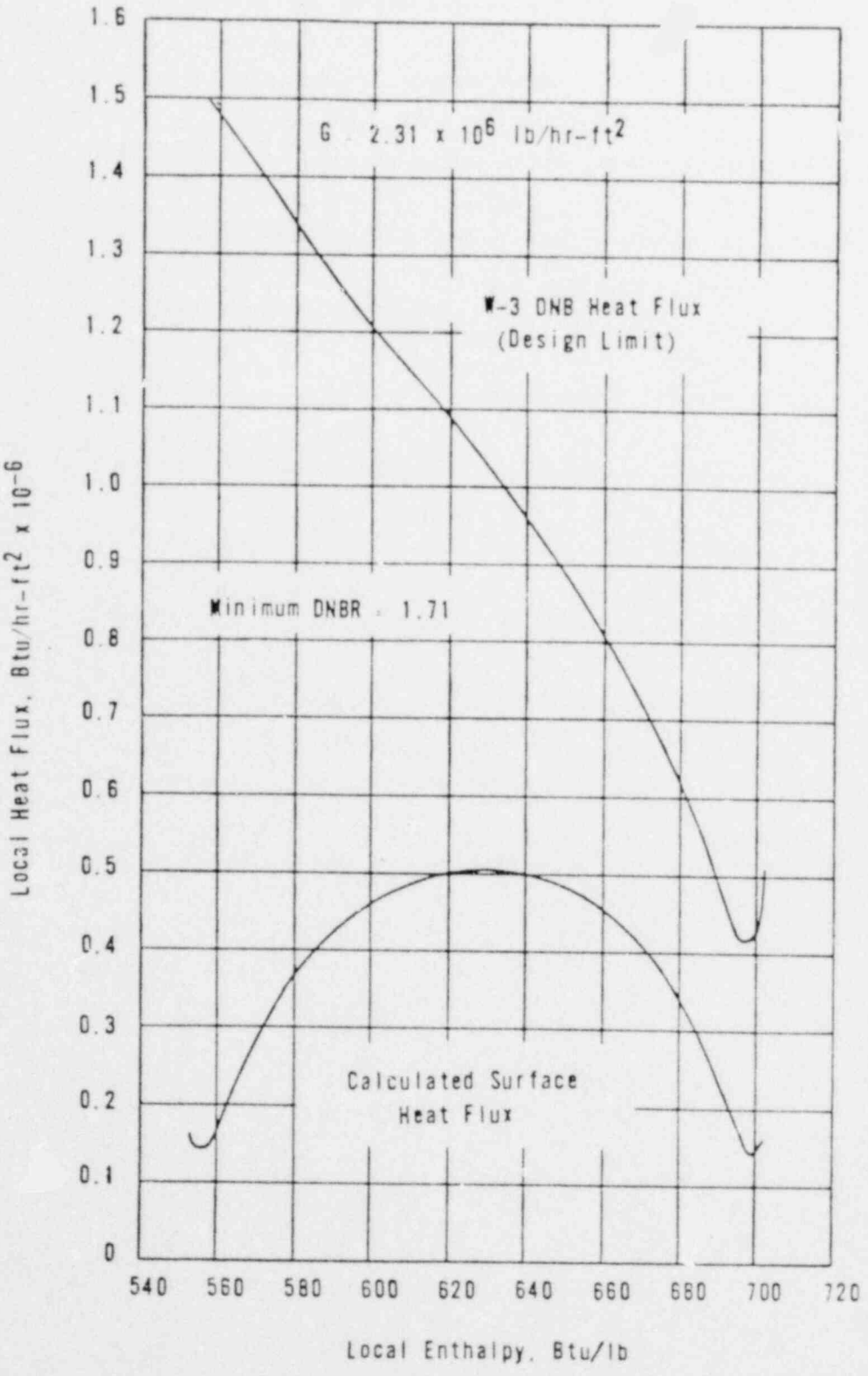

CALCULATED AND DESIGN LIMIT LOCAL HEAT FLUX VS ENTHALPY IN THE HOT UNIT CELL AT THE DESIGN CONDITION

Figure 3-46

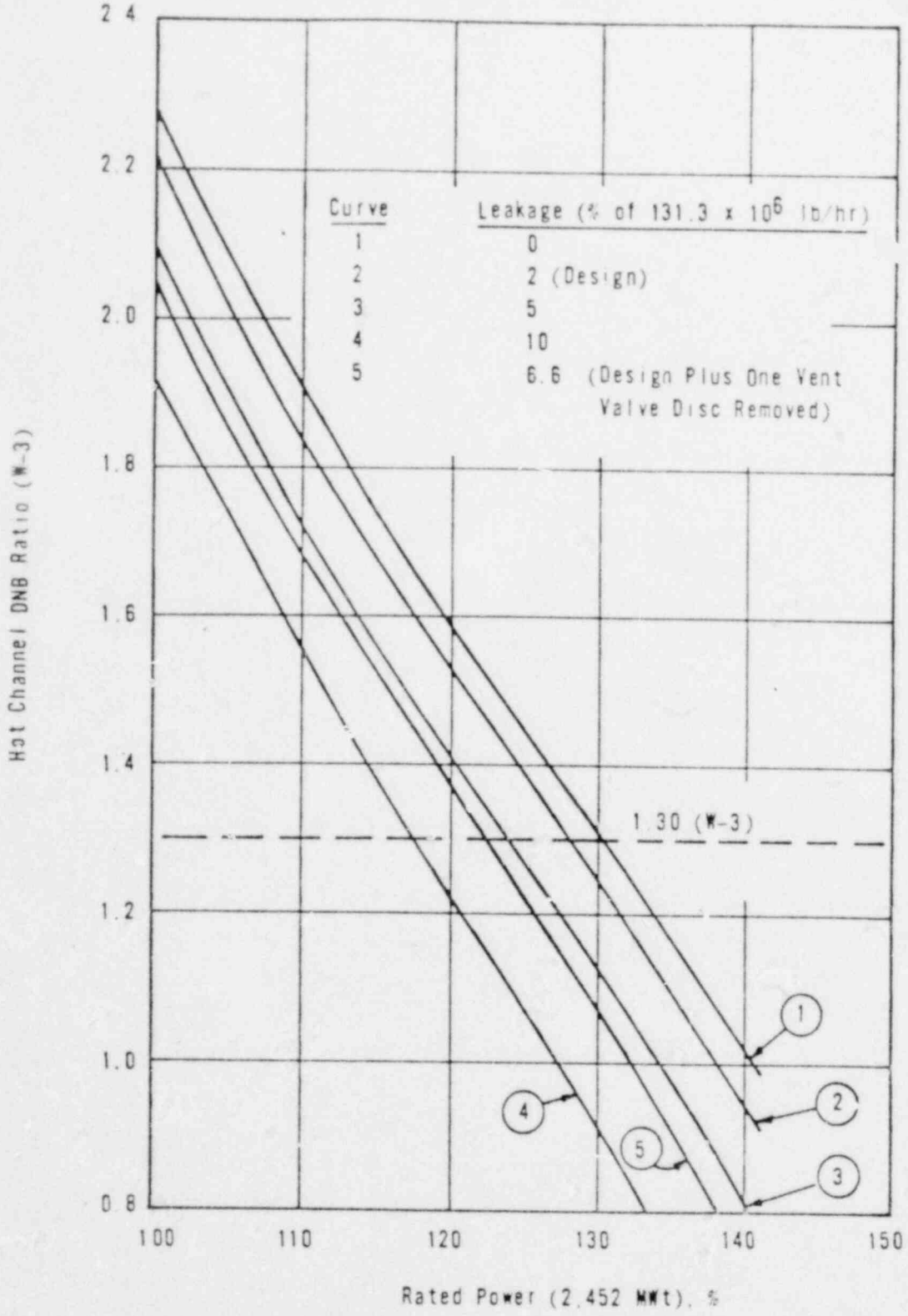

DNB RATIO (W-3) VERSUS POWER FOR VARIOUS INLET-TO-OUTLET CORE BYPASS LEAKAGE

Figure 3-47

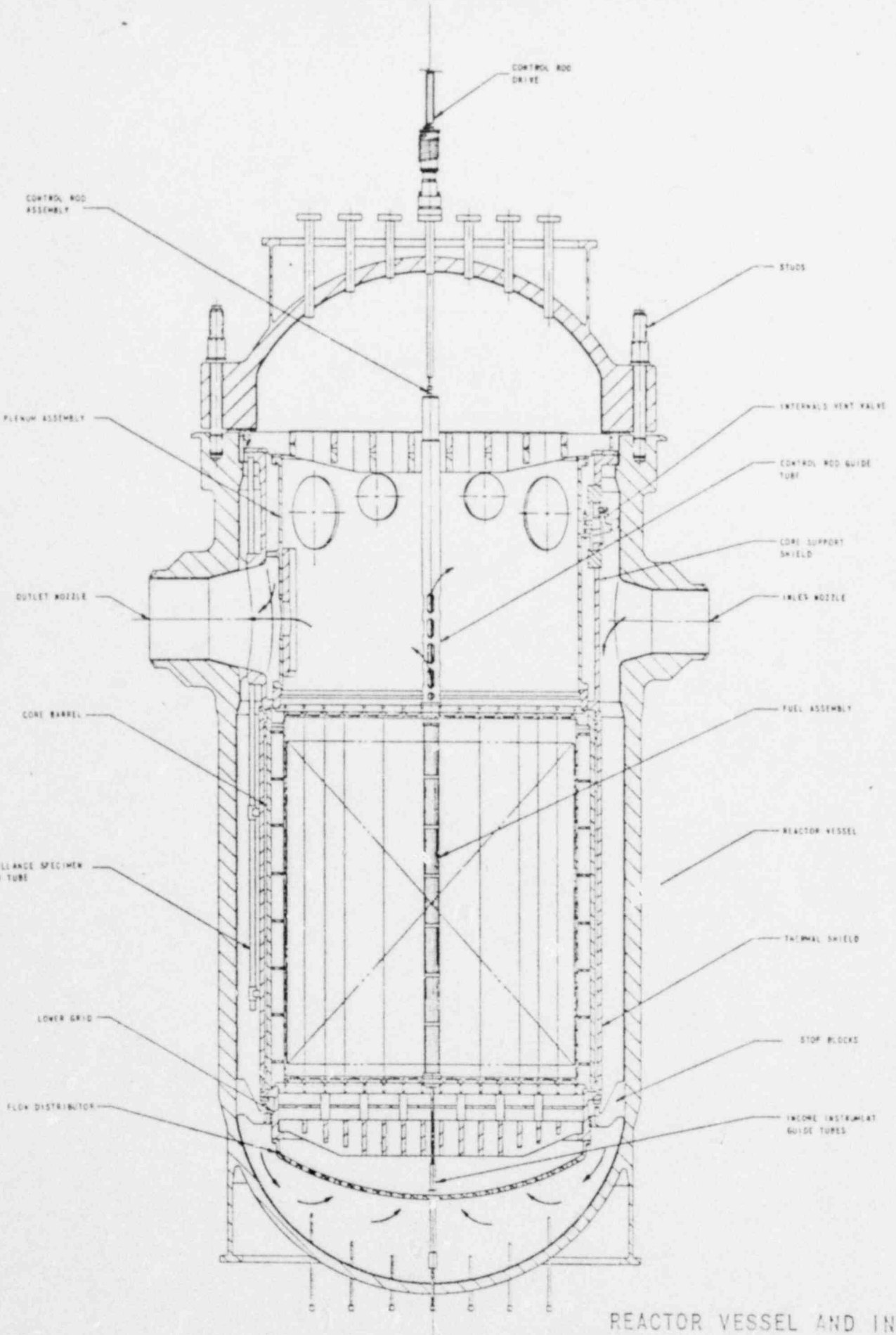

REACTOR VESSEL AND INTERNALS - GENERAL ARRANGEMENT

00008 Figure 3-48

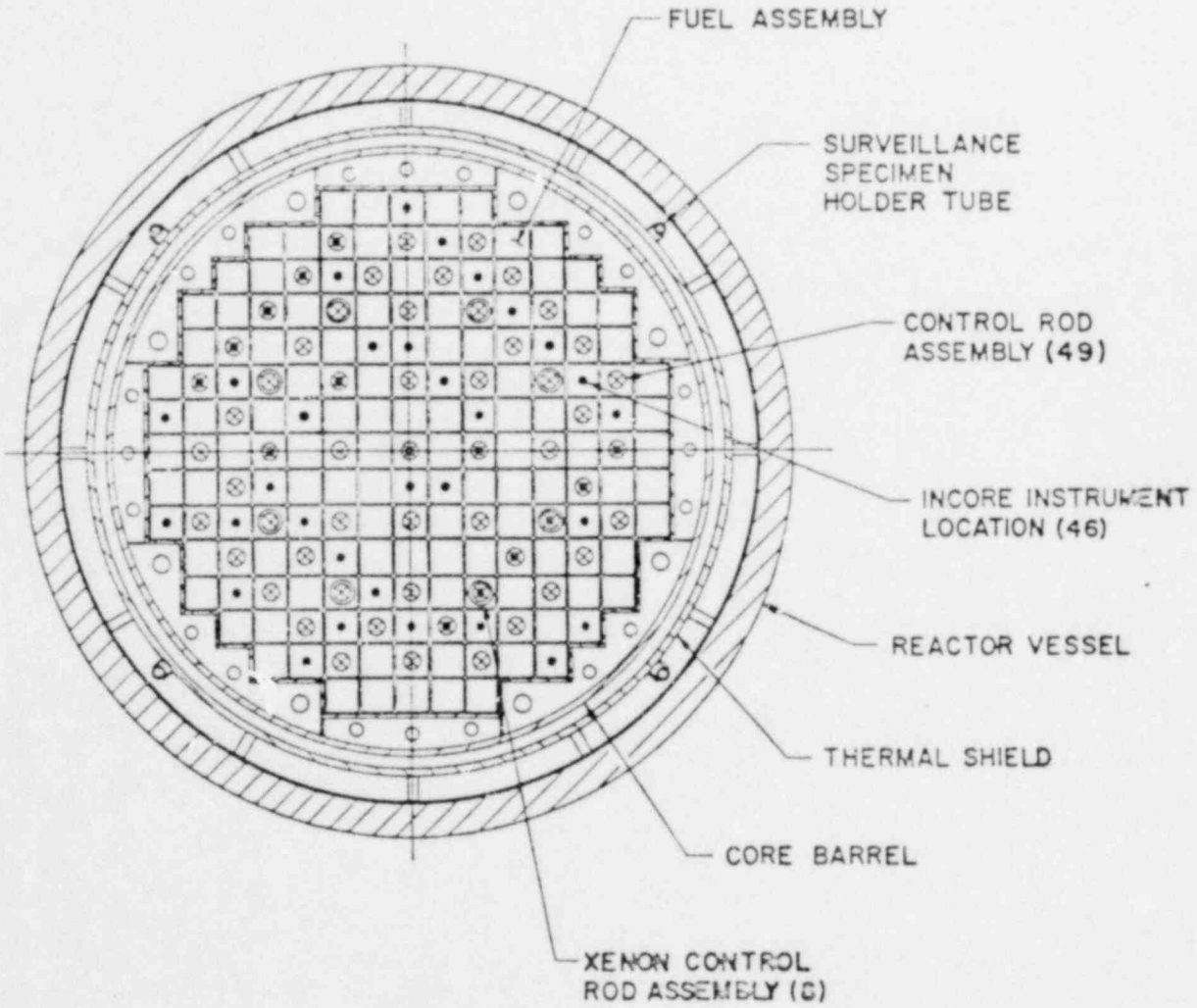

REACTOR VESSEL AND INTERNALS - CROSS SECTION

Figure 3-49

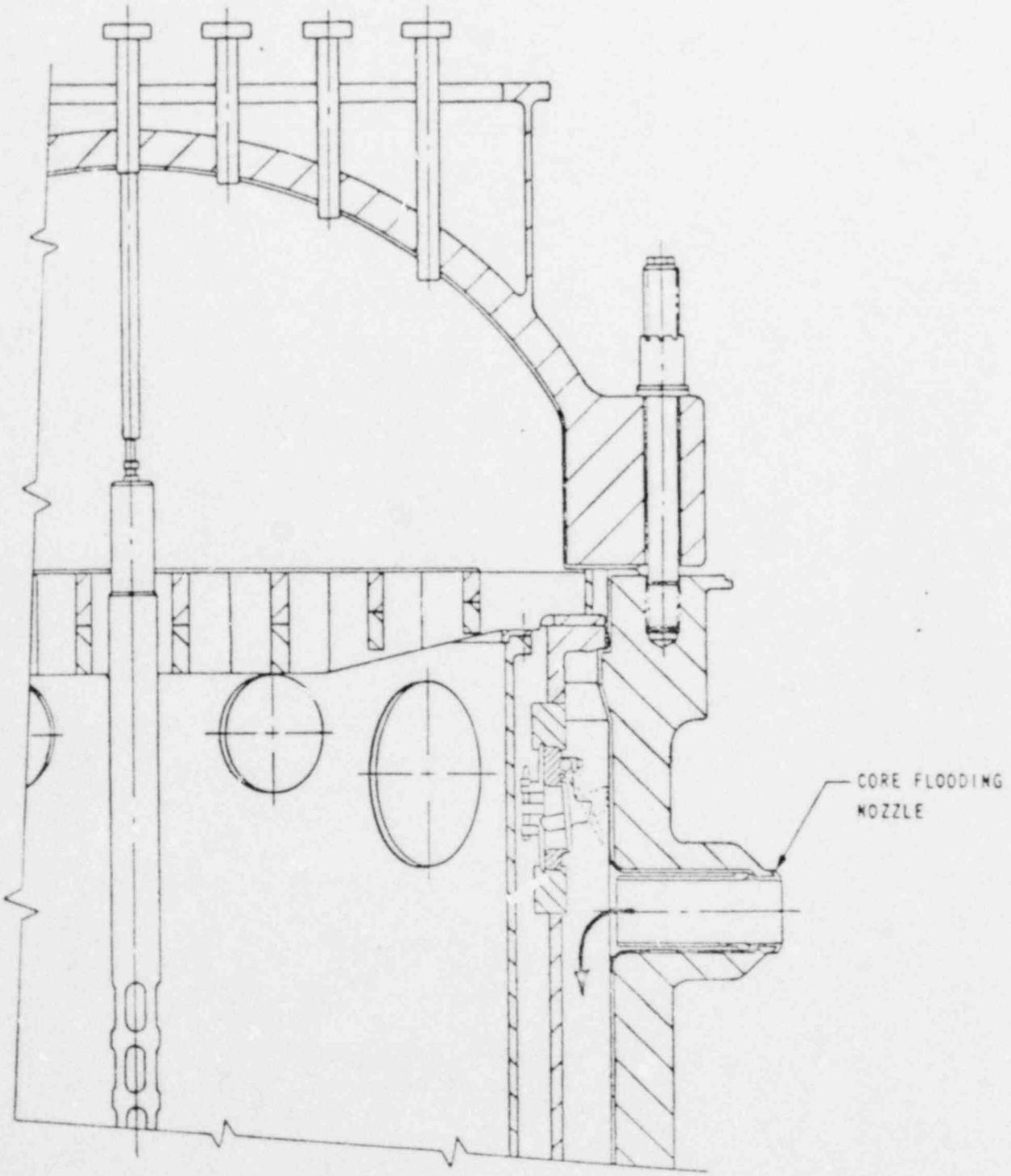

CORE FLOODING ARRANGEMENT

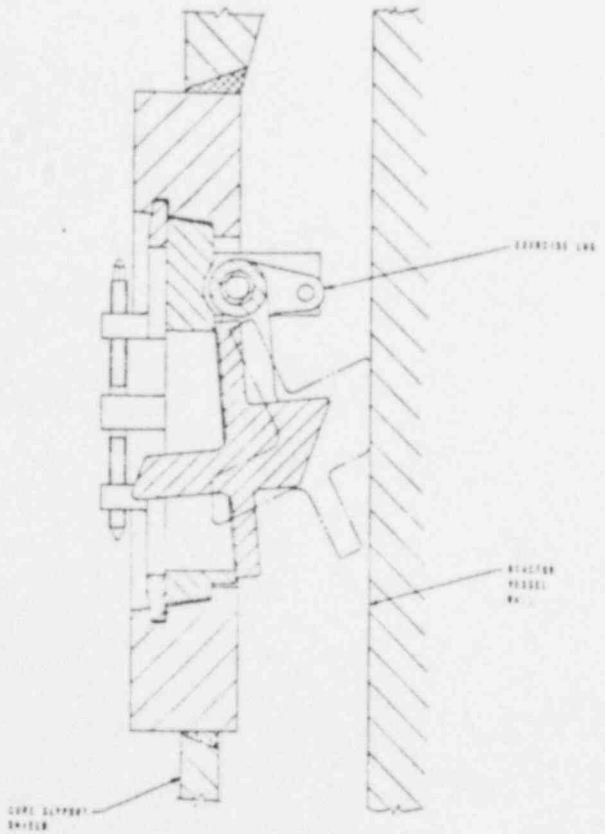

SECTION Z-Z

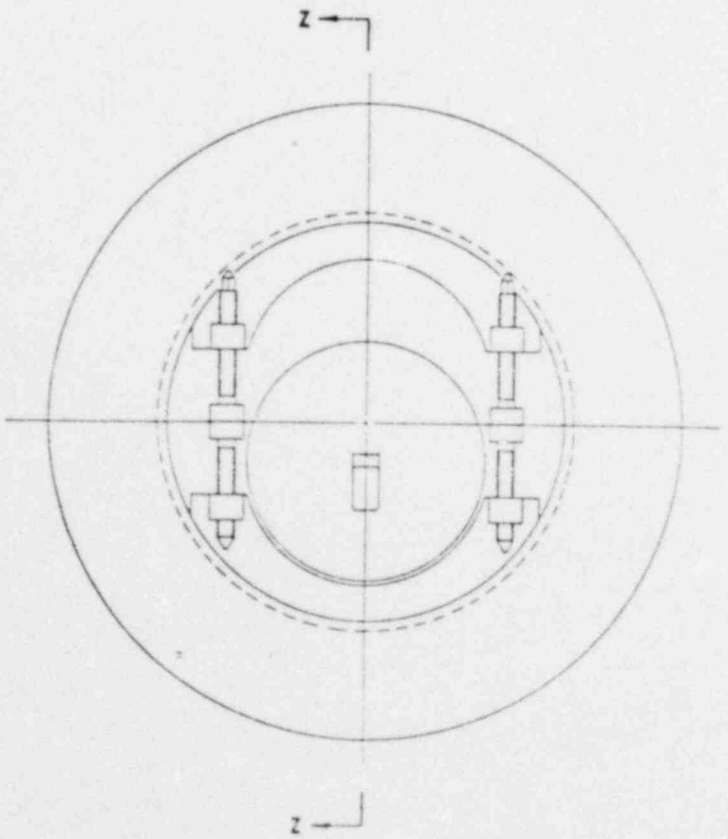

INTERNALS VENT VALVE

00331 Figure 3-51

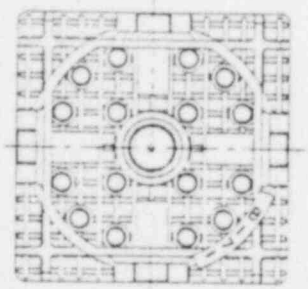

TOP VIEW

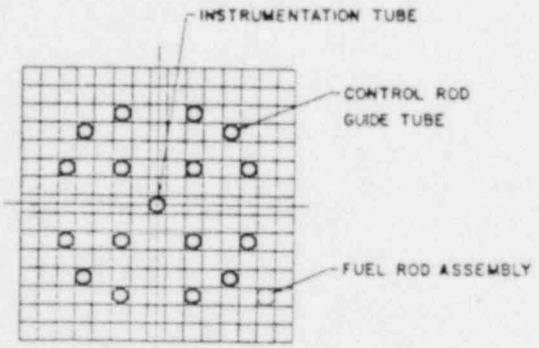

CROSS SECTION

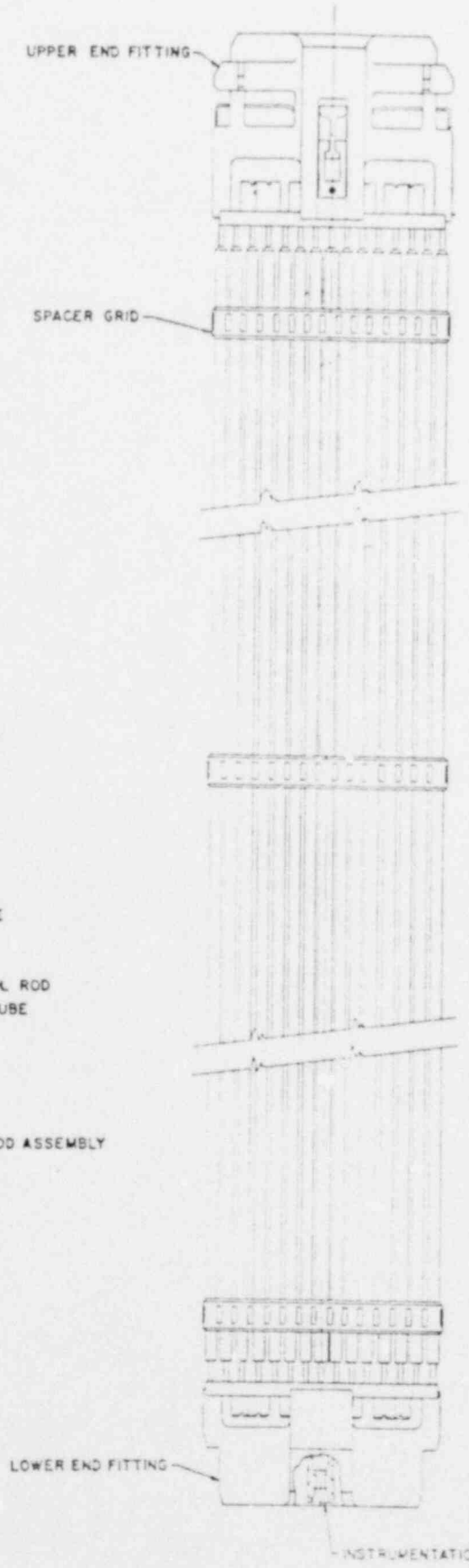

FUEL ASSEMBLY

00332

Figure 3-52

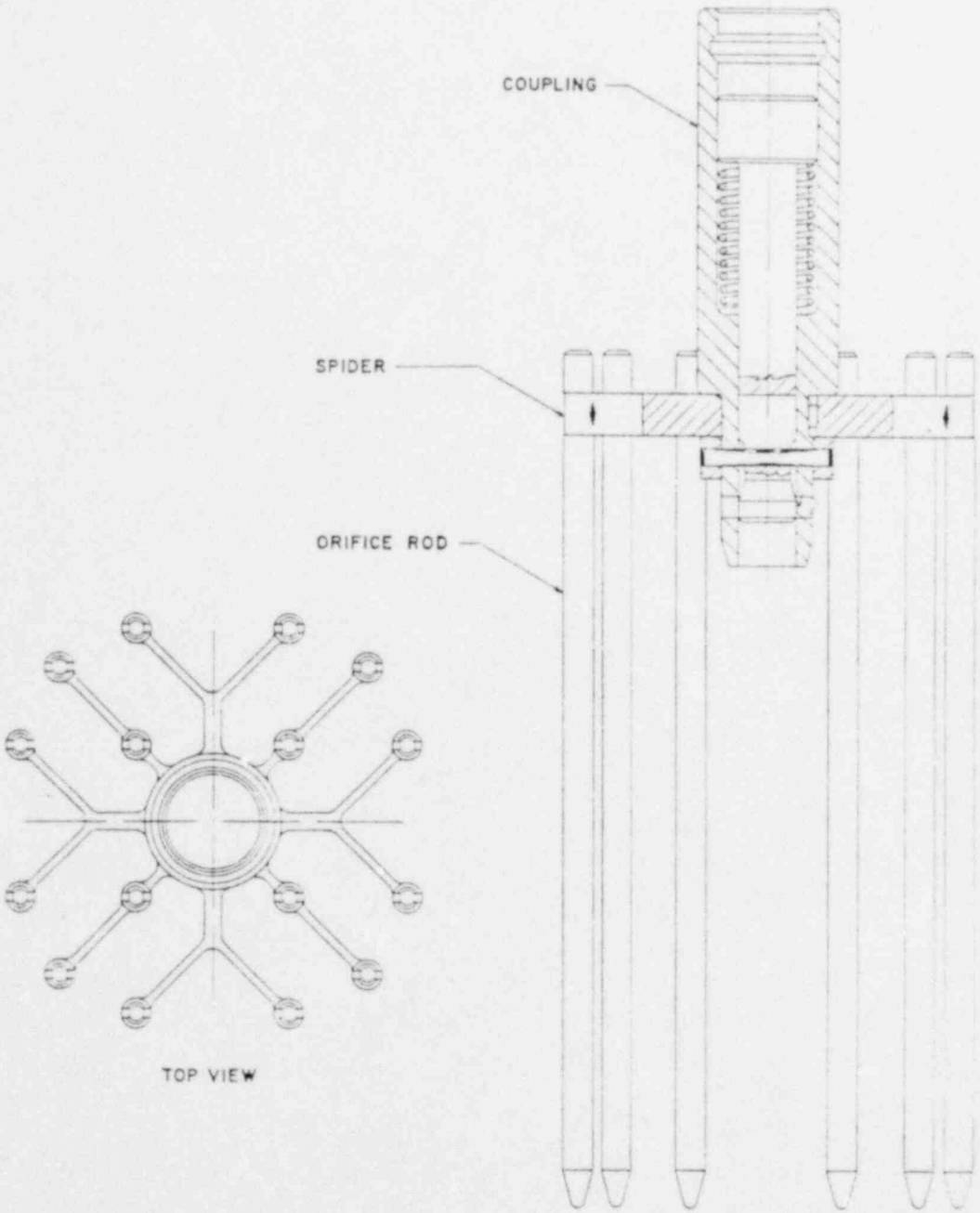

ORIFICE ROD ASSEMBLY

00333

Figure 3-53

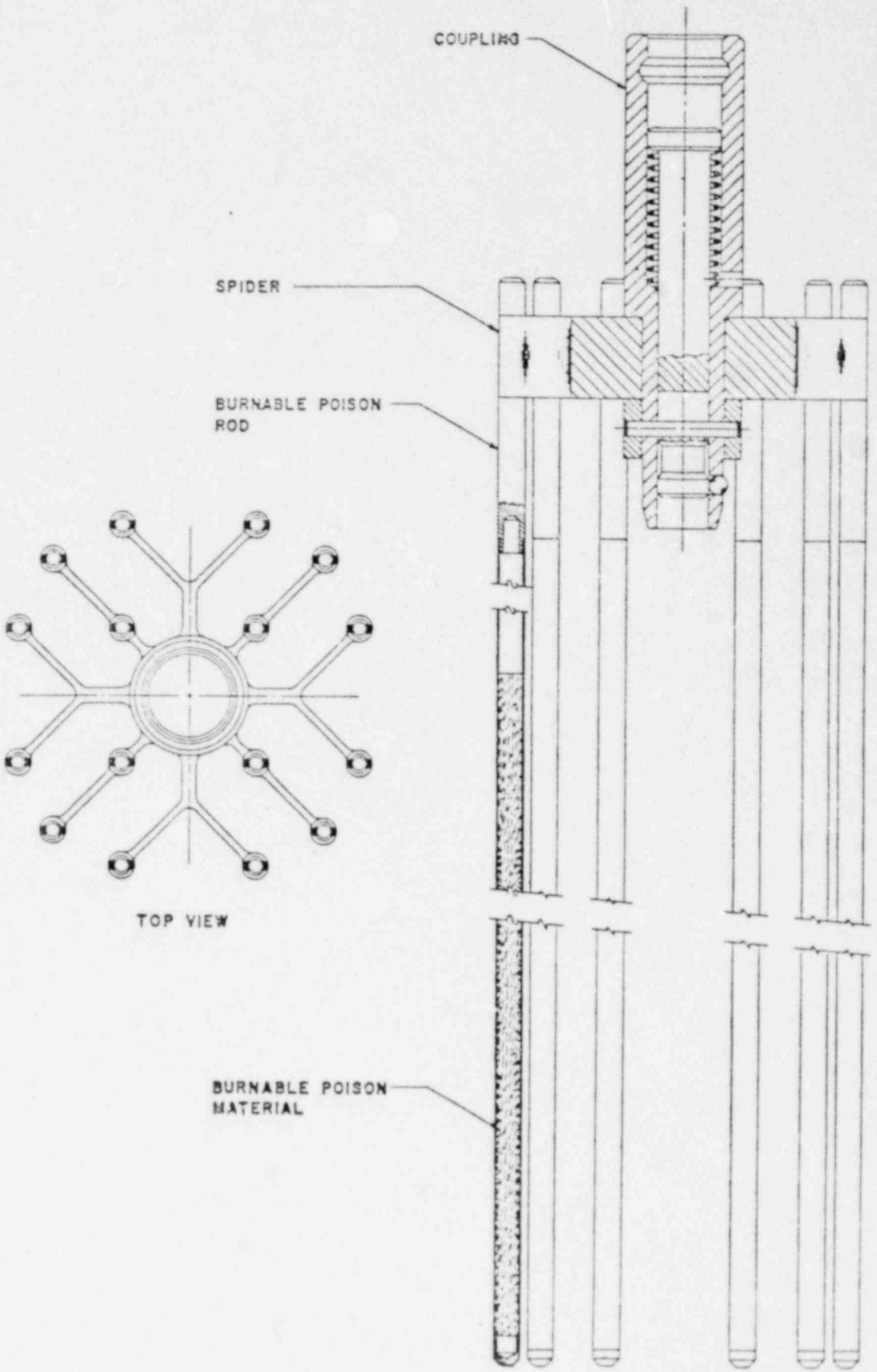

BURNABLE POISON ROD ASSEMBL

Figure 3-5

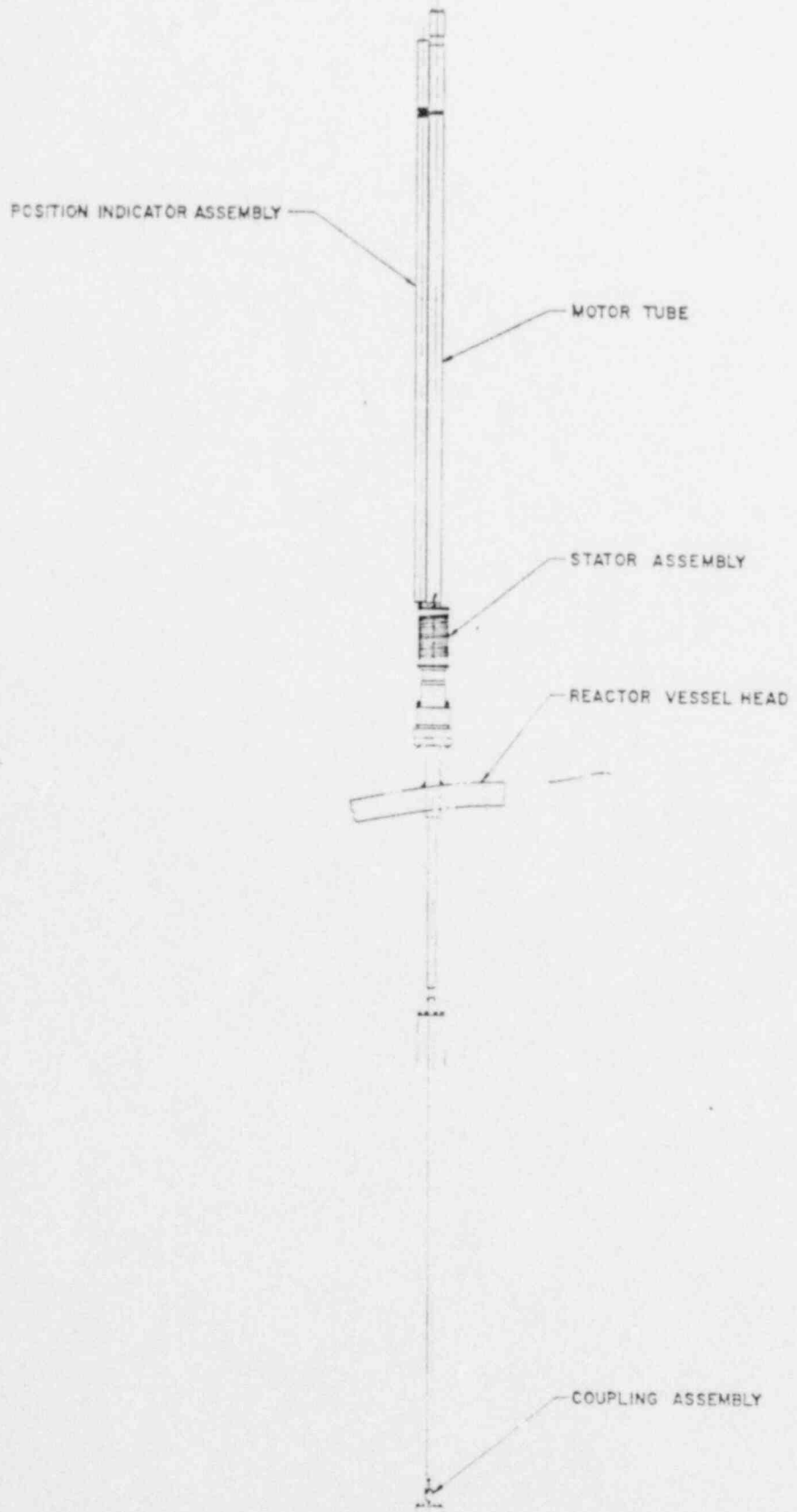

CONTROL ROD DRIVE -
GENERAL ARRANGEMENT

00335

Figure 3-55

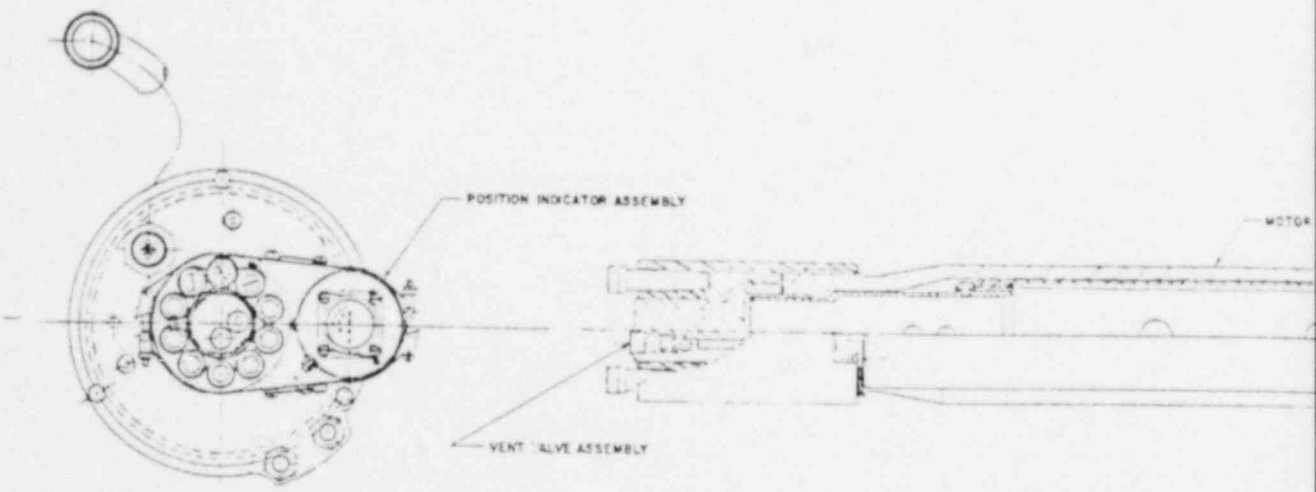
POSITION INDICATOR ASSEMBLY
VENT VALVE ASSEMBLY

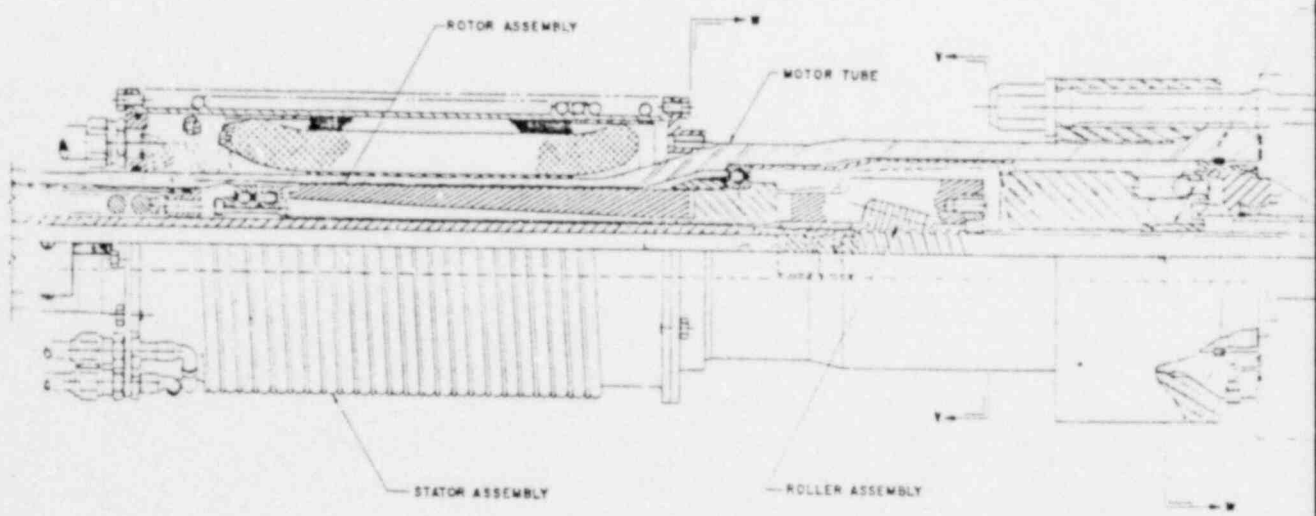
ROTOR ASSEMBLY
MOTOR TUBE
STATOR ASSEMBLY
ROLLER ASSEMBLY

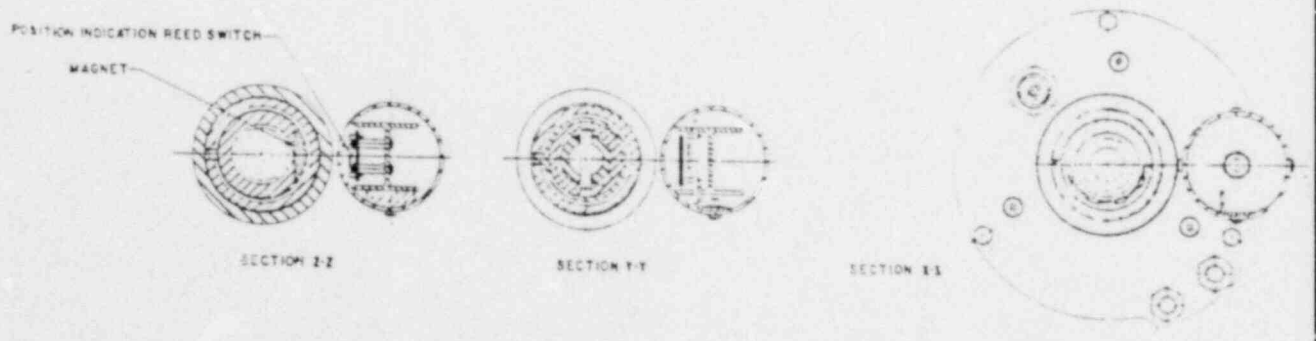
POSITION INDICATION REED SWITCH
MAGNET
SECTION Z-Z
SECTION Y-Y
SECTION X-X

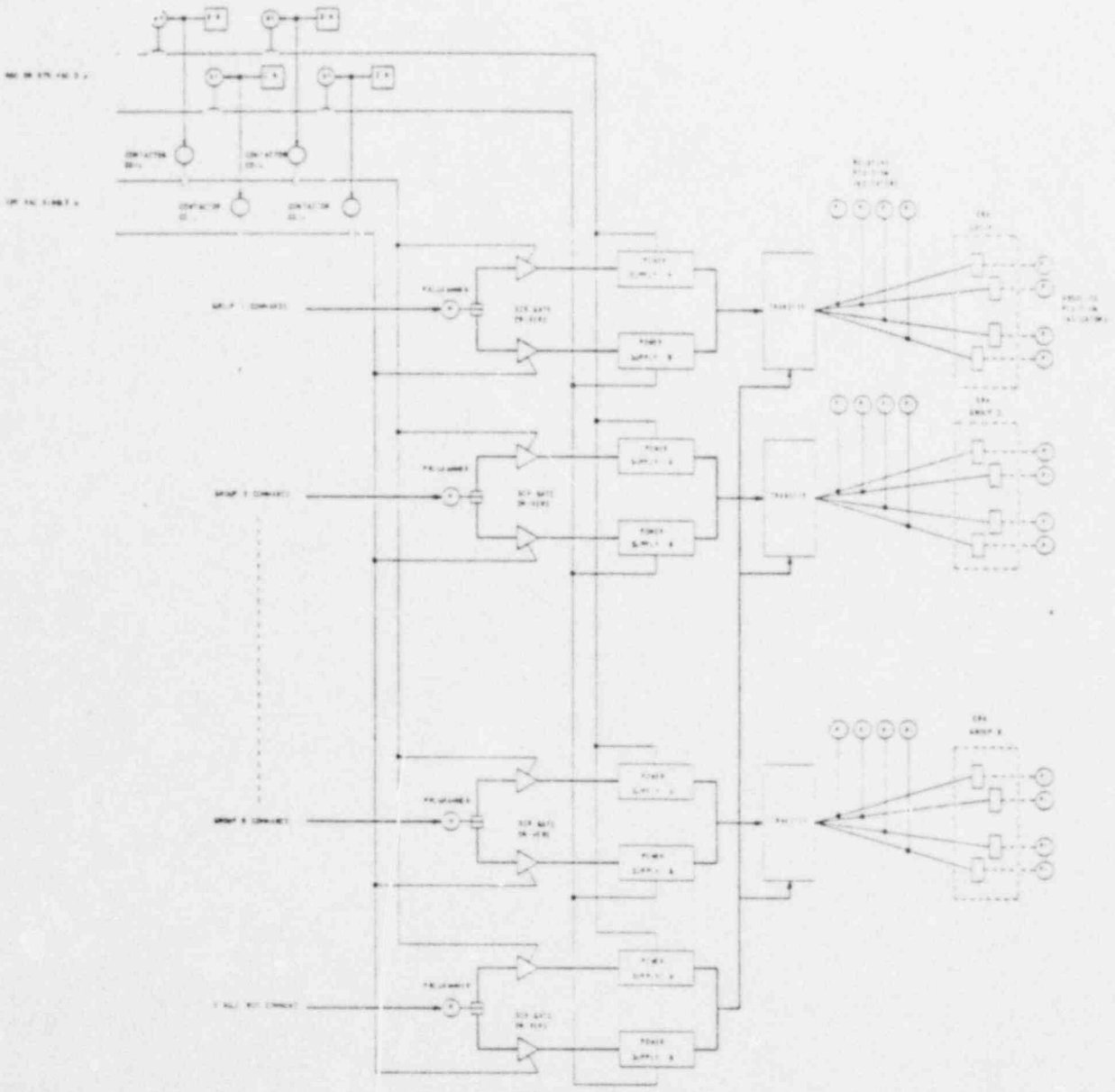

CONTROL ROD DRIVE SYSTEM
AND TRIP BLOCK DIAGRAM

Figure 3-57

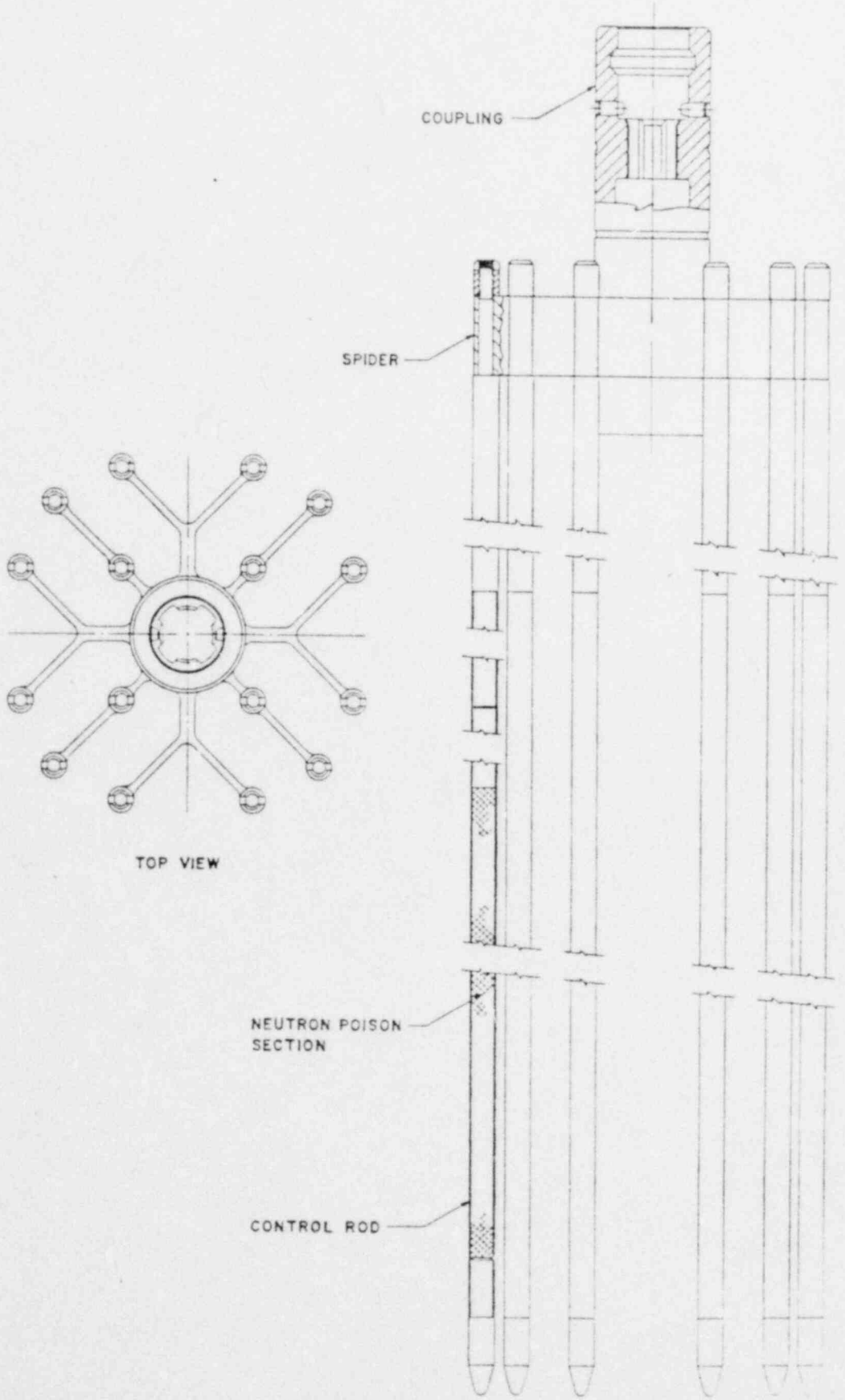

CONTROL ROD ASSEMBLY

00338

Figure 3-58

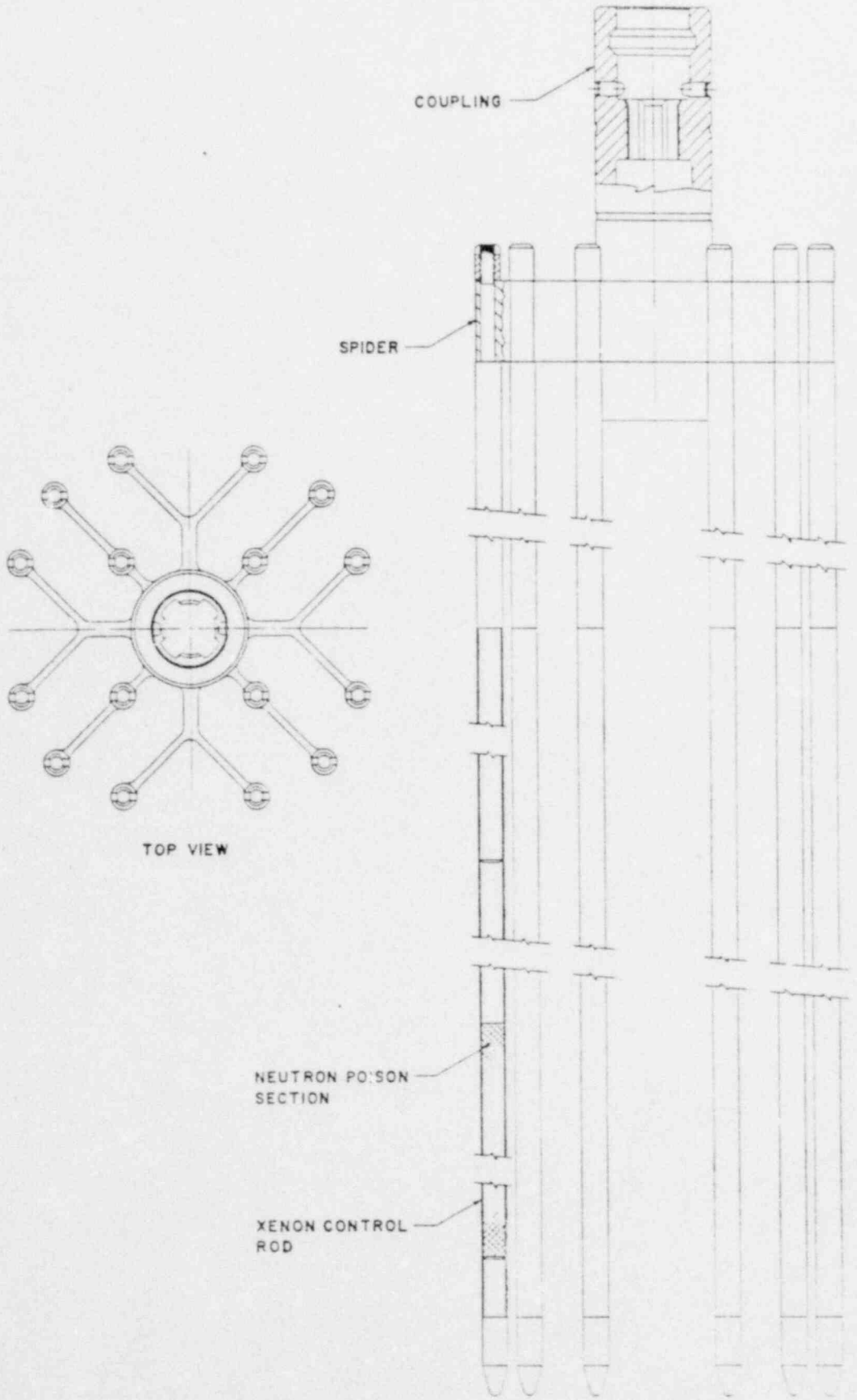

XENON CONTROL ROD ASSEMBLY

Figure 3-59